TECHNISCHE UNIVERSITÄT MÜNCHEN

Lehrstuhl für Bioverfahrenstechnik

Surface Functionalization of Nano-scale Membrane Reactors for Multienzyme Syntheses

Ludwig Johann Klermund, M.Sc.

Vollständiger Abdruck der von der Fakultät für Maschinenwesen der Technischen Universität München zur Erlangung des akademischen Grades eines

Doktors der Naturwissenschaften

genehmigten Dissertation.

Vorsitzender:		Univ.-Prof. Dr.-Ing. Dirk Weuster-Botz
Prüfer der Dissertation:	1.	TUM Junior Fellow Dr. rer. nat. Kathrin Castiglione
	2.	Univ.-Prof. Dr. rer. nat. habil. Dieter Langosch

Die Dissertation wurde am 15.11.2016 bei der Technischen Universität München eingereicht und durch die Fakultät für Maschinenwesen am 22.02.2017 angenommen.

Acknowledgments

This doctoral thesis was prepared at the Institute of Biochemical Engineering (Prof. Dr.-Ing. Dirk Weuster-Botz) of the Technical University of Munich as part of the junior research group of Dr. Kathrin Castiglione. It is a distinct pleasure to thank the many people who contributed to this work.

My sincerest gratitude goes to Dr. Kathrin Castiglione for her guidance and outstanding support. I would like to thank her for four fantastic years I spent in her junior research group, for many lively discussions and the vast knowledge she shared.

I would like to thank Prof. Dr. Dieter Langosch for his role as committee member and Prof. Dr.-Ing. Dirk Weuster-Botz for his role as chairman. Furthermore, I would like to thank Prof. Dr.-Ing. Dirk Weuster-Botz for his excellent support and for providing the necessary equipment and lab space to work on this thesis.

I thank the the BMBF (German Federal Ministry of Education and Research) for funding.

A special thanks goes to all of my current and former colleagues, most of all Sarah Poschenrieder, Tom Schwarzer and Florian Sedlmaier, for all the discussions and debates and the excellent collaboration. I would also like to thank Dr. Dirk Hebel for introducing me to the Institute of Biochemical Engineering.

I deeply acknowledge my students for their great experimental assistance, especially Miguel Valderrama, Hannah Rosner, Bettina Frank, Simone Gruber, Annique Hunger, Caroline Weinzierl, Tom Wyrobnik, Johannes Müller, Lena Dübbel, Marita Deuschle, Arabella Essert, Gerassimos Kolaitis, Julia Keim, and Jennifer Herrmann.

Furthermore, I would like to thank Ellen Truxius, Gabriele Herbrick, Markus Amann, Georg Kojro and Norbert Werth for their support in administrative and technical issues.

Last and most important, I would like to thank my family, most of all my wife and little M.K., for all the support and love.

Table of content

1. Introduction

An increasing awareness toward sustainable industrial processes has shifted the focus of chemical synthesis in industry and academia to develop more environmentally friendly processes (Sheldon, 2008; Woodley, 2008; O'Reilly and Turner, 2015). At the same time, economic aspects play a major role for the implementation of these processes at the industrial scale (Woodley, 2008; Santacoloma *et al.*, 2011). The field of biotechnology provides many aspects of environmentally friendly, safe, but economic syntheses and thus gains an increasing interest in the chemical, pharmaceutical and nutritional industry (Sheldon, 2008; Woodley, 2008; Noyori, 2009). Whereas chemical syntheses often require extreme temperatures and pressures as well as large amounts of organic solvents, biocatalytic processes use enzymes as catalysts that operate at mild conditions in the range of 20 to 40°C, ambient pressure and neutral pH (Faber, 2011). Thus, significantly less energy is required and fewer waste products are produced compared to conventional chemical syntheses, contributing to a greener environment (Schmid *et al.*, 2001; Hatti-Kaul *et al.*, 2007; Liese and Hilterhaus, 2013).

Yet, the use of conventional biocatalytic methods using either whole cells or isolated enzymes encounters several limitations. For example, complex reaction cascades in cells allow the synthesis of high-value products via several reaction steps with cheap biocatalysts. However, despite advances in the development of optimized bacterial strains, the formation of side products still poses a major issue in whole cell biocatalysis (Bommarius and Riebel, 2004; Lopez-Gallego and Schmidt-Dannert, 2010). In turn, advances in enzyme discovery and protein engineering to increase the stability of enzymes and change the substrate specificity have greatly expanded the use of isolated enzymes (Bommarius and Riebel, 2004; Findrik and Vasic-Racki, 2009). However, because isolated enzymes are usually expensive due to extensive purification procedures, retention and reuse of the biocatalyst is of interest (Lee, 2006).

In view of the growing demand for alternative, environmentally friendly industrial processes, the trend in biocatalysis to further increase the sustainability and cost effectiveness goes toward the use of multienzyme cascade reactions, combining the pros and reducing the cons of whole cells and isolated enzymes (Santacoloma *et al.*, 2011). The sequential performance of reactions without intermediate isolation can enhance the performance of bioconversions compared to step-by-step biosynthesis by pulling reversible reactions to completion while at

the same time reducing operational units, thus saving time, costs and chemicals required for intermediate purification (Oroz-Guinea and Garcia-Junceda, 2013). Furthermore, reactions with harmful or unstable intermediates can be performed by immediate scavenging of the intermediate by a subsequent reaction (Ricca *et al.*, 2011). These considerable advantages of multienzyme syntheses in increasing the sustainability as well as the economic viability of biotechnological processes have led to designing interesting and highly economic systems (Santacoloma *et al.*, 2011). However, although enzymatic cascade reactions have great potential for the establishment of sustainable chemical processes (Noyori, 2009), many cascade reactions suffer from incompatibilities, for example different reaction conditions or cross-inhibitions by components of the reaction system, which greatly limit their applicability in biocatalysis (Ricca *et al.*, 2011).

2. Motivation and objectives

Polymeric nanocompartments, so-called polymersomes, are hollow membrane vesicles formed from amphiphilic block copolymers that spontaneously self-assemble when added to aqueous solutions. In their structure, they resemble lipid membrane vesicles, so-called liposomes, however, have a much higher mechanical stability and a lower membrane permeability (Discher and Eisenberg, 2002). This allows retaining encapsulated proteins and molecules within the vesicles' lumen under process conditions (Poschenrieder, 2016). So far the potential of polymer-based vesicles has mainly been investigated in view of therapeutic and diagnostic applications, for example as drug delivery systems (Discher *et al.*, 2007; Christian *et al.*, 2009; Jain *et al.*, 2011; Palivan *et al.*, 2016) or as biosensors (Gonzalez-Perez *et al.*, 2009). By entrapping enzymes in polymersomes, nano-scale enzyme membrane reactors can be created. Within these vesicles, multi-step enzymatic syntheses can be performed in separate reaction chambers without the formation of by-products due to the lack of competing enzymes. As an alternative to whole cells and isolated enzymes, polymersomes may overcome limits to multienzyme reactions which encounter cross-inhibitions by mimicking two fundamental principles of natural cells, compartmentalization and selective mass transport. Hereby, polymersomes made of the block copolymer poly(2-methyloxazoline)-poly(dimethylsiloxane)-poly(2-methyloxazoline) (PMOXA-PDMS-PMOXA) have highly beneficial characteristics as they have a low membrane permeability compared to lipid membranes but allow the incorporation of highly selective natural or engineered membrane transport proteins (Nardin *et al.*, 2000b; Nallani *et al.*, 2006; Kumar *et al.*, 2007). However, in contrast to the use of polymersomes in medical applications, the potential of polymersomes for preparative biotechnological applications has so far not been extended beyond *proof-of-concept* studies (Schoonen and van Hest, 2016). These systems have been limited to compatible reaction cascades that allow for non-selective mass transport to ensure sufficient exchange of substrates and products, which to some extent limits the necessity for using compartmentalization (Schmitt *et al.*, 2016; Schoonen and van Hest, 2016).

The presentation of molecules on the surface of polymersomes is desired in all fields of polymersome applications (Egli *et al.*, 2011b). Surface functionalization of nano-scale membrane reactors, that is the immobilization of enzymes on the polymer membrane, can make the environment surrounding the polymersomes available for multienzyme syntheses

while retaining the possibility to remove or recover the catalytic species as a whole entity (van Dongen *et al.*, 2008).

To date, numerous approaches have been pursued to functionalize the surface of polymer membranes indicating the need for quick and simple strategies to immobilize proteins on polymersome surfaces. Focus has been laid on chemical conjugations (Christian *et al.*, 2007; Opsteen *et al.*, 2007; van Dongen *et al.*, 2008; van Dongen *et al.*, 2009; Egli *et al.*, 2011a; Debets *et al.*, 2013) and on non-covalent binding of interaction partners (Broz *et al.*, 2005; Lin *et al.*, 2006; Hammer *et al.*, 2008; Grzelakowski *et al.*, 2009). These methods require the pre-conjugation of the polymer and the protein with reactive groups such as azides and alkynes, or interaction partners such as biotin and streptavidin, thereby adding multiple additional steps toward polymersome functionalization. Especially the extensive chemical modifications of the polymer usually result in a profound change of the hydrophilic weight fraction of the copolymer. This can significantly alter polymer characteristics and influence polymersome formation (van Dongen *et al.*, 2008). Furthermore, the number of proteins immobilized per polymersome is typically low, which has been either attributed to steric hindrance (Egli *et al.*, 2011a) or to the surface ligand being inaccessibly buried in the hydrophilic brush of the polymer membrane (Pang *et al.*, 2008).

As an alternative approach, proteins may be anchored on the polymersome surface by fusion to a hydrophobic protein domain on gene level. Due to the polymer membrane's resemblance to lipid membranes in terms of fluidity and compressibility, polymer membranes have been demonstrated to allow the integration of biological membrane domains. This strategy offers a strong hydrophobic interaction between the polymer and the protein and is not constrained to pre-conjugated polymers (Noor *et al.*, 2012). Although Noor *et al.* (2012) were able to display the enhanced green fluorescent protein (eGFP) on poly(isobutylene)-poly(ethylene glycol)-poly(isobutylene) (PIB-PEG-PIB) polymersomes via its fusion to the antibacterial peptide cecropin A, the potential of antibacterial peptides to form pores in polymeric membranes has been demonstrated for alamethicin (Wong *et al.*, 2006) and gramicidin (Gonzalez-Perez *et al.*, 2009). These antibacterial, pore-forming peptides readily inserted into and destabilized PMOXA-PDMS-PMOXA polymersomes. Because the polymersomes are to be used as nano-scale membrane reactors for multienzyme syntheses, uncontrolled diffusion across the polymer membrane can lead to the abolition of the compartmentalization, making antibacterial peptides not applicable for surface functionalization. In turn, natural membrane anchors exist which tether their adjacent protein or enzyme to but do not form pores or disintegrate lipid membranes (Kutay *et al.*, 1993).

In view of the utilization of polymeric nanocompartments as reaction chambers for multienzyme syntheses, the main objective of this study was the assessment of hydrophobic, non-antibacterial membrane domains as membrane anchors for a simple surface

functionalization method of nano-scale enzyme membrane reactors. Thus, natural and artificial non-antibacterial membrane anchors that are suitable for the surface functionalization of $PMOXA_{15}$-$PDMS_{68}$-$PMOXA_{15}$ polymersomes were to be identified and characterized in terms of their insertion into the polymer membrane.

A successful immobilization would make the surrounding environment available as additional reaction space without losing the ability to retain the biocatalyst as a whole entity. Furthermore, it would allow the spatial separation of the reactions by a membrane by entrapping enzmyes in the lumen and immobilizing enzymes on the surface of the polymersomes. Thus, through the spatial separation of reactions in the inner and the outer compartment, polymersomes have the potential to enhance reaction cascades with incompatible reactions steps in one pot. On the basis of the three-step enzymatic synthesis of cytidine-5'-monophospho-*N*-acetylneuraminic acid (CMP-Neu5Ac), it was to be evaluated whether the application of functionalized $PMOXA_{15}$-$PDMS_{68}$-$PMOXA_{15}$ polymersomes as nano-scale enzyme membrane reactors has advantages over the corresponding reaction systems based on isolated enzymes free in solution. The reaction cascade involves three enzymes, an *N*-acyl-D-glucosamine 2-epimerase (AGE), an *N*-acetylneuraminate lyase (NAL) and a CMP-sialic acid synthetase (CSS) producing CMP-Neu5Ac from *N*-acetylglucosamine (GlcNAc), pyruvate and cytidine 5'-triphosphate (CTP) via the intermediates *N*-acetylmannosamine (ManNAc) and *N*-acetylneuraminic acid (Neu5Ac) (Figure 2.1) (Kittelmann *et al.*, 1992). The cascade reaction suffers from several cross-inhibitions with the main incompatibility arising from a strong inhibition of the substrate CTP of the third reaction, the activation of Neu5Ac with CTP to form CMP-Neu5Ac, on the enzyme of the first reaction, the AGE.

To ensure a compartmentalization that has the potential to enhance the reaction cascade by reduction of the cross-inhibition, a selective mass transport across the polymer membrane must be provided to differentiate between substrates and inhibitors of the encapsulated enzyme. Thus, selective membrane channel proteins were to be identified and reconstituted into the polymer membrane, with the aim to allow the separation of the AGE from its inhibitor CTP, thereby potentially enhancing the synthesis of CMP-Neu5Ac in a one-pot multienzyme cascade reaction.

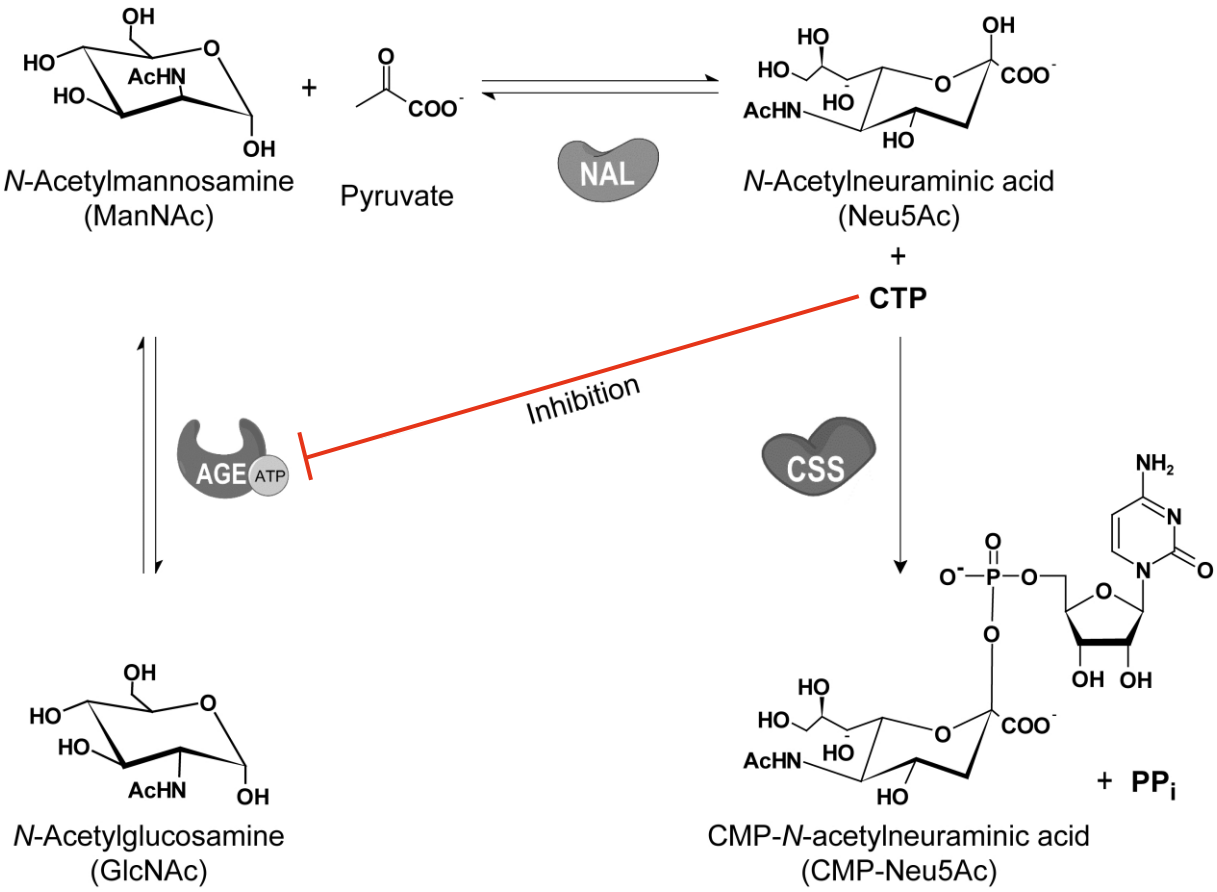

Figure 2.1 – CMP-Neu5Ac synthesis via a three-enzyme cascade reaction. *N*-Acetylglucosamine (GlcNAc) is converted to *N*-acetylmannosamine (ManNAc) by an *N*-acyl-D-glucosamine 2-epimerase (AGE). ATP serves as allosteric activator of the enzyme. ManNAc then reacts with pyruvate to form *N*-acetylneuraminic acid (Neu5Ac) in an aldol condensation reaction catalyzed by an *N*-acetylneuraminic acid lyase (NAL). Neu5Ac is then activated with CTP by a CMP-sialic acid synthetase (CSS) to form CMP-Neu5Ac and inorganic pyrophosphate (PP_i). The reaction suffers from a strong cross-inhibition of CTP on the AGE.

Furthermore, to reduce tedious protein purification steps of membrane bound proteins from recombinant expression hosts, the potential of cell-free protein synthesis (*in vitro* protein synthesis, IVPS) in synthesizing membrane proteins is to be investigated. In the presence of polymersomes, the hydrophobic membrane can salvage the nascent hydrophobic membrane anchor, resulting in a combined protein preparation and polymersome surface functionalization. Although this has already been demonstrated for the functionalization of giant liposomes (Nomura *et al.*, 2008) and the production and integration of transmembrane proteins into polymersomes (Nallani *et al.*, 2011; May *et al.*, 2013), it remains unclear whether this approach is suitable for presenting target proteins on polymersome surfaces using hydrophobic membrane anchors.

This thesis is divided into the following work packages:

- Identification of suitable peptide anchors for the surface functionalization of $PMOXA_{15}$-$PDMS_{68}$-$PMOXA_{15}$ polymersomes using enhanced green fluorescent protein (eGFP) as model protein, including:
    - Preparation of functional eGFP in fusion with hydrophobic peptide anchors
    - Determination of the effect of peptide anchors on eGFP fluorescence
    - Qualitative and quantitative characterization of the peptide insertion into the polymer membrane

- Implementation of the multienzyme biosynthesis of CMP-Neu5Ac in functionalized polymersomes, including:
    - Assessment of the membrane permeability and selection of a suitable membrane channel protein for selective mass transport
    - Positional assembly of the enzymes within the nano-scale enzyme membrane reactors
    - Selection of suitable peptide anchors for enzyme immobilization and determination of the effect of the peptide anchors on enzyme characteristics
    - Evaluation of the performance of the nano-scale enzyme membrane reactors in comparison to the non-compartmentalized reaction cascade

- *Proof-of-principle* of the combined *in vitro* synthesis of proteins with hydrophobic membrane anchors and the simultaneous surface functionalization of polymersomes

3. Theoretical background

3.1 Polymer vesicles

Polymersomes are hollow spherical vesicles made of amphiphilic block copolymers (Discher *et al.*, 1999). These polymer vesicles closely resemble liposomes, vesicles made of natural or artificial lipids, and have thus been termed polymersomes (Discher and Eisenberg, 2002) (Figure 3.1). In contrast to homopolymers, which consist of a single repetitive monomeric subunit, copolymers are made of at least two different monomers A and B. Depending on the alignment of the monomeric subunits, copolymers are subdivided into alternating (ABABABAB), statistical (ABBABBAA), or block (AAAABBBB) copolymers. By covalently linking a hydrophobic homopolymer to a hydrophilic homopolymer, amphiphilic block copolymers can be formed. Similar to amphiphilic lipids, which contain a hydrophilic head group and hydrophobic tails, the amphiphilicity of the block copolymer can lead to the spontaneous self-assembly of the single polymer strands to highly structured membranes when added to aqueous solutions. Thereby, the membrane can form around an inner aqueous phase to form vesicles, separating it from the continuous outer phase. Hydrophilic molecules can be entrapped in the lumen or inner cavity of the polymersomes, whereas hydrophobic molecules can be incorporated in the hydrophobic membrane (Palivan *et al.*, 2012).

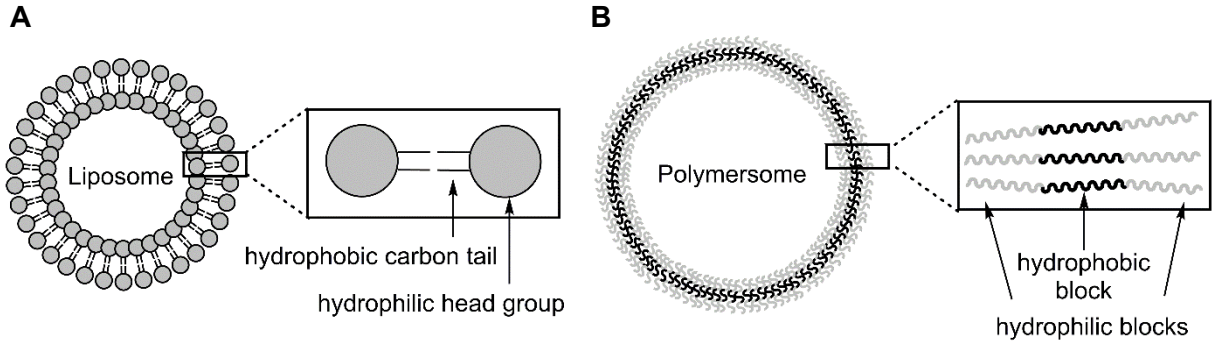

Figure 3.1 – Schematic depiction of a liposome (A) and a polymersome (B) separating an inner aqueous phase from a continuous outer phase. The membrane is made of amphiphilic molecules, either amphiphilic lipids with a hydrophilic head group oriented toward the aqueous phases and a hydrophobic tail oriented toward each other, or amphiphilic block copolymers, in this case a triblock copolymer with two hydrophilic side blocks and a hydrophobic middle block.

Polymersomes share many structural characteristics with liposomes, however, usually have a much higher mechanical stability and a lower membrane permeability compared to liposomes (Discher and Eisenberg, 2002). The fluidity, stability and permeability of the membrane are thereby dependent on the molecular mass of the copolymer and thus the membrane thickness (Figure 3.2). Opposed to lipid membranes, which have a thickness of 3 – 5 nm (Le Meins *et al.*, 2011), the membrane thickness of polymersomes can be significantly varied by changing the block lengths of the copolymer, ranging from 2.4 – 40 nm (Battaglia and Ryan, 2005; Chen *et al.*, 2009). Due to their increased mechanical stability and the ability to control vesicle characteristics by appropriate choice of the block copolymer, polymersomes are a promising tool for various biotechnological applications (Graff *et al.*, 2010).

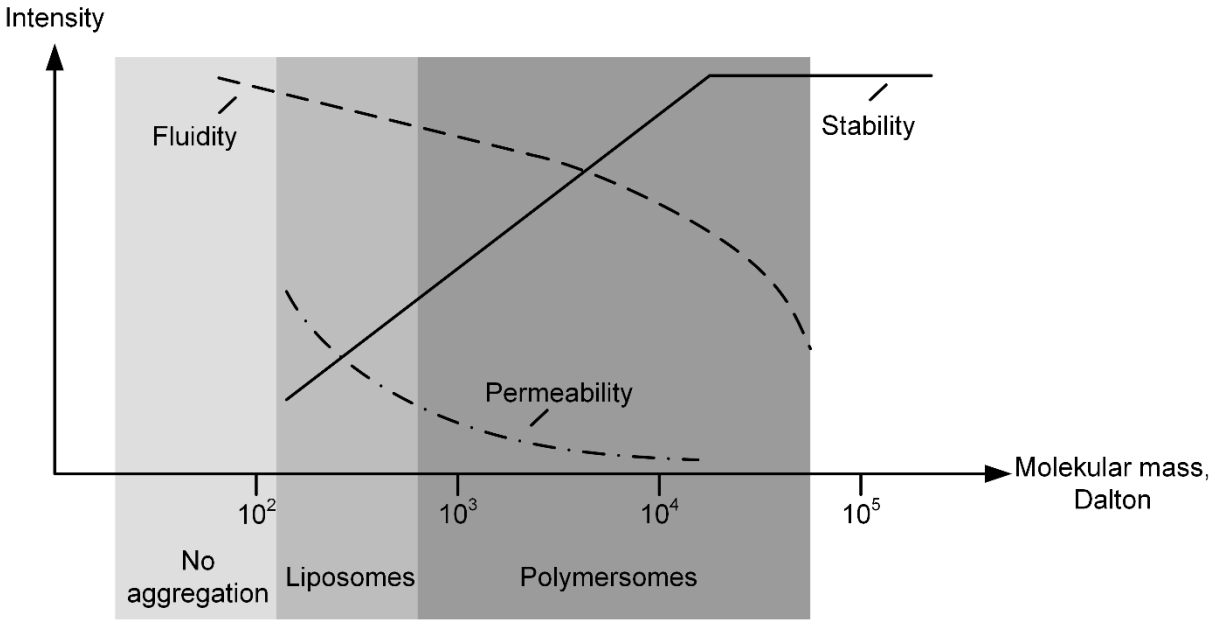

Figure 3.2 – Dependency of the fluidity, stability and permeability of membranes on the molecular mass of the amphiphilic molecule. With increasing size of the amphiphile, the stability of the membrane increases, while the fluidity and the permeability decrease (modified from Discher and Eisenberg (2002)).

Polymersome diameters can range from a few nanometers to up to a few micrometers. For most applications, however, diameters of 100 – 500 nm have been reported. Hereby, the size of polymersomes is highly dependent on the type and the block lengths of the copolymer as well as the production process and post-production processing steps (Graff *et al.*, 2010).

Due to the similarities between lipid and polymer vesicles, the procedures described for polymersome formation are essentially the same as for liposome formation including direct dispersion of the solid polymer in an aqueous solution (Ahmed and Discher, 2004), injection

of a polymer solution dissolved in a cosolvent into an aqueous solution (Nardin *et al.*, 2000b), film rehydration (Ranquin *et al.*, 2005; Battaglia *et al.*, 2006) and electroformation (Angelova *et al.*, 1992; Discher *et al.*, 1999). Recently Poschenrieder *et al.* (2016a) introduced a scalable polymersome production process based on the cosolvent method, in which the dissolved polymer is injected into a standard bioreactor under vigorous stirring (Poschenrieder *et al.*, 2016a; Poschenrieder *et al.*, 2016b). With this method, a one-step polymersome production process was established yielding high quality polymersomes, greatly facilitating the preparation of polymersome dispersions in laboratory and industrial scale.

3.1.1 Amphiphilic block copolymers

Several amphiphilic block copolymers have been described in literature that are able to spontaneously self-assemble to vesicles. The most common type of copolymers used for polymersome formation are A_XB_Y diblock or $A_XB_YC_Z$ triblock copolymers, where A and C refer to hydrophilic blocks and B refers to hydrophobic blocks (Figure 3.3). The lowercase X, Y and Z refer to the degree of polymerization, which is the average number of monomeric subunits of each block. In many cases, A and C are composed of the same monomeric subunits and are thus referred to as ABA triblock copolymers.

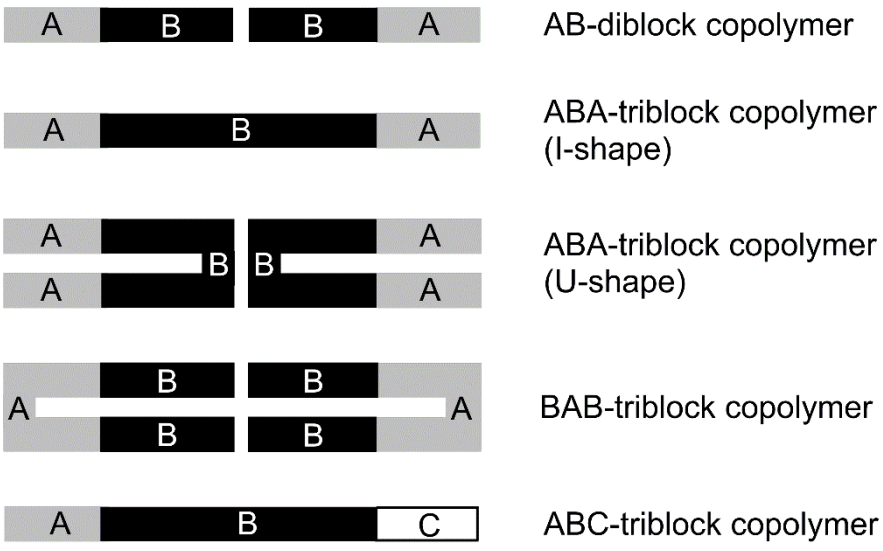

Figure 3.3 – Structure of diblock and triblock copolymers to form polymer membranes. Whereas diblock copolymers form bilayers similar to lipids, triblock copolymers can either form I-shaped monolayers or U-shaped bilayers. Current opinion is that ABA triblock copolymers form a mixture of I and U configuration (Itel *et al.*, 2014).

The properties of the polymer membrane can be controlled by choice of the type and block lengths of the copolymer. Polymersome characteristics such as permeability and size can be varied by changing the block lengths and the weight fraction of hydrophilic to hydrophobic blocks. Furthermore, the versatility of available polymers has led, for example, to the formation of polymersomes that respond to certain external stimuli such as pH (Lomas *et al.*, 2011), temperature (Qin *et al.*, 2006), light (Liu *et al.*, 2014), and the presence of certain molecules (Kim *et al.*, 2012) for various medical applications. Similarly porous polymersomes (Cornelissen *et al.*, 1998) have been created that facilitate diffusion of molecules across the membrane for biochemical applications.

A commonly used copolymer for polymersome formation is the ABA triblock copolymer poly(2-methyloxazoline)-poly(dimethylsiloxane)-poly(2-methyloxazoline) (PMOXA-PDMS-PMOXA) (Baumann *et al.*, 2011). PMOXA-PDMS-PMOXA polymersomes have a high stability and a low membrane permeability (Kumar *et al.*, 2007) while being biocompatible and low protein binding (Woodle *et al.*, 1994; Broz *et al.*, 2005; Ranquin *et al.*, 2005). These characteristics allow retaining encapsulated drugs or enzymes within the vesicles with high efficiency, while the low protein binding properties are required to evade the immune system or prevent unspecific protein adsorption to the polymersomes' surface. $PMOXA_{15}$-$PDMS_{110}$-$PMOXA_{15}$ polymersomes have been shown to be substantially less permeable for water with a permeability coefficient *Pe* of 10^{-5} cm s^{-1} compared to lipid membranes with a *Pe* of 10^{-2} cm s^{-1} (Kumar *et al.*, 2007; Alberts, 2015). Due to the PDMS middle block, PMOXA-PDMS-PMOXA membranes have an extremely high fluidity that is comparable to the fluidity of lipid bilayers (Itel *et al.*, 2014). The high lateral diffusion of single polymer strands in the membrane allows the integration of functional membrane proteins. Furthermore, the lateral mobility of the polymers has been suggested to promote shorter polymers to diffuse into the vicinity of the reconstituted protein, thereby reducing the energetic strain of hydrophobic mismatch between the polymer membrane thickness and the membrane protein size due to an increased apparent compressibility of the membrane (Itel *et al.*, 2015). The hydrophobic mismatch denotes the difference in membrane thickness of the hydrophobic fraction and the hydrophobic length of the protein, which can be quite high when reconstituting natural transmembrane proteins into artificial polymer membranes, due to the unnatural thickness of many polymer membranes and most natural proteins being adapted in length to fit into their respective natural membrane (Itel *et al.*, 2014; Itel *et al.*, 2015). The fluidity of PMOXA-PDMS-PMOXA membranes is maintained up to -123°C, which is the glass transition temperature of the hydrophobic PDMS block (Prinos and Panayiotou, 1995). This glass transition temperature denotes the temperature at which the fluid polymer membrane transitions into a crystalline state. In this study, PMOXA-PDMS-PMOXA was used as

copolymer with hydrophilic block lengths of 15 units and a hydrophobic block length of 68 units (Figure 3.4).

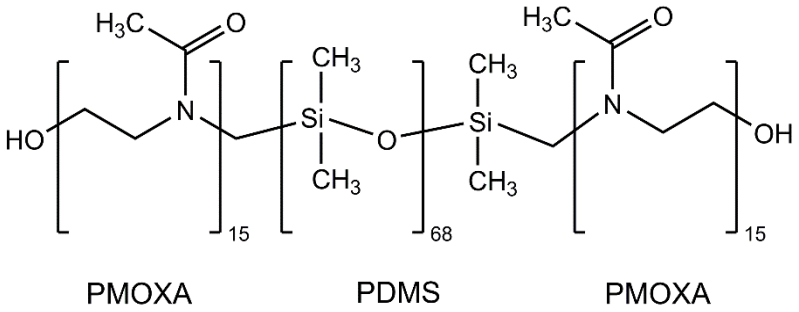

Figure 3.4 – Structure of the amphiphilic triblock copolymer poly(2-methyloxazoline)-poly(dimethylsiloxane)-poly(2-methyloxazoline) (PMOXA-PDMS-PMOXA). The lowercase numbers denote the repetitive chain length of the bracketed part.

3.1.2 Polymersome applications

The increased stability and decreased permeability of the polymersomes compared to liposomes are beneficial characteristics for several medical and biotechnological applications. Polymersomes have been investigated as drug delivery systems, as biosensors in diagnostics and as nano-scale enzyme membrane reactors for catalytic conversions. In drug delivery systems, polymersomes are loaded with drugs or active molecules. The polymersomes enclose the encapsulated molecules with a polymer membrane to shield the encapsulated molecules from degradation or untargeted diffusion within the body until the destined site of action is reached. There, a controlled release of the molecules can be evoked by certain stimuli, depending on the cell target and the polymer used (Palivan *et al.*, 2016). Through the surface functionalization of the membrane, for example with antibodies, cell-targeting mechanisms can be introduced. Such mechanisms have been demonstrated for targeting breast cancer and lung cancer cells with fibronectin mimic-functionalized and anisamide-functionalized polymersomes (Pangburn *et al.*, 2012; Lu *et al.*, 2015). Antibody-conjugated polymersomes have been successfully constructed to target and cross the blood-brain barrier, which is required to deliver cargo to the brain (Pang *et al.*, 2008). In diagnostics, polymersomes have been functionalized to yield biosensors for various applications (Lecommandoux *et al.*, 2005; Ghoroghchian *et al.*, 2007; Gonzalez-Perez *et al.*, 2009).

Whereas the use of polymersomes for drug delivery and as biosensors has been extensively studied (Palivan *et al.*, 2016), their use as nano-scale enzyme membrane reactors has so far only been covered in general *proof-of-principle* studies. This is mainly attributed to substantially different requirements in biochemical applications compared to medical

applications. Whereas in drug delivery systems, the low permeability of the membrane is highly beneficial to keep molecules entrapped within the lumen, nano-scale enzyme membrane reactors require a controlled exchange of low molecular mass substrates, also termed small molecules or micromolecules, between the compartments while retaining the macromolecular biocatalyst within the lumen (Renggli *et al.*, 2011; Schmitt *et al.*, 2016). To this means, substantial reduction in mass transport limitations of substrates and products across the membrane have been achieved with porous poly(styrene)-poly(isocyanoalanine(2-thiophen-3-yl-ethyl)amide) (PS-PIAT) or pH-responsive poly(ethylene glycol)-poly(diethylaminoethylmethacrylate)-poly(3,4-dimethylmaleinimidoethylmethacrylate) (PEG-PDEAEM-PDMIEM) or poly(ethylene glycol)-poly(diethylaminoethylmethacrylate)-poly(3,4-dimethylmaleinimidobutylmethacrylate) (PEG-PDEAEM-PDMIBM) polymer membranes and by the integration of natural porins into PMOXA-PDMS-PMOXA membranes.

The porous PS-PIAT polymersomes allow, for example, the diffusion of several molecules including glucose, glucono-1,5-lactone, 2,2'-azino-bis(3-ethylbenzothiazoline-6-sulphonic acid) (ABTS) and its radical, as well as $NADP^+$ and NADPH, while successfully retaining enzymes within the polymersomes (Kuiper *et al.*, 2008; Meeuwissen *et al.*, 2011). Enzymatic reactions based on encapsulated glucose oxidase (GOx), horseradish peroxidase (HRP), alcohol dehydrogenase (ADH), *Candida antarctica* lipase B (CalB), glucose-6-phosphate dehydrogenase (G6PDH) and phenylacetone monooxygenase (PAMO), including cascades thereof, have been reported in PS-PIAT polymersomes (Vriezema *et al.*, 2003; Vriezema *et al.*, 2007; Kuiper *et al.*, 2008; van Dongen *et al.*, 2008; de Hoog *et al.*, 2009; van Dongen *et al.*, 2009; Meeuwissen *et al.*, 2011; Peters *et al.*, 2014; van Oers *et al.*, 2014; van Oers *et al.*, 2015).

Similarly, the pH-responsive PEG-PDEAEM-PDMIEM and PEG-PDEAEM-PDMIBM copolymers were used to successfully incorporate and retain enzymes such as myoglobin, HRP and GOx (Gaitzsch *et al.*, 2012; Gräfe *et al.*, 2014). By shifting the pH below the pK_a of the hydrophobic block of the copolymer, the copolymer is deprotonated and the positively charged middle block repels adjacent polymers to evoke an increased permeability. The loss of hydrophobicity of the middle block and the expected disintegration of the polymer membrane was circumvented by cross-linking the hydrophilic PDMIEM or PDMIBM block prior to changing the pH. In its permeable state the polymer membrane was highly permeable allowing the diffusion of guaiacol (124 Da), quinone (240 Da), glucose, glucono-1,5-lactone and ABTS as well as the ABTS radical.

Yet, the main purpose of all cascade reactions to date was to demonstrate the general applicability of polymersomes as nano-scale enzyme membrane reactors in terms of an outstanding control over the positional assembly of enzymes in single and multicompartment

systems (Vriezema *et al.*, 2007; van Dongen *et al.*, 2009; Schoonen and van Hest, 2016). None of the reactions has been incomaptible *per se*, and thus no enhanced reaction was expected in any case. In accordance, the reaction performed by Meeuwissen *et al.* (2011) was substantially worse than the non-compartmentalized reaction cascade, taking 28 h to convert 32 % of the substrate as opposed to the reaction free in solution yielding full conversion in 30 min. Likewise, Peters *et al.* (2014) were able to almost completely alleviate mass transport limitations using PS-PIAT polymersomes and a three-enzyme cascade of CalB, GOx and HRP, however, because of the compatibility of the cascade reaction free in solution, the compartmentalized reaction did not perform better than the non-compartmentalized reaction. The cascade reaction performed by Peters *et al.* (2014) reached approximately 80 % of the product concentration after 15 h when performed in polymersomes compared to the reaction taking place free in solution.

A first step toward highly selective nano-scale enzyme membrane rectors was the functional integration of the outer membrane porin F (OmpF) of *E. coli* into PMOXA-PDMS-PMOXA polymersomes by Nardin *et al.* (2000b), thereby leveraging the low permeability of the polymer membrane to allow encapsulated ß-lactamase inside the polymersomes to hydrolyze ampicillin to ampicillinoic acid. Since then, several membrane proteins have been successfully integrated into PMOXA-PDMS-PMOXA polymersomes in functional form highlighting the potential of using membrane proteins as selective transporters for polymersome applications. These include the bacteriophage lambda receptor protein LamB (Graff *et al.*, 2002), the water channels aquaporin Z and aquaporin 0 (Stoenescu *et al.*, 2004; Kumar *et al.*, 2007), the nucleoside transporter Tsx (Ranquin *et al.*, 2005), the ferric hydroxamate protein uptake component A (Onaca *et al.*, 2008), the proton transporter Complex I (Graff *et al.*, 2010), the ion channel MspA of *Mycobacterium smegmatis* (Morton *et al.*, 2015) and the *E. coli* glycerol facilitator GlpF (Zhang *et al.*, 2016). The light-driven transmembrane proton pump bacteriorhodopsin and the F_0F_1-ATP synthase motor protein have been incorporated into similar poly(2-ethyl-2-oxazoline)-poly(dimethylsiloxane)-poly(2-ethyl-2-oxazoline) (PEtOz-PDMS-PEtOz) polymersomes (Choi and Montemagno, 2005). Recently, the incorporation of a synthetic DNA channel into poly(2-(methacryloyloxy)ethyl phosphorylcholine)-poly(2-(diisopropylamino)ethyl methacrylate) (PMPC-PDPA) polymersomes has been demonstrated (Messager *et al.*, 2016).

To this end, only Siti *et al.* (2014) have used a membrane channel for multienzyme cascade reactions in polymersomes. The outer membrane porin OmpF was incorporated into PMOXA-PDMS-PMOXA polymersomes carrying HRP to allow the diffusion of the profluorescent dye amplex red and the release of resorufin (Siti *et al.*, 2014). These polymersomes were encapsulated together with GOx in semi-porous PS-PIAT polymersome creating a multicompartment, multienzyme system. However, so far only unspecific OmpF,

which allows diffusion of molecules based on size with a high molecular mass cut-off (MMCO) of 600 Da, has been used for implementing enzymatic cascade reactions in polymersomes. Thus, OmpF is able to differentiate between macromolecules and low molecular mass molecules but is not sufficiently selective to enhance cascade reactions that suffer from cross-inhibitions on a micromolecule level. Yet, the integration of membrane channels into polymer membranes has the potential to introduce selective mass transport, which is a prerequisite for compartmentalizing reaction cascades that are not compatible with each other and are thus a promising strategy to overcome mass transport limitations across polymer membranes (Schmitt *et al.*, 2016). So far, an enhancement of the space-time-yield of reaction cascades by compartmentalization in polymersomes compared to the same reaction cascade free in solution has not been achieved (Schoonen and van Hest, 2016).

3.1.3 Surface functionalization of polymersomes

The immobilization of proteins on the surface of polymersomes can aid in the specific targeting, cellular uptake or controlled degradation of polymersomes employed as drug carriers, thus allowing a controllable distribution within the body, lead to functional biosensors or add an additional reaction space for multistep syntheses. Although the surface functionalization of polymersomes is highly desired in all fields of applications, which is evidenced by the many different approaches that have been pursued to immobilize proteins on polymersome surfaces, research has been mainly driven in view of highly sophisticated drug delivery systems. Generally, conventional immobilization strategies have been employed making use of various chemical and non-covalent interactions. The first strategy to immobilize proteins on polymersome surface has been performed using the interaction of biotin and streptavidin (Lin *et al.*, 2006). Polymersomes were chemically biotinylated and incubated in an excess of streptavidin. The biotin-conjugated polymersomes could then be functionalized with biotin-labeled proteins or ligands, which has been demonstrated for the immobilization of antibodies (Lin *et al.*, 2006), polyguanylic acid (Broz *et al.*, 2005; Grzelakowski *et al.*, 2009) and fluorescent dyes (Lin *et al.*, 2004; Rigler and Meier, 2006). Although the biotin-streptavidin interaction exhibits a dissociation constant of 10^{-15} M, the affinity of the two species was considerably lower when conjugated to polymersomes of approximately 10^{-8} M (Egli *et al.*, 2011b). A more simple strategy was used by Nehring *et al.* (2010) who immobilized His_6-tagged maltose binding protein (MBP) labeled with fluoresceine and His_6-tagged red fluorescent protein (RFP) on Ni^{2+}-NTA functionalized polymersomes. Although the dissociation constants were typical for Ni^{2+}-His_6 interactions, these are usually only in the micromolar range and non-covalent interactions are susceptible to ligand exchange (Egli *et al.*, 2011b). Furthermore, adamantane-labeled HRP has been immobilized on ß-cyclodextrin-conjugated polymersomes (Felici *et al.*, 2008; Guo *et al.*, 2008). Although

immobilization was successful, the non-covalent interactions were too weak to withstand extensive washing to remove excess, non-bound protein.

In contrast, covalent bonding using chemical conjugation is essentially more stable. Three examples of chemical conjugation are shown in Figure 3.5. A common method applied in immobilization of proteins is the covalent binding of azide and alkyne moieties in the Huisgen cycloaddition. Alkyne-conjugated polymersomes have been used by van Dongen *et al.* (2008, 2009) and Meeuwissen *et al.* (2011) immobilizing azide-conjugated HRP, CalB and PAMO. These represent the only surface functionalizations for biocatalytic applications. Similarly, alkyne-conjugated eGFP has been immobilized on azide-conjugated polymersomes by Opsteen *et al.* (2007). In all azide-alkyne cylcoadditions either toxic Cu^{+} or high temperatures were used to catalyze the reaction. Less harsh conditions have been employed for the surface functionalization using the covalent binding of polymersomes conjugated with *N*-hydroxysuccinimidyl ester or vinyl sulfone to the surface exposed thiol groups of the antibody OX26 (Pang *et al.*, 2008) and short, cysteine-labeled peptides made of arginine, glycine and aspartate, which are important cell surface peptides for cell adhesion (Petersen *et al.*, 2010), respectively. Since the formation of the C-S bond requires reduced thiol groups, the reaction is required to take place at oxygen-free conditions. This was achieved either by a constant nitrogen flow through the reaction medium or by the reaction taking place under nitrogen atmosphere. Other covalent immobilization techniques include the formation of amide bonds using copolymers with a terminal amine group to fluorescently labeled succinimidyl esters or the formation of a bis-aryl hydrazine. The latter was achieved by coupling enhanced yellow fluorescent protein (eYFP), the anti-biotin-IgG and the antibody trastuzumab with a 6-hydrazinonicotinic amide and immobilizing the respective proteins on 4-formyl benzoic amide-functionalized polymersomes (Egli *et al.*, 2011a).

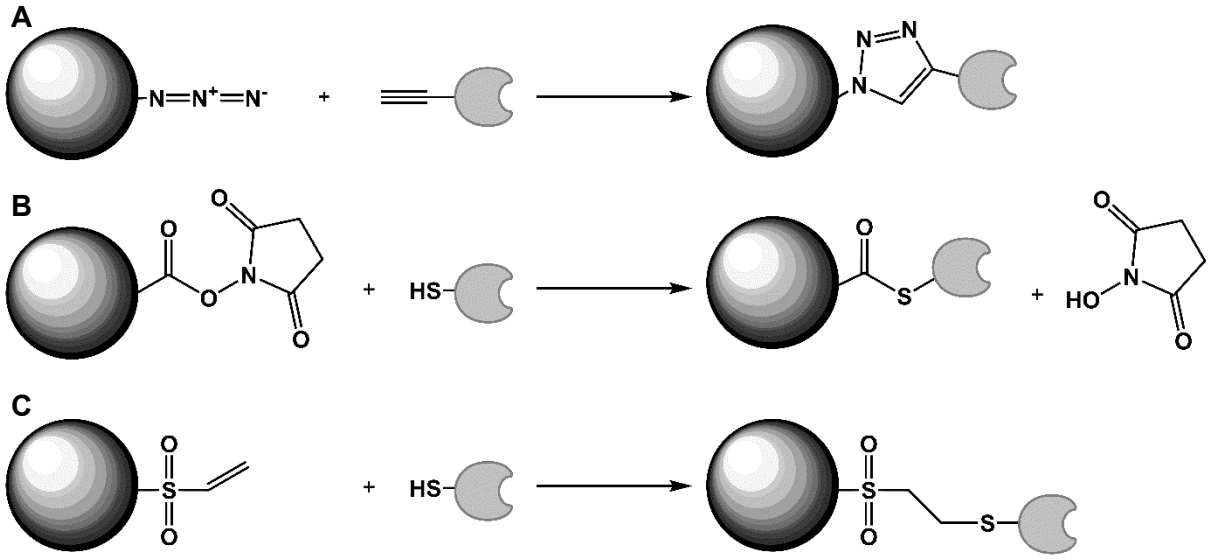

Figure 3.5 – Exemplary chemical conjugations of proteins to polymersome surfaces via azide-alkyne cycloadditon (A), thiol-*N*-hydroxysuccinimidyl esters (B) or vinyl-sulfone-thio esters (C). Polymersomes are represented as shaded spheres and proteins are schematically represented in gray.

Noor *et al.* (2012) have successfully immobilized eGFP on the surface of poly(isobutylene)-poly(ethylene glycol)-poly(isobutylene) (PIB-PEG-PIB) polymersomes via fusion of the eGFP to an antibacterial peptide, cecropin A. This technique of spontaneous peptide insertion was based on the ability of amphiphilic antibacterial peptides to be both soluble in aquoues solution and in amphiphilic membranes as well as their ability to penetrate not only lipid membranes but also polymer membranes. The latter was demonstrated in various studies for the short antibacterial peptides gramicidin (15 amino acids), alamethicin (20 amino acids) and mellitin (26 amino acids), which were reconstituted into polymersomes to study the functional integration and phase behavior of amphiphilic peptides in polymer membranes (Kita-Tokarczyk *et al.*, 2005; Vijayan *et al.*, 2005; Haefele *et al.*, 2006; Wong *et al.*, 2006; Gonzalez-Perez *et al.*, 2009). However, the natural function of antibacterial peptides is a destabilization of the membrane to deploy their antibacterial effect, either by forming small ion channels or larger pores. After association with and integration into the membrane, the peptide monomers aggregate in a concentration dependent manner to form pores that disrupt the membrane integrity and cause uncontrolled leakage of ions and/or small molecules (Bechinger, 1997). Although Noor *et al.* (2012) argued that cecropin A did not form pores in PIB-PEG-PIB polymersomes, the antibacterial peptides alamethicin and gramicidin led to a destabilization of the relatively thick $PMOXA_{13}$-$PDMS_{33}$-$PMOXA_{13}$ (6.1 nm membrane thickness) and $PMOXA_{7}$-$PDMS_{60}$-$PMOXA_{7}$ (10.2 nm membrane thickness) membranes, respectively, and the leakage of small ions, such as K^+ and Cl^-, which are usually not able to permeate across the membrane. Similarly, alamethicin and mellitin have been shown to be able to integrate and disrupt poly(ethylene oxide)$_{40}$-poly(ethylethylene)$_{37}$ (PEO-PEE) (8 nm

membrane thickness) and poly(ethylene oxide)$_{80}$-poly(butadiene)$_{125}$ (PEO-PBD) (14 nm membrane thicknes) membranes causing leakage of even large molecules such as the 623 Da-sized fluorescent dye calcein (Vijayan *et al.*, 2005). Thus, these antibacterial peptides were able to insert into relatively thick polymer membranes of 6 – 14 nm, compared to the natural thickness of lipid membranes of 3 – 5 nm, in a functional, destabilizing form, most likely due to the high compressibility of the polymer membrane. However, although disruption of the membrane integrity is not desired in this study, these findings demonstrate that polymer membranes can harbor several different types of membrane associated proteins and that spontaneous insertion of peptides into the relatively thick polymer membranes is possible.

3.2 Membrane proteins

Membrane proteins constitute a major class of proteins found in nature and make up approximately 30 % of all naturally occurring proteins (Tan *et al.*, 2008). Membrane proteins are divided into two groups, peripheral and integral membrane proteins. Peripheral membrane proteins are attached to the membrane surface via electrostatic interactions between parts of the protein and the hydrophilic head groups of the lipid membrane or hydrophilic domains of integral membrane proteins but do not interact directly with the hydrophobic core of the membrane. The dissociation of peripheral membrane proteins from the lipid membranes can usually be achieved by high salt concentrations or a change in pH to break the electrostatic and hydrogen bonds. In contrast, integral membrane proteins associate with the hydrophobic core of the membrane via strong hydrophobic interactions (Lodish, 2003). As such, integral membrane proteins are permanently integrated within or anchored to the hydrophobic core of the membrane and are most often transmembrane proteins that span the inner hydrophobic core of the membrane for binding. However, they may also only protrude or dip into the hydrophobic core (Berg *et al.*, 2002). Integral membrane proteins can usually only be extracted from the membrane by the use of detergents to solubilize the membrane and dissociate the lipids from the hydrophobic part of the protein (Berg *et al.*, 2002).

Integral membrane proteins can further be divided into membrane transport proteins that are fully embedded in and act within the membrane and membrane associated proteins that act in the cytosol or peripheral space (Berg *et al.*, 2002).

3.2.1. Membrane transporters and outer membrane porin OmpF

The boundaries of natural cells are constituted of a lipid membrane that keeps molecules and cellular components from leaking out of the cell and unwanted molecules of diffusing in. Since mass transport across the membrane is vital, membrane channels in form of proteins are embedded in the membrane to facilitate transport. Thus, membrane channel proteins play a major role in the survival and proper functioning of cells by translocating ions, small molecules and macromolecules across the cell membrane (Lodish, 2003). Like enzymes, membrane transporters usually display a high substrate specificity, thus selectively controlling membrane permeability (Berg *et al.*, 2002). Thereby, they allow the uptake of nutrients and the removal of waste products that are usually not able to pass the membrane by simple diffusion. Whereas lipophilic molecules permeate across the lipid bilayer of the cell membrane, the diffusion across the membrane of polar and charged molecules is limited and usually requires specialized translocating mechanisms. Membrane channels can be classified into active transporters and those facilitating passive diffusion across the membrane. Whereas active transporters require energy for the translocation of molecules to pump these against the concentration gradient, passive transporters facilitate diffusion of molecules across the membrane. Hereby, the passive diffusion always occurs along the concentration gradient until equilibrium is reached (Berg *et al.*, 2002; Lodish, 2003).

The membrane channel OmpF of *Escherichia coli* is one of the most studied membrane proteins and belongs to the class of passive transporters. OmpF is a non-specific porin that allows the passive diffusion of ions and small, hydrophilic molecules across the outer membrane of gram negative bacteria. OmpF associates to a trimer when embedded in the membrane (Nikaido, 2003; Alcaraz *et al.*, 2004). Each monomer consists of 16 antiparallel ß-sheets that form a barrel-like structure around a water-filled pore or channel and 16 loops (L1 – L16) that connect the ß-sheets. L3 serves as a constriction loop that protrudes into the cavity of the pore and limits the channel size to 7 x 11 Å (Cowan *et al.*, 1992). Due to its role as mediator of passive diffusion from the external space into the periplasm, OmpF is not selective but allows diffusion of several different molecules based on size. Restricted by the pore size, the channel allows the passive diffusion of molecules with a molecular mass (MM) below 600 Da while retaining molecules exceeding 600 Da (Nikaido, 1992). Negative charged amino acids in L3 lead to a slight preference for positively charged (cationic) molecules. Mutations in L3 have shown to have a strong impact on the size of the channel as well as the cation selectivity (Delcour, 2009). Mutation of the aspartate at position 113 to glycine, for example, led to an increased pore size allowing a faster diffusion of disaccharides such as lactose and sucrose. In contrast, mutation of the glycine at position 119 to aspartate led to the protrusion of the larger and negatively charged amino acid into the central cavity of the porin, thereby separating the channel into two smaller subchannels

of approximately 3 x 4 Å (Figure 3.6) (Jeanteur *et al.*, 1994). The molecular mass cut-off (MMCO) of the OmpF G119D variant was reduced to 300 Da, keeping lactose and sucrose from diffusing through the channel, while the negative charge of the aspartate that protrudes into the inner cavity led to a 2.3-fold increased cation selectivity compared to wildtype OmpF (Jeanteur *et al.*, 1994, Saint *et al.*, 1996).

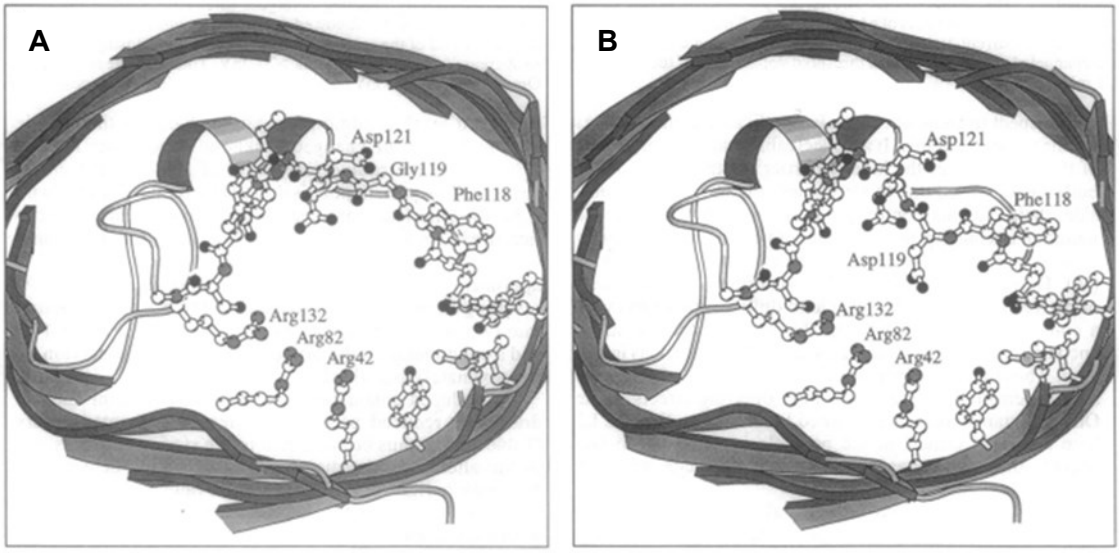

Figure 3.6 – Top view of the constriction zone of OmpF (A) and OmpF G119D (B). The single amino acid substitution of glycine to aspartate at position 119 leads to separation of the channel (7 x 11 Å) into two smaller constriction zones of (3 x 4 Å) reducing the molecular mass cut off from 600 Da to 300 Da. The negative charged aspartate further increases the cation selectivity of the channel (from Jeanteur *et al.* (1994)).

3.2.2. Membrane associated proteins

Several membrane associated proteins exist that are permanently attached to the membrane but function in the aqueous phase. These include, amongst others, receptor proteins involved in cell signaling, soluble *N*-ethylmaleimide-sensitive-factor attachment receptor (SNARE) proteins that act in membrane fusion, and enzymes involved in processes that require concentration gradients or membranes such as the cytochrome b_5 involved in cellular respiration and the prostaglandin H_2 synthase-1, which converts a hydrophobic substrate present in the membrane (Kutay *et al.*, 1993; Berg *et al.*, 2002).

Among the membrane associated proteins, Kutay *et al.* (1993) described a class of integral membrane proteins that is capable of spontaneously inserting into lipid membranes without the help of the signal recognition particle (SRP). The SRP is often required to locate integral membrane proteins to specific membranes due to their increased hydrophobicity and thus their potential to aggregate in aqueous solution. Binding to the SRP is conferred by an N-terminal signal peptide. The class of integral membrane proteins described by Kutay *et al.*

(1993), in contrast, are hydrophilic proteins that act in the cytosol but are tethered to the membrane via a single hydrophobic membrane domain or membrane anchor at the C-terminus. Due to the position of the hydrophobic anchoring domain, these integral membrane proteins have been termed tail-anchored proteins. Since the proteins are synthesized from the N- to the C-terminus, membrane integration occurs posttranslationally. This class of integral membrane proteins includes enzymes such as oxygenases, dehydrogenases and phosphatases as well as proteins with various functions such as hemeproteins, syntaxins, synaptobrevins and several membrane receptors (Kutay *et al.*, 1993). Although hundreds of tail-anchored proteins in several organisms and in all types of membrane have been identified to date the exact mechanisms of membrane targeting and peptide insertion are not fully understood and can substantially differ among different tail-anchored proteins and organisms (Marty *et al.*, 2014).

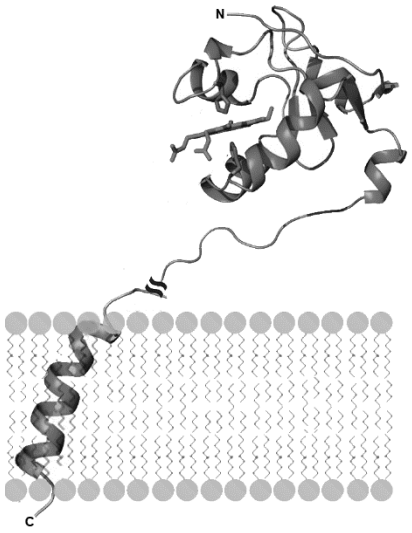

Figure 3.7 – Graphic representation of membrane-associated cytochrome b_5 according to X-ray crystallographic data. The enzyme is located in the mitochondrial lumen and is tethered to the mitochondrial membrane via a 38 amino acid long hydrophobic peptide anchor. The peptide anchor forms an integral α-helix that spans the membrane (modified from Ahuja *et al.* (2013).

One of the best studied members of the tail-anchored integral protein class is the microsomal or mitochondrial cytochrome b_5 found in mammals (Figure 3.7). Cytochrome b_5 is an electron transfer hemeprotein that is involved in the respiratory pathway. Purified cytochrome b_5 has been demonstrated to integrate spontaneously into artificial liposomes *in vitro*, demonstrating that membrane integration is spontaneous and independent of other proteins or factors (Strittmatter *et al.*, 1972; Rogers and Strittmatter, 1975). Resolution of the crystal structure revealed that the enzyme is tethered to membranes via a 38 amino acid peptide anchor,

which forms an α-helix inside the membrane (Ahuja *et al.*, 2013). Similarly, the ubiquitine conjugating enzyme 6 and most of the SNARE proteins of *Saccharomyces cerevisiae* have been demonstrated to spontaneously insert into liposomes in a transmembrane manner (Kutay *et al.*, 1993; Burri and Lithgow, 2004).

3.2.3. Artificial membrane anchoring

The spontaneous insertion of tail-anchored and antibacterial peptides has been used in several studies and applications to tether heterologous fusion proteins to natural or artificial membranes. Especially cytochrome b_5 has been used in different applications to tether recombinant fusion proteins to membranes. George *et al.* (1989) reported the immobilization of ß-galactosidase in the inner membrane of *E. coli* using the hydrophobic domain of cytochrome b_5. After recombinant expression of the fusion protein in *E. coli* and subsequent cell lysis, 90 % of the ß-galactosidase activity was found in the membrane containing fraction as opposed to 80 % of the ß-galactosidase activity being present in the soluble fraction when the peptide anchor was omitted. ß-Galactosidase was 50 % active in fusion to the hydrophobic peptide anchor, indicating that the peptide anchor had an influence on the enzyme activity. Similarly, Nomura *et al.* (2008) fused cytochrome b_5 to eGFP and dehydrofolate reductase (DHFR) and synthesized the fusion protein *in vitro* in the presence of liposomes. Nomura *et al.* (2008) used the apoenzyme of cytochrome b_5, which does not contain the heme group and is thus inactive, tethering eGFP and DHFR to the liposomes after protein synthesis.

In an interesting approach to construct non-living vaccines, Szostak *et al.* (1996) prepared *E. coli* devoid of their cytoplasmic content that displayed proteinaceous antigens in the inner membrane via recombinant fusion to hydrophobic domains. The inactivation of the *E. coli* was induced by a phage lysis system mediated by the expression of the bacteriophage protein E to avoid antigen denaturation by heat or X-ray inactivation of the bacterial cells. Aggregation of the E protein in the membrane forms a pore which leads to the loss of the cytosplsamic content and cell death. To retain the antigens in the lysed *E. coli*, Szostak *et al.* (1993, 1996) and Szostak and Lubitz (1991) used the hydrophobic domains of the lysis proteins E or L of the bacteriophage MS2, designated E' and L', to anchor several antigens, including antigens from the human immunodeficiency virus (HIV), the simian immunodeficiency virus, the hepatitis B virus and the herpes simplex virus, to the inner membrane of *E. coli*. Notably, the hydrophobic domains of the E and L protein were not able to mediate cell lysis without their hydrophilic domain and were thus able to anchor sufficient amounts of the antigen to the inner membrane without inducing cell lysis. The controlled cell lysis was performed by thermal induction of E-mediated lysis by a temperature shift from

28°C to 42°C by cloning a temperature sensitive promotor upstream of full length protein E (Szostak and Lubitz, 1991; Szostak *et al.*, 1993; Szostak *et al.*, 1996; Sachse *et al.*, 2014).

Sührer (2015) used the same E-mediated lysis system for biocatalytic purposes. With the aim of producing *E. coli* cells devoid of cytoplasmic proteins for side-reaction free whole-cell biocatalysis, Sührer (2015) investigated several hydrophobic domains, including the tail-anchoring hydrophobic domains of cytochrome b_5 and ubiquitin conjugating enzyme 6 as well as E' and L', to tether ß-galactosidase and a fusion protein of a ketoreductase and a formate dehydrogenase to the inner membrane of *E. coli* (Sührer, 2015; Sührer *et al.*, 2015).

3.3 Biocatalysis

Biocatalysis is the chemical conversion of organic compounds using natural organic catalysts. Advances in life sciences have immensely expanded the use of biocatalysis for industrial applications in the last decades, which today has become an inherent part of organic chemistry (Bommarius and Riebel, 2004). Especially the safe and environmentally friendly use of enzymes has led to a wide acceptance among organic chemists as well as in various industries, including the food and feed industry, the pharma- and cosmetics industry and the chemical industry (Woodley, 2008). Furthermore, biocatalysis is highly sustainable employing natural or non-natural resources and, as opposed to chemical catalysts which are often heavy metals or strong acids and bases, biocatalysts are biodegradable. Due to society's increasing awareness for sustainable, environmentally friendly industrial processes, developments in the field of biocatalysis are further stressed in academia and industry.

In the past decades, technological advances in genome sequencing, enzyme discovery and protein engineering have intensified research on biocatalytic applications. For biotechnological processes, biocatalysts are either employed in whole cells or as isolated enzymes. Benefits of whole cells are a cheap production of the biocatalyst and the ability to engineer complex cascades to produce high-value products. However, their use is limited to non-toxic substances and mass transfer limitations of complex compounds across the cell membrane as well as unwanted side reactions catalyzed by endogenous enzymes are often observed. Thus, extensive strain development is often required (Bommarius and Riebel, 2004). In contrast, isolated enzymes are highly specific in the reaction they catalyze and offer side reaction free conversions.

The increasing demand for enzymes as biocatalysts can be attributed to the ability of enzymes to catalyze a variety of reactions in a highly chemo-, regio-, and stereoselective manner. Furthermore, enzymes allow the performance of chemical reactions under mild

conditions, usually in the range of 20 – 40°C at physiological pH and atmospheric pressure (Faber, 2011).

On the downside, enzymes usually only work in a narrow operational window. High and low temperatures or unfavorable pH can significantly reduce the catalytic efficiency or inactivate the enzymes (Faber, 2011). Thus, although enzymes are considered to be easily combinable due to the similar reaction conditions required, small changes in the operational parameters can have a significant effect on the enzyme activity. Additionally, many enzymes require cofactors such as adenine 5'-triphosphate (ATP), nicotinamide adenine dinucleotides (phosphates) ($NAD(P)^+$ / NAD(P)H), flavin adenine dinucleotides (FAD / $FADH_2$) or flavin mononucleotides (FMN / $FMNH_2$), which are usually unstable and expensive (Faber, 2011).

Through the identification and characterization of novel enzymes and advances in the fields of DNA technology and protein engineering, the scope of chemical conversions as well as the substrate promiscuity of already available enzymes has increased significantly. These advances have enabled complex chemical reactions by use of natural or engineered enzymes that are hardly accessible for conventional organic chemistry (Bommarius and Riebel, 2004).

3.3.1. Enzyme immobilization

A disadvantage of isolated enzymes as biocatalysts is their limited stability at non-physiological conditions. High temperatures, acidic or basic pH, high salinity or organic solvents can denature and thus inactivate enzymes. Furthermore, enzymes are considered expensive compared to chemical catalysts. Depending on the purity of the enzyme, the expenses for the biocatalyst can be considerable. The immobilization of the biocatalyst on a solid support represents a main strategy to resolve both issues. Although the primary goal of enzyme immobilization is the retention of the biocatalyst, immobilized enzymes are often more stable than the soluble counterpart. This has been attributed to a restriction of translational motion and volume-enhancing unfolding and thus a conformational stabilization of the enzymes (Bommarius and Riebel, 2004). In continuous processes, the retention of the biocatalyst by immobilization, in contrast, allows an easy way to recover and reuse the biocatalyst. With more stable and reusable enzymes, the costs for biocatalysts can be significantly reduced.

Enzymes are often immobilized on solid surfaces such as ceramics, glass, metallic oxides, synthetic polymers, polysaccharides or membranes via covalent or non-covalent binding. A different strategy is the immobilization by entrapment of the enzyme in a solid matrix such as a polymeric gel, by encapsulation of the enzyme by a membrane such as in hollow fibers or microcapsules, or by cross-linking the enzymes (Bommarius and Riebel, 2004; Lee, 2006).

Either method has advantages and disadvantages. For example, whereas immobilization via adsorption is easily performed, desorption of the biocatalyst from the solid support may occur during operation. In contrast, covalent binding is highly stable but is usually performed under harsh conditions which may result in a loss of activity of the enzyme due to conformational changes (Bommarius and Riebel, 2004; Lee, 2006).

3.3.2. Kinetic parameters of enzymes

Enzymes are usually characterized in terms of the catalytic turnover k_{cat} and the half-saturation constant K_M which determine the catalytic efficiency $k_{cat} \cdot K_M^{-1}$ of each specific enzyme for a specific substrate. These values are derived from simplified reaction models based on the work of Leonor Michaelis and Maud Menten (Michaelis and Menten, 1913). Michaelis and Menten (1913) described a reaction model based on the simplest form of an enzyme catalyzed reaction, an irreversible reaction with one substrate and one product (Figure 3.8). The substrate S binds to the enzyme E at the active site at a rate k_1, resulting in the enzyme-substrate complex ES. The substrate may either desorb off the enzyme, thus reversing the binding (k_{-1}), or be converted into the product P, which then dissociates into the free enzyme and the product in an irreversible manner (k_2).

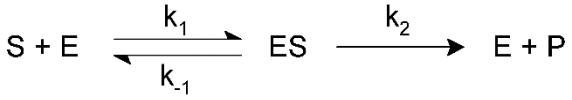

Figure 3.8 – Reaction scheme of an irreversible reaction with one substrate S and one product P. The substrate binds to the enzyme E forming the enzyme-substrate complex ES. The substrate may either dissociate from the enzyme in is unchanged state or be converted to the product before dissociation. The constants k denote the rate constants of each step.

The kinetic model described by Briggs and Haldane (Briggs and Haldane, 1925) is based on three assumptions:

- One molecule of substrate binds to one molecule of enzyme to form the activated substrate-enzyme complex (ES).
- The activated ES complex is in a steady-state equilibrium so that $\frac{d[ES]}{dt} = 0$.
- The reaction is irreversible or proceeds far from its thermodynamic equilibrium so that a possible backwards reaction can be neglected. For reversible reactions, this is achieved when measuring the initial reaction rates with $[P] \cong 0$.

Under these conditions, the reaction rate can be described in dependency of the rate constants and the substrate concentration according to Equation 3.1.

$$\boldsymbol{v = v_{max} \cdot \frac{[S]}{K_M + [S]}} \qquad \text{Equation 3.1}$$

with v = reaction rate, U mg^{-1}

v_{max} = maximal reaction rate, U mg^{-1}

$[S]$ = substrate concentration, mol L^{-1}

K_M = half-saturation constant, mol L^{-1}

The reaction rate is given as unit (U) per mg of enzyme, where one unit refers to the conversion of one µmol of substrate per minute. The maximal reaction rate v_{max} is dependent on the catalytic constant k_{cat}, which denotes the catalytic turnover of one substrate by one active site per second, and the molecular mass of one active monomeric unit of enzyme (Equation 3.2).

$$\boldsymbol{v_{max} = \frac{k_{cat}}{M_E} \cdot 60,000} \qquad \text{Equation 3.2}$$

with k_{cat} = catalytic constant (turnover number), s^{-1}

M_E = Molecular mass of one enzyme monomer, g mol^{-1}

The half-saturation constant K_M is a product of the rate constants of the individual reaction steps (Equation 3.3) and specifies the substrate concentration at which the reaction proceeds at its half maximal reaction rate.

$$\boldsymbol{K_M = \frac{k_2 + k_{-1}}{k_1}} \qquad \text{Equation 3.3}$$

Although multi-substrate reactions, for example reactions with substrate A and B, are markedly more complex, the above rate equations for substrate A can be obtained by keeping substrate B in excess and vice versa. Thus, the change in concentration of the substrate in excess is negligible over time and the half-saturation constants can be determined by measuring initial reaction rates as described above, giving individual K_M values for each substrate.

Furthermore, the activity of enzymes can be modified by binding of certain reactants to the enzyme. Depending on whether these effectors positively or adversely affect the enzyme activity, they are referred to as activators or inhibitors. Whereas activators are usually allosteric and thus bind to the enzyme at a distal position from the active site, inhibitors can either bind to an allosteric site or to the active site. Allosteric effectors act by stabilizing or destabilizing the enzyme's active conformation. In contrast, competitive inhibitors compete with the substrate for binding to the active site (Figure 3.9).

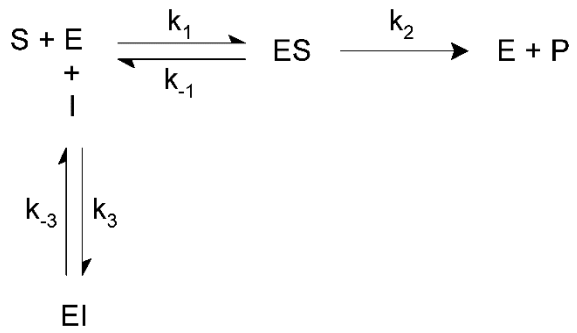

Figure 3.9 – Reaction scheme of an irreversible reaction with one substrate S and one product P. In the presence of a competitive inhibitor I, the enzyme E can either form the enzyme-substrate-complex ES or the enzyme-inhibitor-complex EI. The inhibitor cannot be converted into a product. Since the binding of the inhibitor is reversible, the inhibitor is considered to be competitive with respect to the substrate. The constants k denote the rate constants of each step.

The reaction rate v is thus also dependent on the inhibitor concentration and the inhibition constant K_i according to Equation 3.4, which represents a competitive inhibition.

$$\boldsymbol{v = v_{max} \cdot \frac{[S]}{K_M \cdot (1 + \frac{[I]}{K_i}) + [S]}}$$ Equation 3.4

with $[I]$ = inhibitor concentration, mM

K_i = inhibition constant, mM

The strength of an inhibitor is commonly described by the inhibition constant K_i, which reflects the binding affinity of the inhibitor to the enzyme with small values representing a high affinity (Equation 3.5).

$$\boldsymbol{K_i = \frac{k_{-3}}{k_3}}$$ Equation 3.5

For reversible reactions, the product P can be defined as a substrate for the reverse reaction yielding a $K_{M,product}$ and a maximum reaction rate for the reverse reaction $v_{max,reverse}$. The thermodynamic equilibrium K_{eq} can be described by the Haldane relationship (Haldane, 1930) (Equation 3.6).

$$\boldsymbol{K_{eq} = \frac{[P]_{eq}}{[S]_{eq}} = \frac{v_{max,forward} \cdot K_{M,product}}{v_{max,reverse} \cdot K_{M,substrate}}}$$ Equation 3.6

with K_{eq} = Equilibrium constant

$[P]_{eq}$ = Product concentration at thermodynamic equilibrium

$[S]_{eq}$ = Substrate concentration at thermodynamic equilibrium

3.3.3. Enzyme stability

Enzymes usually function in a narrow range of conditions. High temperatures and non-physiological pH can effectively inactivate enzymes by denaturation (Bisswanger, 2008; Ringe and Petsko, 2009).

Under fixed conditions, the stability can be expressed as a first-order decay function of the enzyme activity (Equation 3.7).

$$\boldsymbol{A = A_0 \cdot e^{-k_{inact} \cdot t}} \qquad \text{Equation 3.7}$$

with A = activity

A_0 = initial activity at t = 0

t = time

k_{inact} = inactivation constant

The half-life τ denotes the time required for the activity of the enzyme to reach half the initial activity and is thus a measure of the stability of an enzyme at defined process conditions. The half-life τ can be obtained from the inactivation constant k_{inact} (Equation 3.8).

$$\boldsymbol{\tau = \frac{\ln(2)}{k_{inact}}} \qquad \text{Equation 3.8}$$

3.3.4. Multienzyme syntheses

Many chemical products, especially in the pharmaceutical industry, require multiple reactions to be converted from a readily available substrate to the target product. In chemical syntheses, this is usually done by a step-by-step approach in which each reaction is performed separately. The product is removed and purified after each step, which then serves as substrate for the next reaction. This is usually required due to an incompatibility of the reactions or the reactions taking place under substantially different conditions. Biocatalytic reactions, in turn, are considered to be easily combinable due to most reactions taking place at similar conditions and in aqueous media. Although step-by-step approaches allow the optimal adjustment of the reaction conditions for each biocatalyst, purification of each intermediate leads to extensive work-up and results in low yields, often due to unfavorable thermodynamic equilibria, long production times and high amounts of waste chemicals. Consequently, this leads to expensive products (Findrik and Vasic-Racki, 2009; Santacoloma *et al.*, 2011). These issues are addressed by performing multienzyme reactions in one pot without intermediate product purification, which are often referred to as domino, cascade or more generally as multistep reactions (Figure 3.10) (Findrik and Vasic-Racki,

2009). There are several set-ups for multistep syntheses. For one, the reactions can still be performed sequentially, similar to step-by-step biocatalysis, however, without intermediate purification. After the first reaction is completed, the second enzyme is added to allow the second reaction to proceed. Where applicable, reaction conditions can be adjusted, for example by regulation of the pH and the temperature, to fit the optimal requirements of the subsequent reaction. Furthermore, substrates that are required for later steps in the biosynthesis can be added when required reducing the risk of side product formation or cross-inhibitions (Ricca *et al.*, 2011). However, since most reactions are reversible and are thus controlled by a thermodynamic equilibrium, low yields of one or more reactions in the cascade can significantly limit the overall yield.

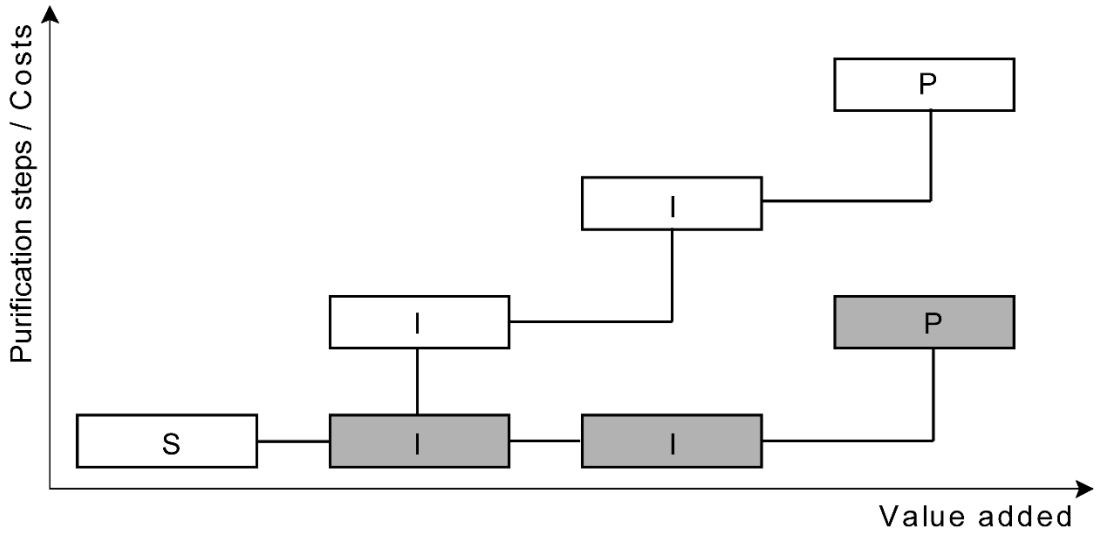

Figure 3.10 – Schematic diagram of the purification steps and costs versus the value generated for multienzyme syntheses using a step-by-step approach with intermediate purification (*white*) and a one-pot cascade without intermediate purification (*gray*).

This disadvantage can be circumvented by one-pot reactions, where all enzymes required for the biosynthesis are combined in a cascade reaction under identical reaction conditions and at the same time. The most often described multistep reactions involve cofactor regeneration. Many industrially relevant enzymes require cofactors such as $NAD(P)^+$, NAD(P)H, FAD^{2+} or $FADH_2$. Because these cofactors are expensive, cofactor regeneration can substantially reduce costs by reducing the amount of cofactor from stoichiometric to catalytic amounts. In these reactions, the cofactor required for the enzymatic reaction is recycled by addition of a second enzyme. An industrial example is the production of L-tert-leucine by an L-leucine dehydrogenase (LeuDH) from trimethylpyruvate. The LeuDH requires NADH as cofactor which is oxidized to NAD^+. To recycle NAD^+, formate dehydrogenase (FDH) is added, which oxidizes formate to CO_2 by reducing NAD^+ to NADH. Besides

significantly reducing the amount of cofactor required (Kragl *et al.*, 1996), the irreversible FDH reaction shifts the reaction equilibrium toward product formation by constantly converting NAD^+ to NADH, driving the reaction to completion. Thus, one-pot reactions allow reactions with favorable thermodynamic equilibrium or irreversible reactions to push or pull the cascade toward higher product yields. This approach is highly attractive to increase the yields of otherwise highly unfavorable reactions. Furthermore, reactions with unstable intermediates, such as radicals or volatile compounds, can be performed as the intermediate is immediately processed by the subsequent reaction. However, although all enzymes are considered to work under mild conditions of physiological temperatures and pH, optimal reaction conditions can vary greatly and thus can lead to incompatibilities (Ricca *et al.*, 2011). Furthermore, cross-inhibitions of substrates, intermediates and products of one reaction on the biocatalyst of other reactions can pose a major challenge.

3.4 Synthesis of cytidine-5'-monophospho-*N*-acetylneuraminic acid

A good example of the benefits and problems encountered in multienzyme synthesis is the three-enzyme cascade reaction for the synthesis of cytidine-5'-monophospho-*N*-acetylneuraminic acid (CMP-Neu5Ac). CMP-Neu5Ac is a key component in the formation of sialylated oligosaccharides. Sialic acids are acidic 9-carbon sugars that are usually present at the terminal position of glycan chains of glycoconjugates displayed on mammalian cell surfaces (Schauer and Shaw, 1991). In humans, *N*-acetylneuraminic acid (Neu5Ac) is the most abundant sialic acid (Varki, 2008; Tao *et al.*, 2010) and, due to its anionic charge and exposed position on cell surfaces, is involved in several cellular processes. At the end of glycan chains, Neu5Ac interacts with sialic acid recognizing lectins to mediate cell-cell recognition and signaling. Furthermore, the terminal display of Neu5Ac on glycan chains plays a major role in embryogenesis, cell development and neural plasticity and thus makes Neu5Ac an interesting compound for the food industry (Varki, 2009). Neu5Ac has further been described as a masking agent for pathogenic bacteria to evade the immune system. Thus, several pathogenic bacteria are capable of Neu5Ac production and its presentation on their cell surface, thereby mimicking eukaryotic cells (Varki and Gagneux, 2009). Hence, sialylated glycoconjugates play an important role in the pharmaceutical industry (von Itzstein, 2007). The transfer of Neu5Ac to the glycan chain is catalyzed by sialyltransferases with high selectivity and high yield. Sialyltransferases require an activated form of Neu5Ac for glycoconjugation with a high specificity for the nucleotide sugar CMP-Neu5Ac. However, the availability of nucleotide sugars is a major limitation for the synthesis and study of glycoconjugates *in vitro* (Seeberger *et al.*, 2009).

CMP-Neu5Ac can be either synthesized chemically or enzymatically. Sugar chemistry in general is complicated due to the many similar reactive groups and thus, chemical synthesis of CMP-Neu5Ac requires complicated protecting group chemistry (Martin and Schmidt, 1993; Zimmermann *et al.*, 2007; Wolf *et al.*, 2012).

The first biocatalytic synthesis of CMP-Neu5Ac has been described by Roseman in 1962, who isolated and characterized the enzyme CMP-sialic acid synthetase (CSS), which effectively catalyzed the activation of Neu5Ac via cytidine 5'-triphosphate (CTP). To provide Neu5Ac, Uchida *et al.* (1984) proposed its enzymatic synthesis from pyruvate and *N*-acetylmannosamine (ManNAc), which is catalyzed by the *N*-acetylneuraminate lyase (NAL). The reaction was coupled to the CSS reaction to produce CMP-sialic acid from ManNAc, pyruvate and CTP at high yields of up to 96 % (Simon *et al.*, 1988; Song *et al.*, 2003; Yu *et al.*, 2004). Since ManNAc is expensive and not readily available in large scale, ManNAc was chemically epimerized from *N*-acetylglucosamine (GlcNAc) at alkaline conditions. The chemoenzymatic one-pot reaction, however, yielded low conversions of only 15 % due to unfavorable alkaline conditions of pH 10.5 required for the chemical epimerization reaction (Yu *et al.*, 2004). Thus, the reaction is usually carried out in two steps with intermediate product isolation, which involves large amounts of strong bases and organic solvents needed for the epimerization and the product purification, respectively (Liese *et al.*, 2006; Tao *et al.*, 2010). In contrast, the *N*-acyl-D-glucosamine 2-epimerase (AGE) catalyzes the conversion of GlcNAc to ManNAc. The combined AGE and NAL reaction was used for the production of Neu5Ac and has the potential to be a more cost-efficient and environmentally sustainable alternative to the chemo-enzymatic synthesis (Maru *et al.*, 2002; Tao *et al.*, 2010). However, a main drawback of the AGE is its requirement for adenosine 5'-triphosphate (ATP) as allosteric activator. Although ATP is not consumed in the reaction, ATP is required for stabilization of the AGE and thus for full catalytic activity.

Thus, CMP-Neu5Ac can be synthesized from GlcNAc, pyruvate and CTP by a three-enzyme cascade reaction employing an AGE, a NAL and a CSS (Kittelmann *et al.*, 1992) (Figure 3.11). The cascade reaction is highly efficient in terms of theoretical yield and atom economy. Both the epimerization and the aldol condensation reaction have unfavorable thermodynamic equilibria that lie on the substrate side ($K_{eq,AGE}$ = 0.26 at 30°C, pH 7.5; $K_{eq,NAL}$ = 20.7 L mol^{-1} at 25°C, pH 7.5) (Groher and Hoelsch, 2012; Klermund *et al.*, 2013), whereas the thermodynamic equilibrium of the CSS-catalyzed reaction lies far on the product side. Thus, although reversibility of the CSS reaction has been demonstrated at certain conditions, the reaction is considered to be quasi-irreversible (Kean and Roseman, 1966), pulling the cascade reaction toward completion. Furthermore, only inorganic pyrophosphate (PP_i) is produced as by-product, resulting in an efficient conversion of the substrates into the target product.

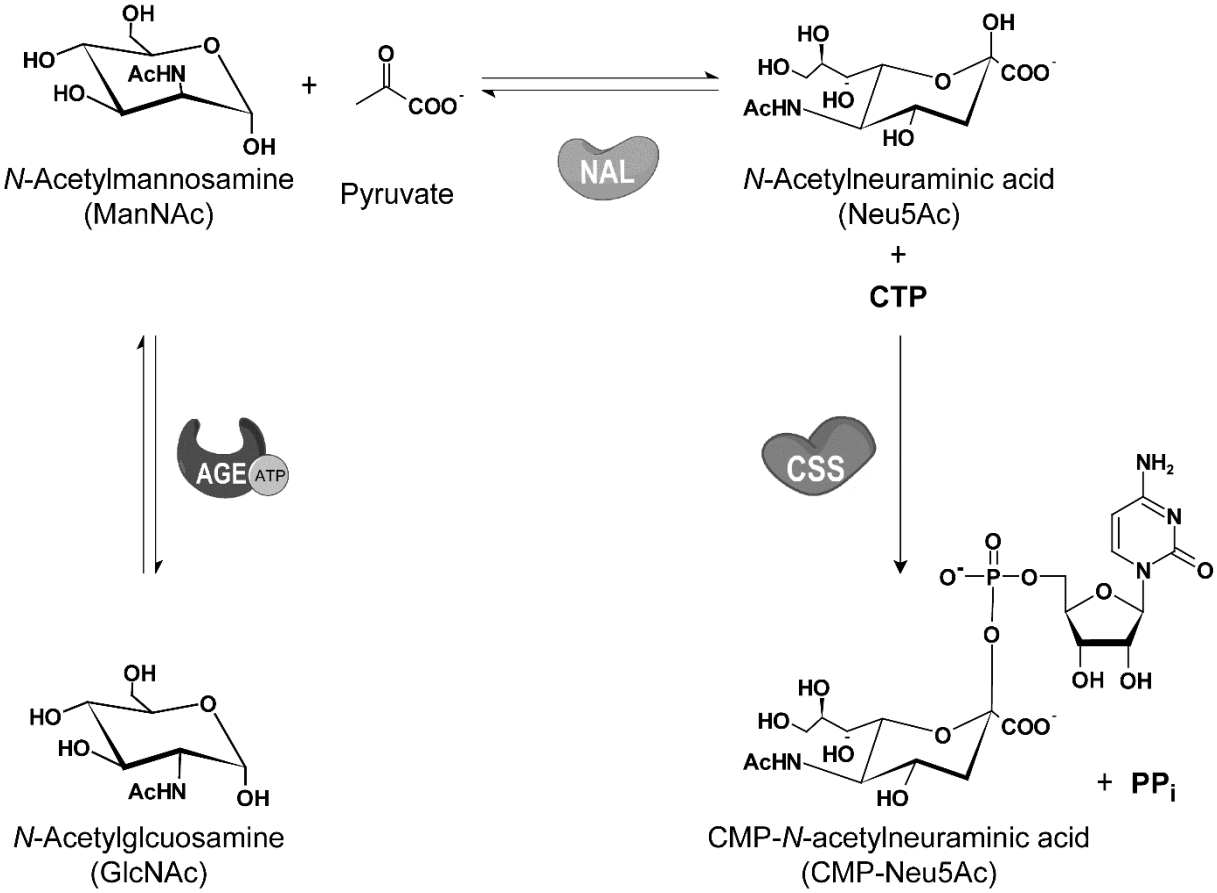

Figure 3.11 – CMP-Neu5Ac synthesis via a three-enzyme cascade reaction. *N*-Acetylglucosamine (GlcNac) is converted to *N*-acetylmannosamine (ManNAc) by an *N*-acyl-d-glucosamine 2-epimerase. ATP serves as allosteric activator of the enzyme. ManNAc then reacts with puyruvate to form *N*-acetylneuraminic acid (Neu5Ac) in an aldol condensation reaction catalyzed by an *N*-acetylneuraminic acid lyase (NAL). Neu5Ac is then activated with CTP by a CMP-sialic acid synthetase (CSS) to form CMP-Neu5Ac and inorganic pyrophosphate (PP_i).

Even though the reaction is intriguing in terms of theoretical yield and atom economy, Kittelmann *et al.* (1992) yielded only 10.6 % CMP-Neu5Ac based on CTP when producing CMP-Neu5Ac using the three-enzyme cascade reaction in one pot. At the same conditions but starting from ManNAc, pyruvate and CTP, the reaction yielded conversions of up to 37 % based on ManNAc, indicating an incompatibility between the AGE and reactants of the second and third reaction.

3.4.1 *N*-Acyl-D-glucosamine 2-epimerase

The AGE catalyzes the interconversion of GlcNAc and ManNAc and thus belongs to the class of isomerases and to the subclass of racemases/epimerases. All known AGEs form an active dimer and promote the epimerization of the C2-bond, which contains the acetylated

amino group, between the *S* and the *R* configuration. AGEs have initially been isolated from mammals including humans (Takahashi *et al.*, 1999), rats (Takahashi *et al.*, 2002) and pigs (Maru *et al.*, 1996). In the last decades, novel AGEs from bacteria including *Bacteroides ovatus* ATCC 8483 (Sola-Carvajal *et al.*, 2012) and cyanobacteria including *Synechocystis* sp. PCC 6803 (Tabata *et al.*, 2002), *Anabaena* sp. CH1 (Lee *et al.*, 2007), *Acaryochloris marina* MBIC 11017, *Anabaena variabilis* ATCC 29413, *Nostoc* sp. PCC 7120 and *Nostoc punctiforme* PCC 73102 (Klermund *et al.*, 2013), have been isolated to find variants with beneficial properties for industrial purposes. Especially the AGEs from the *Anabaena* strains displayed considerably improved kinetic parameters compared to the mammalian AGEs (Lee *et al.*, 2007; Klermund *et al.*, 2013). All known AGEs to date require ATP as an allosteric activator. For the AGE from *Anabaena* sp. CH1, a specific loop region exposed on the protein surface was determined to be responsible for ATP binding (Liao *et al.*, 2012).

Research on the two-enzyme synthesis of Neu5Ac from GlcNAc and pyruvate via AGE and NAL have elucidated a high susceptibility of the AGE to reactants of the three-enzyme cascade. Strong inhibitions of Neu5Ac and/or pyruvate have been reported for various AGEs (Lee *et al.*, 2004; Zimmermann *et al.*, 2007; Klermund *et al.*, 2013). However, especially the high similarity between ATP and CTP and the AGE requiring ATP for activity and the CSS requiring CTP as substrate are substantially limiting the cascade efficiency. Lee *et al.* (2007) demonstrated that CTP readily displaced ATP from the ATP-binding site of the AGE from *Anabaena* sp. CH1, resulting in no AGE activity even in the presence of ATP. CTP seemed to have the strongest ability to displace ATP compared to GTP, UTP and the respective deoxyribonucleotides (Lee *et al.*, 2007), suggesting that nucleotide inhibition on the AGE from *Anabaena* sp. CH1 is strongest for CTP.

In this study, the AGE from *Anabaena variabilis* ATCC 29413 was used. This AGE displays a high catalytic efficiency with a k_{cat} K_M^{-1} of 4.96 s^{-1} mM^{-1} for the conversion of GlcNAc to ManNAc and a strong affinity for the allosteric activator ATP of 3.3 µM. Moreover, the AGE has an exceptionally high activity in the absence of ATP of up to 32 % compared to the activity determined with ATP in excess. This is considerably more than has been reported for other AGEs of approximately 5 %, including the AGE from *Anabaena* sp. CH1 (Lee *et al.*, 2007; Klermund *et al.*, 2013). Furthermore, high-level expression of the AGE using a chaperone system has recently been described (Klermund *et al.*, 2015). In contrast, the AGE is highly susceptible to various reactants. Apart from the known Neu5Ac and pyruvate inhibitions, pyruvate has been found to inactivate the AGE of *Anabaena variabilis* ATCC 29413 presumably by formation of a Schiff's base with the primary amine of the lysine at residue 160 in the ATP-binding region. By a single amino acid substitution of the lysine to isoleucine, the pyruvate inactivation could be completely abolished, resulting in the same stability of the AGE K160I at high pyruvate concentrations compared to the AGE stability

without pyruvate (Klermund *et al.*, 2016b). Since the mutation was in the ATP binding site, the kinetic parameters were slightly altered, resulting in a catalytic turn over k_{cat} of 21.6 s^{-1} and half-saturation constants of 28.7 mM for the substrate GlcNAc and 95 µM for the allosteric activator ATP. Furthermore, an extremely low inhibition constant K_i of CTP on the AGE K160I of 1 mM was determined (unpublished data). The CTP inhibition on the AGE K160I was determined to be competitive in respect to ATP. In the presence of high CTP concentrations, the AGE K160I activity resembled its activity without ATP, reaching approximately 16 % of the maximum activity with ATP in excess, indicating that CTP competes with ATP for the ATP binding site but does not lead to an activation of the AGE K160I (unpublished data). Thus, at full CTP inhibition, the AGE K160I was still active, although the activity was substantially reduced.

3.4.2 *N*-Acetylneuraminate lyase

The NAL catalyzes the aldol condensation of ManNAc and pyruvate to form Neu5Ac. The enzyme is involved in the sialic acid metabolism and has been first isolated from pathogenic bacteria such as *Vibrio cholerae* and *Clostridium perfringens* (Heimer and Meyer, 1956; Popenoe, 1959) but can also be found in mammalian tissues (Comb and Roseman, 1960; Brunetti *et al.*, 1962; Sirbasku and Binkley, 1970). In 1984, the NAL from *E. coli* was isolated and characterized by Uchida *et al.* (1984). The NAL forms a tetrameric enzyme that remains fully active in the presence of several heavy metals and is thermostable with 100 % activity remaining after 24 h at 37°C and up to 10 min at 60°C (Uchida *et al.*, 1984). Furthermore, the pH optimum is between 6 and 9 (Uchida *et al.*, 1984). The NAL from *E. coli* K12 has been thoroughly characterized by Groher and Hoelsch (2012) who elucidated the reaction mechanism as a rapid-equilibrium ordered reaction with pyruvate binding first. The NAL from *E. coli* K12 displayed a catalytic activity k_{cat} of 8.53 s^{-1} and half-saturation constants of 2.25 mM and 141 mM for pyruvate and ManNAc, respectively, at 25°C, pH 7.5 (Groher and Hoelsch, 2012).

3.4.3 CMP-sialic acid synthetase

The CSS has been isolated from several mammalian organisms and pathogenic bacteria such as *E. coli* and *Neisseria meningitidis* (Warren and Blacklow, 1962; Mizanur and Pohl, 2008). The CSS of *Neisseria meningitidis*, which was used in this study, has been thoroughly characterized and high-level expression in *E. coli* has been achieved (Gilbert *et al.*, 1997; Karwaski *et al.*, 2002; Horsfall *et al.*, 2010). The CSS of *Neisseria meninigitidis* has an outstanding catalytic efficiency which is due to a high catalytic activity (k_{cat} = 54 s^{-1}) and low half-saturation constants ($K_{M,Neu5Ac}$ = 130 - 250 µM; $K_{M,CTP}$ = 50 – 560 µM) (Warren and

Blacklow, 1962; He *et al.*, 2011). Although the CSS of *Neisseria meninigitidis* has been demonstrated to have a broad substrate spectrum for different sugar moieties, it is highly dependent on CTP as nucleotide and does not accept ATP, GTP or UTP (Knorst and Fessner, 2001). In turn, the similarity of the nucleotides leads to an inhibition of the CSS by ATP with an inhibition constant K_i of 5 mM (unpublished data).

3.5 Green fluorescent protein

The green fluorescent protein (GFP) has been first isolated from the jellyfish *Aequorea victoria*. The protein forms a robust barrel structure composed of 11 ß-sheets that harbors a green fluorescing chromophore in the center of the cavity. The protein has been shown to be highly resistant to heat, high pH, high salt concentrations and detergents (Ehrmann *et al.*, 2001). The chromophore is formed by an intramolecular autocatalytic cyclization of the six amino acids from position 64 to 69, Phe-Ser-Tyr-Gly-Val-Gln, to form green fluorescing 4-(*p*-hydroxybenzylidene)-imidazolid-5-one. Fluorescence is dependent on oxidation of the chromophore, which is the rate limiting step during chromophore formation with half the chromophores oxidized in 76 min (Zimmer, 2002).

GFP fluorescence is evoked by excitation of the chromophore at a wave length of 395 nm (maximum), which emits light at a wavelength of 504 nm (maximum). Several mutants have been created to enhance or alter GFP characteristics. The most prominent variant of GFP is a double mutant with a phenylalanine to leucine substitution at position 64 (F64L) and a serine to threonine substitution at position 65 (S65T) in the chromophore region of GFP. These substitutions lead to an increased quantum yield of the chromophore and thus an enhanced fluorescence of the protein. The GFP F64L S65T mutant was thus termed enhanced green fluorescent protein (eGFP). The maximum excitation and emission wavelengths of eGFP are slightly shifted toward 488 and 507 nm, respectively, and a slightly increased pH sensitivity compared to wildtype GFP has been observed (Topell *et al.*, 1999).

GFP and its variants have been used in widespread applications. GFP is, amongst many other applications, used as a reporter gene to monitor gene expression levels when cloned under control of certain promotors or protein localization when fused to endogenous proteins. Adverse effects of its fusion to proteins have rarely been observed and no additional substrates or cofactors are required for GFP fluorescence, making it an ideal reporter protein (Zimmer, 2002).

3.6 In *vitro* protein synthesis

In vitro protein synthesis (IVPS), or cell-free protein synthesis, is the production of proteins in cell-derived lysates. Cell-free systems offer several advantages over conventional heterologous expression systems, including the ability to produce toxic and hard-to-express proteins, the suitability for high-throughput screening, for example for directed protein evolution studies, as well as the easy modification of the reaction conditions and the introduction of unnatural or isotope-labeled amino acids. Thus, applications for IVPS range from structural proteomics, high-throughput and functional proteomics, protein evolution studies and *in vitro* protein labeling to genetic diagnostics for the detection of non-sense or frame-shift mutations in marker genes and has been used in therapeutic applications, for example the synthesis of infectious virus particles for the development of antiviral agents (Gite *et al.*, 2003; Neuman *et al.*, 2004; Katzen *et al.*, 2005; Rosenblum and Cooperman, 2014).

IVPS lysates can theoretically be prepared from any cell by extracting the cytosol from the cell, usually by physical disruption of the cell (Fujiwara and Doi, 2016). In the recent decades, the lysates used for IVPS have greatly improved due to optimization of the buffer composition, introduction of energy recycling machineries and by exchanging components, such as the endogenous RNA polymerase by the T7 or SP6 RNA polymerase, to enhance the efficiency of the systems (Katzen *et al.*, 2005).

The simplest IVPS systems translate mRNA directly into the target protein thus uncoupling the transcription from the translation. These uncoupled approaches require the addition of amino acids and an energy source, usually in the form of ATP, while the lysate provides the translation machinery. Tedious mRNA preparation and low stability of the mRNA in the IVPS have, however, shifted the favor toward coupled IVPS that combine transcription and translation in one pot (Rosenblum and Cooperman, 2014). The mRNA required for translation is directly generated by endogenous RNA polymerases from DNA in the form of either plasmid DNA or purified PCR products, thereby increasing the stability of the whole system. The exchange of the endogenous polymerases with highly active T7 or SP6 polymerases, led to coupled IVPS with significantly increased yields of several micrograms of protein per milliliter within 1-2 h (Kigawa *et al.*, 1999) and allowed the use of standard expression plasmids encoding a T7 or SP6 promotor. Thus, the ease of handling and the high yields have propelled the use of coupled IVPS in the recent years (Rosenblum and Cooperman, 2014).

The use of highly purified IVPS from separately purified components was introduced by Shimizu *et al.* (2001). The developed PURExpress kit, which is commercially distributed by New England Biolabs, is devoid of any components not involved in the IVPS, including

metabolites, nucleases and proteases, that can lower synthesis yields, however are substantially more expensive (Shimizu *et al.*, 2001; Rosenblum and Cooperman, 2014). Despite the advantages of IVPS, cell-free protein synthesis is limited by a short lifetime due to a fast depletion of the energy source required to drive the transcription and translation machinery and the accumulation of phosphate, consequently lowering the yield of batch systems (Katzen *et al.*, 2005; Rosenblum and Cooperman, 2014). The accumulation of phosphate results in the precipitation of magnesium, which is an essential component due to its stabilizing effect on DNA, RNA and nucleotides, as magnesium phosphate. Although these problems have been addressed by the introduction of continuous-flow and semi-continuous cell-free translation systems, these setups are considerably more complex (Katzen *et al.*, 2005; Rosenblum and Cooperman, 2014).

Today, several cell-free extracts are commercially available, including *E. coli*, wheat germ, insect cell and rabbit reticulocyte lysates (Fujiwara and Doi, 2016). These commercial lysates are commonly designed to allow the coupled transcription and translation from plasmid DNA or PCR products. The choice of the IVPS source is highly dependent on the application and the target protein to be expressed. Whereas *E. coli* lysates usually produce protein in high yields, eukaryotic lysates usually achieve lower yields but are better suited for functional studies and protein folding as well as for producing eukaryotic proteins with posttranslational modifications (Hillebrecht and Chong, 2008). Furthermore, the protein yield is dependent on the reaction conditions, which may vary from protein to protein. For example, reducing the optimal temperature of *E. coli*-based cell lysate from 37°C to 30°C significantly slowed down the protein synthesis but increased the amount of functional GFP by almost 2-fold (Iskakova *et al.*, 2006).

Through the addition of lipids or mild detergents, IVPS allows the production of functional membrane proteins without tedious membrane solubilization steps (Wang *et al.*, 2011; Sachse *et al.*, 2014). The ability to synthesize membrane proteins in a functional form by providing a suitable environment *in vitro* has facilitated the screening for suitable detergents and membranes for membrane protein stabilization in solution and analysis of correct folding and functioning of the membrane proteins. Several membrane proteins have been synthesized and characterized recently, including several membrane receptors and transporters (Sachse *et al.*, 2014). However, the functional synthesis and incorporation of membrane proteins strongly depends on the membrane characteristics, including composition, fluidity, curvature and thickness of the hydrophobic region to minimize the hydrophobic mismatch. Thus, even in IVPS systems, membrane protein synthesis is not trivial and requires a careful adjustment of the parameters for each individual membrane protein (Sachse *et al.*, 2014).

4. Materials and methods

4.1 Materials

4.1.1 Chemicals and equipment

Equipment and consumables used in this work were from various suppliers and are listed in the appendices A1 and A2. Chemicals were purchased from various suppliers and were of various analytical grades as listed in the appendix A3. The composition of cultivation media and buffers are listed in the appendices A4 and A5, respectively. Used software is described in the methods section where applicable and listed in the appendix A6.

$PMOXA_{15}$-$PDMS_{68}$-$PMOXA_{15}$ was purchased from Polymer Source Inc. (Dorval, Canada). The polymer has a total mass of 7600 g mol^{-1} with block masses of 1300-5000-1300 g mol^{-1} The polymer has an M_W/M_N of 1.23, where M_W is the mass-average molecular mass and M_N is the number-average molecular mass. The polymer contains hydroxyl end groups on both sides and the blocks are linked by methyl groups. The polymer was ground at -196°C in a cryo mill and the powder was stored at -20°C to avoid agglomeration.

4.1.2 Biological materials

Enzymes required for molecular cloning were purchased from New England Biolabs and are listed in the appendix A7. Genes, primers and vectors were from various suppliers and are listed in appendices A8 – A10. The *E. coli* strains used in this study are described in the appendix A11. Amino acid sequences of the peptide anchors are given in appendix A12.

4.2 Molecular cloning

4.2.1 Polymerase chain reaction

DNA fragments were amplified via polymerase chain reaction (PCR) in a BioRad Thermo Cycler with a Phusion® High-Fidelity DNA polymerase. DNA fragments were amplified with 0.02 U μL^{-1} of Phusion™ DNA polymerase in 1x Phusion HF buffer, 0.2 mM desoxyribonucleotide triphosphates (dNTPs), 0.5 µM of each primer and 2 µL template DNA. Denaturing and elongation steps were chosen according to the supplier's manual and the

lengths of the respective amplicons (Appendix A9). Annealing temperatures were determined by the melting temperatures of the respective primers (Appendix A8).

4.2.2 Isolation of plasmid DNA from *Escherichia coli*

For plasmid isolation and recovery, 4 mL Luria Broth (LB) medium supplemented with the appropriate antibiotics (30 mg L^{-1} kanamycin, 50 mg L^{-1} ampicillin, and 20 mg L^{-1} chloramphenicol) was inoculated with a single colony containing the desired plasmid from LB agar plates. Plasmids were purified using the spin method of the GenElute™ HP Plasmid Miniprep Kit according to the supplier's manual.

4.2.3 Agarose gel electrophoresis

PCR products were analyzed by gel electrophoresis. Agarose gels were run in 1x Tris-acetate-ethylenediaminetetraacetic acid (TAE) buffer at 120 V for 25-45 min. For samples exceeding 1000 bp, 1 % agarose gels were used. DNA samples smaller than 1000 bp were analyzed on 2 % agarose gels. Samples were stained with 16.7 % v/v 6x loading dye. DNA was visualized under UV light. An extended 100 bp DNA marker by Carl-Roth was used to verify strand length.

4.2.4 DNA purification

DNA was purified via the GenElute™ PCR Clean-Up Kit. PCR products were purified from agarose gels via the GenElute™ Gel Extraction Kit. The spin-methods were used according to the supplier's manuals.

4.2.5 Restriction and ligation of DNA

PCR products and plasmids were digested with the appropriate restriction enzymes at 37°C for 1 h according to the supplier's manual. 10 µL of PCR product were digested in a total volume of 20 µL with the appropriate restriction buffer and 10 U of each restriction enzyme. Approximately 500 ng of plasmid were digested in a total volume of 50 µL with the appropriate restriction buffer and 10 U of each restriction enzyme. The digested plasmid was dephosphorylated with 5 U of antarctic phosphatase in 60 µL 1x antarctic phosphatase buffer. Dephosphorylation took place at 37°C for 15 min. After dephosphorylation, the phosphatase was heat-inactivated at 65°C for 5 min. PCR products and plasmids were ligated using a Quick T4 DNA Ligase according to the supplier's manual.

4.2.6 Site-directed mutagenesis

Site-directed single nucleotide mutagenesis was performed with and according to the Stratagene QuikChange® Lightning Site-Directed Mutagenesis Kit. Primers were designed based on the DNA sequence to be mutated using the QuikChange Primer Design tool (http://www.genomics.agilent.com/primerDesignProgram.jsp) (Table A 23).

Mutagenized plasmids were transferred into *E. coli* XL-Gold® Ultracompetent cells according to the QuikChange® Lightning Site-Directed Mutagenesis manual and the cells were plated onto LB agar plates containing the appropriate antibiotics.

4.2.7 Preparation of $CaCl_2$-competent cells

For the preparation of competent cells for plasmid transformation, the respective *E. coli* strain was grown at 37°C to an optical density at 600 nm (OD_{600}) of 0.3 - 0.6 in 100 mL LB medium. The cells were pelletized by centrifugation at 3260 xg for 10 min at 4°C and the supernatant was discarded. The cells were resuspended in 20 mL sterile 0.1 M $CaCl_2$ and incubated on ice for 30 min. The cells were again pelletized by centrifugation at 3260 xg for 10 min at 4°C, the supernatant was discarded and the cells were resuspended in 10 mL sterile 0.1 M $CaCl_2$ supplemented with 20 % v/v sterile glycerol. The cells were aliquoted in 90 µL aliquotes and immediately frozen at -80°C.

4.2.8 Transformation of competent cells

Cells were transformed by heat-shock. *E. coli* DH5α were used for plasmid recovery, *E. coli* XL-Gold® Ultracompetent cells were used for recovery of mutagenized plasmids, *E. coli* BL21 (DE3) were used for protein expression of proteins and proteins fused to peptide anchors, and *E. coli* BL21 (DE3) *omp8* were used for expression of membrane proteins. 90 µL of the respective $CaCl_2$-competent cells were thawed on ice and mixed with 2 µL of plasmid DNA or 10 µL of ligation product. The cells were chilled on ice for 30 min before being heat-shocked at 42°C for 30 s in a thermoshaker. *E. coli* XL-Gold® Ultracompetent cells were incubated for 90 s. The cells were chilled on ice for 2 min. 900 µL of LB medium were added to the transformed cells and the cells were incubated for 1 h at 37°C and 600 rpm in a thermomixer. When introducing plasmid DNA, 150 µL of the cell suspension was plated onto LB agar plates containing the appropriate antibiotics (30 mg L^{-1} kanamycin, 50 mg L^{-1} ampicillin, and 20 mg L^{-1} chloramphenicol). When introducing ligation products, the cells were pelletized in a microcentrifuge for 10 min at 1000 rpm, the supernatant was discarded and the cells were resuspended in 150 µL LB medium prior to being transferred to LB agar plates containing the

appropriate antibiotics (30 mg L^{-1} kanamycin, 50 mg L^{-1} ampicillin, and 20 mg L^{-1} chloramphenicol).

4.2.9 Colony polymerase chain reaction

Colony-PCRs were performed in a BioRad Thermo Cycler to verify successful transformation of bacterial cells. One pipette tip of a bacterial colony was resuspended in 20.8 µl deionized water. 1.25 U of Taq DNA polymerase in 1x ThermoPol buffer, 0.2 mM dNTPs and 0.2 µM of the T7 and T7 terminator primers (Table A 23) were added to the resuspended colony. After an initial denaturation step of 10 min at 95°C, the colony PCRs were run for 30 cycles. Denaturation was set to 30 s at 95°C, annealing was set to 1 min at 55°C and elongation was set according to the supplier's manual and the lengths of the respective amplicons (Appendix A9). Final elongation was 7 min at 68°C. The hold temperature was set to 12°C.

4.2.10 DNA sequencing

DNA sequencing was performed by Eurofins Genomics and verified using the software GENtle (www.gentle.magnusmanske.de).

4.2.11 Molecular cloning of the fusion proteins

The nucleotide sequences of the peptide anchors are listed in (Table A 20). The gene fragment *cytb$_5$'* was synthesized by biomers.net. The gene fragments *vam3p'* and *polyAL* were synthesized by Eurofins Genomics. The gene fragments *ubc6'* and *l'* were already available at the Institute of Biochemical Engineering (TUM). The gene fragment *ceca* was assembled via assembly PCR according to the Assembly PCR Oligo Maker (http://www.yorku.ca/pjohnson/).

Egfp was amplified from the respective plasmids (Table A 24) using the respective primer pairs with either NdeI and EcoRI or EcoRI and XhoI restriction sites (Table A 21). *Egfp* was digested with NdeI and EcoRI for ligation into a NdeI/EcoRI-digested, linearized pET28a(+) vector for fusion with C-terminal peptide anchors or EcoRI and XhoI for ligation into a EcoRi/XhoI-digested, linearized pET21a(+) vector for fusion with N-terminal peptide anchors. *Cytb$_5$'*, *l'*, *ubc6'* and *vam3p'* were amplified with the respective primers from Table A 21, digested with EcoRI and XhoI and cloned into EcoRI/XhoI-digested, linearized pET28a(+)-eGFP. *Ceca* and *polyAL* were amplified with the respective primers (Table A 21), digested with NdeI and EcoRI and cloned into NdeI/EcoRi-digested, linearized pET21a(+)-eGFP. A decaalanine linker with an EcoRI restriction site on both sides was cloned between eGFP

and each respective anchor via EcoRI, except for the construct containing *ceca* because it already contained a decaalanine sequence.

Analogously, *nal* and *css* were amplified from the respective plasmids (Table A 24) using the respective primer pairs (Table A 22). *Nal* and *css* were digested with NdeI and EcoRI for ligation into NdeI/EcoRI-digested, linearized pET28a(+) vector. *Cytb$_5$'*, *I'*, *ubc6'* and *vam3p'* were amplified with the respective primers (Table A 22), digested with SalI and XhoI and cloned into SalI/XhoI-digested, linearized pET28a(+)-NAL and pEt28a(+)-CSS. A decaalanine linker containing the EcoRI and SalI restriction sites and was cloned between the target enzyme and each respective anchor via EcoRI and SalI. *E. coli* DH5α were transformed with each vector for selection and plasmid propagation.

4.2.12 Cloning of the MBP-TEV-PolyAL-eGFP fusion protein

To enhance the solubility of the PolyAL-eGFP construct, the maltose binding protein (MBP) was cloned adjacent (N-terminal) to the peptide anchor via the pETM41 plasmid. The plasmid contains the MBP-tag upstream of a tobacco etch virus (TEV) cleavage site to be able to cleave the MBP moiety from the target protein. The MBP-TEV-PolyAL-eGFP fusion protein was cloned using standard cloning procedures. The PolyAL-eGFP construct was amplified from pET21a(+)-PolyAL-eGFP with the primers PolyAL-eGFP_for (NdeI) and PolyAL-eGFP_rev (KpnI) (Table A 23). The PCR product was digested with the restriction enzymes NcoI and KpnI. The digested gene was cloned into the pETM41 vector containing an N-terminal MBP moiety upstream of a TEV protease cleavage site. The plasmid was transformed into *E. coli* DH5α for selection and plasmid propagation.

4.3 Microbiological methods

4.3.1 Strain maintenance

E. coli strains were either stored on agar plates containing the appropriate antibiotics (30 mg L^{-1} kanamycin, 50 mg L^{-1} ampicillin, and 20 mg L^{-1} chloramphenicol) at 4°C or, for prolonged storage, as cryo stocks in 25 % v/v glycerol at -80°C. For cryo stocks, the respective culture was grown in 5 mL LB medium supplemented with the appropriate antibiotics (30 mg L^{-1} kanamycin, 50 mg L^{-1} ampicillin, and 20 mg L^{-1} chloramphenicol) at 37°C and 250 rpm overnight. After addition of sterile glycerol, the cells were immediately frozen at -80°C.

4.3.2 Precultures for heterologous protein expression

A 4 mL preculture was inoculated with a single colony from LB agar plates or by scraping a pipette tip across the respective frozen cryo stock before adding it to the preculture. The precultures were grown in LB medium supplemented with the appropriate antibiotics (30 mg L^{-1} kanamycin, 50 mg L^{-1} ampicillin, and 20 mg L^{-1} chloramphenicol) in a wise cube incubator over night at 30°C and 200 rpm (2.5 cm excentricity). The main cultures were inoculated with 1 mL L^{-1} preculture.

4.3.3 Heterologous expression of fusion proteins

Heterologous expression of proteins fused to peptide anchors was performed in terrific broth (TB) medium supplemented with the appropriate antibiotics (30 mg L^{-1} kanamycin, 50 mg L^{-1} ampicillin) in shaking flasks with a filling volume of 20 % of the nominal volume. The cells were grown to an OD_{600} of 0.6 - 0.8 at 37°C and 250 rpm (3.5 cm excentricity) before protein expression was induced with isopropyl β-D-1-thiogalactopyranoside (IPTG) to a final concentration of 1 mM. Protein expression was allowed to proceed for at least 16 h at 20°C and 250 rpm (3.5 cm excentricity).

4.3.4 Heterologous expression of enzymes

Heterologous expression of NAL and CSS was performed in LB medium supplemented with the appropriate antibiotics (30 mg L^{-1} kanamycin, 50 mg L^{-1} ampicillin) in shaking flasks with a filling volume of 20 % of the nominal volume. The cells were grown to an OD_{600} of 0.6 - 0.8 at 37°C and 250 rpm (3.5 cm excentricity) before protein expression was induced with IPTG to a final concentration of 1 mM. Protein expression was allowed to proceed for at least 16 h at 20°C and 250 rpm (3.5 cm excentricity).

4.3.5 Heterologous expression of *N*-acyl-D-glucosamine 2-epimerase K160I

AGE K160I was prepared by co-expression of the chaperone system GroEL/GroES (pGro7, TaKaRa Bio, Inc., Otsu, Japan) according Klermund *et al.* (2015). Heterologous expression was performed in LB medium supplemented with 30 mg L^{-1} kanamycin and 20 mg mL^{-1} chloramphenicol in shaking flasks with a filling volume of 20 % of the nominal volume. 0.5 g L^{-1} L-arabinose was added for the co-expression of the chaperone system. The cultures were grown to an OD_{600} of 0.6 - 0.8 at 37°C and 250 rpm (3.5 cm excentricity) before protein expression was induced with IPTG to a final concentration of 1 mM. Protein expression was allowed to proceed for 4 h at 37°C and 250 rpm (3.5 cm excentricity).

4.3.6 Heterologous expression of membrane channel proteins

Membrane channel proteins were expressed in *E. coli* BL21 (DE3) *omp8* cells. Heterologous expression was performed in TB medium supplemented with 50 mg L^{-1} ampicillin in shaking flasks with a filling volume of 20 % of the nominal volume. The cells were grown to an OD_{600} of 0.6 - 0.8 at 37°C and 250 rpm (3.5 cm excentricity) before protein expression was induced with IPTG to a final concentration of 1 mM. Protein expression was allowed to proceed for at least 16 h at 20°C and 250 rpm (3.5 cm excentricity).

4.3.7 Determination of optical density

The optical density (OD_{600}) of cell cultures was measured photometrically at 600 nm. Linearity was warranted until an OD_{600} of 0.3. Measurements exceeding an OD_{600} of 0.3 were appropriately diluted with medium.

4.3.8 Cell lysis

After heterologous expression, cells were harvested by centrifugation at 3260 xg for 10 min at 4°C. The cell pellets were resuspended in 5 mL IMAC binding buffer per g cell wet weight and supplemented with 1 mM phenylmethylsulfonyl fluoride (PMSF), 0.2 mg mL^{-1} lysozyme and 0.1 U mL^{-1} DNase I. The cells were lysed by sonication with a Sonoplus HD 2070 equipped with a sonotrode MS73. The Sonoplus HD 2070 was set to 5 min in countdown mode at cycle 5 and a power of 90 %. These settings are equivalent to a sonication for 5 min at an amplitude of 245–260 µm in 0.5 s pulses.

4.4 Protein purification

4.4.1 Membrane solubilization

Cell lysates containing target protein with peptide anchors were solubilized in 2 % v/v nonident P-40 (NP-40) for 1 h at room temperature or overnight at 4°C in an overhead rotator at 8 rpm to solubilize the membrane and extract the target protein. Cell lysates containing membrane protein were solubilized in 3 % n-ocytl glucoside (OG) for 2 h at room temperature in a rotary shaker at 8 rpm.

4.4.2 Immobilized metal affinity chromatography

Protein purification was performed via immobilized metal affinity chromatography (IMAC) with 1 mL HisTrap FF crude columns at a flow rate of 1-2 mL min^{-1}. The column was equilibrated with 5 column volumes (CVs) of IMAC binding buffer. Proteins without peptide anchor were eluted with a linear gradient of 0 - 100 % IMAC elution buffer over 20 CVs. Proteins with peptide anchor were washed with 10 CVs IMAC washing buffer prior to being eluted with 5 CVs 100 % IMAC elution buffer. For the purification of membrane proteins, IMAC-MB binding and IMAC-MB elution buffers containing 0.6 % of the detergent n-octylpolyoxyethylene (O-POE) were used and the proteins were eluted with a linear gradient of 0 - 100 % IMAC-MB elution buffer over 20 CVs. All buffer solutions were filtered (Pore size: 0.22 µm, Steritop) prior to use. All chromatographic procedures were performed at room temperature.

4.4.3 Dialysis

Purified protein was usually dialyzed against the respective storage and/or reaction buffer. AGE K160I, NAL without peptide anchor and CSS without peptide anchor were dialyzed against 50 mM bicin, pH 8.0, and 100 mM NaCl. If not already present in the appropriate buffer, target proteins with peptide anchor were dialyzed against 100 % IMAC elution buffer. The protein solutions were dialyzed overnight at 4°C against a buffer volume of at least 100 times the protein stock solution volume.

4.4.4 Hydrophobic interaction chromatography

Proteins containing peptide anchors were polished via hydrophobic interaction chromatography (HIC) using a HiTrap Butyl FF column. The column was equilibrated with 20 mM phosphate buffer, pH 7.4 and 3 M NaCl. Protein was applied in IMAC elution buffer and the column was washed with 10 mL HIC washing buffer. Target proteins were eluted with bidistilled water. After elution, target protein containing eGFP was dialyzed against IMAC elution buffer. Target protein containing NAL or CSS were eluted in 50 µL increments directly into 50 µL 2x IMAC elution buffer due to the enzymes not being stable in bidistilled water. After elution, the fusion proteins containing NAL and CSS were thus present in 1x IMAC elution buffer. CecA-eGFP was washed with 20 mM phosphate buffer, pH 7.4, and 1 M NaCl, and eluted in 20 mM phosphate buffer, pH 7.4.

The ionic strength I of the buffer was calculated according to Equation 4.1.

$$I = \frac{1}{2} \cdot \sum_i c_i \cdot z_i^2$$ Equation 4.1

with c_i = Molar concentration of ion *i*, mol L^{-1}

z_i = Charge number of ion *i*

4.4.5 Anionic exchange chromatography

Membrane channel proteins were polished and concentrated via anionic exchange chromatography (AEX). The membrane proteins were dialyzed against 10 mM Tris-HCl, pH 8.0, and applied to HiTrap Capto Q columns. The columns were washed with 10 CVs AEX washing buffer and the membrane channel proteins were eluted with 2 CVs AEX elution buffer.

4.4.6 Storage of proteins

Proteins were stored at 4°C in their respective buffer solution. Proteins with peptide anchor were stored in IMAC elution buffer, membrane channel proteins were stored in 50 mM bicin buffer, pH 8.0, containing 0.6 % O-POE, and proteins without peptide anchor were stored in 50 mM bicin, pH 8.0, and 100 mM NaCl.

4.4.7 Sodium dodecyl sulfate polyacrylamide gel electrophoresis

Protein purity was validated via sodium dodecyl sulfate polyacrylamide gel electrophoresis (SDS-PAGE) with a 12.5 % resolving gel and a 3 % stacking gel. Polymerization of the polyacrylamide gels was induced with 100 µL 10 % ammonium persulfate (APS) and 10 µL tetramethylethylenediamine (TEMED). Protein samples were incubated for 5 min at 95°C in 1x application buffer prior to application. Membrane channel proteins were incubated for 15 min at 99°C. SDS-PAGE was run in 1x SDS-PAGE running buffer at 30 mA per gel and maximum voltage for 60-75 min.

The gels were stained according to Fairbanks *et al.* (1971). The polyacrylamide gels were successively boiled in Fairbanks' solution A, Fairbanks' solution B and 20 % acetic acid with intermediate incubation times of 5 min at room temperature and low agitation. Polyacrylamide gels were digitalized by scanning.

4.4.8 Determination of protein concentration

Protein concentrations were determined with the bicinchoninic acid (BCA) assay using the BCA Assay Kit according to the supplier's manual. Bovine serum albumin served as reference protein. Membrane channel protein concentrations were determined by absorbance at 280 nm using quartz cuvettes according to the Lambert-Beer law and a molar extinction coefficient ε of 54,000 M^{-1} cm^{-1} (Equation 4.2).

$$A_{280} = c_{Protein} \cdot \varepsilon \cdot d \qquad \text{Equation 4.2}$$

4.5 Polymersome production and characterization

4.5.1 Polymersome preparation

To obtain a 20 % w/v polymer solution, 2 g of $PMOXA_{15}$-$PDMS_{68}$-$PMOXA_{15}$ polymer powder were dissolved in 10 mL ethanol (99.8 %, undenatured). The polymer solution was added to deionized water in a 1:20 ratio to obtain a 1 % w/v polymersome dispersion and stirred in 12 mL-stirred tank reactors in a bioREACTOR 48 at 4000 rpm with an S-type stirrer for 1.25 h at room temperature according to the method of Poschenrieder *et al.* (2016b). Polymersome concentrations above 1 % w/v were obtained by concentrating the polymersome dispersion after polymersome formation with 10 kDa Vivaspin 20 ultrafiltration units at 3260 xg.

Encapsulation of substrates, calcein and enzymes was performed by adding the respective enzyme or reactant to the bulk solution during polymersome formation. Polymersome formation was performed as described above with minor adjustments. Deionized water during the polymersome formation was exchanged by the respective enzyme or substrate in 50 mM bicin buffer and 100 mM NaCl. The 12 mL-stirred tank reactors were cooled to 4°C using an integrated cooling system in the bioREACTOR 48 block to counteract enzyme denaturation. After addition of the polymer solution, the dispersion was stirred for 7 h due to a prolonged formation process of polymersomes in bicin buffer at 4°C.

4.5.2 Dynamic light scattering

The polydispersity index (PDI), the intensity-based mean hydrodynamic diameter (z-average) and the number-based mean diameter (d_P) of the polymersomes were measured via dynamic light scattering on a ZetaSizer Nano-S. The light scattering was measured at 173°. Polymersomes were diluted to a concentration of 0.1 % w/v and 500 µL were measured in

standard cuvettes. Each measurement was performed in triplicates of 10 runs with automatic attenuation and measurement position.

For each polymersome preparation, the polydispersity index was ≤ 0.25, the z-average was approximately 185 nm in a narrow, monomodal size distribution and the d_P was approximately 110 nm. The average aggregation number has been determined to 43,000 polymer chains per polymersome (Poschenrieder *et al.*, 2016b).

4.5.3 Polymersome concentration measurements

The polymersome concentration was measured via absorbance at 350 nm. For each polymersome preparation, a standard curve was produced immediately after preparation to account for slight differences in polymersome size. The polymersome absorbance at 350 nm was linear in a range of 0 – 1 % w/v. Samples exceeding 1 % w/v were diluted appropriately.

4.5.4 Size exclusion chromatography

Functionalized polymersomes were separated from free proteins by size exclusion chromatography (SEC) using Sepharose 4B. Samples were applied on 2.5 mL or 12.5 mL laboratory columns at a volume equivalent to 4 % of the total bed volume. 1.5 CVs SEC running buffer were added in 100 µL or 500 µL increments, respectively, allowed to pass through the column by gravitational force, and collected in microcentrifuge tubes in 100 µL or 500 µL fractions, respectively. Protein or enzyme concentrations were determined by fluorescence or activity measurements. The polymersome concentration was determined via absorbance at 350 nm.

For larger polymersome quantities of up to 10 mL, a 140 mL preparative SEC column was used to separate functionalized polymersomes from free proteins. The preparative SEC was operated with an ÄKTAPure purification system at a flow rate of 1 mL min^{-1}.

4.5.5 Permeability assay

The permeability of the $PMOXA_{15}$-$PDMS_{68}$-$PMOXA_{15}$ membrane was determined by measuring the influx of the reactants into empty polymersomes. Empty polymersomes at a final concentration of 0.5 % w/v were added to 50 mM of each reactant and were incubated for at least 2 weeks at 30°C. At set time intervals, 100 µL samples were taken and purified via 2.5 mL-SEC. The short purification time of the SEC of approximately 5 min was substantially lower than the measured time allowed for passive diffusion of the molecules into the polymersomes of at 24 h for GlcNAc and ManNAc, 48 h for pyruvate and up to 336 h for

Neu5Ac, ATP and CTP. Thus, an error due to diffusion of the substances out of the polymersomes during the purification step can be neglected. After purification, the fractions containing polymersomes were pooled. The polymersomes were disintegrated with 1 % O-POE and the reactant concentrations were determined via enzymatic assays. For each assay polymersomes at a final concentration of 0.2 % w/v were added. Each reaction was performed at 30°C in 50 mM bicin, pH 8.0.

GlcNAc, ManNAc and Neu5Ac concentrations were determined via an *N*-acetylmannosamine dehydrogenase (ManDH) assay. The ManDH from *Flavobacterium* sp. 141-7 was used. The ManDH converts ManNAc to *N*-acetylmannosaminolactone by reducing NAD^+ to NADH and does not accept GlcNAc or Neu5Ac as substrate. *N*-acetylmannosaminolactone is readily hydrolyzed in aqueous solution, making the ManDH reaction irreversible (Figure 4.1) (Yamamoto-Otake *et al.*, 1991). Samples containing ManNAc were added to a reaction mixture containing 50 µg mL^{-1} ManDH and 5 mM NAD^+. Samples containing GlcNAc were added to a reaction mixture containing 50 µg mL^{-1} ManDH, 150 µg mL^{-1} AGE, 1 mM ATP and 5 mM NAD^+. Samples containing Neu5Ac were added to a reaction mixture containing 50 µg mL^{-1} ManDH, 150 µg mL^{-1} NAL and 5 mM NAD^+. Each reaction was allowed to proceed to completion, which was reached after 20 min. The substrate conversion was determined by measuring the NADH concentration in the sample after 20 min at 340 nm. Reactant concentrations were determined from a respective standard curve with known reactant concentrations in the range of 0 - 70 µM.

Pyruvate concentrations were determined via a lactate dehydrogenase assay (LDH). LDH was purchased from Sigma-Aldrich. The LDH reduces pyruvate to lactate by oxidizing NADH to NAD^+. The equilibrium lies far on the product side and thus the reaction is quasi-irreversible (Brooks *et al.*, 1999). Samples containing pyruvate were added to a reaction mixture containing 10 µg mL^{-1} LDH and 1 mM NADH. The reaction was allowed to proceed to completion, which was reached after 20 min. The substrate conversion was determined by measuring the NADH consumption after 20 min at 340 nm. Pyruvate concentrations were determined from a standard curve with known pyruvate concentrations in the range of 0 - 70 µM.

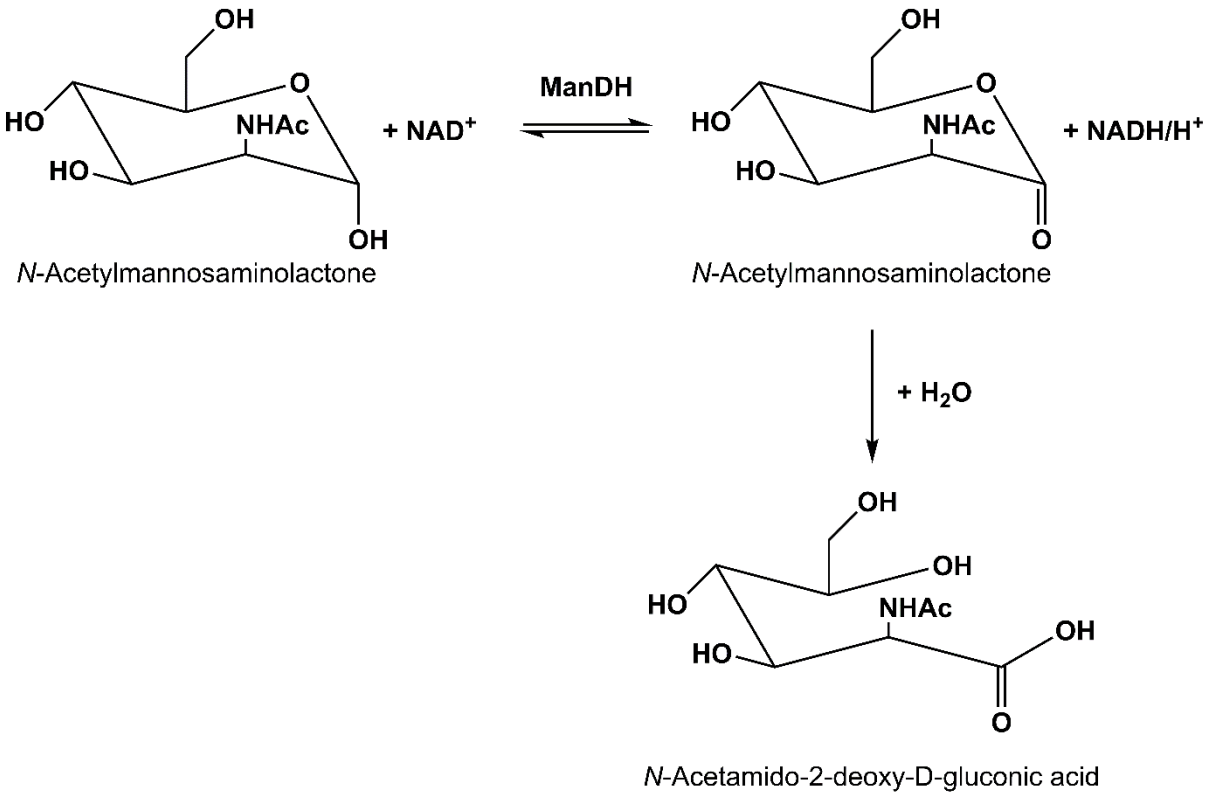

Figure 4.1 – Schematic reaction of the ManDH assay. The ManDH converts *N*-acetylmannosamine (ManNAc) to *N*-acetylmannosaminolactone by reducing NAD^+ to NADH and H^+. The *N*-acetylmannosaminolactone readily hydrolyzes in aqueous media to *N*-acetamido-2-deoxy-D-gluconic acid making the ManDH reaction irreversible.

CTP concentrations were determined via the quasi-irreversible CSS reaction. Because O-POE interfered with the CSS reaction, the polymersomes were pretreated with 1 % OG for 1 h at room temperature prior to CTP concentration measurements. The reaction mixture contained 50 µg mL^{-1} CSS, 3 mM Neu5Ac, 10 mM $MgCl_2$, 0.2 mM dithiothreitol (DTT) and 4 U mL^{-1} inorganic pyrophosphatase. The reaction was allowed to proceed to completion, which was reached after 5 min. CTP concentrations were determined from a standard curve with known CTP concentrations in the range of 0 – 70 µM.

ATP concentrations were determined using the Kinase-Glo® Luminescent Kinase Assay according to the supplier's manual. ATP concentrations were determined from a standard curve with known ATP concentrations in the range of 0 – 70 µM.

The reactant concentrations were used to determine the permeability *Pe* according to Equation 4.3.

$$\boldsymbol{Pe} = -\frac{\boldsymbol{V_A \cdot V_D}}{\boldsymbol{(V_A + V_D) \cdot A \cdot t}} \cdot \boldsymbol{ln}\left(\mathbf{1} - \frac{\boldsymbol{c_A}}{\boldsymbol{c_{eq}}}\right) \qquad \text{Equation 4.3}$$

with V_A = Total volume of the acceptor phase, cm^3

V_D = Total volume of the donor phase, cm^3

A = Total surface area of the polymer membrane, cm^2

t = Incubation time, s

c_A = Reactant concentration in the acceptor phase, mM

c_{eq} = Equilibrium concentration of the reactant, mM

The total volumes of the acceptor phase is the sum of all inner volumes of the polymersomes present in the sample. The inner volume of a polymersome was calculated from the number-based mean diameter d_P of 110 nm and the membrane thickness d_M of 14 nm. At 0.5 % w/v polymersomes and a total sample volume of 200 µL (0.2 cm^3), V_A was 0.62 µL ($6.2 \cdot 10^{-4}$ cm^3). The total volume of the donor phase was calculated by subtracting the total volume occupied by 0.5 % w/v polymersomes from the total sample volume and amounted to 198.57 µL ($1.9857 \cdot 10^{-1}$ cm^3). The remaining volume was occupied by the membrane and amounted to 0.81 µL ($8.1 \cdot 10^{-4}$ cm^3). The total outer surface area of the polymersomes under these conditions was 753.67 cm^2. The reactant concentration in the acceptor phase was determined as described above. The equilibrium concentration c_{eq} was determined according to Equation 4.4 and was 50.21 mM in all cases. Due to the volume occupied by the polymersomes, the initial concentration in the donor phase c_D was 50.36 mM of each reactant.

$$\boldsymbol{c_{eq}} = \frac{\boldsymbol{c_A \cdot V_A + c_D \cdot V_D}}{\boldsymbol{V_A + V_D}} \qquad \text{Equation 4.4}$$

4.5.6 Substrate diffusion through channel proteins

For measuring reactant diffusion through the membrane channel proteins, each reactant was first encapsulated in polymersomes by adding the reactant to the bulk solution during polymersome formation. Encapsulation concentrations were 500 mM GlcNAc, 500 mM ManNAc, 300 mM pyruvate, 100 mM Neu5Ac and 1 mM ATP. 10 % v/v of the respective membrane channel protein stock (1 mg mL^{-1} in 50 mM bicin, pH 8.0, and

0.6 % v/v O-POE) was added to purified, reactant-loaded polymersomes in the presence of the reaction mixtures described in Section 4.5.4. The final detergent concentration was 0.06 % w/v O-POE. Total sample volume was 100 µL with a polymersome concentration of 0.25 % w/v. The NADH or NAD^+ concentration was determined photometrically at 340 nm after 20 min. ATP release was determined after 20 min using the Kinase-Glo® Luminescent Kinase Assay according to the supplier's manual. As a negative control, polymersomes without channel proteins were investigated in parallel. 10 % v/v of a 0.6 % v/v O-POE solution was added to the negative control to account for potential detergent effects on the membrane permeability. As positive control, polymersomes were disintegrated with 3 % triton X-100 or 1 % O-POE to measure the maximum substrate concentration in the samples.

4.5.7 Peptide anchor insertion

Purified peptides anchors were added to preformed polymersomes and incubated at various temperatures for up to 72 h at 600 rpm in a thermal shaker. If not stated otherwise, surface functionalization with eGFP was performed for 4 h at 37°C. Surface functionalization with NAL and CSS was performed for at least 48 h at 4°C. Prolonged incubation at 4°C had no positive or negative effect on the peptide anchor insertion. The insertion buffer contained 10 mM phosphate buffer, pH 7.4, 250 mM NaCl and 135 mM imidazole.

4.5.8 Channel protein integration

For biosynthesis using polymersomes, membrane channel proteins were reconstituted in the polymer membrane during polymersome formation. The bulk solution and the components to be encapsulated were preassembled in the bioreactor. Since a rapid dilution of the membrane channel protein into the bioreactor would cause a dilution of the detergent below its critical micelle concentration and thus a precipitation of the membrane channel, the membrane channel protein was added to the ethanolic polymer solution and the mixture was instantly injected into the preassembled bioreactor under stirring at 4000 rpm. The amount of detergent injected during the polymersome formation process had a profound influence on the self-assembly of the polymer vesicles. Even at low detergent concentrations of 0.02 % v/v O-POE, no polymersome formation occurred. At 0.01 % v/v O-POE, no influence of the detergent on the polymersomes in terms of quality and quantity was observed. Because at least 0.6 % O-POE was required in the channel protein stock solution to keep the channel protein stable in aqueous solution, the addition of channel protein was restricted to a volume of 200 µL for a 12 mL nominal filling volume of the bioreactor (1.67 % v/v). With a maximum concentration of 2 mg mL^{-1} of OmpF and OmpF G119D in the stock solution, 33 µg mL^{-1}

were added to the bioreactor for both OmpF and OmpF G119D, corresponding to a protein-to-polymer ratio of 1:1500.

4.5.9 Confocal microscopy

Confocal microscopy images were taken on a FV-1000/IX81 confocal laser scanning microscope equipped with GaAsP detectors, an UPlanSApo ×60/1.20 objective and a 488 nm laser (Olympus, Tokyo, Japan). Exposure time was set to 2 µs/pixel, the laser was set to 500 *hv* with a gain of 1 and 3 % offset. Polymersomes were imaged at concentrations between 0.14 – 0.22 % w/v with 30 – 170 eGFP molecules immobilized per polymersome.

4.5.10 Calcein leakage experiments

For leakage experiments, calcein (25 mM) was dissolved in 0.1 M Tris–HCl, pH 8.0, and the polymersomes were formed in the calcein solution according to the method described in 4.5.1. Polymersomes and free calcein were separated on a preparative 140 mL SEC column. 50 µL of the purified polymersome dispersion were added to 50 µL of the protein solution in 96 well, chimney, black polystyrene assay plates immediately before fluorescence measurements. The sample fluorescence was measured for 12 h in an Infinite M200 microplate reader. Measurements were taken every 5 min with excitation and emission wavelengths of 485 and 515 nm, respectively, in top mode at gain 50. Negative controls were always included to differentiate between eGFP fluorescence and calcein fluorescence. The positive control included 3 % triton X-100 to disintegrate the polymersomes and force calcein release.

4.6 Protein and enzyme characterization

4.6.1 Fluorescence measurements

EGFP fluorescence was measured with an Infinite M200 microplate reader using 96 well, half area, black polystyrene assay plates and excitation and emission wavelengths of 485 and 515 nm, respectively.

The amount of immobilized eGFP was calculated from the effective fluorescence intensity *fl* of the functionalized polymersomes. Inner filter effects were observed during eGFP measurements caused by light absorption and light scattering of the polymersomes at the excitation (485 nm) and emission (515 nm) wavelengths of eGFP. This led to a reduction of eGFP fluorescence with increasing polymersome concentration. To account for the inner

filter effects when measuring eGFP fluorescence, eight standard curves of each eGFP fusion protein were analyzed at 0 – 0.5 % w/v polymersome concentration, resulting in eight straight lines according to Equation 4.5 with eight slopes, a_0 – a_7, per fusion protein (Appendix B, Figure B1).

$$\boldsymbol{fl = a_i \cdot c_{eGFP}} \qquad \text{Equation 4.5}$$

For each fusion protein, the slopes a_0 through a_7 decreased with increasing polymersome concentration, leading to the expected reduction in fluorescence in the presence of polymersomes.

Slopes a_0 – a_7 were plotted against the respective polymersome concentration to obtain a straight line according to Equation 4.6 with a slope *a'* and a y-intercept at slope a_0 without polymersomes (Appendix B, Figure B2).

$$\boldsymbol{a_i = a' \cdot c_{polymersomes} + a_0} \qquad \text{Equation 4.6}$$

After purification of eGFP-functionalized polymersomes from free eGFP, the polymersome concentration in each fraction was determined photometrically by measuring the absorbance at 350 nm. The absorbance of polymersomes at 350 nm was not significantly altered when adding 0 – 50 µg mL^{-1} eGFP (Appendix B, Figure B3). Subsequently, the eGFP concentration in each fraction was calculated from the effective fluorescence *fl* and the slope *a* at the given polymersome concentration according to Equation 4.7.

$$\boldsymbol{c_{eGFP} = \frac{fl}{a} = \frac{fl}{a' \cdot c_{polymersome} + a_0}} \qquad \text{Equation 4.7}$$

The standard curves were used for the determination of the correct eGFP concentration at a known polymersome concentration between 0 – 0.5 % polymersomes and the respective fluorescence intensity.

4.6.2 Enzyme activity assays

Enzyme activities were measured at 30°C and 600 rpm in a thermal shaker if not stated otherwise. Each assay was performed in 50 mM bicin buffer, pH 8.0, and 100 mM NaCl.

4.6.3 *N*-Acyl-D-glucosamine 2-epimerase assay

The encapsulation efficiency of the AGE K160I was determined enzymatically via a coupled assay with ManDH. The assay was performed in transparent 96 well plates in an Infinite M200 microplate reader set to 30°C with 2 s orbital shaking before each measurement. 128 mM GlcNAc, 1 mM ATP, 5 mM NAD^+, 25 µg mL^{-1} ManDH and 1 % v/v O-POE were added to polymersomes containing AGE K160I at a final concentration of 0.2 % w/v. O-POE was added to disintegrate the polymersomes and release encapsulated AGE K160I. The reaction kinetics was followed by determining the stoichiometric production of NADH for 20 min at a wavelength of 340 nm. The AGE K160I concentration was calculated from the initial reaction rate according to the Lambert-Beer law (described in Section 4.4.7) in 96 well plates with d = 0.3 cm and ε = 6220 L mol^{-1} cm^{-1}. Because O-POE had a negative effect on the reaction rate of the AGE K160I, the AGE K160I concentration was calculated from either a standard curve or a single reference measurement performed with soluble AGE K160I in known concentrations.

4.6.4 *N*-Acetylneuraminate lyase assay

The NAL activity was determined via high pressure liquid chromatography (HPLC). To determine the amount of NAL immobilized on the polymersomes, 250 mM ManNAc and 50 mM pyruvate were added to polymersomes at a final concentration of 0.1 - 0.2 % w/v and incubated for 2 to 24 h. The reaction was stopped by addition of 250 µL of the sample to 750 µL of 0.1 M H_2SO_4. The NAL concentration was calculated from the determined volumetric activity and the specific activity of the NAL under these conditions of 15.28 U mg^{-1}.

The kinetic parameters v_{max} and K_M for ManNAc of soluble and immobilized NAL were determined by measuring the initial reaction rates at varying substrate concentrations from 0-300 mM ManNAc at constant 50 mM pyruvate. The K_M for pyruvate was determined at 0-50 mM pyruvate at constant 250 mM ManNAc. The reaction rates at given substrate concentrations were plotted in SigmaPlot 12.8. Kinetic parameters were determined by fitting Equation 3.1 to the data by non-linear regression using a least square fit.

4.6.5 CMP-sialic acid synthetase assay

The CSS activity was determined via the Phosphate Colorimetric Assay Kit according to the supplier's manual. To determine the amount of CSS immobilized on the polymersomes, 3 mM CTP, 5 mM Neu5Ac, 10 mM $MgCl_2$, 0.2 mM DTT and 4 U mL^{-1} inorganic pyrophosphatase to convert the product PP_i to 2 P_i were added to the polymersomes at a final concentration of 0.1 – 0.2 % w/v. The production of P_i was quantified photometrically at

650 nm. The CSS concentration was calculated from the determined volumetric activity and the specific activity of the CSS under these conditions of 159.9 U mg^{-1}.

The kinetic parameters v_{max} and K_M of soluble and immobilized CSS were determined by measuring the initial reaction rates at varying substrate concentrations from 0-25 mM CTP at constant 5 mM Neu5Ac and 0-50 mM Neu5Ac at constant 3 mM CTP. Each reaction included 10 mM $MgCl_2$ and 0.2 mM DTT and 4 U mL^{-1} inorganic pyrophosphatase to convert the product PP_i to 2 P_i. The reaction rates at given substrate concentrations were plotted in SigmaPlot 12.8. Kinetic parameters were determined by fitting Equation 3.1 to the data by non-linear regression using a least square fit.

The stability of soluble and immobilized CSS was determined at standard reaction conditions of 3 mM CTP, 5 mM Neu5Ac, 10 mM $MgCl_2$, 0.2 mM DTT and 4 U mL^{-1} inorganic pyrophosphatase to convert the product PP_i to 2 P_i.

4.6.6 CMP-*N*-acetylneuraminic acid synthesis in nano-scale enzyme membrane reactors

The three-enzyme cascade reaction was performed by adding 0.13 – 0.24 % w/v of the nano-scale enzyme membrane reactors to a reaction mixture containing 128 mM GlcNAc, 80 mM pyruvate, 3 mM or 50 mM CTP, 10 mM $MgCl_2$ and 0.2 mM DTT to a final volume of 350 µL. The reaction was allowed to proceed for at least 93 h. Reactant concentrations were determined at least twice a day. CMP-Neu5Ac production was determined indirectly by measuring the produced P_i via the Phosphate Colorimetric Assay Kit according to the supplier's manual. The P_i was generated from the by-product PP_i by adding 4 U mL^{-1} inorganic pyrophosphatase to the reaction mixture. Final intermediate concentrations were determined via HPLC by adding 250 µL of the sample to 750 µL of 0.1 M H_2SO_4.

4.6.7 High pressure liquid chromatography

HPLC was performed with an Agilent 1100 HPLC-System equipped with a Biorad Aminex HPX-87H column at 60°C and a Micro-Guard Cation H Cartridge as pre-column. The flow-rate was set to 0.5 mL min^{-1} with an injection volume of 20 µL per sample. Samples were run for 18 min with 5 mM H_2SO_4 as running buffer. Product and intermediate concentrations were determined by correlation of the peak area of the UV/Vis detector signal at 210 nm to appropriate standard curves.

4.7 *In vitro* protein synthesis

4.7.1 Template DNA preparation

Template DNA for IVPS was propagated using *E. coli* DH5α and was purified using the GenElute Maxiprep Kit according to the supplier's manual. All work was carried out under RNase-free conditions by treating the workspace and the equipment with RNase AWAY® prior to use.

4.7.2 *In vitro* protein synthesis in the presence of polymersomes

IVPS were carried out according to the suppliers' manuals in a total volume of 100 µL. *E. coli* lysate and wheat germ extract were purchased from Promega, insect cell and Chinese hamster ovary (CHO) lysate were generously provided by the Bioanalytics and Bioprocesses (IZI-BB) group (Dr. Kubick) of the Fraunhofer Institute for Cell Therapy and Immunology (IZI) in Potsdam, Germany.

RNase-free polymersomes were prepared in sterile 12 mL-reactors equipped with RNase-free water. To avoid any RNase contamination during the polymersome formation procedure, the lid and the stirrers of the bioREACTOR 48 were soaked in water containing 0.1 % diethylpyrocarbonate (DEPC) for at least 12 h at room temperature. The DEPC was removed by autoclaving the reactor lid and the stirrers at 121°C for 20 min prior to use. The RNase-free polymersomes were added to the IVPS systems at a final concentration of 0.2 % w/v. To reduce any residual RNase activity, the RNase inhibitor RNasin® Ribonuclease Inhibitor was added to all IVPS runs to minimize RNA degradation. Each IVPS was assembled in 0.5 mL PCR tubes to a final volume of 0.1 mL. Incubation was performed in a BioRad Thermo Cycler. *E. coli* lysate was incubated at 37°C for 2 h, insect cell lysate was incubated at 32°C for 2 h, CHO lysate was incubated at 30°C for 2 h, and wheat germ extract was incubated at 25°C for 1.5 h. After synthesis, IVPS samples containing eGFP were incubated at 37°C for another 4 h to allow chromophore formation of eGFP and peptide insertion. Subsequently, the IVPS was chilled on ice for 15 min. IVPS samples containing CSS were incubated at 4°C over night. Each sample was centrifuged at 50,377 xg for 30 min before being loaded onto 2.5 mL-SEC columns to separate the functionalized polymersomes from other IVPS components.

5. Surface functionalization of polymersomes using hydrophobic peptide anchors[1]

5.1 Selection of peptide anchors

For the surface functionalization of polymersomes using hydrophobic peptide anchors, five peptides were selected from literature. These comprised the hydrophobic peptide anchors of cytochrome b_5 (Cytb_5') from rabbit liver (Spatz and Strittmatter, 1971) and the ubiquitine-conjugating enzyme 6 (UBC6') from *Saccharomyces cerevisiae* (Kutay *et al.*, 1993), the membrane-binding domain of the syntaxin Vam3p (Vam3p') from *S. cerevisiae* (Hofmann *et al.*, 2006), the membrane-associated domain of the lysis protein L (L') of the bacteriophage MS2 (Szostak *et al.*, 1996) and an artificial transmembrane peptide consisting of an alpha-helical repetition of alanines and leucines (PolyAL) (Whitley *et al.*, 1994). Since the required properties of the peptides for their ability to insert into polymeric membranes were unknown, the hydrophobic peptides were selected on the basis of different characteristics including their origin, the type of membrane they naturally attach to, the peptide length and their hydrophobicity. The properties of each peptide anchor are listed in Table 5.1. Whereas the origin and the type of membrane they insert into may play a crucial role for the general ability of peptide insertion into the polymer membrane, different peptide lengths were chosen to minimize possible mismatch phenomena between peptide length and membrane thickness which may be crucial for or influence peptide insertion. Furthermore, a certain hydrophobicity may be required as driving force for penetration of the hydrophilic PMOXA block and peptide insertion into the hydrophobic PDMS block. Important for the selection was a general inability of the peptide anchors to form pores in lipid membranes and thus disturb membrane integrity. Cytb_5' and L' represent moderately hydrophobic peptide anchors with lengths of 43 and 55 amino acids, respectively, whereas UBC6' and Vam3p' represent short peptides with 17 and 19 amino acids with a high content of hydrophobic amino acids of above 80 %. The artificial peptide PolyAL has a medium length of 31 amino acids and represents the most hydrophobic anchor with a content of hydrophobic amino acids of 96 %. The antibacterial Cecropin A (CecA) of the moth *Hyalophora cecropia* served

[1] Parts of the results shown here have been published in Klermund, L., Poschenrieder, S. T. and Castiglione, K., 2016a, Simple surface functionalization of polymersomes using non-antibacterial peptide anchors, *J Nanobiotechnol* **14**

as a reference peptide, whose integration into PIB-PEG-PIB polymersomes has been previously demonstrated (Noor *et al.*, 2012).

Table 5.1 – Peptide anchor characteristics

Peptide anchor	Origin	Natural membrane	Length, # amino acids	Hydrophobic amino acids, %	Location
Cytb_5'	Rabbit liver	Mitochondrial	43	56	C-terminal
L'	Phage	Bacterial	55	47	C-terminal
UBC6'	Yeast	Yeast	17	83	C-terminal
Vam3p'	Yeast	Vacuolal	19	84	C-terminal
PolyAL	Artificial	-	31	96	N-terminal
CecA	Moth	Bacterial	37	46	N-terminal

5.1.1 Expression and purification

For easy detection and quantification of the peptide insertion, each peptide anchor was fused to eGFP on gene level. This allowed for a fast quantification of the peptide insertion via fluorescence. Cytb_5', L', UBC6' and Vam3p' naturally occur at the C-terminus, thus *cytb_5'*, *l'*, *ubc6'* and *vam3p'* were cloned C-terminal of *egfp* while *polyAL* was cloned N-terminal of *egfp* resulting in the fusion proteins eGFP-Cytb_5', eGFP-L', eGFP-UBC6', eGFP-Vam3p' and PolyAL-eGFP (Figure 5.1). The gene of the antibacterial CecA was cloned N-terminal of *egfp* (CecA-eGFP) according to Noor *et al.* (2012). The fusion constructs contained a His_6-tag adjacent to the eGFP moiety and opposite of the peptide anchor to allow purification via IMAC without interfering with peptide insertion.

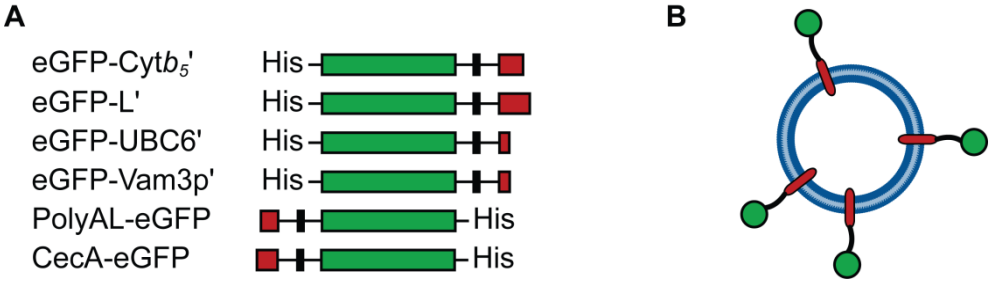

Figure 5.1 – Schematic depiction of eGFP-fused peptide anchors (A) and functionalized polymersomes (B), with eGFP (*green*), the respective peptide anchor (*red*) and a decaalanine linker (*black*). The hexahistidine tag (His) was cloned opposite of the peptide anchor to not interfere with peptide insertion.

The fusion proteins were heterologously expressed in *E. coli* BL21 (DE3). In accordance with the ability of the hydrophobic peptide anchors to tether eGFP to the cytosolic membrane, the yield of soluble fusion protein did usually not exceed 1 mg per liter shake flask expression culture. SDS-PAGE analysis revealed that the majority of the target protein was present in the insoluble cell debris. Thus, a membrane solubilization step was introduced to extract the target protein from the membrane. The addition of 2 % v/v NP-40 to the cell lysate and subsequent incubation in a rotary shaker for 2 h significantly increased the purification yields by 2.9 – 6.1-fold depending on the respective peptide anchor (Figure 5.2).

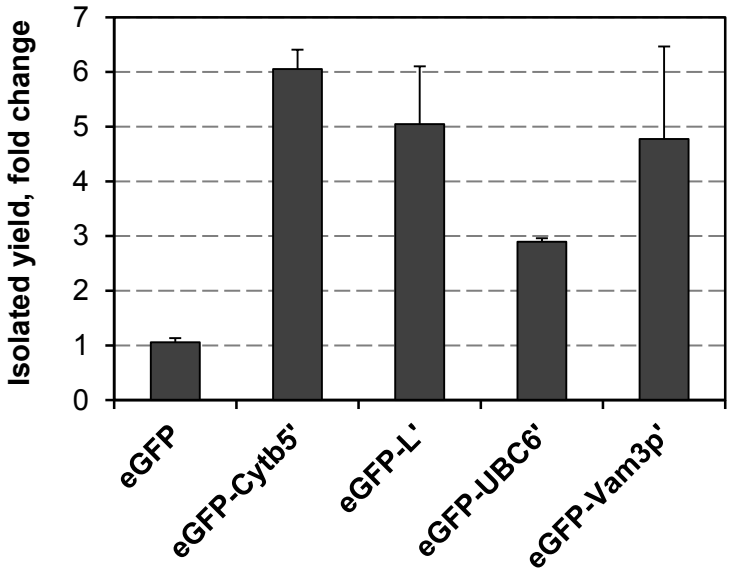

Figure 5.2 – Fold change of isolated yield obtained with solubilization step with the detergent NP-40 compared to the isolated yield without solubilization step. Whereas the yield of eGFP without peptide anchor is not increased, eGFP with peptide anchors can be solubilized from the membrane using NP-40, demonstrating a binding of the eGFP to the membrane conferred by the peptide anchors.

Since NP-40 affected the integrity of the polymer membrane (Appendix B, Figure B4), no detergent was used during purification via IMAC to reduce residual NP-40 to a minimum. Omitting detergent during the purification step had no apparent effect on the purification yield as judged by fluorescence and protein concentration measurements (data not shown). For each peptide anchor, SDS-PAGE analysis revealed two distinct bands after purification corresponding in mass to eGFP and eGFP fused to the respective peptide anchor, as exemplarily shown for eGFP-Cytb_5' in Figure 5.3 B (lane 1). Depending on the peptide anchor and the expression batch, 25-80 % of the protein was not conjugated to the respective peptide anchor, suggesting a partial cleavage of the hydrophobic peptides from the eGFP. Since the hydrophobic peptide anchors substantially increase the hydrophobicity of the target protein, the target proteins were polished using hydrophobic interaction chromatography (HIC). The exemplary elution profile of eGFP-Cytb_5' and the subsequent

SDS-PAGE analysis shown in Figure 5.3 demonstrate that the two protein species could be successfully separated using HIC. Both protein species displayed typical eGFP fluorescence, further demonstrating that both species indeed contained eGFP. After purification and polishing, isolated expression yields of 2.7, 5.5, 0.6, 2.1 and 1.2 mg per liter shake flask expression culture were generally obtained for eGFP-Cytb_5', eGFP-L', eGFP-UBC6', eGFP-Vam3p' and CecA-eGFP, respectively. EGFP without peptide anchor reached expression yields of 24 mg L^{-1} under the same conditions. Typical protein concentrations after purification ranged from 50 to 500 µg mL^{-1}. Interestingly, high salt concentrations (0.5 M NaCl, 0.27 – 0.5 M imidazole) stabilized the fusion proteins in solution and prevented protein precipitation during storage. Especially eGFP-UBC6' and eGFP-Vam3p' quickly precipitated when dialyzed against low salt buffers (e.g. 0.1 M Tris–HCl, pH 8.0). Except for eGFP-UBC6' and eGFP-Vam3p', which could be stored for 2 - 5 days, the fusion proteins were stable for several weeks at protein concentrations of up to 500 µg mL^{-1} when stored in high salt buffers. Thus, Cytb_5', L' and CecA were most suitable for application in terms of protein preparation and storage stability.

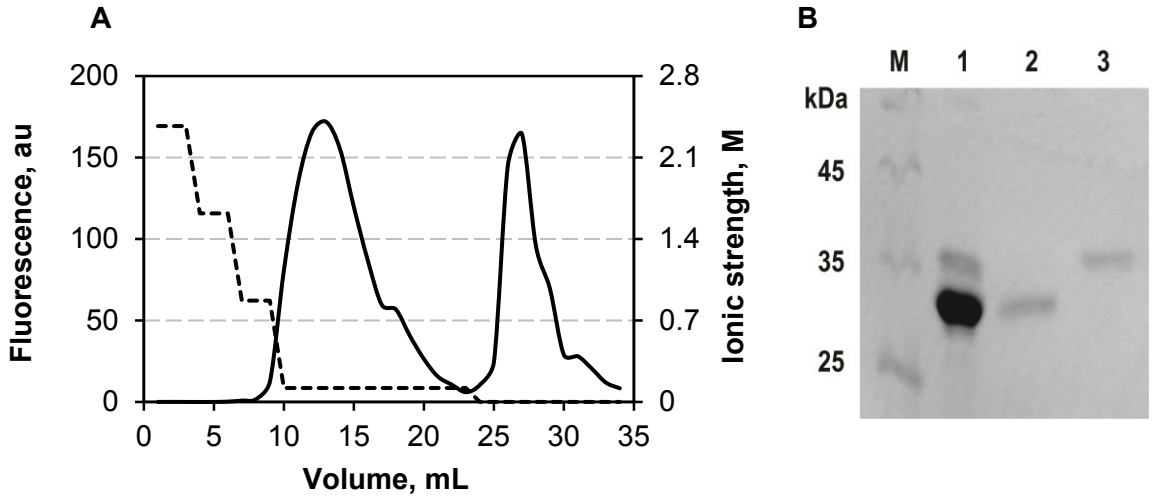

Figure 5.3 – Elution profile of the measured fluorescence (*solid line*) at decreasing ionic strength (*dashed line*) (A) and SDS-PAGE analysis (B) of the protein polishing using hydrophobic interaction chromatography. EGFP without peptide anchor eluted in fraction 10 – 20, eGFP-Cytb_5' eluted in fraction 25 – 30. SDS-PAGE of purified target protein before HIC (*lane 1*) as well as fraction 13 (*lane 2*) and fraction 27 (*lane 3*) after HIC. Fluorescence is given in arbitrary units (au).

In contrast, no detectable fluorescence was measured when expressing PolyAL-eGFP, indicating that the extremely hydrophobic PolyAL hindered functional expression of eGFP. SDS-PAGE revealed that small amounts of PolyAL-eGFP were present in the insoluble cell debris, however, treatment with NP-40 led to no increase in fluorescence or protein yield. Since a solubilization of the other peptide anchors upon NP-40 treatment was observed, the low protein yield suggests that the hydrophobic peptide PolyAL is not inserted into the

membrane but strongly aggregates to inclusion bodies. To prevent the peptide anchor from aggregating, the solubility-enhancing maltose binding protein (MBP), including a tobacco etch virus (TEV) protease cleavage site, was cloned N-terminal of PolyAL-eGFP, leading to a cleavable MBP-TEV-PolyAL-eGFP fusion protein. Since the solubility tag was cloned at the membrane interacting side of the peptide anchor, potential peptide insertion into the membrane was also prevented. Although the expression of MBP-TEV-PolyAL-eGFP could be increased to some extent at 20°C and 37°C expression temperatures, no fluorescence of the target protein was detected and, unfortunately, the MBP-TEV moiety did not render the protein more soluble as judged by SDS-PAGE (data not shown). Thus, due to its strong hydrophobicity, PolyAL could not be expressed in soluble form and was therefore not further considered a suitable peptide anchor for the spontaneous insertion into polymer membranes and no further attempts to express the protein were performed.

5.1.2 Characteriztaion of eGFP-fusion proteins

Important for a suitable and applicable peptide anchor for the surface functionalization of polymersomes is a low impact of the peptide anchor on the protein function. To assess the influence of the peptide anchors on the correct folding of eGFP, the fluorescence intensity of each purified fusion protein was compared to eGFP without peptide anchor (Figure 5.4). EGFP retained full fluorescence when fused to Cytb_5' and L' with 103 ± 6 % and 103 ± 10 % relative fluorescence. In contrast, eGFP-UBC6' and eGFP-Vam3p' had relative fluorescence intensities of 12 ± 2 and 27 ± 6 %, respectively, indicating a profound effect of the small and highly hydrophobic peptides UBC6' and Vam3p' on protein folding and chromophore formation of eGFP. The reference peptide CecA had a relative fluorescence of 38 ± 4 % which is in congruence with a decrease in eGFP fluorescence observed by Noor *et al.* (2012).

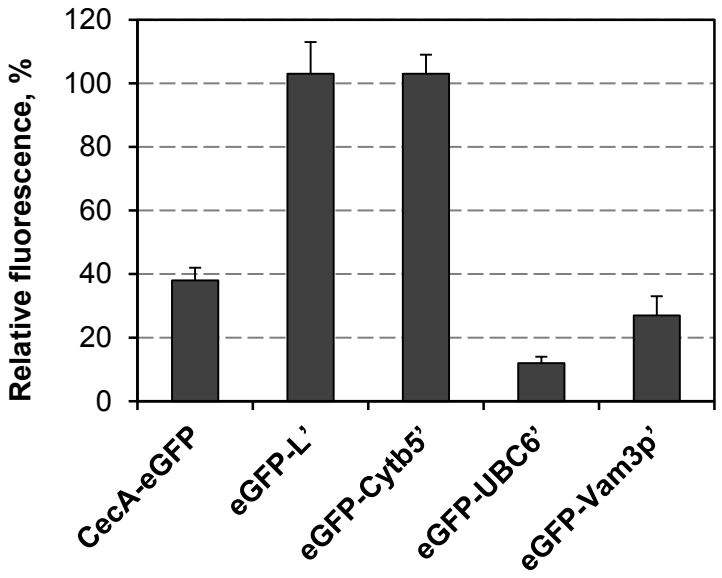

Figure 5.4 – Relative fluorescence of the eGFP fused to each peptide anchor compared to eGFP without peptide anchor as reference. The moderately hydrophobic peptide anchors Cytb_5' and L' have no impact on eGFP fluorescence. In contrast, the highly hydrophobic peptide anchors UBC6' and Vam3p' reduce eGFP fluorescence significantly. CecA, although less hydrophobic, also reduces eGFP fluorescence.

5.2 Characterization of peptide anchor insertion

Since adding fusion protein during the polymersome formation would lead to a non-directional integration of the peptide anchor, yielding eGFP on the outer and the inner surface of the membrane, the insertion of the peptide anchors into $PMOXA_{15}$-$PDMS_{68}$-$PMOXA_{15}$ membranes was studied by adding eGFP-Cytb_5', eGFP-L', eGFP-UBC6', eGFP-Vam3p' and CecA-eGFP to preformed polymersomes. $PMOXA_{15}$-$PDMS_{68}$-$PMOXA_{15}$ polymersomes were thus formed by self-assembly in 12 mL-stirred tank reactors under vigorous stirring according to the method of Poschenrieder *et al.* (2016b) until a particle size distribution with a polydispersity index (PDI) below 0.2 was reached. After addition of the fusion proteins to the preformed polymersomes and subsequent incubation, functionalized polymersomes were separated from free protein by size-exclusion chromatography (SEC). Figure 5.5 shows a schematic representation of the surface functionalization procedure. The insertion was characterized by detecting and quantifying the fluorescence in the polymersome fractions. The polymersomes were detected and quantified via absorbance at 350 nm and qualitatively analyzed via dynamic light scattering (DLS).

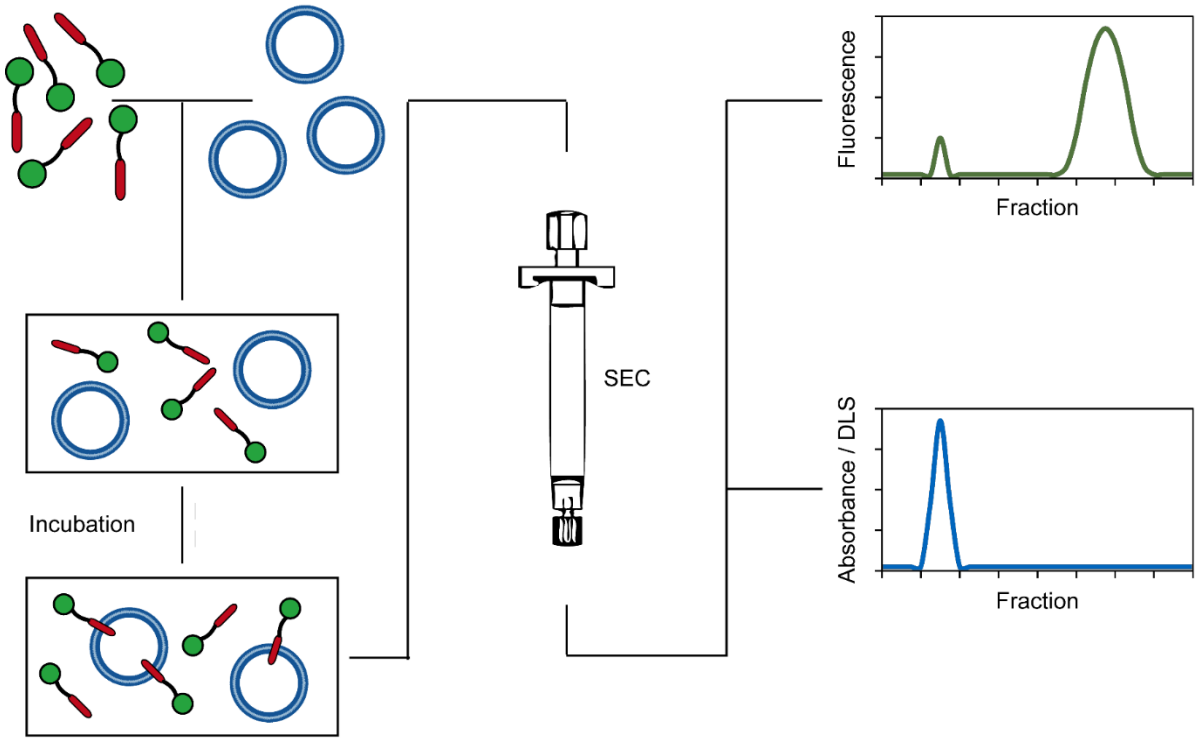

Figure 5.5 – Schematic depiction of the spontaneous peptide insertion. Purified fusion proteins are added to preformed polymersomes and incubated under various conditions. Surface functionalized polymersomes and free fusion proteins are separated by size exclusion chromatography (SEC) and detected and quantified via absorbance and dynamic light scattering (DLS), and fluorescence, respectively. A co-localization of the absorbance and fluorescence peak indicates successful peptide insertion.

5.2.1 Spontaneous peptide insertion

Figure 5.6 A-F depict the fluorescence and absorbance chromatograms after the addition of eGFP and eGFP fused to each peptide anchor to polymersomes for 4 h at 37°C in 0.02 M phosphate buffer, pH 7.4 with 0.25 M NaCl and 0.14 M imidazole. Without peptide anchor, eGFP was separated from the polymersomes at high resolution, indicating no unspecific interactions between the eGFP moiety and the polymersomes. When adding eGFP fused to either peptide anchor, fluorescence was detected in the fractions containing polymersomes. Thus, a co-localization of the absorbance peak and the fluorescence peak was observed, demonstrating that each peptide anchor was capable of tethering eGFP to the polymersomes' surface. The lack of interaction between the eGFP moiety and the polymersomes validates that adhesion of eGFP to the polymersomes was indeed conferred by the peptide anchors. Negative controls without polymersomes did not show fluorescence in the respective fractions where polymersomes were usually detected (data not shown).

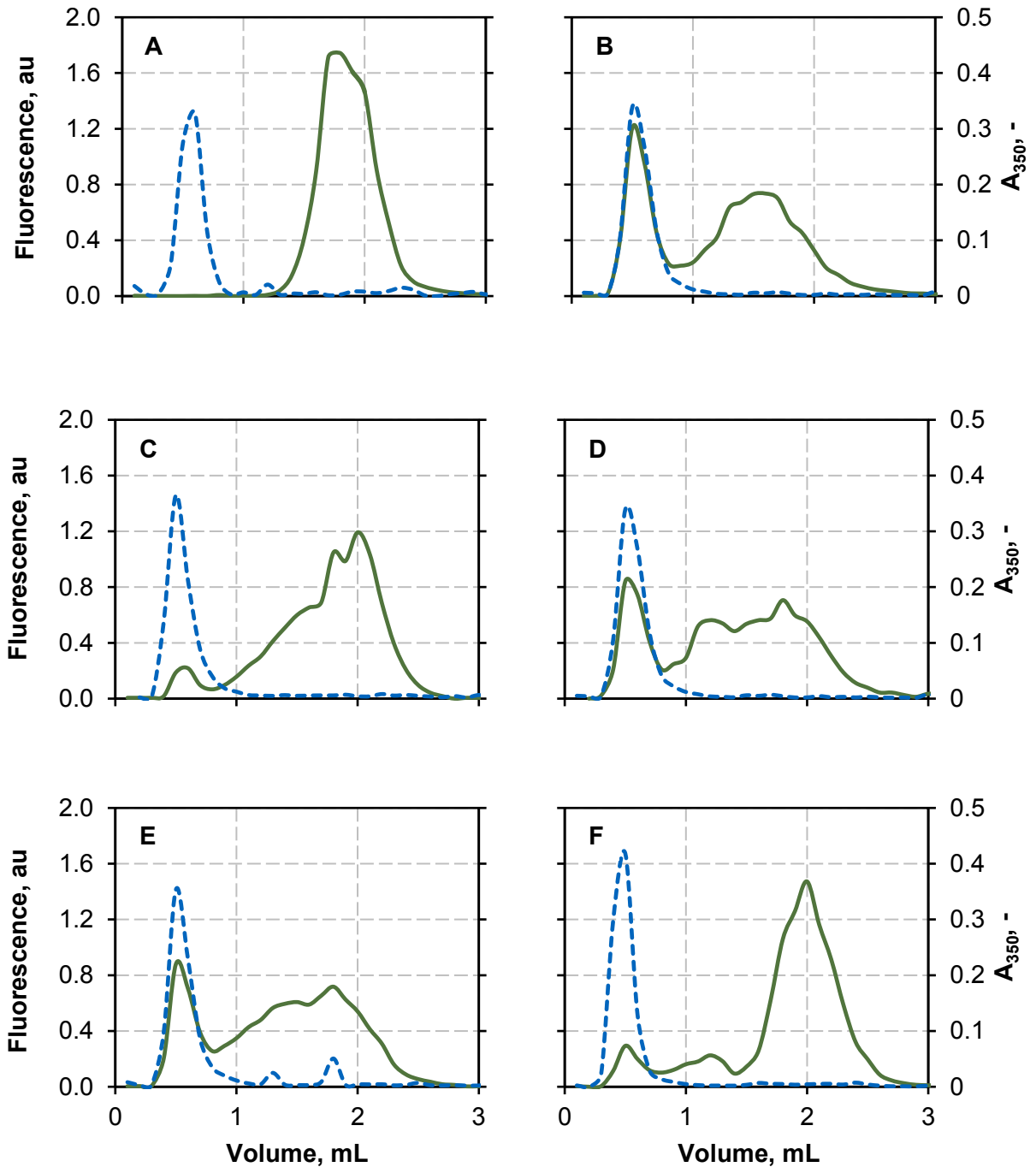

Figure 5.6 – Size-exclusion chromatography of $PMOXA_{15}$-$PDMS_{68}$-$PMOXA_{15}$ polymersomes. EGFP (A), eGFP-Cytb_5' (B), eGFP-L' (C), eGFP-UBC6' (D), eGFP-Vam3p' (E) and CecA-eGFP (F) after surface functionalization for 4 h at 37 °C. Polymersomes were quantified by measuring light absorbance at 350 nm (*black, dashed*), the presence of eGFP was verified by fluorescence signal (*green, solid*). Each run is the mean of a triplicate determination. Fluorescence is given in arbitrary units (au).

To visualize the adhesion of eGFP to the polymersomes, confocal microscopy images of purified polymersomes before and after functionalization with peptide anchors were taken. Although the resolution of the confocal microscope was not sufficient to depict the surface localization of eGFP on single polymersomes, a clustering of the fluorescence to the

polymersomes was observed after functionalization with peptide anchor-fused eGFP only. This clustering further demonstrates peptide insertion and eGFP immobilization on the polymersome surfaces, as exemplarily shown for eGFP-Cytb_5' (Figure 5.7). Polymersomes incubated with eGFP without peptide anchor showed no fluorescence before or after functionalization.

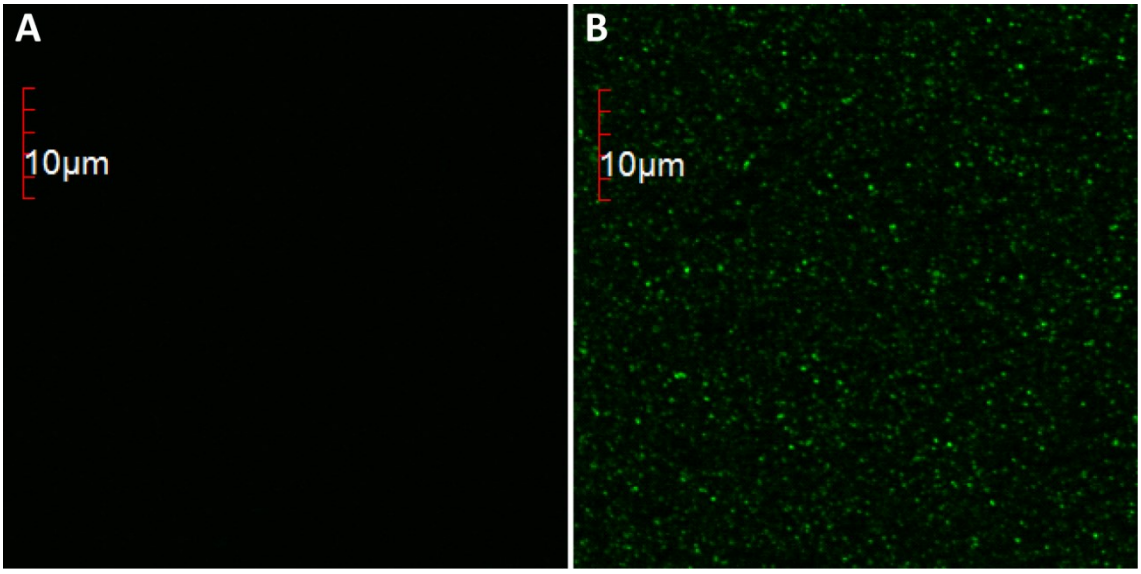

Figure 5.7 – Confocal microscopy images of non-functionalized polymersomes (A) and purified, eGFP-functionalized polymersomes with Cytb_5' as peptide anchor containing on average 170 molecules per polymersome (B). The scale bar is 10 µm.

Qualitative comparison of the peptide anchor insertion revealed that approximately 26 % of the total amount of eGFP-Cytb_5' and 21 % of the total amount of eGFP-UBC6' inserted into the polymersomes. Employing Vam3p' as peptide anchor, approximately 10 % of the fluorescence was measured in the fractions containing polymersomes, whereas for eGFP-L′ and CecA-eGFP approximately 6 % of the total fluorescence was co-localized with the polymersomes, indicating that a majority of the protein remained in solution.

Reloading of functionalized polymersomes onto SEC columns after 6 weeks of storage, as exemplarily shown for eGFP-Cytb_5' and eGFP-Vam3p' in Figure 5.8, led to a single fluorescence peak co-localized with the absorbance peak of the polymersomes without the presence of free eGFP. The same fluorescence to absorbance ratio as before the reapplication to the column was obtained. The reduced fluorescence and absorbance signal was due to dilution effects of the SEC. No dissociation of the hydrophobic peptide anchors from the membrane was observed within the measured time span of 6 weeks of storage, which clearly demonstrates a strong hydrophobic interaction between the peptide anchors and the membrane core and a high stability of immobilized eGFP.

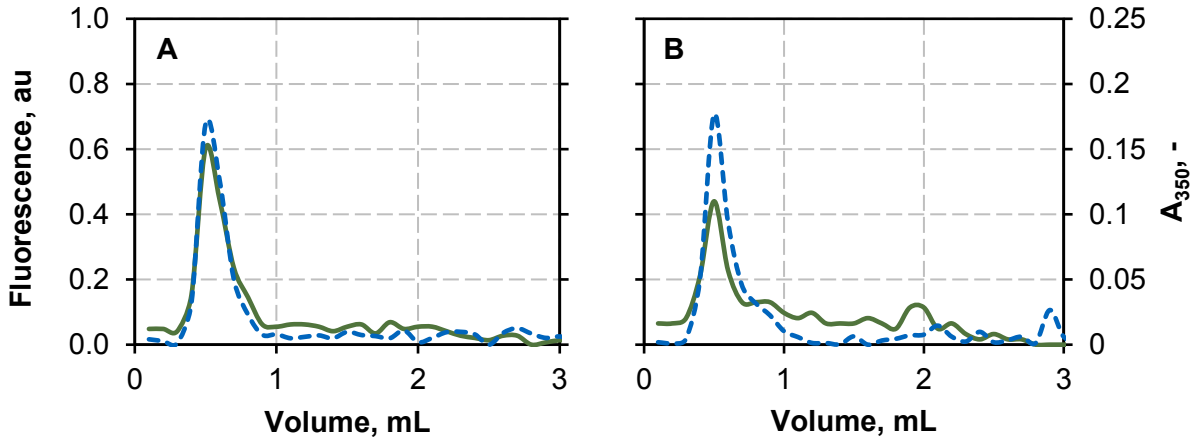

Figure 5.8 – Reapplication of surface functionalized polymersomes with eGFP-Cytb_5' (A) and eGFP-Vam3p' (B) on SEC columns after 6 weeks of storage at 4°C. Polymersomes were determined via A_{350} (*blue, dashed*) and eGFP was detected via fluorescence (*green, solid*). No dissociation of the protein from the polymersomes could be detected.

5.2.2 Insertion kinetics

To optimize the peptide insertion into the polymer membrane, the insertion of each peptide anchor was analyzed over a time period of 48 h to investigate the insertion kinetics at various temperatures (Figure 5.9).

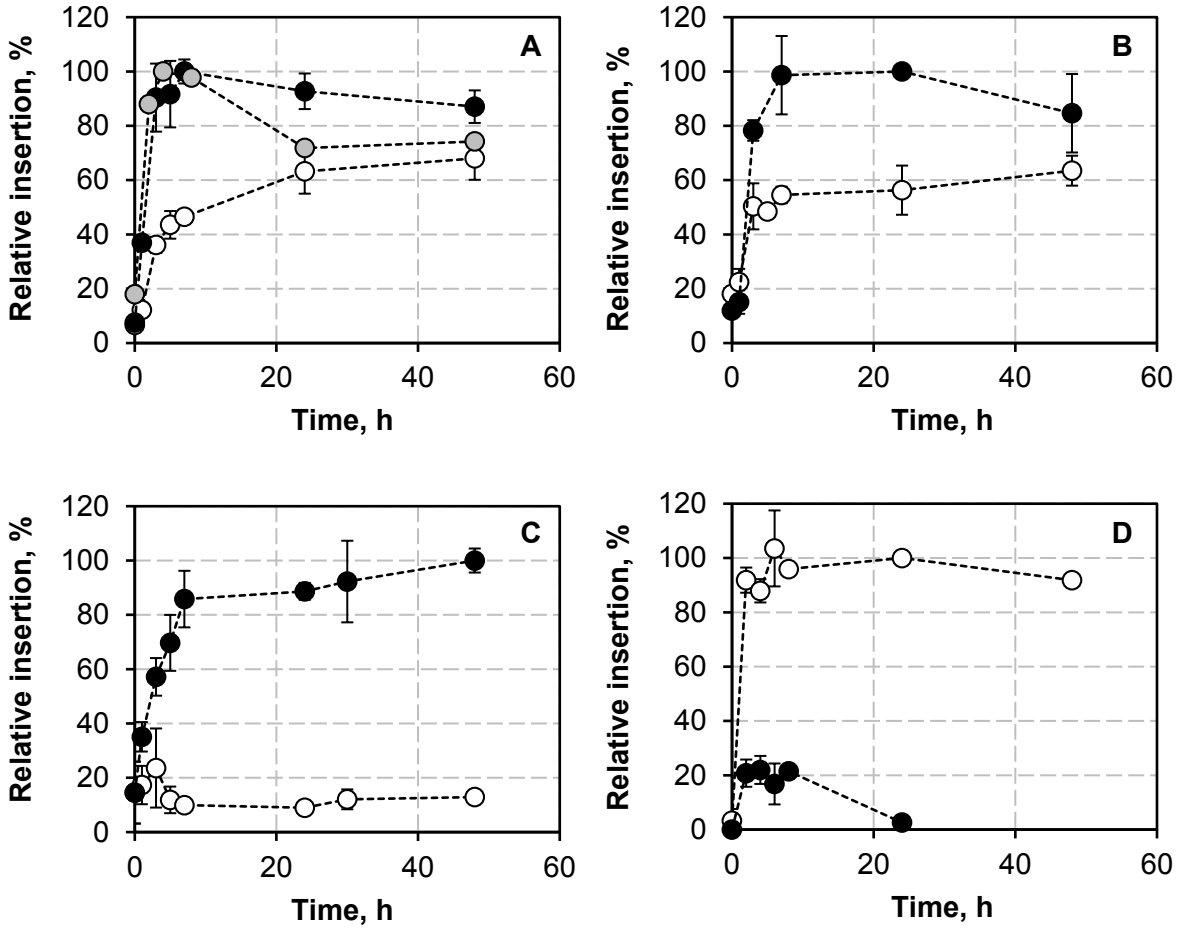

Figure 5.9 – Insertion kinetics of eGFP-Cytb_5' (A), eGFP-L' (B), eGFP-UBC6' (C) and eGFP-Vam3p' (D) into $PMOXA_{15}$-$PDMS_{68}$-$PMOXA_{15}$ polymersomes at insertion temperatures of 4°C (*white*), 37°C (*black*) and, where applicable, at 42°C (*gray*). The highest measured insertion was set to 100 %. The lines serve for visualization.

The data revealed that the peptide anchors inserted spontaneously into the polymer membrane at temperatures ranging from 4 to 42°C (Figure 5.9). Cytb_5' showed a maximum insertion into the polymer membrane within 3 – 7 h at 37°C and 42°C, with a slightly faster insertion at 42°C (Figure 5.9 A, B). Incubation for more than 12 h led to a decrease in fluorescence, which was more prominent at 42°C and may be due to heat denaturation of eGFP. Similarly, L' inserted into the polymer membrane within 3-7 hours at 37°C with a slight reduction in fluorescence after incubations exceeding 12 h. At 4°C, maximum insertion of Cytb_5' and L' was reached after approximately 48 h and was approximately 60 – 70 % of the maximum insertion obtained at 37°C. Prolonged incubation for 72 h led to no further insertion, indicating that peptide insertion is equilibrium controlled (data not shown). In contrast, UBC6' insertion at 4°C was greatly reduced, reaching a relative insertion of 10 % compared to the insertion at 37°C (Figure 5.9 C). At 37°C, peptide insertion increased almost linearly for 7 h and remained stable with a slight increase for the next 40 h. Vam3p', on the

other hand, showed a strongly reduced insertion at 37°C (Figure 5.9 D), which was mainly due to an instability of eGFP-Vam3p' in solution at elevated temperatures.

5.2.3 Quantitative analysis of peptide insertion

To obtain a quantitative measure of the peptide insertion, the amount of eGFP molecules per polymersome was calculated from the effective fluorescence intensity *fl* of the functionalized polymersomes (details in section 4.6.1). The number of polymersomes n_{Pol} per liter was estimated from the concentration of polymer in the dispersion m_{Pol} in g L^{-1}, the molar mass of the copolymer MM_{Pol} of 7600 g mol^{-1}, the average aggregation number N_{Agg} of 43,000 mole polymers per mole polymersome (Poschenrieder *et al.*, 2016b) and the Avogadro's constant N_A of $6.022 \cdot 10^{23}$ mol^{-1} according to Equation 5.1.

$$\boldsymbol{n_{Pol} = \frac{m_{Pol} \cdot N_A}{MM_{Pol} \cdot N_{Agg}}} \qquad \text{Equation 5.1}$$

At a constant polymersome concentration, a linear increase of immobilized eGFP per polymersome was observed with increasing protein concentration, which is demonstrated in Fig. 5.10 for eGFP-Cytb_5' and eGFP-L', in which the slope denotes the insertion efficiency of the respective peptide. Thus, by doubling the protein concentration, double the amount of eGFP was immobilized on the polymersomes' surface.

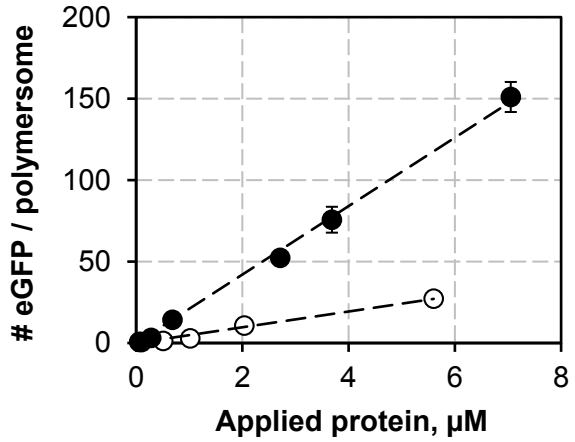

Figure 5.10 – Linear dependency of the presented eGFP molecules per polymersome on the applied protein concentration as exemplarily shown for eGFP-Cytb_5' (*black*) and eGFP-L' (*white*). The lines were calculated by fitting the data by linear regression.

At 0.5 % w/v polymersomes, eGFP-UBC6' showed the highest insertion with an insertion efficiency of 26.8 ± 2.6 molecules per polymersome per micromolar concentration of applied protein (pol^{-1} μM^{-1}) (Figure 5.11). For eGFP-Cytb_5' an insertion efficiency of 20.7 ± 0.7 eGFP-Cytb_5' pol^{-1} μM^{-1} was calculated, followed by eGFP-L′, eGFP-Vam3p′ and CecA-eGFP with insertion efficiencies of 4.8 ± 0.2, 3.7 ± 0.4 and 1.6 ± 0.1 pol^{-1} μM^{-1}, respectively (Figure 5.11 A). At the highest protein concentration of 7.1 μM eGFP-Cytb_5', Cytb_5' immobilized approximately 150 eGFP molecules per polymersome with a total of 9.2 × 10^{15} polymersomes per liter (0.5 % w/v), whereas up to 49 eGFP-UBC6', 27 eGFP-L′, 16 eGFP-Vam3p′ and 10 CecA-eGFP molecules were immobilized per polymersome, however, at lower initial protein concentrations of 1.6 μM eGFP-UBC6', 5.6 μM eGFP-L′, 4.6 μM eGFP-Vam3p′ and 6.4 μM CecA-eGFP. A further increase in the amount of eGFP immobilized per polymersome was limited by the solubility of the respective fusion protein in solution, which was approximately 0.5 mg mL^{-1} for eGFP-Cytb_5', eGFP-L' and CecA-eGFP and below 0.25 mg mL^{-1} for eGFP-Vam3p' and eGFP-UBC6'.

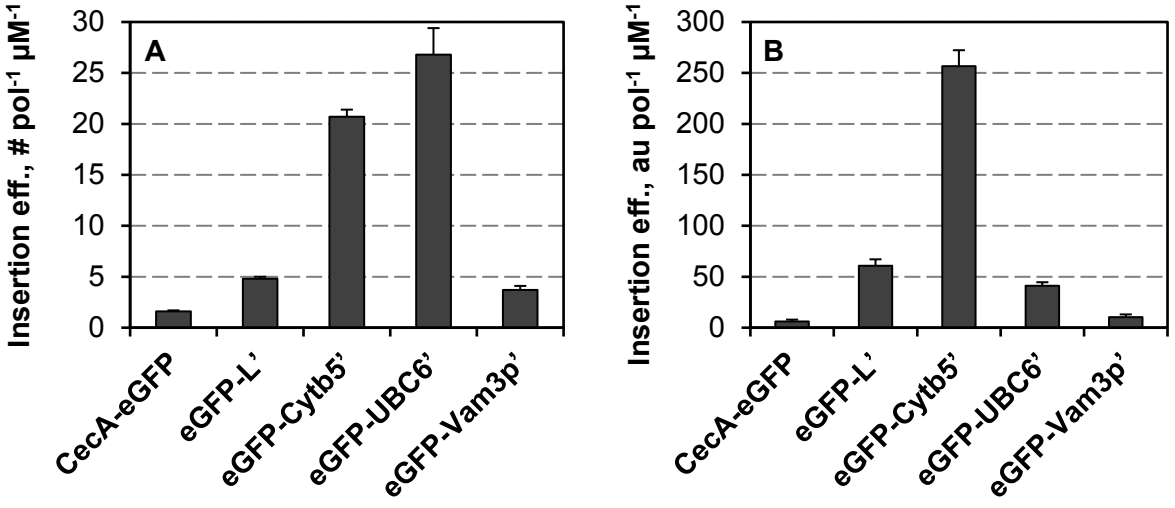

Figure 5.11 – Insertion efficiency (Insertion eff.) of each peptide anchor in terms of eGFP molecules (#) immobilized per polymersome per applied protein concentration (A) and fluorescence (au) per polymersome per applied protein concentration (B). The peptide anchors are sorted after increasing hydrophobicity from left to right. The number based insertion efficiency increases with increasing hydrophobicity. EGFP-Vam3p' aggregated at the insertion conditions. The fluorescence based insertion efficiency is dependent on the number based insertion efficiency and the relative fluorescence of the respective eGFP with peptide anchor (Figure 5.4). Fluorescence is given in arbitrary units (au).

With no influence of Cytb_5' on the eGFP fluorescence and a high insertion efficiency, Cytb_5' was able to mediate 256.6 ± 15.7 au per polymersome and micromolar applied protein (au pol^{-1} μM^{-1}) (Figure 5.11 B). Although UBC6' displayed the highest insertion efficiency, its strong influence on the eGFP fluorescence resulted in 41.2 ± 3.4 au pol^{-1} μM^{-1} only. In turn,

the high relative fluorescence of eGFP when fused to L' balanced the low insertion efficiency resulting in 60.8 ± 6.3 au pol^{-1} μM^{-1}. With relatively low insertion effiencies and low relative fluorescences, eGFP-Vam3p' and CecA-eGFP resulted in a polymersome fluorescence of 10.4 ± 2.7 and 6.1 ± 1.8 au pol^{-1} μM^{-1}.

In contrast to the linear dependency of the insertion on the applied protein concentration, increasing or decreasing the polymersome concentration, which is equivalent to a change in the available surface area for peptide insertion, had no effect on the absolute amount of eGFP that was immobilized at a constant applied protein concentration. For example, the absolute amount of immobilized eGFP per polymersome concentration followed an apparent saturation kinetics with a maximum of 38 μg mL^{-1} immobilized eGFP-Cytb_5' at an initially applied 130 μg mL^{-1} eGFP-Cytb_5' (29 % insertion) (Figure 5.12 A). Thus, peptide insertion seemed to be controlled by an equilibrium between immobilized and free protein independent of the available surface area. In log-log scale this behavior is represented by an inversely proportional dependency of the immobilized eGFP molecules per polymersome with increasing polymersome concentration (Figure 5.12 B).

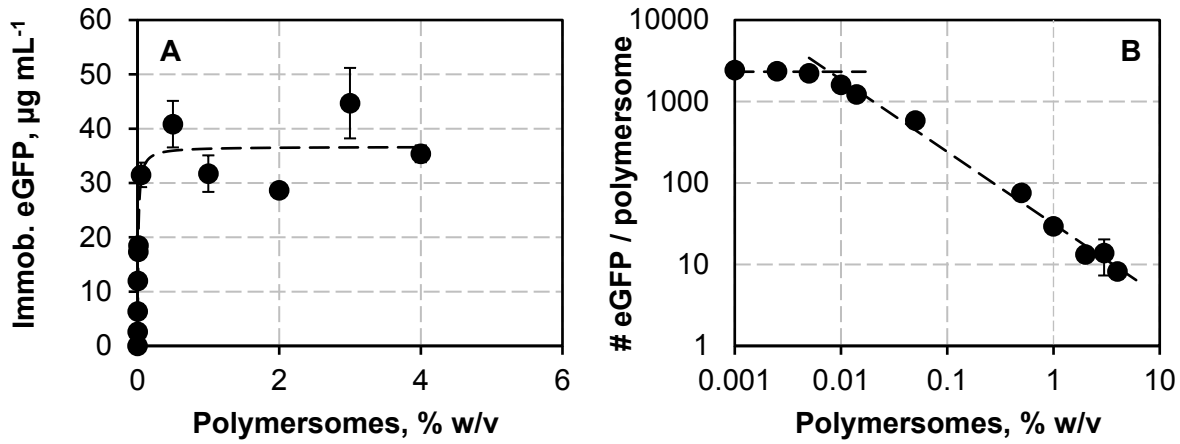

Figure 5.12 – Immobilized (Immob.) eGFP-Cytb_5' (A) and immobilized eGFP molecules (#) per polymersome in log-log scale (B) at varying polymersome concentrations. The amount of immobilized eGFP is independent of the polymersome concentration until the maximum loading capacity of the polymersomes of 2320 ± 280 eGFP molecules per polymersome is reached. The line in (A) was obtained by fitting the data to a saturation kinetics according to Equation 3.1. The lines in (B) were obtained by fitting the data points from 0.5 - 4.0 % w/v and 0.001 – 0.005 % w/v polymersomes to a power function of the form $y = a \cdot x^b$ by non-linear regression.

Below 0.05 % w/v polymersomes, the insertion behavior started to deviate from the linear trend as the polymersome surface area became limiting, resulting in a reduced insertion efficiency of only 14 % at 0.014 % w/v polymersomes and 13 % at 0.010 % w/v polymersomes. Below 0.005 % w/v polymersomes, the amount of eGFP per polymersome

reached a constant value of 2320 ± 280. This value is in perfect agreement with the theoretical maximum loading capacity of 2254 eGFP molecules that can be presented on a single polymersome at the densest two dimensional packing arrangement of eGFP without steric hindrance (Figure 5.13). The maximum loading capacity was calculated from the available surface area A_S of a single polymersome (Equation 5.2) and the largest two-dimensional area A_{eGFP} that is occupied by each eGFP on the surface, which can be calculated from any plane going through the center of a globular protein according to Equation 5.3.

$$\boldsymbol{A_S = 4\,\pi\,\cdot\,r_S^2} \qquad \text{Equation 5.2}$$

$$\boldsymbol{A_{eGFP} = \pi\,\cdot\,r_{eGFP}^2} \qquad \text{Equation 5.3}$$

For the case of the eGFP molecules lying directly on the polymersome's surface, the radius r_S determines the available surface area and must be extended by the distance from the polymersome's surface to the protein core according to Equation 5.4.

$$\boldsymbol{r_S = r_P + r_{eGFP} = \frac{d_P}{2} + r_{eGFP}} \qquad \text{Equation 5.4}$$

Thus, the radius r_S, as depicted in Figure 5.13, was derived from the number-based mean diameter of the polymersomes d_P of 110 nm, which was measured by dynamic light scattering, and the hydrodynamic radius r_{eGFP} of eGFP of 2.3 nm (Hink *et al.*, 2000). At the highest-density hexagonal packing arrangement of equal circles, which is equivalent to the two dimensional packing of spheres, 90.7 % of the available surface area A_S (90.7 % A_S = 37,422.8 nm^2) can be covered by the circular areas occupied by eGFP (A_{eGFP} = 16.6 nm^2), resulting in a maximum loading capacity of 2254 eGFP molecules per polymersome.

The perfect agreement of the experimental and the theoretical data demonstrate that the polymersomes could be fully loaded with eGFP using peptide anchors, completely covering the surface of polymersomes.

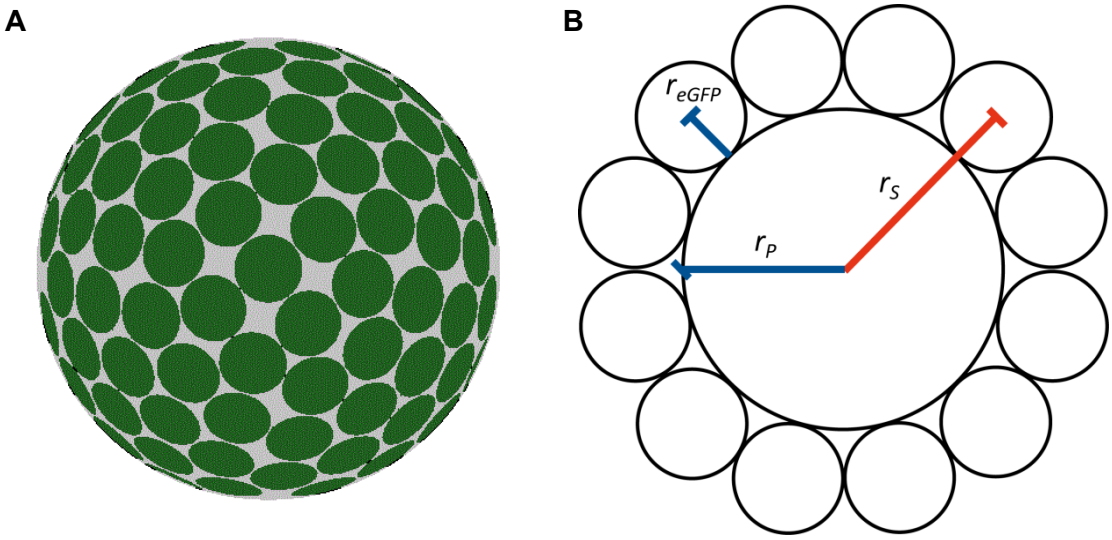

Figure 5.13 – Schematic representation of the highest-density hexagonal packing of circles on a sphere (A) and schematic depiction of the radii used for the calculation of the theoretical maximal loading capacity (B). The total radius r_s is calculated from the polymersome radius r_p of 55 nm and the hydrodynamic radius of eGFP r_{eGFP} of 2.3 nm.

5.2.4 Polymersome stability during peptide insertion

Because membrane integrity is crucial for polymersome applications, calcein leakage experiments were performed to investigate membrane integrity during peptide anchor insertion. Polymersomes were loaded with calcein at a self-quenching concentration of 25 mM and the calcein release during peptide insertion was monitored via an increase in fluorescence, as exemplarily shown for eGFP-L' and eGFP-Cytb_5' (Figure 5.14). As expected, no calcein leakage was detected within 12 h of incubation of each peptide anchor with calcein-loaded polymersomes at 37°C. Thus, none of the peptides substantially destabilized or formed pores within the polymer membrane. Notably, the insertion of CecA, which is known to form pores in lipid membranes, led to no calcein leakage when added at a peptide-to-polymer ratio of 1:200. Although CecA-induced calcein release is concentration dependent, calcein release from liposomes has been demonstrated for peptide-to-lipid ratios of 1:280 and lower (Silvestro *et al.*, 1997), indicating that either polymersomes are more stable than liposomes, pore formation is sterically hampered by the hydrophilic eGFP moiety or CecA insertion is not as efficient in the polymer membrane as in lipid membranes.

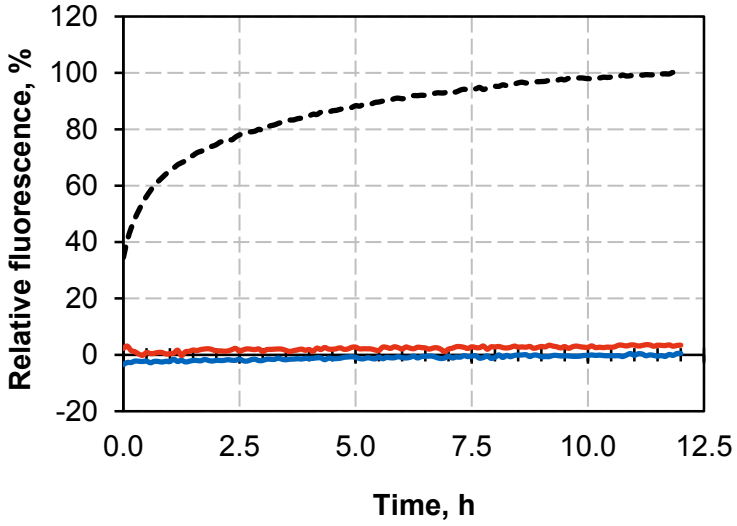

Figure 5.14 – Calcein leakage experiments during peptide insertion of Cytb_5' (*blue*) and L' (*red*) into calcein-loaded polymersomes. A reduction in membrane integrity leads to the release of self-quenched calcein from the polymersome interior and a subsequent increase in fluorescence and was only observed for the positive control, which was treated with 3 % triton X-100 to rupture the polymer membrane (*black dashed*). The highest fluorescence obtained in the positive control was served as 100 % reference.

5.3 Discussion

The insertion of antibacterial peptides such as alamethicin, gramicidin and cecropin A into polymeric membranes has been shown to occur spontaneously and without the addition of additives (Kita-Tokarczyk *et al.*, 2005; Vijayan *et al.*, 2005; Haefele *et al.*, 2006; Wong *et al.*, 2006; Gonzalez-Perez *et al.*, 2009). Yet, the factors influencing peptide insertion as well as insertion kinetics have not been investigated. Furthermore, natural, non-antibacterial peptides are usually highly hydrophobic and do not possess the same amphiphilicity as antibacterial peptides, which by nature need to be both soluble in aqueous solution and in hydrophobic membranes. Nevertheless, the hydrophobic, non-antibacterial peptide anchors Cytb_5', L', UBC6' and Vam3p' readily inserted into preformed $PMOXA_{15}$-$PDMS_{68}$-$PMOXA_{15}$ polymersomes in a similar manner to the various membrane proteins (Wong *et al.*, 2006; Kumar *et al.*, 2007; Onaca *et al.*, 2009; Graff *et al.*, 2010; Nallani *et al.*, 2011) and antibacterial peptides (Vijayan *et al.*, 2005; Haefele *et al.*, 2006; Wong *et al.*, 2006; Noor *et al.*, 2012) that have been incorporated into polymer membranes in the recent years. Peptide insertion occurred immediately after addition of the peptide anchors to the polymer vesicles, which is evidence that the hydrophobic driving force of non-antibacterial peptides is strong enough to penetrate and insert into polymeric membranes despite being soluble in aqueous solution without stabilization by detergents.

A similar stabilizing effect of high salt concentrations on amphiphilic fusion proteins observed in this study was described by the group of Strittmatter, who purified the membrane-bound

NADH-cytochrome b_5 reductase from calf and steer liver using the detergent triton X-100 (Spatz and Strittmatter, 1971). Although the amphiphilic protein was stabilized with deoxycholate during the purification process, subsequent removal of the detergent led to water-soluble NADH-cytochrome b_5 reductase (Spatz and Strittmatter, 1971). In low salt concentrations of 0.02 M Tris acetate and 2 mM ethylenediaminetetraacetic acid (EDTA), pH 8.1, the protein precipitated, leading to a 50 % reduction in activity. The precipitate could be resolved and the activity restored by incubating the protein solution in 0.1 M NaCl for 5 h at 25°C (Spatz and Strittmatter, 1971; Rogers and Strittmatter, 1975). Since the protein has a large hydrophilic domain of 264 amino acid (Ozols *et al.*, 1985) as opposed to a hydrophobic domain of 36 amino acids (Ozols *et al.*, 1984), the increased stability of the protein at high salt concentrations may be due to a conformational stabilization of the hydrophilic moiety in aqueous solution rather than a stabilization of the membrane anchor.

Overall, the data suggest that a certain hydrophobicity of the peptide anchor is required for spontaneous peptide insertion, as CecA and L′ are the least hydrophobic peptides. Furthermore, peptide length may influence the peptide insertion efficiency due to mismatch phenomena. This mismatch between peptide length and membrane thickness arises from the larger thickness of the polymer membrane of approximately 14 nm (Poschenrieder *et al.*, 2016b) compared to the thickness of natural lipid bilayers of 3 – 5 nm (Le Meins *et al.*, 2011). Yet, it has been demonstrated that polymer membranes are highly compressible (Pata and Dan, 2003; Itel *et al.*, 2015) and the relatively high insertion of the 17 amino acid UBC6' anchor seems to validate these results. Yet, naturally occurring membrane peptides and integral membrane proteins are evolutionarily optimized to span natural bilayers, which in turn may impose a negative effect on peptide insertion into the polymer membrane (Pata and Dan, 2003). However, the length of the peptide anchors had no clear effect on membrane insertion, despite covering a broad range of 17–55 amino acids. Each peptide anchor was capable of anchoring eGFP to the polymersomes' surface, regardless of the differences in hydrophobicity and peptide length, establishing a general feasibility of spontaneously inserting non-antibacterial peptide anchors into polymer membranes and suggesting that other non-antibacterial peptides which have not been covered in this study, also integrate into polymer membranes.

Remarkably, the insertion kinetics of the peptide anchor Cytb_5' into polymersomes was strikingly similar to full length cytochrome b_5 insertion into liposomes despite the differences in membrane composition and thickness. Rogers and Strittmatter (1975) obtained a maximum cytochrome b_5 insertion within 50 h at 4 °C and within 10 h at 32 °C which is in congruence with a maximum insertion obtained after 48 h at 4 °C and within 7 h at 37 °C for peptide anchor insertion of Cytb_5' into polymersomes. The similar behavior of polymersomal and liposomal integration of hydrophobic peptides is supported by a recent study by Itel *et al.*

(2014, 2015) who report that the lateral diffusion of proteins within polymer membranes is intriguingly similar to lipid membranes and that the polymer compressibility allows the incorporation of hydrophobic peptides, regardless of size and structure. With a glass transition temperature of the PDMS block of −123 °C (Prinos and Panayiotou, 1995), no glass transition of the hydrophobic block occurs between 4 and 42 °C and the increase in the time required for insertion at lower temperatures is expected to be mainly due to reduced Brownian motion rather than a more condensed membrane structure.

Furthermore, a concentration dependent increase in peptide insertion for cytochrome b_5 into liposomes with a maximum loading capacity of 244 molecules per liposome was observed, which is equivalent to a peptide-to-lipid ratio of 1:11 (Rogers and Strittmatter, 1975). With a liposome diameter of 60 nm, Rogers and Strittmatter (1975) estimated that approximately 82 % of the total surface are occupied by cytochrome b_5. Using polymer vesicles, a similar insertion with a peptide-to-polymer ratio of 1:17 at the maximum loading capacity of 2320 ± 280 molecules per polymersome was achieved. With an average number-based mean diameter of 110 nm of the polymersomes and a hydrodynamic radius of eGFP of 2.3 nm, a theoretical 2254 molecules can be presented on a single polymersome at the highest-density hexagonal packing arrangement of equal circles, indicating that the surface of the polymersomes is completely occupied by the hydrophilic eGFP moiety.

For the potential use of polymersomes in medical and biotechnological applications, the surface functionalization of polymer membranes plays a major role, which is reflected in the many different strategies that have been proposed for immobilizing proteins and other ligands on polymer surfaces. These include non-covalent interactions of biotinylated polymers and ligands (Rigler and Meier, 2006), non-covalent interactions of Ni^{2+}-NTA-conjugated polymers with His_6-tagged proteins (Nehring *et al.*, 2010), chemical conjugation using click-chemistry (Egli *et al.*, 2011a) and thioether bonds (Pang *et al.*, 2008), as well as genetic fusion of antibacterial peptides (Noor *et al.*, 2012) to the target protein.

Although several immobilization strategies have been investigated, only few data exist that allow for a quantitative comparison. Noor *et al.* (2012), who have investigated the immobilization of eGFP using the antibacterial peptide CecA, unfortunately gave no quantified data on the immobilization events. The highest degree of polymersome surface functionalization has been reported by Pang *et al.* (2008), who chemically coupled thiolated antibody OX26 to maleimide-conjugated poly(ethyleneglycol)-poly(ε-caprolactone) (PEG-PCL) polymersomes (d_P ≈ 100 nm) immobilizing up to 162 OX26 per polymersome. The polymersomes In contrast, the non-covalent immobilization employing Ni^{2+}-NTA-functionalized PB-PEO polymersomes (d_P > 100 nm) report a maximum of 24 immobilized red fluorescent protein molecules per polymersome (Nehring *et al.*, 2010). The numbers of molecules immobilized per polymersome are in range with our measurements with

0.5 % w/v polymersomes harboring up to 16 - 150 eGFP molecules depending on the peptide anchor. With a maximum loading capacity of 2320 ± 280 eGFP molecules that could be immobilized using the peptide anchor Cytb_5' per single polymersome (d_P = 110 nm), the use of non-antibacterial peptides for surface functionalization reaches similar values as the maximum loading capacity of biotinylated PMOXA-PDMS diblock polymersomes of 1921 ± 357 fluorescently labeled avidin molecules (Rigler and Meier, 2006). In contrast, Egli *et al.* (2011) have reported the immobilization of 57 molecules of the fluorescent dye Alexa Fluor 633 but only 5 enhanced yellow fluorescent protein molecules per polymersome using chemical conjugation of 4-formylbenzoate-conjugated PMOXA-PDMS diblock polymersomes to 6-hydrazinonicotinate acetone hydrazine, suggesting that the accessibility of the pre-conjugated polymer may be a problem when immobilizing proteins compared to significantly smaller fluorescent dyes.

Thus, the surface functionalization of polymersomes with hydrophobic, non-pore forming peptide anchors performs extremely well compared to other, more complex immobilization techniques. The simplicity of the protein immobilization elevates the surface functionalization using hydrophobic peptide anchors to an easy to use, versatile and simple surface functionalization tool that can be performed at extremely mild conditions (e.g., 4 °C, pH 8.0) and does not require tedious chemical pre-conjugation of the polymer. Furthermore, it does not require an optimization of a conjugated-to-non-conjugated polymer ratio due to polymersome formation problems caused by changes in the hydrophilic weight fraction of the copolymer.

The main challenge for using peptide anchors to immobilize target proteins on polymer surfaces was not the insertion of the peptide into the membrane but finding a peptide anchor with sufficient amphiphilicity to be recombinantly expressible in soluble form, have little effect on the target protein and exhibit enough hydrophobic force to spontaneously insert into the membrane. With Cytb_5' and L', two suitable peptide anchors were identified that readily insert into $PMOXA_{15}$-$PDMS_{68}$-$PMOXA_{15}$ polymersomes, have no effect on eGFP fluorescence and are stable in aqueous solution after recombinant expression in *E. coli*. Although UBC6' showed a good insertion efficiency, the low stability in solution and the strong influence on the eGFP fluorescence make UBC6' unfit for the surface functionalization of polymersomes. Similarly, the impact of Vam3p' and CecA on eGFP fluorescence combined with the low insertion efficiencies are unfavorable for the surface functionalization of polymersomes.

Conclusively, the surface functionalization of polymersomes with a hydrophilic protein could be mediated by several hydrophobic peptide anchors and is not limited to antibacterial peptides or pre-conjugated polymers. The purified eGFP-coupled peptide anchors Cytb_5', L', UBC6' and Vam3p' spontaneously inserted into $PMOXA_{15}$-$PDMS_{68}$-$PMOXA_{15}$ membranes in a concentration dependent manner at a broad temperature range from 4 to 42 °C. Up to

2320 ± 280 eGFP-Cytb_5' molecules were immobilized per polymersome with an average of 9.2×10^{13} polymersomes per liter. This exceeds the largest amount of protein that has been immobilized on a single polymersome found in literature by a 14-fold. Furthermore, the peptide insertion is not limited to antibacterial peptides, which are amphiphilic by nature to be both soluble in aqueous solution and to insert spontaneously into membranes, but could be performed with eukaryotic and viral peptides that are not capable of pore formation. Since the capability of pore formation is an intrinsic property of the peptide, no pore formation is expected for Cytb_5', L', UBC6' and Vam3p' in any polymeric membrane, regardless of the peptide concentration and the thickness, compressibility and fluidity of the membrane, making these peptide anchors universally applicable for any type of polymersome.

6. CMP-Neu5Ac synthesis with functionalized nano-scale enzyme membrane reactors

Enzymatic cascade reactions, that is the combination of several enzyme reactions in one pot without the isolation of intermediates, have great potential for the establishment of sustainable chemical processes. However, many cascade reactions suffer from cross-inhibitions by components of the reaction system. By immobilizing enzymes on the outer surface and entrapping enzymes in the inner lumen of polymersomes, nano-scale enzyme membrane reactors can be created that are capable of spatially separating the incompatible reactions. Thus, polymersomes may overcome limits to multienzyme reactions which encounter cross-inhibitions by compartmentalizing the reaction space. To assess the applicability of $PMOXA_{15}$-$PDMS_{68}$-$PMOXA_{15}$ polymersomes as nano-scale enzyme membrane reactors for the performance of incompatible reaction cascades, the exemplary three-step biosynthesis of CMP-*N*-acetylneuraminic acid (CMP-Neu5Ac) from *N*-acetylglucosamine (GlcNAc), pyruvate and CTP was performed. The incompatibility of the system mainly arises from a strong inhibition of the substrate CTP of the third reaction, the activation of *N*-acetylneuraminic acid with CTP to form CMP-Neu5Ac by a CMP-sialic acid synthetase (CSS), on the enzyme of the first reaction, the epimerization of GlcNAc to *N*-acetylmannosamine (ManNAc) by an *N*-acyl-D-glucosamine 2-epimerase (AGE). In this study, the AGE K160I variant from *Anabaena variabilis* ATCC 29413, the NAL from *E. coli* K12 and the CSS from *Neisseria meningitidis* were used.

Figure 6.1 shows the devised nano-scale enzyme membrane reactor. To shield the AGE K160I from cross-inhibitions of components of the cascade reaction, especially the strong inhibition of CTP (inhibition constant K_i = 1 mM), the AGE K160I was to be encapsulated within the polymersomes and the NAL and the CSS were to be presented in the outer reaction space, thereby compartmentalizing the cascade reaction. To yield a single biocatalytic entity and thus be able to retain and recover the biocatalyst, the NAL and the CSS were to be immobilized on the surface of the polymersomes rendering highly functionalized nano-scale enzyme membrane reactors.

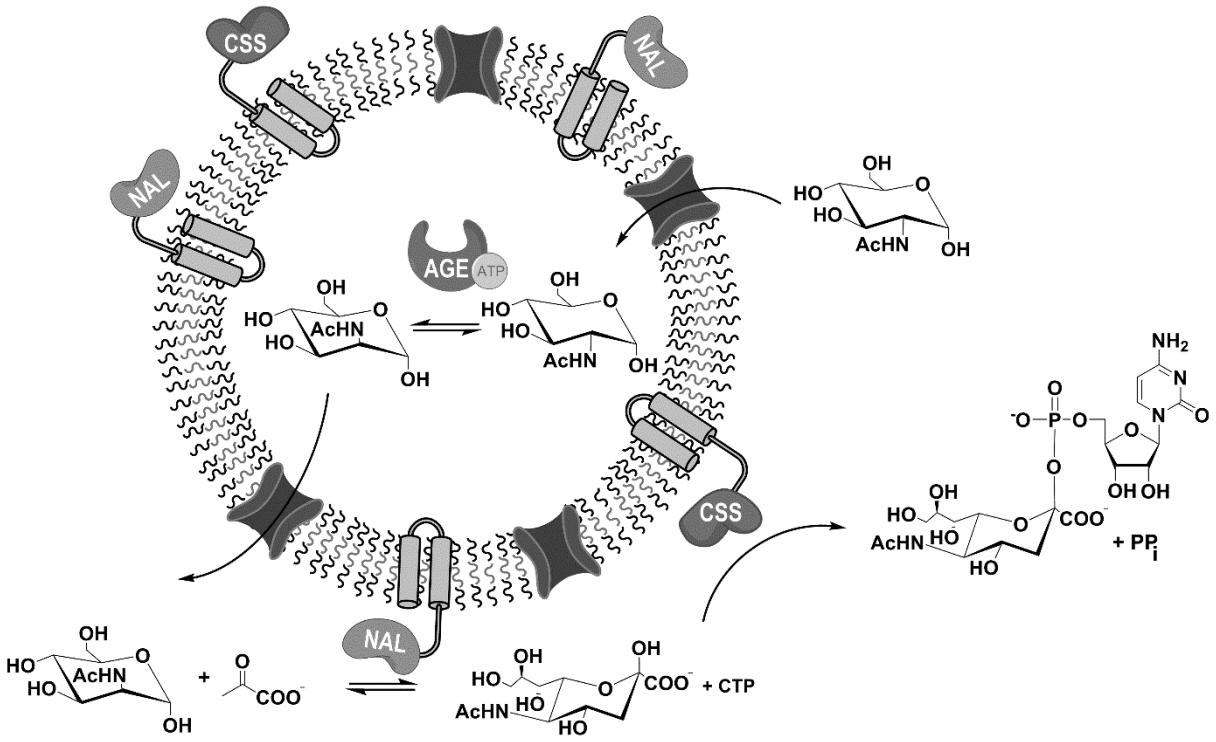

Figure 6.1 – Schematic representation of the nano-scale membrane reactor for the biosynthesis of CMP-Neu5Ac. AGE is encapsulated in the polymersome lumen to shield it from cross-inhibitions by pyruvate, Neu5Ac and CTP. NAL and CSS are immobilized on the polymersome surface via hydrophobic peptide anchors to yield a single biocatalytic entity. Selective mass transport of GlcNAc and ManNAc across the membrane is introduced by a membrane protein.

6.1 Preliminary characterization of membrane permeability

Essential for the implementation of a multienzyme cascade reaction that suffers from cross-inhibitions is a highly selective mass transport that allows the diffusion of substrates and products of the encapsulated enzyme, in this case GlcNAc and ManNAc, while being impermeable toward any substrate inflicting inhibition on the encapsulated enzyme, in this case CTP, pyruvate and Neu5Ac. Thus, the permeability of the membrane was investigated first to assess the general feasibility of PMOXA-PDMS-PMOXA polymersomes to function as nano-scale enzyme membrane reactors for the biosynthesis of CMP-Neu5Ac.

6.1.1 Membrane permeability

To quantitatively analyze the permeability of the polymer membrane toward each reactant involved in the cascade reaction, permeability assays were performed that measured the influx of reactants by adding 50 mM of each reactant to empty polymersomes. The polymersomes were incubated at 30°C reaction temperature and the reactant was allowed to permeate into the polymersome lumen. Samples were purified at specific time points via

miniaturized SEC. The reactant concentration within the polymersomes was detected by controlled disintegration of the purified polymersomes with detergent. The permeability of each reactant was calculated from the concentration increase in the polymersome lumen over time at a given polymersome concentration according to Equation 4.3 and is given in cm s^{-1}. Compared to efflux assays, which are commonly used to determine membrane permeability, influx assays have the advantage of being independent of the ability to form polymersomes at sufficiently high reactant concentrations. Due to the small volume of 0.53 % of the total volume that is encapsulated by the polymersomes (at a d_P of 110 nm, a membrane thickness of 14 nm and a polymersome concentration of 1 % w/v), the reactant is diluted more than 200-fold when diffusing out of the polymersomes into the external reaction space. Thus, high reactant concentrations need to be encapsulated, which in turn may interfere with the polymersome formation process or may have an influence on the quality of the polymersomes. Because the influx assays do not require the encapsulation of the reactant, a consistent polymersome quality can be ensured at sufficiently high reactant concentrations.

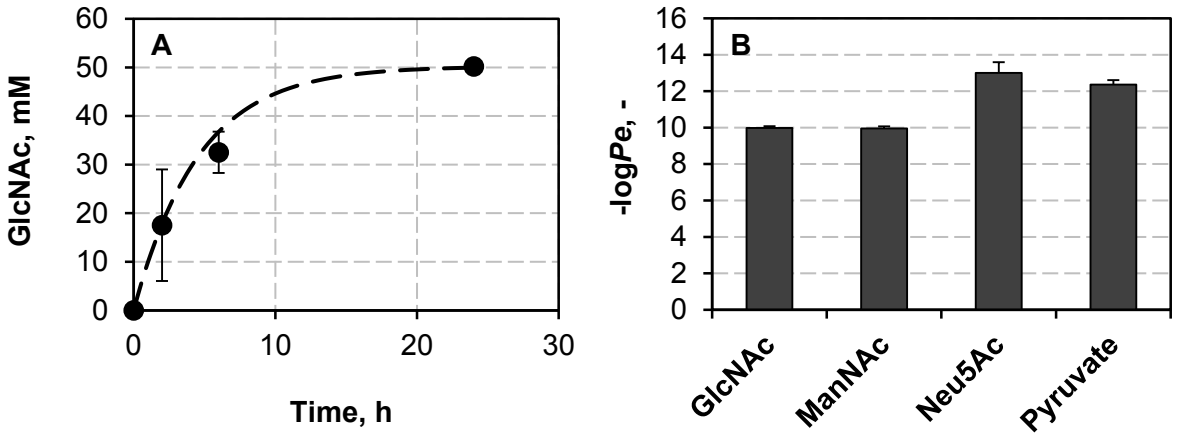

Figure 6.2 – Exemplary diffusion rate of GlcNAc across the polymer membrane as the increase of the GlcNAc concentration within the polymersome after addition of 50 mM GlcNAc to empty polymersomes (c_{eq} = 50.21 mM) (A) and the negative decadic logarithm (-log*Pe*) of the polymer membrane permeability of compounds involved in the CMP-Neu5Ac synthesis (B). A low -log*Pe* represents a high permeability. The line in (A) represents the theoretical course of the GlcNAc concentration calculated from Equation 4.3 with a *Pe* of $1.06 \cdot 10^{-10}$ cm s^{-1}. The -log*Pe* values were calculated from the permeability coefficients in cm s^{-1}.

The data obtained in the permeability studies is represented in Figure 6.2, which exemplarily shows the increase in GlcNAc concentration within the polymersomes over time and the negative decadic logarithm of the permeability coefficients in cm s^{-1} (-log*Pe*) for GlcNAc, ManNAc, Neu5Ac and pyruvate, with a low value indicating a high permeability. Fischer *et al.*

(2007) definied the permeability of lipid membranes toward a certain compound according to the permeability coefficiencts (in cm s^{-1}) as low (-log*Pe* > 7), medium (7 ≥ -log*Pe* > 6) or high (-log*Pe* ≤ 6) (Fischer *et al.*, 2007). The permeability coefficients and -log*Pe* values obtained in this study are listed in Table 6.1.

Because the permeability is a function of the surface area of the membrane and of the incubation time, diffusion of GlcNAc, ManNAc, Neu5Ac and pyruvate into the polymersome was detected, despite the low permeability of the polymer membrane compared to lipid membranes. Thus, theoretically the permeability of any compound can be determined by measuring the permeability for an infinite time period. Especially the extremely large surface area of the membrane (A = 753.67 cm^2) compared to the volume of the acceptor phase (V_A = 0.62 cm^3) leads to a measureable diffusion in a reasonable incubation time. In general, the permeability of a compound across a membrane is considered to be low with a specific a -log*Pe* larger than 7. The polar but uncharged GlcNAc and ManNAc diffused across the polymer membrane with a -log*Pe* of 9.98 ± 0.09 and 9.96 ± 0.11 (Figure 6.2). The similarity of the obtained values for each epimer is in accordance with their identical size and structure. In contrast, the negatively charged and slightly larger Neu5Ac showed a more than 300-fold reduced permeability compared to GlcNAc and ManNAc with a -log*Pe* of 12.70 ± 0.59. For pyruvate a -log*Pe* of 12.04 ± 0.26 was determined. Since both Neu5Ac and pyruvate have pK_a values of 2.5 – 2.6 (Zimmermann *et al.*, 2007), they are present in their deprotonated form at pH 8.0. Thus, permeability across the polymer membrane was considered to be mainly effected by charge and not size of the respective molecule (Table 6.1). In congruence, the large and highly charged nucleotides ATP and CTP could not be detected in the polymersome lumen even after prolonged incubation for more than 2 weeks, indicating that the polymer membrane is completely impermeable toward nucleoside triphosphates. Thus, no permeability could be assigned to the nucleotides.

The data from the permeability assays demonstrate that the $PMOXA_{15}$-$PDMS_{68}$-$PMOXA_{15}$ membrane is capable of discerning between the AGE K160I substrates GlcNAc and ManNAc and the AGE K160I inhibitors pyruvate, Neu5Ac and CTP. Although GlcNAc and ManNAc diffused into the polymersomes reaching the equilibrium concentration within 24 h, the permeability coefficients were very low and diffusion of GlcNAc and ManNAc was significantly hampered by the $PMOXA_{15}$-$PDMS_{68}$-$PMOXA_{15}$ membrane. The impermeability of CTP and ATP, on the other hand, allows keeping CTP from the polymersome lumen, and thus from the AGE K160I, and allows retaining the allosteric activator ATP of the AGE K160I within the polymersomes. The latter significantly reduces the amount of ATP required for the system since no ATP needs to be added to the external compartment to compensate a potential ATP loss by diffusion.

Table 6.1 – Parameters of the compounds involved in the CMP-Neu5Ac synthesis and their permeability across the polymer membrane. The respective charges at pH 8.0 were calculated via Chemicalize Beta by ChemAxon Ltd. (www.chemicalize.org).

Compound	Size, Da	Charge at pH 8.0	Permeability, cm s^{-1}	-log*Pe*, -
GlcNAc	221	0	$1.06 \cdot 10^{-10}$	9.98 ± 0.09
ManNAc	221	0	$1.13 \cdot 10^{-10}$	9.96 ± 0.11
Pyruvate	88	-1	$9.84 \cdot 10^{-13}$	12.04 ± 0.26
Neu5Ac	309	-1	$3.00 \cdot 10^{-13}$	12.70 ± 0.59
CTP	483	-3.8	-	-
ATP	507	-3.9	-	-

6.1.2 Selective modulation of membrane permeability

The increasing size of the reactants along the line of synthesis provides the opportunity to selectively control mass transport on the basis of size. Prerequisite is the identification of a suitable membrane channel with the desired characteristics in terms of selectivity. The membrane channel OmpF G119D, which is a variant of the *E. coli* outer membrane porin OmpF, was selected due to its reported MMCO of 300 Da according to X-ray crystallography (Jeanteur *et al.*, 1994) and its inability to translocate lactose (342 Da) but allow diffusion of acetylated sugars such as GlcNAc (Saint *et al.*, 1996). The diffusion properties of OmpF G119D were qualitatively analyzed by encapsulating ManNAc, pyruvate, Neu5Ac and ATP within polymersomes and determining the diffusion of the reactants into the outer reaction space after external addition of the protein channels. OmpF G119D was compared to wildtype OmpF, which has already been reconstituted into PMOXA-PDMS-PMOXA polymersomes and was successfully used to increase substrate flux of substrates across polymer membranes (Nardin *et al.*, 2000b; Siti *et al.*, 2014).

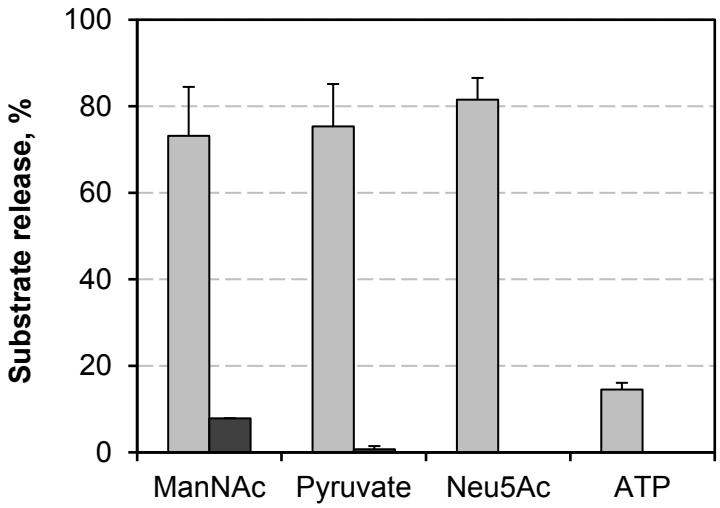

Figure 6.3 – Substrate release of loaded polymersomes after addition of 2.3 µM OmpF (*gray*) and 2.3 µM OmpF G119D (*black*) to 0.2 % w/v polymersomes after 20 min. Each substrate readily diffused through OmpF (*black bars*), whereas diffusion across OmpF G119D (*gray bars*) was greatly impaired and was only detected for ManNAc (7.9 % release in 20 min) and pyruvate (0.7 % release in 20 min). For the 100 % reference, polymersomes were disintegrated and the maximum reactant concentration in the sample was determined.

The results obtained are shown in Figure 6.3. Substantial diffusion of ManNAc, pyruvate and Neu5Ac was detected when reconstituting wildtype OmpF into the polymer membrane, reaching more than 70 % of the equilibrium concentration after 20 minutes in each case. This demonstrates that integration of the channel protein could significantly increase the permeability of the membrane for negatively charged compounds such as Neu5Ac and pyruvate. Although the diffusion of ATP through OmpF was slower compared to the other substrates, 15 % of the encapsulated ATP was lost from the polymersome lumen within 20 minutes, confirming the expectation that nucleotide triphosphates are able to diffuse through OmpF. Thus, although OmpF could substantially increase the permeability of acetylated sugars, it was not selective toward GlcNAc and ManNAc and thus not feasible for the three-enzyme cascade reaction.

In contrast, diffusion through OmpF G119D could only be detected for ManNAc (221 Da) and few amounts of pyruvate (88 Da), which is in congruence with the suggested pore size of OmpF G119D with a MMCO of 300 Da. Although OmpF G119D was capable of increasing the permeation of the acetylated sugars across the membrane, the diffusion rate was much lower compared to wildtype OmpF, releasing approximately 8 % of the encapsulated ManNAc within 20 minutes. In the same time span, no ManNAc diffusion was detected in polymersomes without reconstituted channel protein, indicating that the protein channel was responsible for the increased diffusion. Neither Neu5Ac (309 Da) nor ATP (507 Da) diffused across OmpF G119D in detectable amounts, indicating that the reduced pore size is

effectively keeping molecules above 300 Da from passing through the membrane channel. The 2.3-fold increase in cation selectivity caused by the substitution of glycine to a negatively charged aspartic acid (Jeanteur *et al.*, 1994) may add to the impermeability of Neu5Ac and may also explain the unexpectedly slow diffusion of pyruvate through OmpF G119D. Thus, OmpF G119D was capable of discerning between AGE K160I substrates and AGE K160I inhibitors.

6.2 Positional assembly of enzymes

To determine potential limitations in the positional assembly of the enzymes within the polymersomes, the nano-scale membrane reactors were separately equipped with AGE K160I, NAL and CSS and analyzed in a step-by-step fashion. The encapsulation efficiency of the AGE K160I and factors influencing the surface functionalization with NAL and CSS were investigated.

6.2.1 Encapsulation of *N*-acyl-D-glucosamine 2-epimerase K160I

The AGE K160I was encapsulated within the polymersomes by adding the enzyme to the bulk solution prior to polymersome formation. Thus, the polymersomes form around the enzyme, encapsulating, at best, the same concentration in the lumen as is present in the bulk solution if no interaction with the membrane occurs. In the presence of AGE K160I, polymersome formation required an additional 2 h of vigorous stirring at 4°C to fulfill the quality criteria of a PDI below 0.25, leading to the production process taking a total of 7 h. In comparison, without the addition of protein, polymersomes formed in 5 h at 4°C and 1.5 h at room temperature. Despite the longer exposure to high shear forces, no decline in AGE K160I activity was measured after enzyme encapsulation. This implies that the AGE K160I is sufficiently stable toward the one-step polymersome formation process described by Poschenrieder *et al.* (2016). Figure 6.4 depicts the encapsulation efficiency at various applied protein concentrations. On average, 0.47 ± 0.04 % of the total amount of AGE K160I was encapsulated in 1 % w/v $PMOXA_{15}$-$PDMS_{68}$-$PMOXA_{15}$ polymersomes. With a mean diameter of 110 nm, a membrane thickness of 14 nm and an aggregation number N_{agg} of 43,000, 1 % w/v polymersomes encapsulate 0.53 % of the total volume. Thus, the statistical encapsulation efficiency achieved was in the range of 82 ± 17 % to 89 ± 16 %.

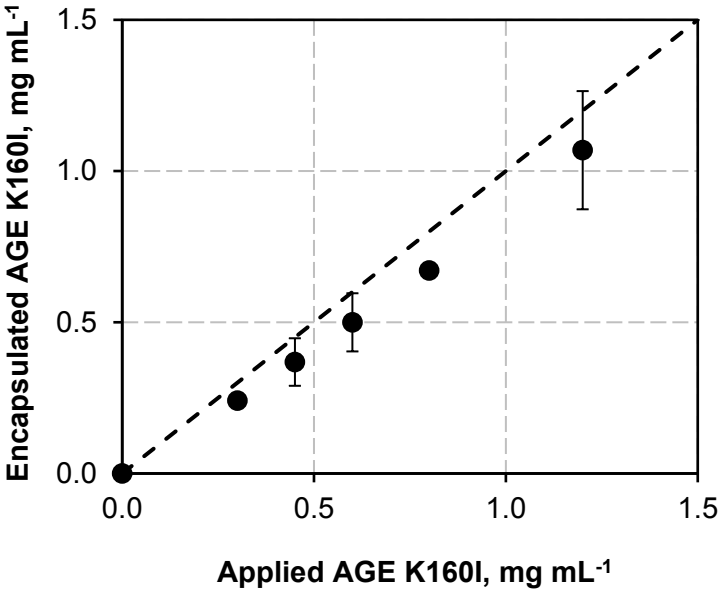

Figure 6.4 – Encapsulation efficiency of AGE K160I in polymersomes. The measured concentration (*black circles*) within the polymersomes in dependency on the AGE K160I concentration in the bulk medium. The encapsulation efficiencies ranged from 82 ± 17 % to 89 ± 16 %. The *dashed line* represents a statistical encapsulation efficiency of 100 %.

To confirm that no unspecific interactions occur between the AGE K160I and the polymer membrane, polymersomes encapsulating AGE K160I were treated with proteinase K to digest any AGE K160I present outside of the polymersomes. With a volumetric activity of 2.40 ± 0.21 U L^{-1}, the AGE K160I activity of the proteinase K treated polymersomes was slightly higher than the activity of untreated polymersomes with a volumetric activity of 2.20 ± 0.01 U L^{-1}. Since in the case of AGE K160I adhering unspecifically to the outer membrane surface, a reduction in the AGE K160I activity should have been observed upon proteinase K treatment, these results confirm that no AGE K160I was present outside of the polymersomes and that the polymer membrane was effectively compartmentalizing macromolecules. Similary, the external addition of 50 mM CTP should reduce the AGE K160I activity if AGE K160I was present on the outside of the polymersomes due to the inhibitory effect of CTP on the AGE K160I. As expected, the activity when adding 50 mM CTP was unchanged with respect to the proteinase K-treated polymersomes and slightly higher compared to the untreated sample with a volumetric activity of 2.49 ± 0.03 U L^{-1}. Thus, by adding a protease and an AGE K160I inhibitor, it could be demonstrated that no unspecific interactions between the AGE K160I and the polymer membranes occur and that no AGE K160I is present on the outside.

The amount of encapsulated AGE K160I was limited by the inability of the amphiphilic copolymer to self-assemble at enzyme concentrations exceeding 1.5 g L^{-1}. This was presumably due to an increased interaction between non-aggregated polymer and the

enzyme. This assumption was supported by the inability of the polymer to self-assemble when other enzymes or proteins were added to the bioreactor at similar concentrations of approximately 1.5 g L^{-1}. Thus, to ensure a high quality of the polymersomes and a maximum encapsulation of AGE K160I within the polymersomes, an initial 1.2 g L^{-1} was applied in the subsequent experiments. At 1.2 g L^{-1}, polymersomes encapsulated approximately 1.0 - 1.1 g L^{-1} AGE K160I in their lumen. With an average d_p of 110 nm, this corresponds to 4 AGE K160I molecules per polymersome. Since the AGE K160I forms active dimers, this corresponds to two active AGE K160I dimers per polymersome.

6.2.2 Surface functionalization with *N*-acetylneuraminate lyase and CMP-sialic acid synthetase

The NAL and the CSS were immobilized on the surface of the polymersomes via hydrophobic peptide anchors. To assess the transferability of the surface functionalization of polymersomes using hydrophobic peptide anchors influential factors previously determined for the surface functionalization of eGFP such as fusion protein preparation, insertion efficiency, and insertion dependencies were reevaluated for the NAL and the CSS. Furthermore, the immobilization of both enzymes on a single polymersome was compared to the immobilization on separate polymersomes in view of the implementation of the three-enzyme cascade reaction in nano-scale membrane reactors. The transferability study was constrained to the non-antibacterial peptide anchors that could be successfully incorporated into the polymer membrane, Cytb_5', L', UBC6' and Vam3p'.

Preparation of NAL and CSS fusion proteins

The preparation and purification of the fusion proteins was investigated since the availability of active fusion protein was considered to be essential. Similar to the expression of peptide-fused eGFP (section 5.1.1), the heterologous expression of the NAL and the CSS in *E. coli* was severely reduced when fused to peptide anchors compared to the expression of the respective enzyme without peptide anchor. After purification and polishing, isolated expression yields of 0.19, 0.51 and 0.21 mg L^{-1} shake flask culture were obtained for NAL-Cytb_5', NAL-L' and NAL-Vam3p', whereas expression of the NAL without peptide anchor typically yielded 12 mg L^{-1}. Interestingly, NAL-UBC6' could not be isolated in functional form. The isolated expression yields of the CSS were typically between 1.2 and 1.5 mg L^{-1} for each fusion protein, including CSS-UBC6', as compared to 15 mg L^{-1} without peptide anchor. Thus, similar to the expression of peptide-fused eGFP, expression yields of less than 10 % compared to the non-fused protein were achieved, indicating a strong impact of the

hydrophobic peptides and the need for further optimization of the expression and purification conditions.

In congruence with data obtained for eGFP, the activity of the NAL was unaffected when fused to L' and Cytb_5', with relative activities of 110 ± 9 % and 104 ± 2 %, respectively, whereas the activity measurements revealed a strong influence of the strongly hydrophobic peptide anchor Vam3p', resulting in a NAL activity of only 12 ± 2 % (Figure 6.5 A). In contrast, the CSS was affected by each peptide anchor (Figure 6.5 B). Whereas UBC6' and Vam3p' almost completely abolished CSS activity with a remaining activity of 3.7 ± 1.3 % and 1.5 ± 0.5 %, L' and Cytb_5' reduced CSS activity to 32.1 ± 10.5 % and 51.0 ± 16.7 %, respectively. Although the tendency of higher activity at moderately hydrophobic peptide anchors was observed for all investigated enzymes, the results of the CSS activity measurements exemplify that the fusion of peptide anchors requires a careful evaluation of the impact of each peptide anchor on the target enzyme activity. Since the activity of the CSS reaches approximately 160 U mg^{-1} at optimal conditions compared to a maximum reaction rate of 27.1 U mg^{-1} and 15.3 U mg^{-1} for the AGE K160I and the NAL, respectively, the reduced activity of the CSS was considered to be tolerable. With a remaining activity of 32.1 % for CSS-L' and 51.0 % for CSS-Cytb_5', the activity of the fusion proteins was 51.4 U mg^{-1} and 81.6 U mg^{-1}, respectively.

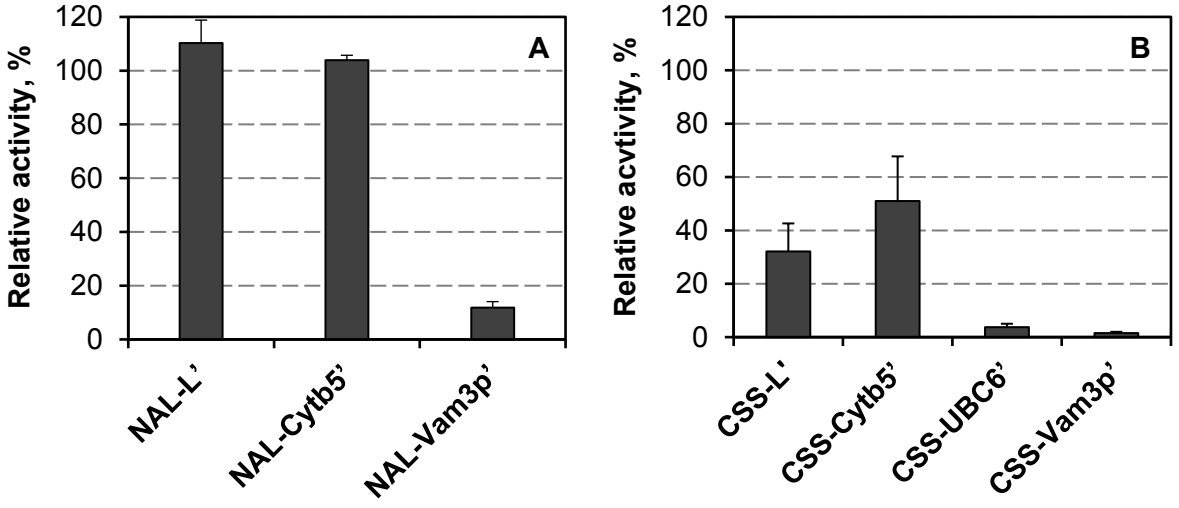

Figure 6.5 – Relative activity of NAL (A) and CSS (B) fused to peptide anchors. The NAL activity is unaffected by fusion peptide anchors L' and Cytb_5'. Vam3p' strongly reduced NAL activity. The CSS was susceptible to each peptide anchor, with L' and Cytb5' having a profound impact on the CSS, whereas UBC6' and Vam3p' almost completely abolished CSS activity. The activity of the NAL and the CSS without peptide anchors served as 100 % reference.

Peptide insertion

Insertion studies were performed at 4°C for 48 h to minimize temperature effects on the enzymes. The amount of enzymes immobilized per polymersome was estimated from the enzyme activity of the fraction containing polymersomes. The results of the insertion studies are summarized in Figure 6.6. In all cases, functional enzymes were displayed on the polymersomes, demonstrating the general feasibility of surface functionalization of polymersomes using hydrophobic peptide anchors and the ability to transfer this immobilization method to enzymes.

The results obtained during the peptide insertion study showed that the NAL and the CSS could be successfully immobilized in active form on the polymer membrane by each peptide anchor (Figure 6.6 A, B). For both NAL and CSS, immobilization with the highly hydrophobic peptide anchor Vam3p' yielded the highest insertion efficiency of 15.38 ± 4.90 NAL and 12.84 ± 3.42 CSS molecules per polymersome per applied protein concentration (molecules pol^{-1} μM^{-1}). This is in congruence with the expectations that a high hydrophobicity of the peptide anchor promotes peptide insertion into the polymer membrane. Whereas for the NAL, the trend of increasing insertion efficiency with increasing hydrophobicity is clearly visible, the insertion efficiency of CSS-Cytb_5' was extraordinarily low, immobilizing only 1.11 ± 0.10 CSS molecules pol^{-1} μM^{-1}. In contrast, the insertion efficiency of CSS-L' with seemed high compared to the immobilization efficiency of NAL-L' with 1.46 ± 0.25 molecules pol^{-1} μM^{-1}.

Since the activity mediated to the polymersomes is a combination of the insertion efficiency of the respective peptide anchor and the relative activity of the fusion enzyme, Cytb_5' and L' performed best in immobilizing NAL and CSS, respectively, in terms of activity per polymersome per applied protein concentration (Figure 6.6 C, D). Although high insertion efficiencies were achieved with Vam3p', the strongly reduced activity of the enzymes in fusion with Vam3p' led to only little activity being conferred to the polymersomes of 1.61 ± 0.49 fU pol^{-1} μM^{-1} and 1.55 ± 0.40 fU pol^{-1} μM^{-1} for NAL and CSS, respectively. With a high insertion efficiency of NAL-Cytb_5' of 9.24 ± 2.05 NAL molecules pol^{-1} μM^{-1} and a high relative activity of 104 ± 2 %, Cytb_5' was able to mediate a NAL activity of 8.20 ± 0.31 fU pol^{-1} μM^{-1} to the polymersomes. Although the relative activity of CSS-L' (31.2 %) was lower than the relative activity of CSS-Cytb_5' (51.0 %), the high insertion efficiency of CSS-L' of 5.19 ± 0.64 molecules pol^{-1} μM^{-1} compared to CSS-Cytb_5' led to the highest CSS activity mediated to the polymersomes of 15.41 ± 1.55 fU pol^{-1} μM^{-1}.

The fact that the NAL and the CSS were immobilized best with two different peptide anchors, Cytb_5' and L', respectively, emphasizes the importance of screening potential candidate peptide anchors for their efficiency to immobilize the respective enzyme similar to assessing the impact of each peptide anchor on the enzyme activity. Furthermore, peptide insertion

was dependent on the respective fusion protein, which is demonstrated by the different insertion efficiencies of the same peptide anchor when fused to eGFP, NAL or CSS. Nevertheless, the moderately hydrophobic but fairly long peptide anchors Cytb_5' and L' generally worked best and may thus represent good candidates for universal peptide anchors for the surface functionalization of polymersomes.

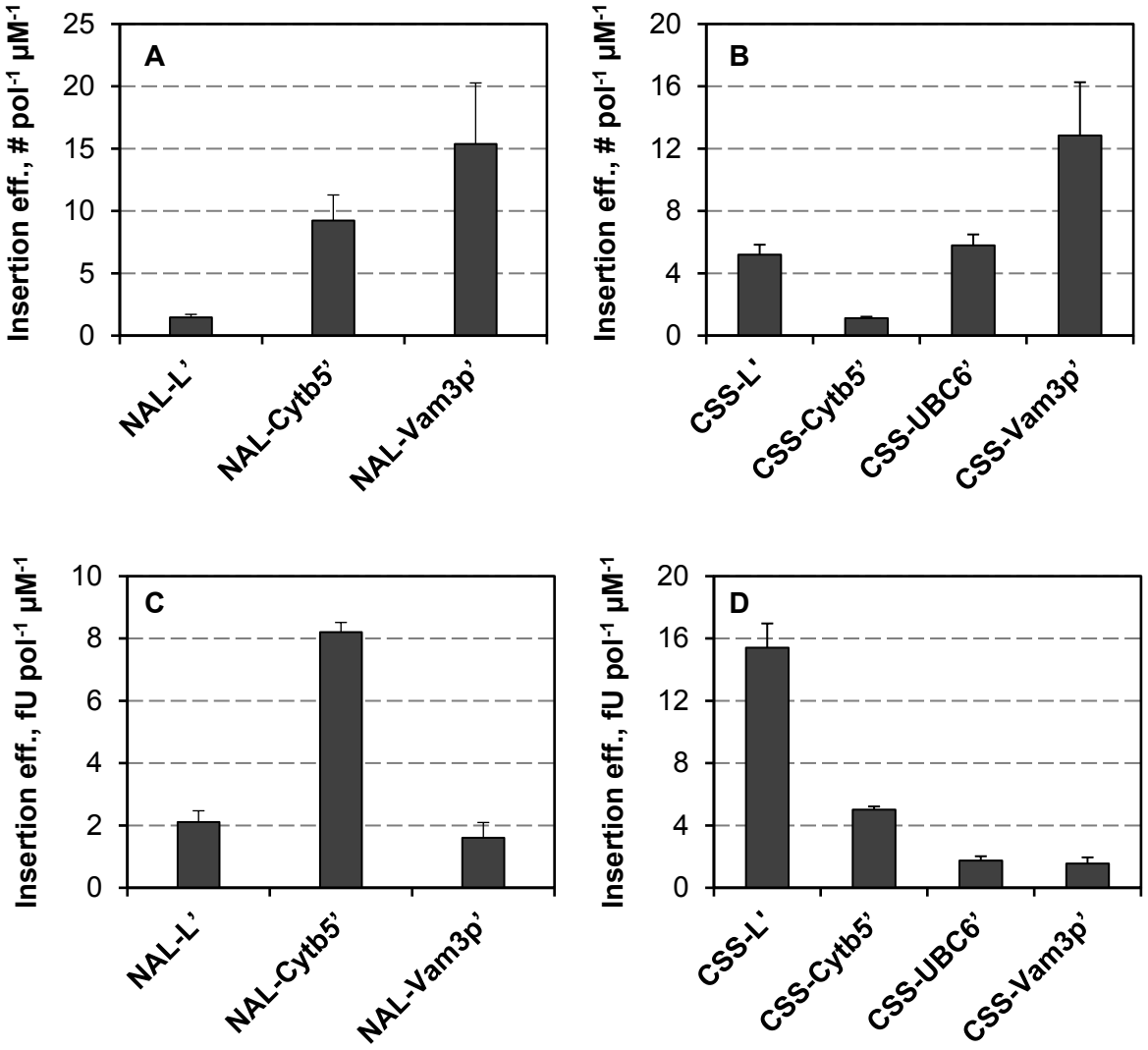

Figure 6.6 – Insertion efficiency (Insertion eff.) of peptide anchors fused to NAL (A and C) and CSS (B and D) at 4°C after 48 h in terms of immobilized molecules (#) per polymersome per applied protein concentration (A and B) and activity (in fU) conferred to the polymersomes per applied protein concentration (C and D). The peptide anchors are sorted according to increasing hydrophobicity from left to right. Except for CSS-Cytb_5', the number based insertion efficiency generally increased with increasing hydrophobicity. The activity based insertion efficiency is dependent on the number based insertion efficiency and the relative activity of the respective fusion protein (Figure 6.5).

To increase the amount of enzyme immobilized per polymersome, the polymersome concentration was gradually reduced. As expected, the peptide insertion was independent of the polymersome concentration in the measured polymersome concentration range, as exemplarily shown for NAL-Cytb_5' (Figure 6.7). Thus, the degree of functionalization with enzymes could be significantly increased by reducing the polymersome concentration. No decrease in insertion efficiency was observed for NAL-Cytb_5' in the measured polymersome concentration range, indicating that higher degrees of functionalization can theoretically be achieved.

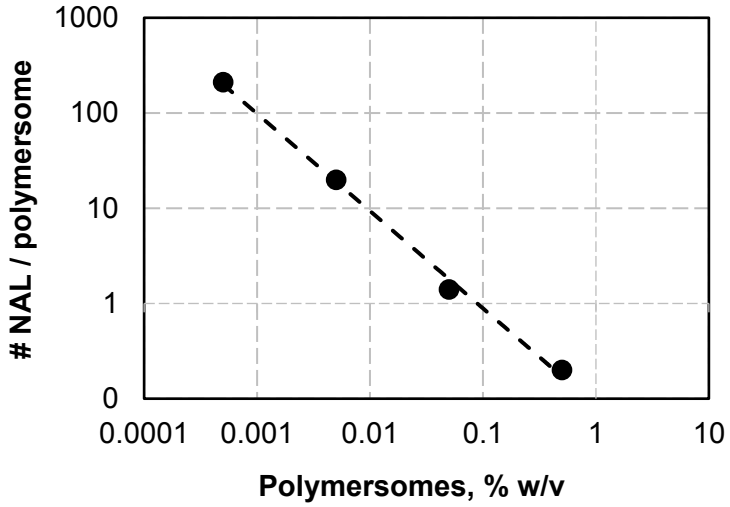

Figure 6.7 – Number of immobilized NAL molecules (#) per polymersome at varying polymersome concentration in log-log scale. The total amount of immobilized NAL is independent of the polymersome concentration in the studied range. The data were fitted to a power function of the form $y = a \cdot x^b$ by non-linear regression (*dashed line*) with an exponent b of -1.

The maximum amount of encapsulated AGE K160I did, however, not exceed 4 molecules per polymersome due to higher AGE K160I concentrations disturbing the polymersome formation process. With an activity of 27.1 U mg^{-1}, the AGE K160I activity per molecule can be calculated according to Equation 6.1 and amounts to 2.15 fU per AGE K160I molecule (the molecular masses M_E can be found in the Appendix Table A 28 and Table A 29).

$$v_m = \frac{v_{max} \cdot M_E}{N_A}$$ Equation 6.1

with v_m = Specific activity per molecule, U

v_{max} = Maximum reaction rate, U mg^{-1}

M_E = Molecular mass of one active monomer, mg mol^{-1}

N_A = Avogadro constant, 6.022 · 10^{23} mol^{-1}

Thus, 4 AGEK160I molecules have an activity of 8.6 fU, which represents the highest achievable AGE K160I activity per polymersome. In a balanced reaction cascade with equivalent activities for each enzyme per polymersome, this would require 8.6 fU NAL and 8.6 fU CSS activity per polymersome. With a v_{max} of 15.3 U mg^{-1} for the immobilized NAL (0.88 fU per NAL molecule), this would require 10 NAL molecules to be immobilized per polymersome. In analogy, with a v_{max} of 51.4 U mg^{-1} for the immobilized CSS (2.3 fU per CSS molecule), a total of 3 CSS molecules are required on the polymersome surface to reach an equivalent 8.6 fU per polymersome. Thus, the degree of surface functionalization achieved via the hydrophobic peptide anchors of up to 200 molecules per polymersome was sufficient to obtain a balanced reaction cascade and higher degrees of functionalization were not required.

Influence of the immobilization on the kinetic parameters

Because the surface functionalization may alter kinetic parameters such as substrate affinity and stability of the immobilized enzymes, the influence of the enzyme immobilization on the kinetic parameters was investigated for NAL-Cyt*b*$_5$' (Table 6.2) and CSS-L' (Table 6.3). Both enzymes were immobilized on polymersomes and the reaction rates of the NAL and CSS reactions were determined.

With a v_{max} of 16.5 ± 0.4 U mg^{-1} and a respective k_{cat} of 11.2 ± 0.3 s^{-1}, the turnover number of the NAL was not changed compared to non-immobilized NAL with a k_{cat} of 11.7 ± 0.2 s^{-1}. Similarly, the half-saturation constants for ManNAc and pyruvate were not significantly altered upon immobilization. Although the NAL forms an active tetramer, the kinetic parameters of the NAL were not affected by the immobilization. This demonstrates the feasibility of immobilizing complex enzymes, such as tetramers, on polymersome surfaces using hydrophobic peptide anchors.

Table 6.2 – Kinetic parameters of NAL and immobilized NAL.

Parameter	NAL	NAL-Cytb_5'
k_{cat}, s^{-1}	11.7 ± 0.2	11.2 ± 0.3
$K_{M,ManNAc}$, mM	131 ± 26	132 ± 7
$K_{M,Pyr}$, mM	4.90 ± 0.25	5.29 ± 0.34

In contrast, the activity of the immobilized CSS-L' was reduced by 67.9 % to a k_{cat} of 23.2 ± 2.1 s^{-1} compared to the free CSS. The K_M for Neu5Ac of 130 ± 50 µM was not significantly altered compared to the K_M of the free CSS whereas the K_M for CTP was increased 3-fold from 80 ± 40 µM of the free CSS to 250 ± 30 µM of the immobilized CSS-L'. Thus, the kinetic parameters were slightly altered, indicating that kinetic parameters should generally be verified when immobilizing enzymes using hydrophobic peptide anchors.

Table 6.3 – Kinetic parameters of CSS and immobilized CSS.

Parameter	CSS	CSS-L'
k_{cat}, s^{-1}	72.3 ± 29.5	23.2 ± 2.1
$K_{M,Neu5Ac}$, µM	190 ± 60	130 ± 50
$K_{M,CTP}$, µM	80 ± 40	250 ± 30
$\tau_{1/2,30°C}$, h	1.47 ± 0.11	36.2 ± 1.5

Even though the activity of the immobilized CSS was decreased, the immobilization of the CSS on the polymersome surface had a marked positive effect on the enzyme stability under process conditions (Figure 6.8). The half-life τ of the CSS was increased 24-fold from 1.47 ± 0.11 h to 36.2 ± 1.5 h when immobilized on the polymersome surface via L'.

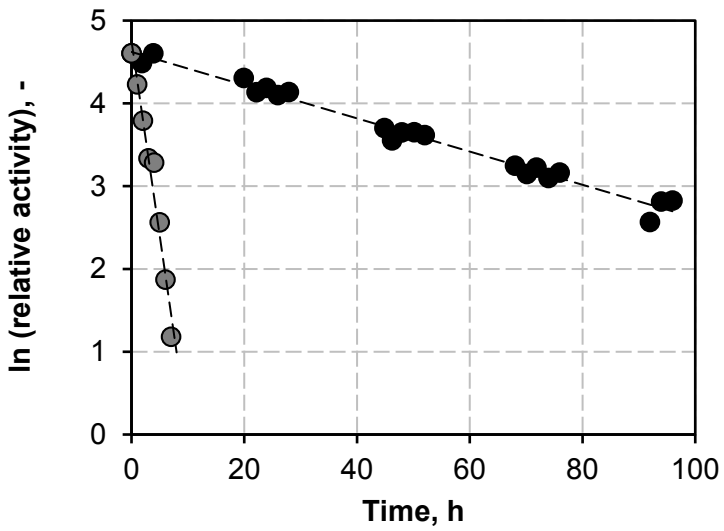

Figure 6.8 – Natural logarithm of the relative activity of the CSS in solution (*gray*) and immobilized on the surface of polymersomes (*black*) over time at 30°C. The immobilized CSS shows an increased stability with a 24-fold increased half-life of 36.2 ± 1.5 h compared to 1.47 ± 0.11 h of the CSS in solution. The lines represent the data fit by linear regression.

Simultaneous peptide insertion

To investigate whether the simultaneous immobilization of multiple enzymes is possible and to check whether it has an effect on the peptide insertion, the simultaneous immobilization of the NAL and the CSS on a single polymersome was compared to the immobilization of the enzymes on separate polymersomes. A schematic representation of the two immobilization modes is shown in Figure 6.9, with either the NAL or the CSS being immobilized on separate polymersomes or both enzymes being immobilized on the same polymersome.

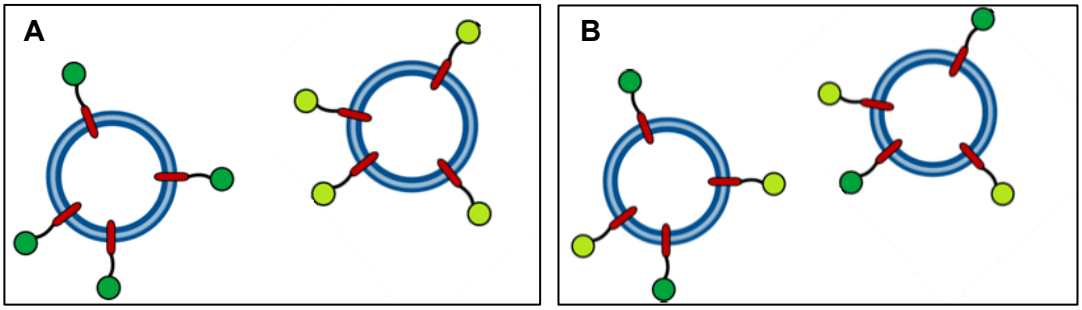

Figure 6.9 – Schematic representation of the separate immobilization of NAL (*light green*) and CSS (*dark green*) on different polymersomes (A) and simultaneous immobilization of both enzymes on a single polymersome (B).

NAL-Cytb_5' and CSS-L' were simultaneously immobilized on the same polymersomes with a constant total protein concentration of 1 µM but at different NAL-to-CSS ratios of 3:1, 1:1 and 1:3. Thus, at the 1:1 ratio, both fusion proteins were present at a concentration of 0.5 µM. At the 3:1 and 1:3 ratios, concentrations of 75 µM NAL-Cytb_5' and 25 µM CSS-L' and 25 µM NAL-Cytb_5' and 75 µM CSS-L' were present, respectively. Analogously, both enzymes were separately immobilized at concentrations of 1 µM and the polymersomes were subsequently mixed in the same ratios.

Because the amount of molecules immobilized per polymersome was found to be dependent on the applied protein concentration, the number of molecules of enzyme A immobilized per polymersome may either be dependent on its own concentration [A] only or on the total protein concentration [A+B]. Whereas the first would result in a linear increase of the peptide insertion with increasing protein concentration [A] and thus result in a constant insertion efficiency with respect to its own applied protein concentration, the latter would result in no change of the peptide insertion because of a constant total protein concentration [A+B] and thus an increased insertion efficiency with respect to its own concentration. Furthermore, a partial effect may be observed, in which the insertion efficiency is increased in the presence of the second fusion protein but is not solely dependent on the total protein concentration. This would result in a change in peptide insertion and an increase in the insertion efficiency at different protein ratios. Lastly, the peptide insertion may be negatively affected by the presence of the second fusion protein, resulting in a decrease in the insertion efficiency at different NAL-to-CSS ratios.

After purification of the functionalized polymersomes, the number of molecules per polymersome and the insertion efficiency was calculated from their respective activities to check for positive or negative effects on the peptide insertion during simultaneous compared to separate surface functionalization. The number of molecules immobilized at the different NAL-to-CSS ratios and the insertion efficiencies of NAL-Cytb_5' and CSS-L' with respect to their applied protein concentration is depicted in Figure 6.10. The results demonstrate that simultaneous peptide insertion was possible at each NAL-to-CSS ratio investigated.

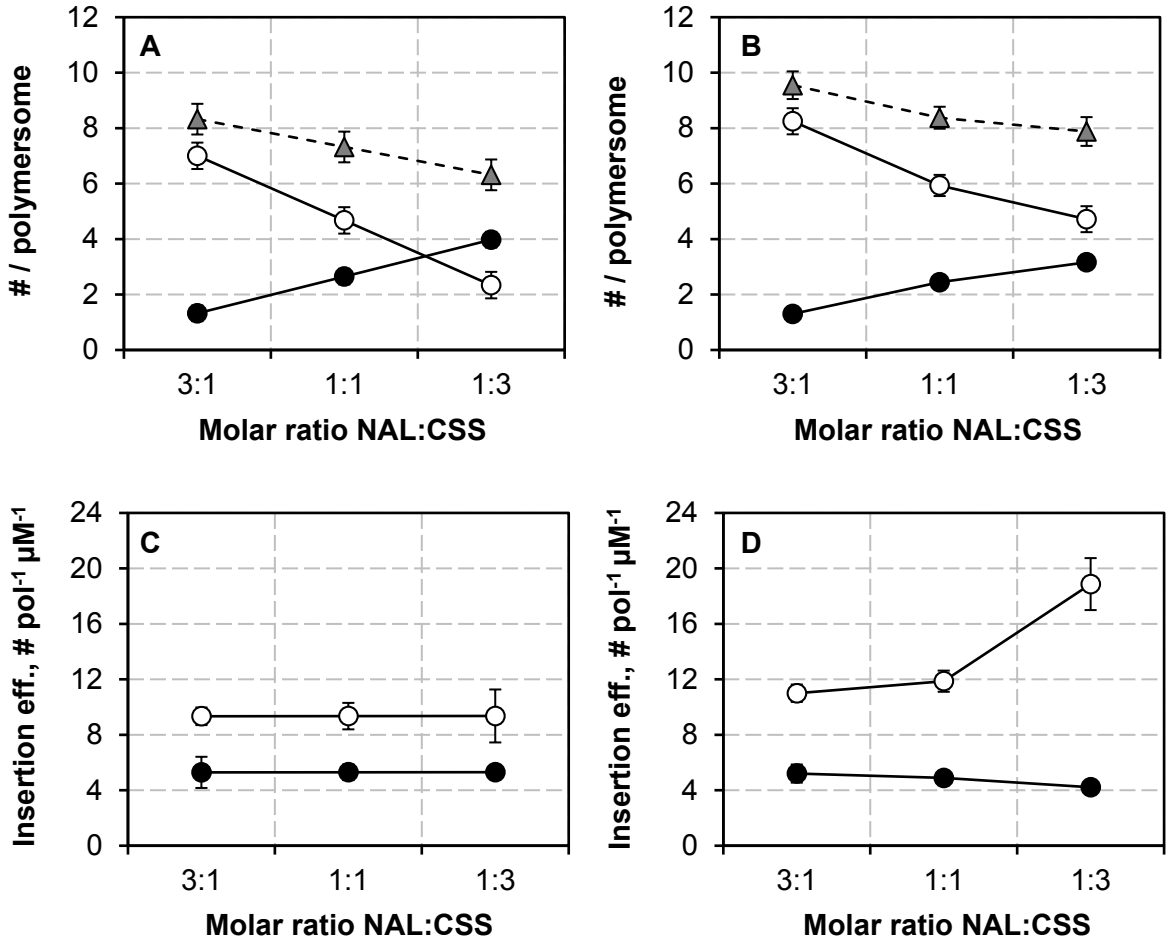

Figure 6.10 – The number of molecules (#) of NAL (*white*) and CSS (*black*) and the total amount of molecules (*gray triangles*) immobilized per polymersome after separate (A) and simultaneous (B) immobilization at decreasing NAL and increasing CSS concentration with a total protein concentration of 1 µM and the insertion efficiency (eff.) with respect to either the NAL-Cytb_5' or the CSS-L' concentration during separate (C) and simultaneous (D) immobilization. NAL immobilization was increased when simultaneously immobilized with CSS, whereas CSS immobilization was slightly reduced at a NAL-to-CSS ratio of 1:3 when simultaneously immobilized. The lines serve the visualization.

The data revealed that the insertion of NAL-Cytb_5' into the polymer membrane was positively affected by the presence of CSS-L', whereas the insertion of CSS-L' was not or slightly negatively affected by the presence of NAL-Cytb_5'. In general, the amount of NAL molecules per polymersome was always higher when immobilized together with CSS-L' compared to when immobilized separately. With increasing CSS-L' concentration the positive effect on the insertion of NAL-Cytb_5' increased with 18 % more NAL molecules being immobilized per polymersome at 0.25 µM CSS-L' and 102 % more NAL molecules being immobilized at 0.75 µM CSS-L' compared to when immobilized separately. Thus, increasing CSS-L' concentrations led to a higher insertion efficiency of NAL-Cytb_5', which could be increased by 2-fold from 9.3 ± 0.4 NAL molecules per polymersome per applied NAL-L' concentration

when immobilized without CSS-L' to 18.9 ± 1.9 NAL molecules pol^{-1} μM^{-1} in the presence of 0.75 µM CSS-L' at a 3-fold molar excess of CSS-L' over NAL-Cytb_5'.

In contrast, the insertion of CSS-L' was either not affected or slightly reduced in the presence of NAL-Cytb_5'. Interestingly, the negative effect seemed to increase with decreasing NAL-Cytb_5' concentration, which is contrary to the expectations. At 0.75 µM NAL-Cytb_5', the CSS-L' insertion was equivalent to when immobilized separately, whereas at 0.25 µM NAL-Cytb_5', only 80 % of the insertion efficiency of CSS-L' was reached. Due to the positive effect of the simultaneous immobilization on the insertion of NAL-Cytb_5' into the polymer membrane, the total amount of protein per polymersome was increased by 15 – 25 %. The increased amount of total molecules per polymersome, however, resulted solely from an increased amount of NAL molecules per polymersome.

6.3 CMP-Neu5Ac synthesis

To assess the applicability of polymersomes as nano-scale membrane reactors to compartmentalize and thereby enhance incompatible multienzyme syntheses, PMOXA-PDMS-PMOXA polymersomes were equipped with AGE K160I in their lumen, NAL and CSS on their surface and OmpF G119D reconstituted in their membrane.

6.3.1 Synthesis of CMP-Neu5Ac using nano-scale enzyme membrane reactors

After assembly of the nano-scale enzyme membrane reactors, the AGE K160I, the NAL and the CSS were separately checked for activity to ensure that each enzyme of the cascade reaction was present at similar volumetric activities (Figure 6.11). The AGE K160I and NAL activities were measured at non-saturated substrate concentrations. The AGE K160I was determined at 128 mM GlcNAc and 1 mM ATP, the NAL concentration was determined at 250 mM ManNAc and 50 mM pyruvate. Under these assay conditions, the nano-scale enzyme membrane reactors constituted an AGE K160I activity of 0.77 ± 0.01 fU pol^{-1}, a NAL activity of 1.99 ± 0.03 fU pol^{-1} and a CSS activity of 2.24 ± 0.11 fU per polymersome. In total, the volumetric activities of each enzyme were in the same order of magnitude with a slight increase in activity along the line of synthesis. When disintegrating the polymersomes, the AGE K160I activity increased to 3.66 ± 0.07 fU pol^{-1}, which represents the actual amount of AGE K160I present per polymersome. This indicates that mass transport limitations were still encountered despite the integration of OmpF G119D.

The integration efficiency of OmpF G119D into the polymersomes was judged by SDS-PAGE analysis to approximately 1 %. With a molar excess of 29 channel proteins per polymersome added to the nano-scale enzyme membrane reactors and an integration efficiency of 1 %,

0.3 OmpF were incorporated per polymersome, which is equivalent to one functional OmpF G119D trimer in every tenth polymersome.

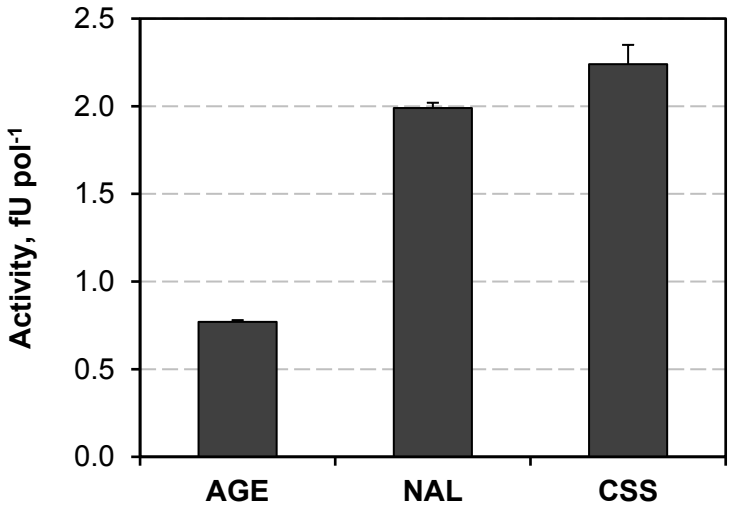

Figure 6.11 – Activities of the three enzymes for the CMP-Neu5Ac synthesis measured per polymersome in the functionalized nano-scale enzyme membrane reactors. The activities increase along the line of synthesis. The activity of the AGE K160I was determined at initial process conditions and does not represent the maximum achievable reaction rate of the AGE K160I. NAL activity was determined at non-saturated ManNAc concentrations (250 mM ManNAc) and does not represent the maximum achievable reaction rate of the NAL.

For the synthesis of CMP-Neu5Ac, 0.13 % w/v nano-scale enzyme membrane reactors were added to initial substrate concentrations of 128 mM GlcNAc, 80 mM pyruvate and 50 mM CTP. To account for background activity, which may result due to a slow epimerization of GlcNAc to ManNAc at pH 8.0 and hydrolysis of CTP, nano-scale membrane reactors without AGE K160I that contained surface displayed NAL and CSS were assembled as negative control. The negative control without AGE K160I was subtracted from all data.

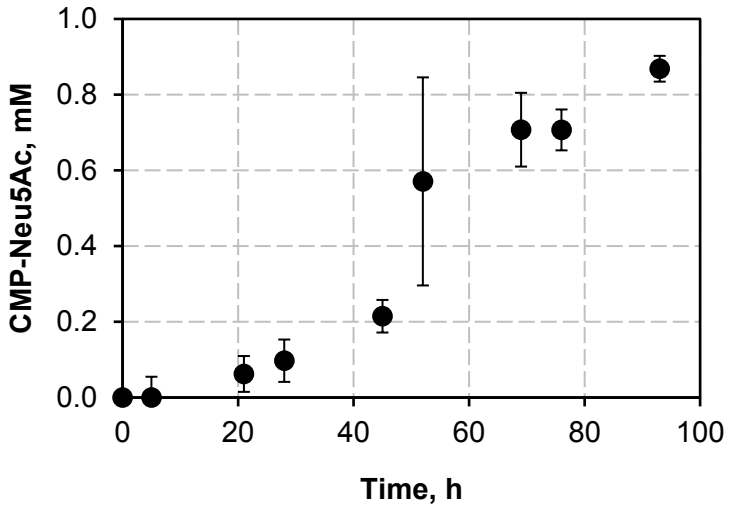

Figure 6.12 – CMP-Neu5Ac synthesis in nano-scale enzyme membrane reactors. The CMP-Neu5Ac concentration steadily increases over the measured time period of 93 h.

As shown in Figure 6.12, CMP-Neu5Ac synthesis was possible in functionalized nano-scale enzyme membrane reactors with a steady increase in the CMP-Neu5Ac reaching a concentration of 0.87 ± 0.03 mM after 93 h. This demonstrates that the reaction could indeed be performed in compartmentalized reaction spaces with functionalized polymersomes. No accumulation of intermediates was detected, indicating that the epimerization of GlcNAc to ManNAc was the rate-limiting step in the cascade. Since ManNAc is only gradually built up inside the nano-scale enzyme membrane reactors, limitations were most likely due to a reduced mass transport of ManNAc across the polymer membrane. Nevertheless, the reaction was significantly faster than the negative control, indicating a successful implementation of the reaction cascade in nano-scale enzyme membrane reactors.

6.3.2 Comparative study of CMP-Neu5Ac synthesis

To evaluate the performance of the compartmentalized reaction cascade, the CMP-Neu5Ac synthesis in nano-scale enzyme membrane reactors with reconstituted OmpF G119D was compared to the same cascade in a non-compartmentalized set-up and to control reactions with no reconstituted membrane channel or unselective OmpF. A schematic representation of the systems compared is shown in Figure 6.13. Two aspects were considered when assessing the applicability of the polymersomes as nano-scale enzyme membrane reactors. First, the performance of the nano-scale enzyme membrane reactors (Figure 6.13 F) was compared to the cascade reaction free in solution (Figure 6.13 A) to evaluate whether polymersome systems can enhance multienzyme syntheses through compartmentalization and selective mass transport. Since the immobilization of the CSS on the polymersome

surface substantially increased the stability of the CSS, a non-compartmentalized reaction cascade with immobilized NAL and CSS on empty polymersomes and addition of AGE K160I and ATP to the outer continuous phase was performed (Figure 6.13 B). To be able to compare the nano-scale enzyme membrane reactors to the non-compartmentalized reaction, the enzyme concentrations for the non-compartmentalized systems were adjusted to fit the volumetric activities of each enzyme. The activity of AGE K160I added to the non-compartmentalized systems was adjusted to be equivalent to the volumetric activity of disintegrated polymersomes. At 0.13 % w/v nano-scale enzyme membrane reactors ($2.4 \cdot 10^{12}$ polymersomes per mL), the reaction contained AGE K160I, NAL and CSS with volumetric activities of 8.77, 4.79 and 5.07 U L^{-1}, respectively. Under the conditions at which the enzyme activities were determined, the AGE K160I had an activity of 15.6 U mg^{-1}, the NAL had an activity of 15.3 U mg^{-1} and the CSS had an activity of 51.4 U mg^{-1}. Thus, the reaction mixture contained 0.56 µg mL^{-1} AGE K160I, 0.31 µg mL^{-1} NAL and 0.10 µg mL^{-1} CSS. Since the CSS activity was reduced by 32.1 % when immobilized on the surface of the nano-scale enzyme membrane reactors, this corresponds to a CSS concentration without peptide anchor of 0.03 µg mL^{-1} at equivlanet CSS activities. Again, the negative control, represented in Figure 6.13 C, was subtracted from all experiments to account for background activity.

Second, the fully functionalized nano-scale enzyme membrane reactors were compared to two control set-ups to evaluate the importance of introducing selective mass transport. Polymersomes were assembled that contained all three enzymes but lacked a membrane channel protein (Figure 6.13 D) and were thus subjected to full mass transport limitations. This allowed to differentiate between membrane diffusion and selective diffusion through OmpF G119D and evaluate whether incorporation of OmpF G119D had a positive effect on the reaction rate. In the second control, the polymer membrane was reconstituted with unselective wildtype OmpF (Figure 6.13 E) to assess the importance of introducing a highly selective mass transport.

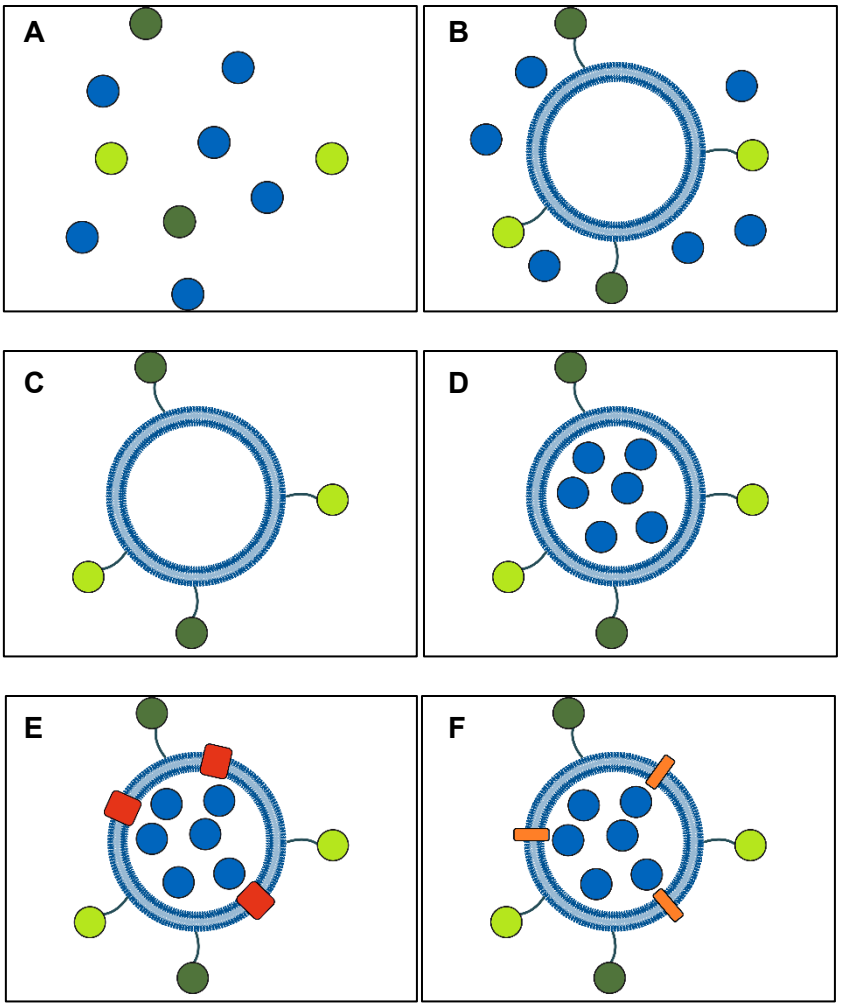

Figure 6.13 – Schematic depiction of the cascade reactions analyzed for the comparative study with AGE K160I (*blue*), NAL (*light green*), CSS (*dark green*), OmpF (*red*) and OmpF G119D (*orange*). Two non-compartmentalized reaction cascades with all enzymes in solution (A) and the NAL and the CSS immobilized on empty polymersomes to increase the stability of the CSS (B). A negative control without AGE K160I (C) was performed to account for base-catalyzed epimerization of GlcNAc to ManNAc at pH 8.0. The CMP-Neu5Ac concentrations measured in the negative control were subtracted from all results. Control experiments without membrane channel (D) and reconstitution of unselective OmpF (E) were performed to evaluate changes in membrane permeability. The nano-scale enzyme membrane reactors with reconstituted OmpF G119D are shown in (F).

The CMP-Neu5Ac concentrations achieved for each set-up after 93 h incubation at 30°C are shown in Figure 6.14. Comparing the nano-scale enzyme membrane reactors to the non-compartmentalized and the control set-ups clearly demonstrated an enhanced production of CMP-Neu5Ac using the compartmentalized system with selective mass transport. Whereas 0.87 ± 0.03 mM CMP-Neu5Ac were produced by the nano-scale enzyme membrane reactors with reconstituted OmpF G119D in 93 h, no CMP-Neu5Ac production was observed with all three enzymes free in solution, which was in part due to the strong cross-inhibitions of the substrates CTP and pyruvate on the AGE K160I and in part due to the low stability of the CSS in solution. The low stability of the CSS may result in an accumulation of the

intermediate Neu5Ac, which further inhibits the AGE K160I. By immobilization and thus stabilization of the CSS, the CMP-Neu5Ac concentration increased to 0.40 ± 0.12 mM CMP-Neu5Ac, which represents the maximum performance of the reaction cascade at full CTP inhibition. Thus, compared to the non-compartmentalized reaction cascade, an increased product formation by 2.2-fold was achieved with the nano-scale enzyme membrane reactors. This demonstrates that nano-scale enzyme membrane reactors can effectively enhance the productivity of multienzyme cascade reactions that suffer from cross-inhibition by compartmentalization.

Furthermore, an increased product formation was only achieved by introducing a highly selective mass transport across the membrane, as demonstrated by comparing the nano-scale enzyme membrane reactors to the control set-ups without membrane channel and with reconstituted unselective OmpF. By encapsulating the AGE K160I without reconstitution of a channel protein, CMP-Neu5Ac formation was reduced to 0.22 ± 0.06 mM in 93 h due to mass transport limitations of GlcNAc and ManNAc across the membrane. Thus, the product yield was increased by 3.9-fold by reconstituting the highly selective OmpF G119D variant and significantly reducing mass transport limitations. This validates that the membrane permeability of GlcNAc and ManNAc was not sufficient for an enhanced synthesis of CMP-Neu5Ac, despite evading the observed cross-inhibitions and that the introduction of channel proteins to increase the permeability of PMOXA-PDMS-PMOXA membranes is required. The high fold-increase observed is especially astonishing keeping in mind that only one in ten nano-scale enzyme membrane reactors harbored a functional OmpF G119D trimer to allow increased mass transport across the membrane. Since mass transport limitations were observed when measuring the AGE K160I activity only, an increase of the amount of reconstituted OmpF G119D may further increase the synthesis rate and thus further enhance the performance of the nano-scale enzyme membrane reactors.

In contrast, the reconstitution of wildtype OmpF into the nano-scale enzyme membrane reactors led to a CMP-Neu5Ac concentration of 0.49 ± 0.08 mM after 93 h, which is an increase of 2.2-fold compared to the control without membrane channel but only 56 % of the product concentration obtained with the selective nano-scale enzyme membrane reactors. SDS-PAGE analysis revealed that 2 OmpF were incorporated per polymersome, which is equivalent to two functional OmpF trimers in three polymersomes. In view of the higher diffusion rate of GlcNAc and ManNAc through OmpF compared to OmpF G119D and the higher functionalization of the polymersomes with two OmpF in three polymersomes compared to one OmpF G119D in ten polymersomes, mass transport limitations should be significantly less in the unselective nano-scale enzyme membrane reactors. Yet, the introduction of unselective mass transport via OmpF did not significantly enhance the CMP-Neu5Ac syntheses with nano-scale enzyme membrane reactors beyond that of the non-

compartmentalized system. This is in perfect agreement with the expectations and validates that unselective mass transport reintroduces the CTP inhibition on the AGE K160I and causes release of ATP from the polymersome lumen, thus, at best resulting in the same reaction rate and product yield as the non-compartmentalized cascade reaction. In conclusion this demonstrates that, although mass transport limitation can be easily bypassed by introducing large channel proteins or porous membranes (Peters *et al.*, 2014; Siti *et al.*, 2014), selectivity plays a crucial role when compartmentalizing multienzyme reactions with cross-inhibitions.

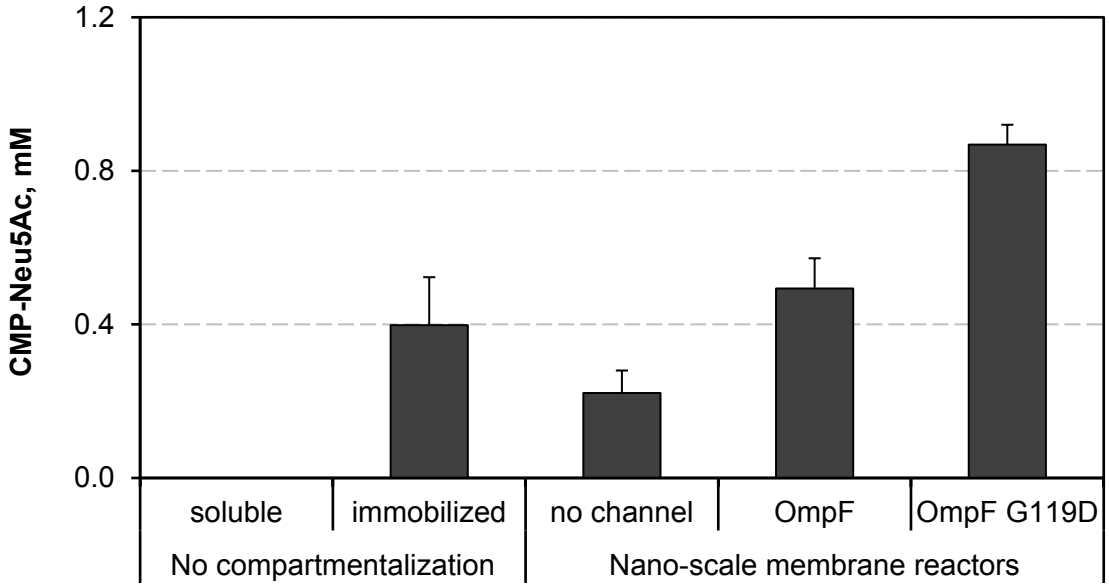

Figure 6.14 – CMP-Neu5Ac yield after 93 h in non-compartmentalized and compartmentalized reaction set-ups. The CMP-Neu5Ac synthesis was increased from no synthesis to 0.4 mM CMP-Neu5Ac by increasing the stability of the CSS via immobilization on the polymersome surface. Both non-compartmentalized reactions are fully subjected to cross-inhibitions. Without membrane channel, synthesis was reduced due to mass transport limitations of GlcNAc and ManNAc across the membrane. Mass transport limitations could be alleviated by reconstitution of the membrane channels OmpF and OmpF G119D. OmpF led to an unselective permeation of the membrane, allowing the diffusion of CTP and ATP, thus resulting in full cross-inhibitions and a similar CMP-Neu5Ac yield as the non-compartmentalized, immobilized system. OmpF G119D induced a selective permeation, allowing diffusion of GlcNAc and ManNAc but retaining CTP and ATP in their respective compartments, thereby increasing the yield by 2.2-fold compared to the non-compartmentalized, immobilized reaction.

Essential for a successful implementation of polymersomes as nano-scale enzyme reactors is the ability to compartmentalize the reaction cascade on a micromolecule level. The segregation of macromolecules, for example enzymes, while allowing the diffusion of low molecular mass molecules, such as substrates and products, has been demonstrated in

several compartmentalized systems (van Dongen *et al.*, 2009; Peters *et al.*, 2014; Schmitt *et al.*, 2016; Schoonen and van Hest, 2016). However, a differentiation between different low molecular mass molecules, in this case substrates and inhibitors, is required for a successful implementation of the CMP-Neu5Ac synthesis cascade. To demonstrate that CTP, the strongest inhibitor of the AGE K160I, was successfully excluded from the polymersome lumen by OmpF G119D, the reaction cascade was performed in the nano-scale enzyme membrane reactor with integrated OmpF G119D at different inhibitor concentrations of 3 mM and 50 mM CTP and compared to the non-compartmentalized reaction (Figure 6.15). In case of CTP entering the polymersomes, a reduction in reaction rate was expected, whereas the reaction rate should be unchanged when selectively compartmentalizing the reaction.

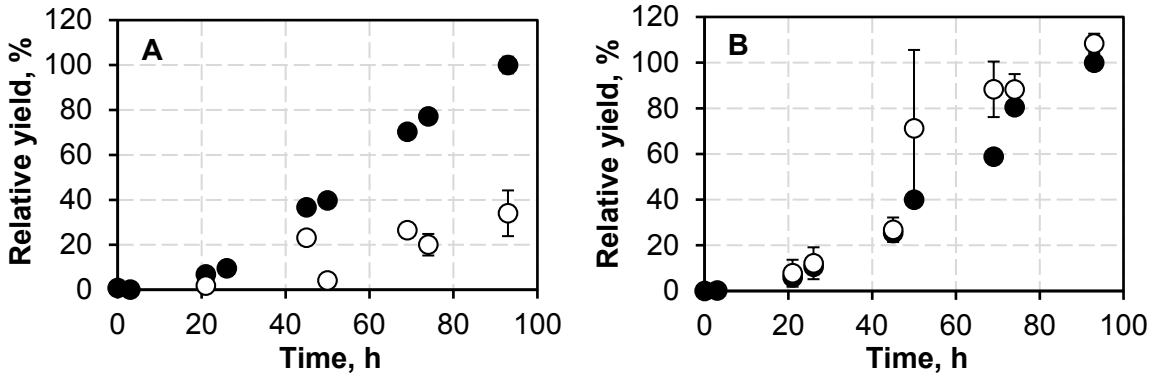

Figure 6.15 – Relative CMP-Neu5Ac production in the non-compartmentalized reaction (A) and the nano-scale enzyme membrane reactors (B) at 3 mM CTP (*black*) and 50 mM CTP (*white*). Whereas the reaction rate in the non-compartmentalized cascade reaction is reduced by high CTP concentrations, the reaction rate in the nano-scale enzyme membrane reactors is uncoupled from the CTP concentration by encapsulation of the AGE K160I in the lumen of the polymersomes, thereby shielding it from cross-inhibition by CTP. For each reaction system, the CMP-Neu5Ac concentration achieved after 93 h at 3 mM initial CTP concentration was set to 100%.

As expected, a strong reduction in the CMP-Neu5Ac yield was observed by increasing the CTP concentration from 3 mM to 50 mM when the cascade was not compartmentalized (Figure 6.15 A). This is in congruence with the inhibitory effect of CTP on the AGE K160I. At 50 mM CTP, the final yield of the non-compartmentalized reaction cascade was reduced to 34 ± 10 % compared to the activity at 3 mM CTP. With an inhibition constant K_i for CTP of 1 mM and a half-saturation constant K_M for ATP of 0.095 mM, the reaction rate of the AGE K160I is reduced to 17 % of the maximum reaction rate at 50 mM CTP and 1 mM ATP (Equation 3.4). Since CTP competes with the activator ATP for allosteric binding and since the AGE K160I has a remaining activity of approximately 16 % in the absence of ATP (unpublished data), a remaining AGE K160I activity of approximately 33 % was expected. At 3 mM CTP, the remaining AGE K160I activity is approximately 88 %, resulting in an overall

remaining activity of 37 % at 50 mM compared to 3 mM CTP. Thus, the results were in range with the expected activity loss of the AGE K160I due to CTP inhibition.

In contrast, the reaction rate of the compartmentalized reaction was successfully uncoupled from the CTP concentration (Figure 6.15 B). Within the nano-scale membrane reactor, the final yield at 50 mM CTP after 93 h was equivalent (108 ± 4 %) to the yield at 3 mM CTP. This uncoupling of the reaction rate from the CTP concentration is essential for the improvement of the reaction cascade, as it successfully eliminates the main cross-inhibition observed in the reaction cascade. Furthermore, it demonstrates that the polymer membrane with integrated OmpF G119D was capable of effectively segregating micromolecules, as it allowed diffusion of the substrates GlcNAc and ManNAc while abolishing CTP inhibition.

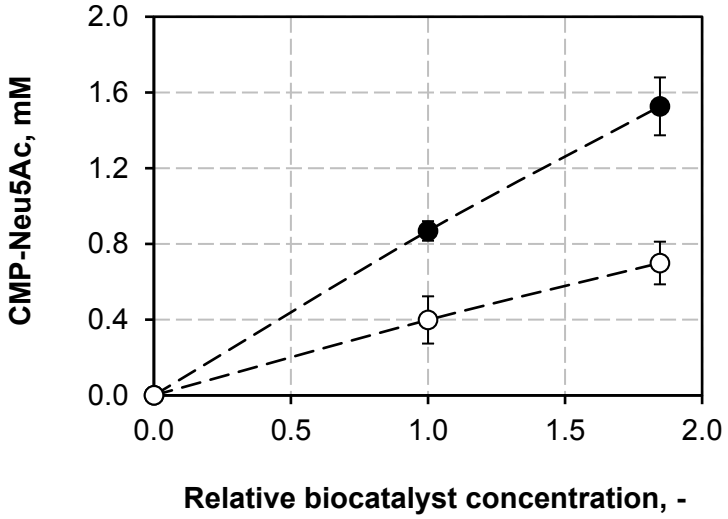

Figure 6.16 – Increase in CMP-Neu5Ac production at increased relative biocatalyst concentration(s) measured for the non-compartmentalized reaction cascade (*white*) and the nano-scale enzyme membrane reactors (*black*). A relative biocatalyst concentration of 1 represents the enzyme concentrations at 0.13 % w/v nano-scale enzyme membrane reactors. The lines are for visualization only.

Although only 1.7 % of the CTP was converted to CMP-Neu5Ac in 93 h, the overall low yield of the reaction was mainly due to the low biocatalyst concentration in the reaction. By increasing the concentration of freshly assembled nano-scale enzyme membrane reactors from 0.13 % w/v to 0.24 % w/v, the amount of CMP-Neu5Ac could be increased from 0.87 ± 0.03 mM to 1.53 ± 0.15 mM CMP-Neu5Ac in the same time (Figure 6.16). Since the enzyme concentrations in the non-compartmentalized reaction were adjusted according to the volumetric activities in the nano-scale membrane reactor set-up, the fold-changes in CMP-Neu5Ac synthesis compared to the non-compartmentalized cascades and the control set-ups were unchanged, resulting in a 2.2-fold increased productivity of the OmpF G119D-

functionalized nano-scale enzyme membrane reactors compared to the non-compartmentalized reaction cascade. Thus, increasing the biocatalyst concentration could increase the overall yield, whereas for a further enhancement of the cascade reaction, higher functionalization of the nano-scale enzyme membrane reactors with OmpF G119D is required to further reduce mass transport limitations.

6.4 Discussion

The use of polymersomes as nano-scale enzyme membrane reactors has been suggested by Discher *et al.* in 1999 when introducing polymer vesicles as alternative to liposomes (Discher *et al.*, 1999). However, compared to medical applications, the requirements for the use of polymersomes in biochemical applications are substantially different. The low permeability of polymer membranes is highly advantageous for medical applications such as drug delivery, in which drug release is at best not triggered before reaching the site of action. Triggering drug release has been extensively studied with various triggering mechanisms and usually aims at releasing all of the cargo (Palivan *et al.*, 2016). In contrast, the exchange of substrates and products across the membrane without a loss of the entrapped biocatalyst is required in biochemical application to alleviate mass transport limitations (Renggli *et al.*, 2011). Several multienzyme syntheses have recently been implemented into single- and multicompartment polymersome systems (van Dongen *et al.*, 2009; van Dongen *et al.*, 2010; Meeuwissen *et al.*, 2011; Gaitzsch *et al.*, 2012; Gräfe *et al.*, 2014; Peters *et al.*, 2014; Siti *et al.*, 2014), demonstrating the general ability to perform cascade reactions in nano-scale membrane reactors. However, none of the reaction cascades performed with nano-scale membrane reactors has been *per se* incompatible as recently emphasized by Schoonen and van Hest (2016). Thus, an improved reaction cascade due to compartmentalization was not expected and not possible. The lack of incompatibility allowed for an unspecific and non-selective mass transport across the membrane, which has been obtained by porous membranes or the integration of the unspecific porin OmpF. However, compartmentalization requires highly specific mass transport to have a positive effect on complex reaction cascades with cross-inhibitions, which has recently be emphasized in a review article by Schmitt *et al.* (2016) and was confirmed in this study.

The two fundamental advantages of PMOXA-PDMS-PMOXA polymersomes for the use as nano-scale enzyme membrane reactors are their low membrane permeability (Discher and Eisenberg, 2002) and the possibility to reconstitute functional membrane proteins, thereby allowing the introduction of a selective mass transport across the membrane to control the flux of desired substrates, intermediates and products (Renggli *et al.*, 2011).

Fundamental for the implementation of the three-step biosynthesis of CMP-Neu5Ac in polymersomes was the ability to establish a highly selective mass transport across the membrane via the reconstitution of an appropriate channel protein, in this case OmpF G119D. Despite the outstanding selectivity of membrane transport proteins on a micromolecule level, their reconstitution in nano-scale membrane reactors for biocatalytic purposes has been limited to OmpF. The unselective channel has the advantage of allowing the diffusion of several compounds and is thus applicable for various enzymatic reactions. However, this unselectivity is disadvantageous when requiring highly selective mass transport due to incompatibilities in the reaction cascade. Since the required selectivity differs depending on the implemented cascade reaction and the predominant incompatibilities, the choice of an appropriate membrane transport protein is crucial. Yet, due to the limited knowledge on the transport properties of many membrane transport proteins, the selection of suitable membrane channel proteins poses a major issue in view of a universal use of nano-scale enzyme membrane reactors for incompatible multienzyme syntheses. Thus, advances in the integration and characterization of novel membrane channels will be a fundamental requirement when extending the application of polymersomes as nano-scale enzyme membrane reactors. Recently, the incorporation of a synthetic DNA channel with a pore size of 1.5 nm into PMPC-PDPA polymersomes has been demonstrated that allows diffusion of molecules across the membrane (Messager *et al.*, 2016). Although the pore size is too large for selective mass transport discerning micromolecules, the ability to easily engineer DNA channels (Burns *et al.*, 2016) is a promising alternative to the use natural or engineered membrane channels.

Although the permeability of GlcNAc and ManNAc across the membrane was sufficient to synthesize CMP-Neu5Ac in nano-scale enzyme membrane reactors without membrane channel, the membrane permeability toward the reactants of the CMP-Neu5Ac synthesis was low according to the definition of Fischer *et al.* (2007), which is in congruence with permeability data for polymer membranes found in literature. For $PMOXA_{15}$-$PDMS_{110}$-$PMOXA_{15}$ polymersomes, a membrane permeability toward water of 10^{-5} cm s^{-1} was determined (Kumar *et al.*, 2007). Although the hydrophobic middle block is substantially longer than the one used in this study, the diffusion of water across the membrane was reduced a 1000-fold compared to lipid bilayers of approximately 10^{-2} cm s^{-1} (Alberts, 2015). This is similar to a 500-fold reduced permeability of GlcNAc (Pe = 10^{-10} cm s^{-1}) and ManNAc (Pe = 10^{-10} cm s^{-1}) across the $PMOXA_{15}$-$PDMS_{68}$-$PMOXA_{15}$ membrane compared to the permeability of glucose ($5 \cdot 10^{-8}$ cm s^{-1}) across lipid membranes (Wood *et al.*, 1968; Alberts, 2015). Likewise, Ca^{2+} has been demonstrated to be unable to diffuse across PMOXA-PDMS-PMOXA membranes with a mass of the hydrophobic block of 5400 g mol^{-1} (polymerization degree of approximately 73 monomeric units) (Sauer *et al.*, 2001), which is in congruence

with the extremely low permeability of the charged reactants pyruvate and Neu5Ac and the inability to detect diffusion of CTP and ATP across the PMOXA-PDMS-PMOXA membrane within 330 h. Despite measuring some degree of membrane diffusion of Neu5Ac and pyruvate, the permeability was in the range of Na^+ ($Pe = 10^{-12}$) and K^+ ($Pe = 5 \cdot 10^{-12}$ cm s^{-1}) ions across lipid membranes, which are considered to be impermeable and thus require specific Na^+/K^+ transporters to translocate across lipid membranes (Alberts, 2015).

Similarly, although OmpF G119D was not able to completely alleviate mass transport limitations, the reduced diffusion rates of monosaccharaides through OmpF G119D compared to wildtype OmpF have been shown before. Saint *et al.* (1996) have shown that the passive diffusion rate of GlcNAc is approximately 25 % compared to its diffusion through wildtype OmpF due to the reduced pore size of the mutated channel. Furthermore, although wildtype OmpF does not distinguish between the epimers glucose and mannose, diffusion of mannose through OmpF G119D was 50 - 65 % slower than diffusion of glucose, indicating that OmpF G119D prefers glucose over mannose. If this is also the case for the epimers GlcNAc and ManNAc, a reduced diffusion rate of 12 % is expected. This is in agreement with a drastically reduced diffusion of ManNAc through OmpF G119D obtained in this study of only 8 % compared to wildtype OmpF. However, it has to be noted that only the added ratio of channel protein-to-polymer of 1:1500 was kept constant, which does not take into account different insertion efficiencies of OmpF and OmpF G119D and thus different amounts of channel per polymersomes. Nevertheless, OmpF G119D could successfully partition the reaction space while maintaining compartmentalization for CTP, pyruvate and Neu5Ac. Since the mass transport can be increased by increasing the amount of membrane channels incorporated into the membrane, the ability to successfully compartmentalize the reaction spaces is more important than alleviating mass transport limitations in multienzyme syntheses suffering from cross-inhibitions. Yet, the extremely low insertion efficiency of OmpF G119D represents a major bottleneck in alleviating the observed mass transport limitations and needs to be addressed. Because OmpF has been added to polymersomes in substantially higher protein-to-polymer rations of 1:100 and 1:10 (Ranquin *et al.*, 2005), a higher degree of functionalization with OmpF G119D is realistic.

To circumvent problems with mass transport limitations, nano-scale enzyme membrane reactors have been based on an unselective exchange of substrates and products between the compartments (Schmitt *et al.*, 2016). Kuiper *et al.* (2008) and Peters *et al.* (2014) demonstrated that mass transport limitations could be almost completely alleviated for glucose, glucono-1,5-lactone, and profluorescent esters and alcohols using porous PS-PIAT polymersomes. Although the membrane effectively retained encapsulated enzymes, its intrinsic porosity allowed the diffusion of even large and charged molecules as demonstrated for ABTS and the $ABTS^+$ radical (Kuiper *et al.*, 2008; van Dongen *et al.*, 2009) and the

744 Da cofactor pair NADPH and $NADP^+$ (Meeuwissen *et al.*, 2011). Similarly, Gaitzsch *et al.* (2012) and Gräfe *et al.* (2014) used pH-responsive PEG-PDEAEM-PDMIBM polymersomes to alleviate mass transport limitations. By switching the pH from 8 to 6, the permeability of the membrane was increased due to the protonation of the hydrophobic middle block and a subsequent swelling of the membrane, allowing the translocation of several molecules including guaiacol, quinone, glucose, glucono-1,5-lactone, ABTS and $ABTS^+$ radicals. Neither PS-PIAT nor pH-responsive polymersomes were, however, sufficiently selective on a small molecule level to allow the performance of reactions with cross-inhibitions, highlighting the advantages of introducing selective membrane channels into a quasi-impermeable membrane.

Although intriguing multicompartment systems to spatially separate enzymes have been created, either using polymersomes with different enzymes as cargo (Gräfe *et al.*, 2014) or encapsulating small polymer vesicles in larger polymer vesicles (Peters *et al.*, 2014; Siti *et al.*, 2014), these set-ups are consequently more complex. Mass transport limitations need to be considered for each membrane compartment in a way that compartmentalization is still maintained, requiring highly sophisticated set-ups. The acquisition of the continuous, outer aqueous phase as a reaction space thus represents an interesting alternative. Although the ability to remove or recover the catalyst as a single entity is an important feature for using polymersomes as nano-scale enzyme membrane reactors (van Dongen et al. 2008 van Dongen *et al.*, 2008), only van Dongen *et al.* (2009) and Meeuwissen *et al.* (2011) addressed this issue by immobilizing the enzymes CalB, HRP and PAMO on polymersomes. Both CalB and HRP were immobilized in functional form via azide-alkyne cycloaddition for 60 - 65 h at 4°C with Cu^+ as catalyst as opposed to an incubation time of 48 - 60 h at 4°C required for peptide insertion. In this study, neither the amount of HRP nor CalB per polymersome nor any effects on enzyme activity have been reported. In contrast, the immobilization of PAMO via the same method led to an inactive enzyme and thus PAMO was added to the outer reaction space in soluble form (Meeuwissen *et al.*, 2011).

To this end, the presentation of more than one enzyme on the surface of a single polymersome has not been reported. The co-immobilization of an NAD^+ reductase and an alcohol dehydrogenase on carbon beads by electrostatic interactions has been reported to increase the reaction rate by 2-fold due to their spatial proximity (Reeve et al. 2015). Thus, a study designed to investigate the optimal distance of NAL and CSS may elucidate whether channeling effects can be evoked when immobilizing enzymes on a single polymersome. Although this was not part of the objectives of this study, the immobilization of multiple enzymes on a single polymersome may extend the scope of polymersome use to several application in which the presentation of two or more enzymes in close proximity may have positive effects.

The main limiting factor apart from mass transport limitations was the low amount of AGE K160I encapsulated in the polymersome lumen and thus the catalytic activity of the nano-scale enzyme membrane reactors as biocatalysts. Although the statistical encapsulation efficiency cannot exceed 100 % unless positive interactions occur between the polymersomes and the target protein (Wang *et al.*, 2012), the amount of encapsulated AGE K160I with 4 molecules was rather low compared to the ability to immobilize up to 2320 molecules on the polymersome surface. Encapsulation of enzymes is usually performed by adding enzymes to the bulk solution prior to polymersome formation and removal of non-encapsulated molecules via filtration or dialysis (O'Neil *et al.*, 2009). Although the amount of molecules that is encapsulated is dependent on the volume encapsulated by a single polymersome, and consequently its size, and the protein concentration in solution, which in turn is limited to a concentration in which polymersome readily form, the number of molecules encapsulated per polymersome reported in literature reach similar values compared to the 4 AGE K160I molecules encapsulated in this study. Vriezema *et al.* (2007) reported 14 GOx molecules in significantly larger PS-PIAT polymersomes of a mean diameter of 517 nm and Noor *et al.* (2012) reported 2 eGFP molecules in 100 nm-sized PIB-PEG-PIB polymersomes. In contrast the insertion efficiency in terms of protein encapsulated per total protein in the bulk solution is dependent on the total volume encapsulated by the polymersomes and is thus dependent on the size of the polymersomes and the polymersome concentration. By increasing the concentration of the polymersomes from typically applied 1 - 3 % w/v to 33 % w/v, O'Neil *et al.* (2009) were able to encapsulate 15-37 % of the protein present in solution using a direct hydration method for polymersome formation. Although this increases the efficiency in terms of encapsulating as much of the enzyme in the bulk solution as possible, excess enzyme can theoretically be reused after polymersome removal. Furthermore, amounts of encapsulated enzyme achieved by O'Neill did not exceed 2.4 - 12.8 µg encapsulated protein per mg polymer for ovalbumin, bovine serum albumin and γ-globulin, which is in range with the encapsulation achieved in this study of 5.64 µg encapsulated AGE K160I per mg polymer. Van Dongen *et al.* (2009) and Meeuwissen *et al.* (2011) reported an encapsulation efficiency of 20 - 25 % for the encapsulation of G6PDH and GOx in PS-PIAT polymersomes of 90 to 180 nm, which is significantly more than the expected value of 0.1 % derived from the polymersome size and concentration. Van Dongen *et al.* (2009) postulate a positive influence on the polymersome formation process by nucleation of polymer aggregates around transient protein aggregates.

An interesting alternative to passive encapsulation of the bulk medium during polymersome formation is the active loading of polymersomes via electroporation. Wang *et al.* (2012) were able to incorporate proteins at the 15 – 21-fold of the maximum statistical encapsulation efficiency using electroporation, reaching a loading of up to 160 BSA molecules per

polymersome. Since the protein loading via electroporation is performed on preformed polymersomes, the protein concentration applied in the bulk solution is not constrained to a concentration at which polymersome formation is still possible. However, Wang et al. (2012) used a polymer with a membrane thickness of 6.5 nm, which is substantially less than the 14 nm thick $PMOXA_{15}$-$PDMS_{68}$-$PMOXA_{15}$ membrane. Thus, the feasibility of encapsulation via electroporation has to be investigated for PMOXA-PDMS-PMOXA polymersomes.

7. Surface functionalization by *in vitro* protein synthesis

The expression and purification of proteins fused to peptide anchors for the surface functionalization of nano-scale enzyme membrane reactors posed a major limiting factor due to the association of the peptide anchor to the membrane or its aggregation in the cytosol, leading to substantial decreases in isolated yields of up to 90 % compared to expression without peptide anchor. To circumvent these issues, the synthesis of eGFP and CSS fused to peptide anchors was investigated with *in vitro* protein synthesis (IVPS) in the presence of polymersomes as salvaging membrane. A schematic representation of the approach is depicted in Figure 7.1.

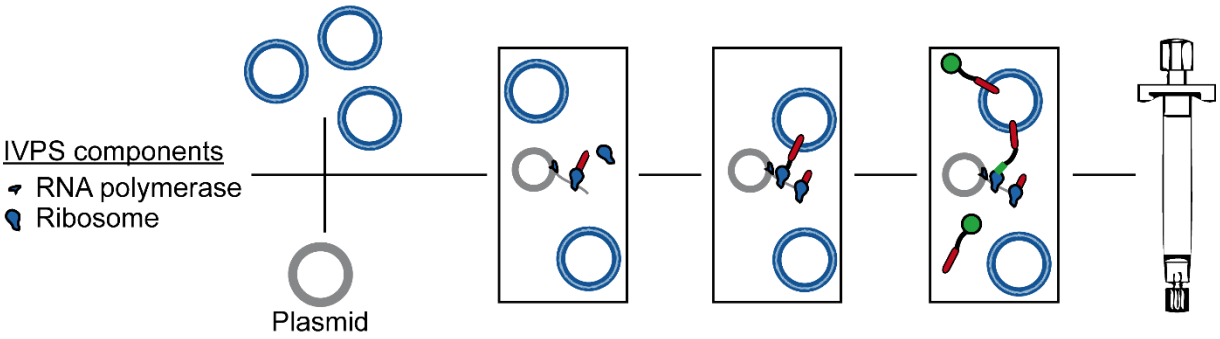

Figure 7.1 – Schematic depiction of the *in vitro* protein synthesis (IVPS) of peptide anchor-fused proteins in the presence of polymersomes. The IVPS including the transcription and translation machinery is assembled together with the plasmid encoding the respective target protein and the preformed polymersomes in one pot. In the first step, the plasmid DNA is transcribed into mRNA. Ribosomes bind to the nascent mRNA strand, which is translated into the target protein. In step two and three, the hydrophobic peptide anchor spontaneously associates with the available hydrophobic membrane. After IVPS is completed, the polymersomes are separated from the IVPS components by SEC.

Since lysates from different organisms can have a profound influence on the expression yield (Hillebrecht and Chong, 2008), four different systems were investigated. These comprised two commercially available expression kits, an *E. coli* lysate and a wheat germ lysate and two expression kits based on lysates from insect cells and Chinese hamster ovary (CHO) cells generously provided by the Bioanalytics and Bioprocesses (IZI-BB) group (Dr. Kubick) of the Fraunhofer Institute for Cell Therapy and Immunology (IZI) in Potsdam, Germany. The insect cell and CHO lysates were prepared for protein encapsulation in microsomes, which are small, lipid-based vesicles, and should thus be compliant with polymersomes. In contrast, the composition of the commercially available *E. coli* and wheat germ extracts was not

available. Since integrity of the polymersomes during peptide insertion is crucial, each lysate was checked for compatibility with the polymersomes. Especially detergents used during lysate preparation or added for the stabilization of lysate components may be detrimental for a combined use with polymersomes.

7.1 Polymersome integrity

The integrity of the polymersomes in the lysates was assessed by encapsulating calcein at a self-quenching concentration within the polymersomes and measuring calcein release after addition of the polymersomes to the lysates. No template DNA was added, thus protein synthesis was not initiated. By following the progression curve of the fluorescence in the sample, a release of calcein was detected in the *E. coli* and the wheat germ lysates, although only approximately 7.66 ± 0.12 % and 6.12 ± 0.37 % of the calcein was released after 2 h, respectively. In comparison, during the incubation of the polymersomes in the insect and CHO lysates, 0.26 ± 0.27 % and 1.32 ± 0.17 % calcein was released, respectively. Thus, the two commercial IVPS kits had a slight adverse effect on the polymersome integrity. As expected, the cell lysates that were optimized for harboring microsomes had little to no influence on the membrane integrity.

7.2 *In vitro* protein synthesis in the presence of polymersomes

The *E. coli* and the wheat germ lysates were checked for synthesis and insertion of eGFP-Cytb_5' and eGFP-L' at a polymersome concentration of 0.1 % w/v. The presence of the polymersomes had no apparent effect on the protein yield of the lysates when synthesizing eGFP-Cytb_5', reaching a final concentration of 12.9 ± 0.5 µg mL^{-1} without polymersomes and 14.3 ± 0.5 µg mL^{-1} with polymersomes after 2 h of incubation at 37°C (Figure 7.2). Interestingly, eGFP-L' synthesis was reduced by approximately 50 % in the presence of polymersomes, reaching 35.1 ± 1.6 µg mL^{-1} without polymersomes and 15.3 ± 0.2 µg mL^{-1} with polymersomes.

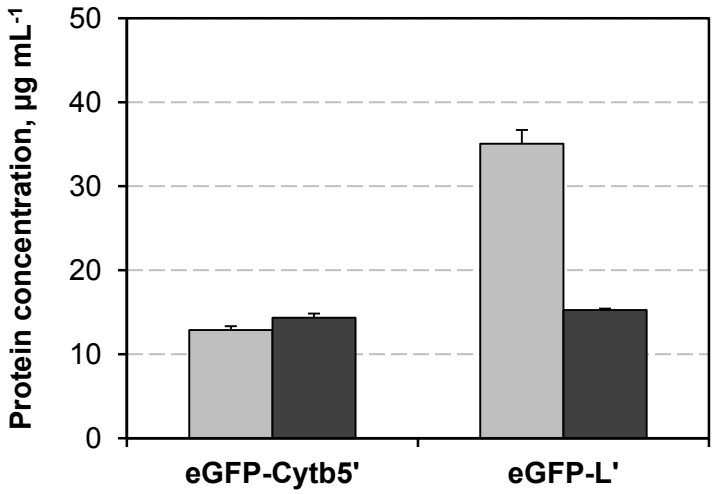

Figure 7.2 – Protein concentration obtained with the *E. coli* lysate after 2 h incubation at 37°C without polymersomes (*gray*) and with polymersomes (*black*) for eGFP-Cytb_5' and eGFP-L'.

Although a slight defect of the polymersomes was observed in the *E. coli* lysate leading to minor calcein release, insertion of the peptide anchors into the polymersomes was detected for both eGFP-Cytb_5' and eGFP-L', measuring substantial fluorescence in the fractions containing polymersomes (Figure 7.3). The co-localization of the fluorescence and the polymersome peak clearly demonstrate the general feasibility of the simultaneous protein synthesis and peptide insertion into the polymer membrane. Quantification of the peptide insertion revealed that with eGFP-Cytb_5' 6.0 eGFP molecules were immobilized per polymersome. With a total eGFP-Cytb_5' concentration of 0.37 µM and a polymersome concentration of 0.1 % w/v, an insertion efficiency of 16.2 eGFP pol^{-1} µM^{-1} applied protein was obtained. For eGFP-L', 4.3 eGFP molecules were immobilized per polymersomes at a total eGFP-L' concentration of 0.39 µM, reaching an insertion efficiency of 11.0 eGFP pol^{-1} µM^{-1} applied protein concentration.

Although demonstrating the ability to combine protein synthesis and surface functionalization using IVPS, the insertion efficiencies of eGFP-Cytb_5' and eGFP-L' were approximately 84 % and 54 % lower than when adding purified proteins to the same amount of polymersomes, which amounted to approximately 100 and 24 eGFP pol^{-1} µM^{-1} at 0.1 % w/v polymersomes for Cytb_5' and L', respectively.

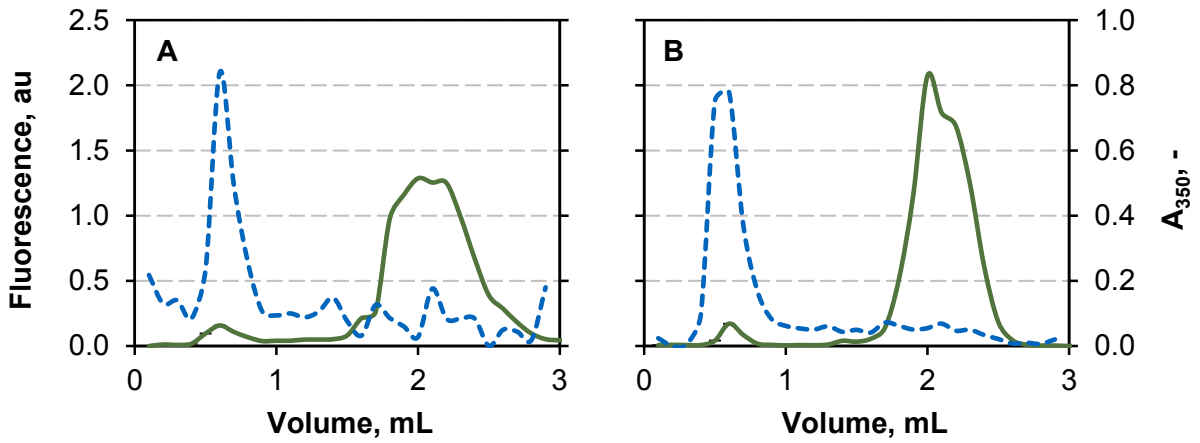

Figure 7.3 – Chromatograms of the eGFP fluorescence (*green*) and the absorbance at 350 nm (*blue, dashed*) of the SEC after peptide insertion during *in vitro* protein synthesis of eGFP-Cytb_5' (A) and eGFP-L' (B). The co-localization of the fluorescence signal and the absorbance signal at an elution volume of 0.3 – 0.8 mL demonstrates a successful coupling of the fusion protein synthesis and the peptide insertion into polymersomes. Fluorescence is given in arbitrary units (au).

In contrast to the *E. coli* lysate, protein concentrations obtained with the wheat germ extract were extremely low and reached only approximately 0.5 - 0.6 µg mL^{-1} for both eGFP-Cytb_5' and eGFP-L'. Although the polymersomes had no adverse effect on the protein synthesis, no fluorescence was detected in the fractions containing polymersomes. Since the peptide insertion is linearly dependent on the protein concentration, the poor results were most likely due to the low synthesis yield of the wheat germ extract. Thus, the wheat germ extract was considered to be not efficient enough for a combined protein synthesis and polymersome functionalization approach.

Whereas a slight destabilization of the polymersomes by the *E. coli* lysate and the wheat germ extract was observed, the insect cell and CHO lysates were fully compatible with polymersomes. Both the insect cell and the CHO lysate were investigated with CSS-L' as target protein. CSS-L' was more difficult to heterologously express in *E. coli* and less stable in solution than eGFP-L' or eGFP-Cytb_5' and would thus benefit from a simultaneous production and immobilization approach. After IVPS with the insect cell lysate in the presence of 0.1 % w/v polymersomes and subsequent purification of the polymersomes, a volumetric CSS activity of 0.42 U L^{-1} was detected in the fractions containing polymersomes (Figure 7.4). No activity was detected in the control experiments that were performed either without template DNA or without polymersomes, indicating that the observed activity was indeed a result of the combined protein synthesis and peptide insertion into the polymersomes. However, although active polymersomes were obtained after IVPS using the insect cell lysate, the activity was extremely low, corresponding to one CSS-L' molecule in every 25 polymersomes. Unfortunately, the high phosphate concentration in the lysate did

not allow for a quantification of the total CSS concentration synthesized with the insect cell lysate. Thus no insertion efficiency could be calculated. The low activities may thus result from a poor protein yield and a resulting low peptide insertion, similar to the low yields obtained in the wheat germ extract.

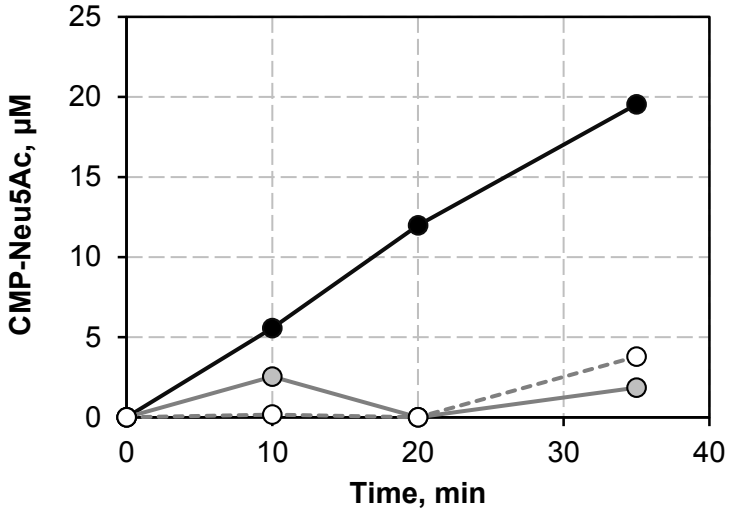

Figure 7.4 – CSS activity in the purified polymersome fraction after *in vitro* protein synthesis with the insect cell lysate in the presence of polymersomes (*black*), in the absence of polymersomes (*gray*) and in the absence of template DNA (*white*). The lines are for visualization.

In contrast to the insect lysate, no CSS activity was detected in the polymersome containing fraction when producing CSS-L' with the CHO lysate. Thus, like the wheat germ extract, CHO lysates were considered not suitable for the combined approach. Since the limiting factor, however, was protein synthesis rather than an incompatibility with the polymersomes, production of other proteins or enzymes may reach higher concentrations and thus a better incorporation of the peptide anchors. Furthermore, optimization of the protein synthesis conditions may substantially improve the protein yield and thus the peptide insertion.

7.3 Discussion

The combined cell-free synthesis and integration into membrane vesicles such as microsomes, micelles and liposomes, has been proposed as a facile way in expressing functional membrane proteins (Sachse *et al.*, 2014). So far, several membrane channels have been synthesized using IVPS, including, amongst others, the MraY translocase (Ma *et al.*, 2011), the mannitol permease (Kuruma *et al.*, 2005; Wuu and Swartz, 2008) and the porin pOmpA (Kuruma *et al.*, 2005). Especially by making tedious expression and purification

steps obsolete and by circumventing problems with protein stability in aqueous solution, IVPS can greatly facilitate the synthesis of correctly folded membrane proteins. Thus, IVPS may be a viable tool for reconstituting membrane channels in polymersomes or presenting hydrophilic enzymes on the surface of polymersomes using hydrophobic peptide anchors without tedious membrane solubilization and protein polishing steps.

A significant factor for protein synthesis using IVPS is the choice of lysate. According to Hillebrecht and Chong (2008), the yield of functional target protein can be influenced by employing eukaryotic lysates for eukaryotic proteins and bacterial lysates for bacterial proteins. This was reflected by the different yields obtained in this study. Yet, although the fusion proteins synthesized in this study were fusions of bacterial, eukaryotic and viral segments, no posttranslational modifications were required allowing the synthesis of the fusion proteins via prokaryotic or eukaryotic lysates. Thus, the differences in the lysates were most likely due to generally lower yields obtained in eukaryotic lysates than in prokaryotic lysates, rendering the *E. coli* lysate most suitable for the coupling of protein synthesis and peptide insertion.

Nallani *et al.* (2011) were the first to use IVPS for the expression and simultaneous incorporation of a membrane protein, claudin-2 (Cldn2), into polymersomes. Since Cldn2 is a eukaryotic protein, a wheat germ extract was used. Cldn2 could be detected in the purified polymersome fraction, however, the amount of protein per polymersome was not quantified. Nevertheless, the presence of the polymersomes did not interfere with protein synthesis, which is in congruence with the presence of polymersomes not interfering with protein synthesis of eGFP-Cytb_5'. Similarly, Nomura *et al.* (2007) reported no adverse or beneficial effect when adding lipid membranes when synthesizing eGFP and dihydrofolate reductase (DHFR) fused to apo-cytochrome b_5 in the presence of giant liposomes. Although Nomura et al. (2007) emphasize that the nascent hydrophobic peptide was salvaged right after synthesis by the immediate insertion of apo-cytochrome b_5 into the lipid bilayer of the giant liposomes, no increased synthesis yield or increased activity of the synthesized proteins was detected. Furthermore, although Nomura *et al.* (2007) argue that most of the eGFP was immobilized on the surface of the liposomes, the DHFR activity in the liposome-containing fraction was relatively low and close to the detection limit. Similarly, May *et al.* (2013) report a high insertion efficiency of 25 % when synthesizing the dopamine receptor D2 (DRD2) in the presence of $PMOXA_{20}$-$PDMS_{54}$-$PMOXA_{20}$ and PBd_{22}-PEO_{12} polymersomes using the same wheat germ extract as used in this study. However, the overall low expression yield obtained by May *et al.* (2013) is indicated by an unspecific binding of the DRD2-specific antibody to non-functionalized polymersomes of 35 – 38 % of that obtained for DRD2-functionalized polymersomes, which seems high considering the specificity of antibodies. Thus, the inability to detect peptide insertion into the polymer membrane when using the wheat germ extract

may be due to protein expression being below the detection limit of the analytical methods used.

The main limitation of using IVPS for the surface functionalization of polymersome was the overall low synthesis yield. Although the *E. coli* lysate can reach protein concentrations of up to 500 µg mL^{-1} according to the suppliers manual, only 20 - 40 µg mL^{-1} of the target protein were synthesized. Similarly, only 0.5 - 0.6 µg mL^{-1} of the target protein were synthesized with the wheat germ extract as opposed to a maximum of 10 µg mL^{-1} that can be obtained according to the supplier. A major concern raised by Iskakova *et al.* (2006) is the uncoupling of the tightly coupled transcription/translation apparatus by introducing the bacteriophage T7 RNA polymerase to commercial lysate systems, which can significantly lowers synthesis yields. The T7 RNA polymerase transcribes DNA more rapidly than *E. coli* or eukaryotic RNA polymerase, which can lead to the destabilization of the mRNA or the formation of secondary RNA structures hindering translation and thus synthesizing less protein (Iskakova *et al.* 2006). For example, synchronizing the transcription and translation by lowering the synthesis temperature or by slowing down the RNA polymerase activity through the introduction of site-directed mutations has been demonstrated to significantly improve the synthesis of eGFP (Iskakova *et al.*, 2006). Thus, optimizing the synthesis conditions, especially in terms of temperature and synthesis duration, may have a significant effect on the overall protein concentrations achieved with IVPS kits and thus improve the overall performance of the surface functionalization using IVPS systems. Furthermore, continuous or semi-continuous IVPS can lead to substantially higher protein concentrations (Katzen *et al.*, 2005; Stech *et al.*, 2014; Quast *et al.*, 2016) and thus lead to improved surface functionalization using a combined synthesis and insertion approach. Nevertheless, the general feasibility of the synthesis of the fusion proteins and the simultaneous peptide insertion into $PMOXA_{15}$-$PDMS_{68}$-$PMOXA_{15}$ polymersomes in a one-pot reaction using IVPS in the presence of polymersomes was successfully demonstrated for the *E. coli* and insect cell lysates.

8. Summary

Hollow vesicles formed from block copolymers have been extensively studied in the last decade for their various applications in drug delivery, in diagnostics and as nano-scale enzyme membrane reactors. For each application, the immobilization of proteins on the polymersome surface is desired as it can aid in cell targeting, lead to functional biosensors or add an additional reaction space for multistep syntheses. In almost all surface functionalization strategies to date, a chemical pre-conjugation of the polymer with a reactive group or ligand and the functionalization of the protein are required, which leads to extensive chemical modification. To avoid this chemical pre-conjugation, the functionalization of unmodified, preformed poly(2-methyloxazoline)$_{15}$-poly(dimethylsiloxane)$_{68}$-poly(2-methyl-oxazoline)$_{15}$ (PMOXA$_{15}$-PDMS$_{68}$-PMOXA$_{15}$) polymersomes through the spontaneous insertion of hydrophobic, non-antibacterial peptide anchors into the membrane was investigated. The enhanced green fluorescent protein (eGFP) served as a model protein for easy detection and quantification of the peptide insertion.

Four of five investigated non-antibacterial peptide anchors, the membrane domains of cytochrome b_5 (Cytb_5') from rabbit liver, of the lysis protein L (L') of the bacteriophage MS2, of the ubiquitin-conjugating enzyme 6 (UBC6') of *Saccharomyces cerevisiae* and of the syntaxin VAM3 (Vam3p') of *Saccharomyces cerevisiae* could be recombinantly expressed as soluble fusion proteins with eGFP (Table 8.1). The fifth peptide, an artificial alpha-helix made of a repetitive sequence of alanines and leucines (PolyAL), could not be expressed in functional form and was thus not further investigated. The antibacterial peptide cecropin A (CecA) served as a reference peptide whose integration into poly(isobutylene)-poly(ethylene glycol)-poly(isobutylene) (PIB-PEG-PIB) polymersomes has already been demonstrated (Noor *et al.*, 2012). Cytb_5' and L' exhibited no influence on the eGFP fluorescence, whereas the highly hydrophobic UBC6' and Vam3p' and the reference peptide CecA, had a strong negative impact on protein folding and chromophore formation, reducing eGFP fluorescence by 62 – 88 %. However, each peptide anchor was capable of spontaneously inserting into PMOXA$_{15}$-PDMS$_{68}$-PMOXA$_{15}$ membranes, thereby tethering eGFP to the surface of the preformed polymersomes. Peptide insertion into the polymer membrane was possible at a broad temperature range of 4 – 42°C and a pH of 8.0, allowing for extremely mild insertion conditions. At 37°C, peptide insertion reached its maximum after approximately 3 – 7 h. At 4°C, peptide insertion took approximately 48 h to reach maximum insertion, which was 60 - 70 % of the maximum insertion obtained at 37°C.

Table 8.1 – Properties of the peptide anchors used in this study and the preparation and insertion properties when fused to the model protein eGFP. (aa = amino acids; pol = polymersome; au = arbitrary units)

	Cytb_5'	**L'**	**UBC6'**	**Vam3p'**	**PolyAL**	**CecA**
Length, # aa	43	55	17	19	31	37
Hydrophobicity, % hydrophobic aa	56	47	83	84	96	46
Isolated yield (shake flask culture), mg L^{-1}	2.7	5.5	0.6	2.1	n/a[b)]	1.2
Rel. fluorescence, %	103 ± 6	103 ± 10	12 ± 2	27 ± 6	n/a	38 ± 4
Inserted molecules pol^{-1} μM^{-1} applied protein [a)]	21 ± 1	4.8 ± 0.2	27 ± 3	3.7 ± 0.4	n/a	1.6 ± 0.1
Fluorescence (au) pol^{-1} μM^{-1} applied protein [a)]	256.6 ± 15.7	60.8 ± 6.3	41.2 ± 3.4	10.4 ± 2.7	n/a	6.1 ± 1.8

[a)] at 37°C for 4 h with 0.5% w/v polymersomes; [b)] n/a: not available

Characterization of the surface functionalization using hydrophobic peptide anchors revealed that the peptide insertion was linearly dependent on the protein concentration with 26.8 ± 2.6, 20.7 ± 0.7, 4.8 ± 0.2 and 3.7 ± 0.4 eGFP molecules being immobilized per polymersome per µM applied protein for UBC6', Cytb_5', L' and Vam3p', respectively. Due to the reduced eGFP fluorescence when fused to UBC6', the peptide anchors Cytb_5' and L' performed best for the surface functionalization of polymersomes with eGFP immobilizing 256.6 ± 15.7 and 60.8 ± 6.3 arbitrary fluorescence units (au) per polymersome and µM applied protein, respectively. The peptide insertion was independent of the polymersome concentration until the available surface area became limiting and the polymersomes were fully loaded with protein. Up to 2320 ± 280 eGFP molecules were immobilized on a single polymersome, which is in congruence with the calculated maximum loading capacity of 2254 molecules per polymersome at the highest-density hexagonal packing of eGFP. Thus, the polymersomes could be completely coated with protein without destabilizing or disintegrating the polymersomes. This represents a 14-fold higher degree of surface functionalization compared to chemical and a 100-fold higher degree compared to non-covalent functionalization of polymersomes found in literature (Pang *et al.*, 2008; Nehring *et al.*, 2010).

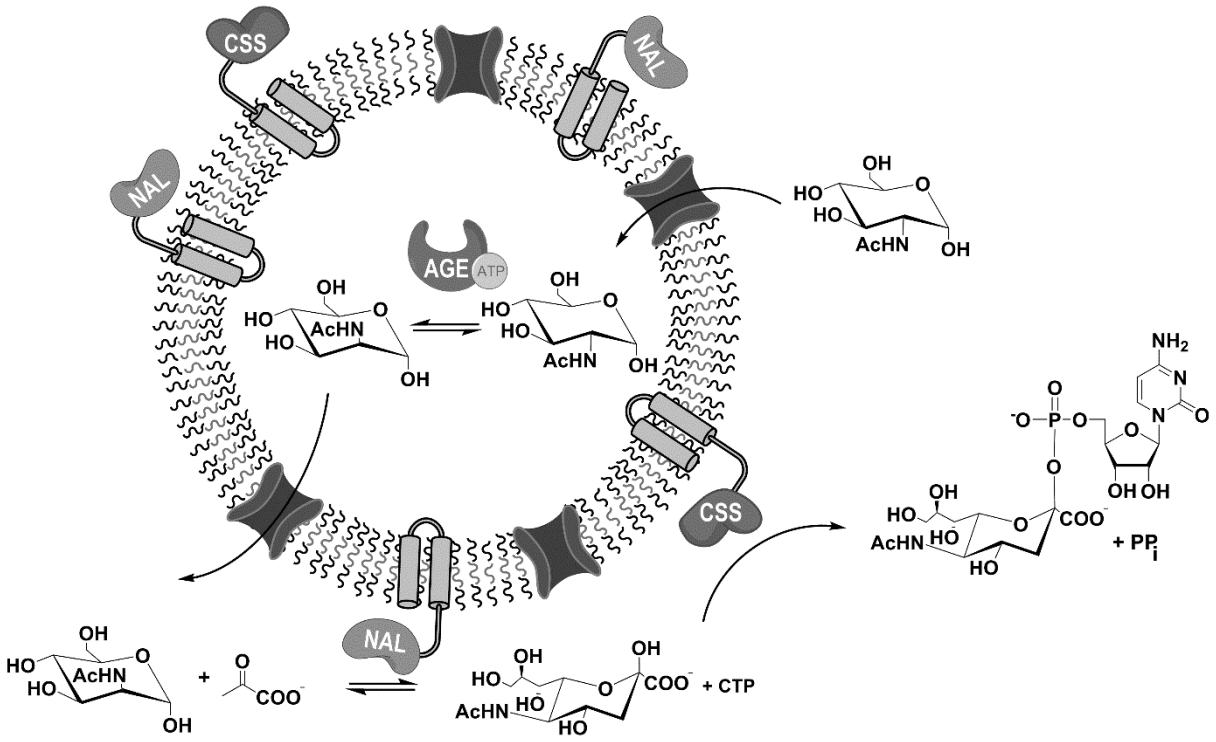

Figure 8.1 – Schematic representation of the nano-scale enyme membrane reactor for the biosynthesis of CMP-Neu5Ac. The *N*-acyl-d-glucosamine 2-epimerase (AGE) is encapsulated in the polymersome lumen to shield it from cross-inhibitions by CTP. The *N*-acetylneuraminate lyase (NAL) and the CMP-sialic acid synthetase (CSS) are immobilized on the polymersome surface via hydrophobic peptide anchors to yield a single biocatalytic entity. Selective mass transport of the substrates of the AGE across the membrane is introduced by a membrane channel protein.

The successful surface functionalization of the polymersomes via hydrophobic peptide anchors can make the outer reaction space accessible for multienzyme syntheses and thus enables a compartmentalization of the reaction via polymersomes as a single biocatalytic unit. The compartmentalization potentially allows the enhancement of incompatible reaction cascades in one pot by spatially separating the incompatible reaction steps. For the assessment of the applicability of $PMOXA_{15}$-$PDMS_{68}$-$PMOXA_{15}$ polymersomes as nano-scale enzyme membrane reactors to enhance reaction cascades that suffer from cross-inhibitions, polymersomes were equipped with the enzymes catalyzing the model three-step enzymatic synthesis of cytidine-5'-monophospho-*N*-acetylneuraminic acid (CMP-Neu5Ac) (Figure 8.1). The incompatibility of the cascade reaction mainly arises from a strong inhibition of the substrate CTP of the third reaction, the activation of *N*-acetylneuraminic acid (Neu5Ac) with CTP to form CMP-Neu5Ac by a CMP-sialic acid synthetase (CSS), on the enzyme of the first reaction, an *N*-acyl-D-glucosamine 2-epimerase (AGE) which epimerizes *N*-acetylglucosamine (GlcNAc) to *N*-acetylmannosamine (ManNAc). Thus, the AGE was spatially separated from CTP by encapsulating the enzyme within the polymersomes

whereas the *N*-acetylneuraminate lyase (NAL) and the CSS were immobilized on the surface of the polymersomes via hydrophobic peptide anchors.

The AGE variant K160I of *Anabaena variabilis* ATCC 29413, which has an improved stability in the presence of pyruvate (Klermund *et al.*, 2016b), was encapsulated within the polymersomes with an encapsulation efficiency of 82 ± 17 % – 89 ± 16 %. The maximum amount of AGE K160I per polymersome was, however, limited by an inability of the polymer to self-assemble to polymersomes at protein concentrations exceeding 1.5 g L^{-1}, resulting in a maximum of four AGE K160I molecules per polymersome. The NAL and the CSS, which catalyze reaction two and three in the three-step biosynthesis of CMP-Neu5Ac were successfully immobilized on the polymersome surface using hydrophobic peptide anchors. The insertion behavior of the peptide anchors in fusion with NAL and CSS was similar to the insertion behavior of the peptide anchors in fusion with eGFP indicating a general transferability of the surface functionalization of polymersomes with peptide anchors to biocatalytically active enzymes. Peptide insertion could be performed with each peptide anchor at mild conditions of 4°C and pH 8.0. In terms of conferring biocatalytic activity to the polymersomes, Cytb_5' performed best in immobilizing the NAL with an insertion efficiency of 9.2 ± 2.1 NAL molecules per polymersome per µM applied protein, whereas the CSS was best immobilized using the L' anchor with an insertion efficiency of 5.2 ± 0.6 CSS molecules per polymersome and µM applied protein. Hereby, the kinetic parameters of the NAL were not altered upon immobilization. In contrast, the activity of the CSS was reduced by 67.9 ± 10.5 % upon immobilization with a moderate increase of the half-saturation constant for CTP from 80 ± 40 µM to 250 ± 30 µM. However, the thermostability of the CSS at 30°C was increased 24-fold with an increased half-life τ of 1.47 ± 0.11 h to 36.2 ± 1.5 h, thus counteracting the reduced activity at long process times. Furthermore, both enzymes could be immobilized on a single polymersome to obtain a single biocatalytic entity. The simultaneous immobilization with both fusion proteins present at the same time had a positive effect on the immobilization efficiency of NAL-Cytb_5', which was increased up to 2-fold in the presence of a 3-fold molar excess of CSS-L' over NAL-Cytb_5', whereas the insertion efficiency of CSS-L' was not affected by the presence of the other fusion protein.

Essential for the implementation of the intrinsically incompatible cascade reaction in polymersomes is a selective permeability across the membrane allowing GlcNAc and ManNAc diffusion while excluding CTP from the polymersome lumen. Although PMOXA-PDMS-PMOXA membranes are considered to have a low permeability, the polymer membrane was slightly permeable toward the AGE K160I substrates GlcNAc and ManNAc with permeability coefficients of $1.06 \cdot 10^{-10}$ and $1.13 \cdot 10^{-10}$ cm s^{-1}, respectively, and hardly permeable toward the charged reactants pyruvate ($9.84 \cdot 10^{-13}$ cm s^{-1}) and Neu5Ac ($3.00 \cdot 10^{-13}$ cm s^{-1}). A diffusion of the highly charged nucleotides CTP and ATP across the

polymer membrane was not detected in the measured time span of two weeks. To increase the flux of the substrates GlcNAc and ManNAc but keep CTP from entering the polymersomes and inhibiting the AGE K160I, the outer membrane porin OmpF of *E. coli* and an OmpF variant, the OmpF mutant G119D, were chosen. With a molecular mass cut-off (MMCO) of 600 Da, OmpF allowed a fast diffusion of GlcNAc, ManNAc, pyruvate and Neu5Ac, but also allowed a slow diffusion of nucleoside triphosphates. In contrast, through the single amino acid mutation at position 119 from glycine to aspartate, the pore size of OmpF G119D is constricted to 300 Da with a 2.4-fold increased cation selectivity (Jeanteur *et al.*, 1994). The reconstitution of OmpF G119D allowed the diffusion of GlcNAc and ManNAc (both 221 Da) across the membrane, while successfully retaining Neu5Ac (309 Da) and the nucleoside triphosphates CTP (483 Da) and ATP (507 Da). The diffusion of pyruvate (88 Da) was strongly reduced, presumably due to the increased cation selectivity of OmpF G119D compared to wildtype OmpF and the negative charge of the pyruvate at pH 8.0. Thus, whereas OmpF effectively alleviated mass transport limitations, only the OmpF G119D variant was selective for the AGE K160I substrates GlcNAc and ManNAc and did not allow diffusion of CTP.

The performance of the nano-scale enzyme membrane reactors with reconstituted OmpF G119D was compared to the reaction cascade performed free in solution without compartmentalization (Figure 8.2). Due to the cross-inhibitions and the low thermostability of the CSS, no product formation was detected after 93 h when performing the non-compartmentalized reaction cascade. By immobilization of the NAL and the CSS on the polymersome surface, thereby increasing the stability of the CSS, the non-compartmentalized reaction cascade reached a CMP-Neu5Ac concentration of 0.40 ± 0.12 mM in 93 h. By compartmentalization of the reaction in nano-scale enzyme membrane reactors with selective mass transport across OmpF G119D, the CMP-Neu5Ac production could be enhanced by 2.2-fold to a CMP-Neu5Ac concentration of 0.87 ± 0.03 mM in the same time interval.

Crucial for the functional compartmentalization was a selective mass transport across the membrane to reduce mass transport limitations while maintaining the compartmentalization, which was demonstrated by incorporating no membrane channel, the unselective channel protein OmpF (MMCO = 600 Da) and the engineered channel OmpF G119D (MMCO = 300 Da). OmpF G119D allowed GlcNAc and ManNAc diffusion while keeping CTP (483 Da) from entering the polymersomes. Whereas the low intrinsic permeability of the polymer membrane toward GlcNAc and ManNAc led to the synthesis of 0.22 ± 0.06 mM CMP-Neu5Ac within 93 h, the observed mass transport limitations could be alleviated by reconstitution of the unselective membrane channel OmpF into the polymer membrane. OmpF led to a fast diffusion of GlcNAc and ManNAc across the membrane,

however, its non-selectivity led to a release of the AGE K160I activator ATP from the polymersome lumen and an influx of the AGE K160I inhibitor CTP. Reconstitution of OmpF into functionalized nano-scale enzyme membrane reactors resulted in a CMP-Neu5Ac synthesis of 0.49 ± 0.08 mM, which was in range with the non-compartmentalized cascade reaction synthesizing 0.40 ± 0.12 mM CMP-Neu5Ac, and could thus not enhance the reaction cascade.

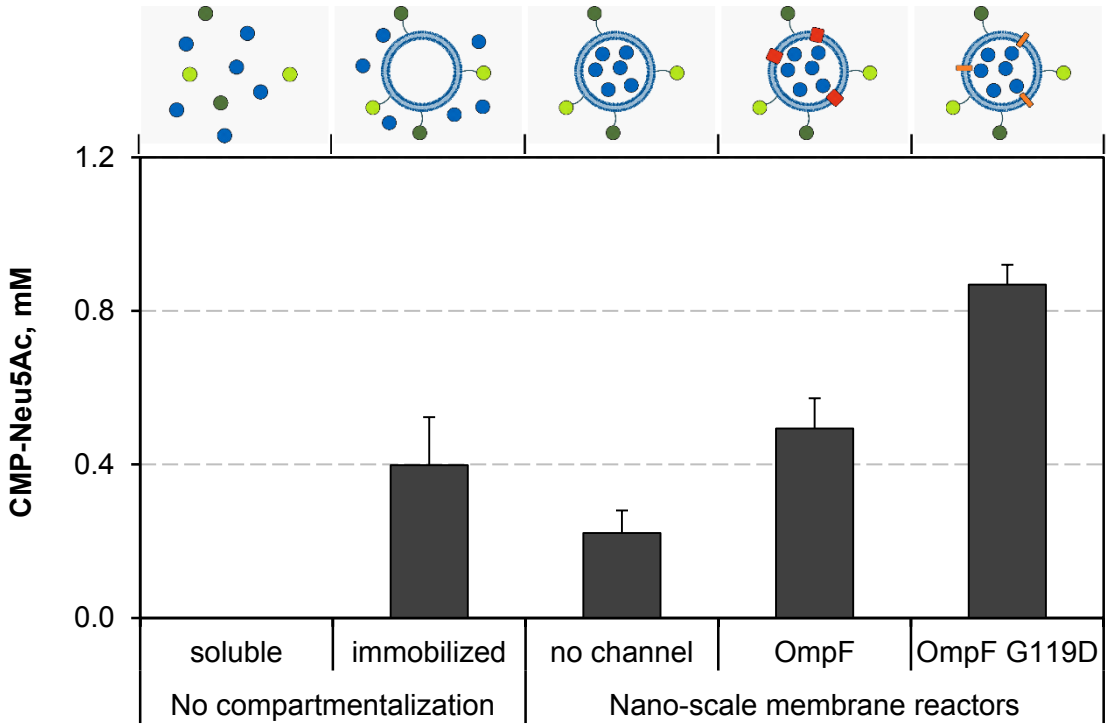

Figure 8.2 – CMP-Neu5Ac yield after 93 h in non-compartmentalized and compartmentalized reaction set-ups. The set-ups are schematically represented above the corresponding bar. The schematic representations of each set-up containing AGE (*blue*), NAL (*light green*), CSS (*dark green*), and OmpF (*red*) or OmpF G119D (*orange*), where applicable, is shown above the respective bar.

The implementation of a reaction cascade that suffers from an incompatibility in form of cross-inhibitions as well as the controlled and highly selective mass transport across the membrane extends the scope of polymersome applications for multienzyme syntheses and addresses two recently emphasized deficits in current polymersome technology, that only compatible reaction cascades have been implemented and that increased mass transport has always been non-selective (Schmitt *et al.*, 2016; Schoonen and van Hest, 2016). Although the results are far from optimized conditions, they demonstrate that by selectively controlling mass transport, multienzyme syntheses that suffer from cross-inhibitions can be enhanced through compartmentalization of the reaction steps in nano-scale enzyme membrane reactors.

Lastly, to reduce tedious preparation of peptide-fused proteins, which yielded only approximately 10 % of the protein produced without peptide anchor and required an additional membrane solubilization and protein polishing step, preliminary studies were performed to investigate the preparation of the fusion proteins with hydrophobic peptides for surface functionalization using *in vitro* protein synthesis (IVPS) in the presence of polymersomes. The simultaneous preparation of functional fusion protein and peptide insertion into the polymer membrane was demonstrated for eGFP-Cytb_5' and eGFP-L' using an *E. coli* lysate and for CSS-L' using an insect cell lysate. In contrast, wheat germ extract and CHO lysate did not produce sufficient amounts of protein to detect peptide insertion into the polymersomes. Protein synthesis yields were generally low, reaching approximately 3 - 6 % of the maximum yields described by the supplier, thus limiting the peptide insertion to 16.2 eGFP-Cytb_5', 11.0 eGFP-L' and 0.03 CSS-L' molecules per polymersome. Yet, the general feasibility of the simultaneous synthesis of the peptide anchors and the surface functionalization of polymersomes was demonstrated. Optimization of the synthesis conditions as well as the use of more sophisticated continuous or semi-continuous IVPS systems may significantly increase the protein yield and thus the peptide insertion, and may greatly facilitate the surface functionalization of nano-scale enzyme membrane reactors.

9. Outlook

The enhanced production of CMP-Neu5Ac in nano-scale membrane reactors via a three-step enzymatic route demonstrates the ability to perform incompatible reaction cascades in polymersomes by selectively controlling mass transport across the membrane on a micromolecule level. Limiting factors were the degree of enzyme encapsulation and of membrane functionalization with membrane channels which reduced the biocatalytic efficiency of a single polymersome. Whereas the incorporation of membrane channels can be increased by increasing the membrane channel concentration added to the polymersomes, new strategies to increase the enzyme load of the encapsulated enzyme are required to further increase the amount of encapsulated enzymes beyond the 5.6 µg protein per mg polymer achieved. Promising alternatives may be electroporation of preformed polymersomes which allow the addition of higher enzyme concentrations in the bulk solution or a directed guidance of enzymes to the polymersome lumen via the generation of interactions with the polymer membrane.

In terms of establishing polymersomes as platform technology for enhancing the performance of incompatible reaction cascades, the main challenge will be the transfer of the system to other cascades reactions. The incompatibility of multienzyme syntheses may arise from manifold reasons, for example from cross-inhibitions, substrate or product inhibitions, different pH optima or the requirement for different solvents, for example when using lipases in multienzyme syntheses. The use of polymersomes in organic solvents has been demonstrated by cross-linking the polymers in the membrane and may be an interesting strategy for many reaction cascades requiring different solvents (Nardin *et al.*, 2000a).

The introduction of selective mass transport via membrane channels will play a crucial role in future studies as each implemented cascade reaction will have different prerequisites on the membrane permeability. Whereas the selective mass transport for the synthesis of CMP-Neu5Ac can be introduced by both size and charge, other reaction cascades may require more sophisticated and more specialized membrane channels, depending on the reactants to be separated. Thus, the characterization and incorporation of highly selective membrane channels should be addressed in the future to generate a toolbox of available membrane proteins for cascade reactions that can greatly benefit from compartmentalization.

10. Literature

Ahmed, F. and Discher, D. E., 2004, Self-porating polymersomes of PEG-PLA and PEG-PCL: hydrolysis-triggered controlled release vesicles, *J Control Release* **96** (1): 37-53

Ahuja, S., Jahr, N., Im, S. C., Vivekanandan, S., Popovych, N., Le Clair, S. V., Huang, R., Soong, R., Xu, J., Yamamoto, K., Nanga, R. P., Bridges, A., Waskell, L. and Ramamoorthy, A., 2013, A model of the membrane-bound cytochrome b5-cytochrome P450 complex from NMR and mutagenesis data, *J Biol Chem* **288** (30): 22080-22095

Alberts, B., 2015, *Molecular biology of the cell*, Garland Science, Taylor and Francis Group

Alcaraz, A., Nestorovich, E. M., Aguilella-Arzo, M., Aguilella, V. M. and Bezrukov, S. M., 2004, Salting out the ionic selectivity of a wide channel: the asymmetry of OmpF, *Biophys J* **87** (2): 943-957

Angelova, M. I., Soleau, S., Meleard, P., Faucon, J. F. and Bothorel, P., 1992, Preparation of Giant Vesicles by External Ac Electric-Fields - Kinetics and Applications, *Prog Coll Pol Sci S* **89** 127-131

Battaglia, G. and Ryan, A. J., 2005, Bilayers and interdigitation in block copolymer vesicles, *Journal of the American Chemical Society* **127** (24): 8757-8764

Battaglia, G., Ryan, A. J. and Tomas, S., 2006, Polymeric vesicle permeability: A facile chemical assay, *Langmuir* **22** (11): 4910-4913

Baumann, P., Tanner, P., Onaca, O. and Palivan, C. G., 2011, Bio-Decorated Polymer Membranes: A New Approach in Diagnostics and Therapeutics, *Polymers-Basel* **3** (1): 173-192

Bechinger, B., 1997, Structure and functions of channel-forming peptides: magainins, cecropins, melittin and alamethicin, *J Membr Biol* **156** (3): 197-211

Berg, J. M., Tymoczko, J. L., Stryer, L. and Stryer, L., 2002, *Biochemistry*, W.H. Freeman

Bisswanger, H., 2008, *Enzyme kinetics : principles and methods*, Wiley-VCH

Bommarius, A. S. and Riebel, B. R., 2004, *Biocatalysis*, Wiley-VCH

Briggs, G. E. and Haldane, J. B., 1925, A Note on the Kinetics of Enzyme Action, *Biochem J* **19** (2): 338-339

Brooks, G. A., Dubouchaud, H., Brown, M., Sicurello, J. P. and Butz, C. E., 1999, Role of mitochondrial lactate dehydrogenase and lactate oxidation in the intracellular lactate shuttle, *Proc Natl Acad Sci U S A* **96** (3): 1129-1134

Broz, P., Benito, S. M., Saw, C., Burger, P., Heider, H., Pfisterer, M., Marsch, S., Meier, W. and Hunziker, P., 2005, Cell targeting by a generic receptor-targeted polymer nanocontainer platform, *J Control Release* **102** (2): 475-488

Brunetti, P., Roseman, S. and Jourdian, G. W., 1962, Sialic Acids .3. Distribution and Properties of Animal N-Acetylneuraminic Aldolase, *Journal of Biological Chemistry* **237** (8): 2447-&

Burns, J. R., Seifert, A., Fertig, N. and Howorka, S., 2016, A biomimetic DNA-based channel for the ligand-controlled transport of charged molecular cargo across a biological membrane, *Nat Nanotechnol* **11** (2): 152-156

Burri, L. and Lithgow, T., 2004, A complete set of SNAREs in yeast, *Traffic* **5** (1): 45-52

Chen, Q., Schonherr, H. and Vancso, G. J., 2009, Mechanical properties of block copolymer vesicle membranes by atomic force microscopy, *Soft Matter* **5** (24): 4944-4950

Choi, H. J. and Montemagno, C. D., 2005, Artificial organelle: ATP synthesis from cellular mimetic polymersomes, *Nano Letters* **5** (12): 2538-2542

Christian, D. A., Cai, S., Bowen, D. M., Kim, Y., Pajerowski, J. D. and Discher, D. E., 2009, Polymersome carriers: from self-assembly to siRNA and protein therapeutics, *Eur J Pharm Biopharm* **71** (3): 463-474

Christian, N. A., Milone, M. C., Ranka, S. S., Li, G. Z., Frail, P. R., Davis, K. P., Bates, F. S., Therien, M. J., Ghoroghchian, P. P., June, C. H. and Hammer, D. A., 2007, Tat-functionalized near-infrared emissive polymersomes for dendritic cell labeling, *Bioconjugate Chem* **18** (1): 31-40

Comb, D. G. and Roseman, S., 1960, Sialic Acids .1. Structure and Enzymatic Synthesis of N-Acetylneuraminic Acid, *Journal of Biological Chemistry* **235** (9): 2529-2537

Cornelissen, J. J. L. M., Fischer, M., Sommerdijk, N. A. J. M. and Nolte, R. J. M., 1998, Helical superstructures from charged poly(styrene)-poly(isocyanodipeptide) block copolymers, *Science* **280** (5368): 1427-1430

Cowan, S. W., Schirmer, T., Rummel, G., Steiert, M., Ghosh, R., Pauptit, R. A., Jansonius, J. N. and Rosenbusch, J. P., 1992, Crystal-Structures Explain Functional-Properties of 2 Escherichia-Coli Porins, *Nature* **358** (6389): 727-733

de Hoog, H. M., Nallani, M., Cornelissen, J. J., Rowan, A. E., Nolte, R. J. and Arends, I. W., 2009, Biocatalytic oxidation by chloroperoxidase from Caldariomyces fumago in polymersome nanoreactors, *Org Biomol Chem* **7** (22): 4604-4610

Debets, M. F., Leenders, W. P., Verrijp, K., Zonjee, M., Meeuwissen, S. A., Otte-Holler, I. and van Hest, J. C., 2013, Nanobody-functionalized polymersomes for tumor-vessel targeting, *Macromol Biosci* **13** (7): 938-945

Delcour, A. H., 2009, Outer membrane permeability and antibiotic resistance, *Biochim Biophys Acta* **1794** (5): 808-816

Discher, B. M., Won, Y. Y., Ege, D. S., Lee, J. C., Bates, F. S., Discher, D. E. and Hammer, D. A., 1999, Polymersomes: tough vesicles made from diblock copolymers, *Science* **284** (5417): 1143-1146

Discher, D. E. and Eisenberg, A., 2002, Polymer vesicles, *Science* **297** (5583): 967-973

Discher, D. E., Ortiz, V., Srinivas, G., Klein, M. L., Kim, Y., Christian, D., Cai, S., Photos, P. and Ahmed, F., 2007, Emerging Applications of Polymersomes in Delivery: from Molecular Dynamics to Shrinkage of Tumors, *Prog Polym Sci* **32** (8-9): 838-857

Egli, S., Nussbaumer, M. G., Balasubramanian, V., Chami, M., Bruns, N., Palivan, C. and Meier, W., 2011a, Biocompatible functionalization of polymersome surfaces: a new approach to surface immobilization and cell targeting using polymersomes, *J Am Chem Soc* **133** (12): 4476-4483

Egli, S., Schlaad, H., Bruns, N. and Meier, W., 2011b, Functionalization of Block Copolymer Vesicle Surfaces, *Polymers-Basel* **3** (1): 252-280

Ehrmann, M. A., Scheyhing, C. H. and Vogel, R. F., 2001, In vitro stability and expression of green fluorescent protein under high pressure conditions, *Lett Appl Microbiol* **32** (4): 230-234

Faber, K., 2011, *Biotransformations in Organic Chemistry*, Springer

Felici, M., Marza-Perez, M., Hatzakis, N. S., Nolte, R. J. and Feiters, M. C., 2008, Beta-cyclodextrin-appended giant amphiphile: aggregation to vesicle polymersomes and immobilisation of enzymes, *Chemistry* **14** (32): 9914-9920

Findrik, Z. and Vasic-Racki, D., 2009, Overview on Reactions with Multi-enzyme Systems, *Chem Biochem Eng Q* **23** (4): 545-553

Fischer, H., Kansy, M., Avdeef, A. and Senner, F., 2007, Permeation of permanently positive charged molecules through artificial membranes—Influence of physico-chemical properties, *European Journal of Pharmaceutical Sciences* **31** (1): 32-42

Fujiwara, K. and Doi, N., 2016, Biochemical Preparation of Cell Extract for Cell-Free Protein Synthesis without Physical Disruption, *Plos One* **11** (4):

Gaitzsch, J., Appelhans, D., Wang, L., Battaglia, G. and Voit, B., 2012, Synthetic bio-nanoreactor: mechanical and chemical control of polymersome membrane permeability, *Angew Chem Int Ed Engl* **51** (18): 4448-4451

Ghoroghchian, P. P., Frail, P. R., Li, G., Zupancich, J. A., Bates, F. S., Hammer, D. A. and Therien, M. J., 2007, Controlling Bulk Optical Properties of Emissive Polymersomes Through Intramembranous Polymer-Fluorophore Interactions, *Chem Mater* **19** (6): 1309-1318

Gilbert, M., Watson, D. C. and Wakarchuk, W. W., 1997, Purification and characterization of the recombinant CMP-sialic acid synthetase from Neisseria meningitidis, *Biotechnol Lett* **19** (5): 417-420

Gite, S., Lim, M., Carlson, R., Olejnik, J., Zehnbauer, B. and Rothschild, K., 2003, A high-throughput nonisotopic protein truncation test, *Nat Biotechnol* **21** (2): 194-197

Gonzalez-Perez, A., Stibius, K. B., Vissing, T., Nielsen, C. H. and Mouritsen, O. G., 2009, Biomimetic triblock copolymer membrane arrays: a stable template for functional membrane proteins, *Langmuir* **25** (18): 10447-10450

Gräfe, D., Gaitzsch, J., Appelhans, D. and Voit, B., 2014, Cross-linked polymersomes as nanoreactors for controlled and stabilized single and cascade enzymatic reactions, *Nanoscale* **6** (18): 10752-10761

Graff, A., Fraysse-Ailhas, C., Palivan, C. G., Grzelakowski, M., Friedrich, T., Vebert, C., Gescheidt, G. and Meier, W., 2010, Amphiphilic Copolymer Membranes Promote NADH:Ubiquinone Oxidoreductase Activity: Towards an Electron-Transfer Nanodevice, *Macromol Chem Phys* **211** (2): 229-238

Graff, A., Sauer, M., Van Gelder, P. and Meier, W., 2002, Virus-assisted loading of polymer nanocontainer, *Proc Natl Acad Sci U S A* **99** (8): 5064-5068

Groher, A. and Hoelsch, K., 2012, Mechanistic model for the synthesis of N-acetylneuraminic acid using N-acetylneuraminate lyase from Escherichia coli K12, *J Mol Catal B-Enzym* **83** 1-7

Grzelakowski, M., Onaca, O., Rigler, P., Kumar, M. and Meier, W., 2009, Immobilized protein-polymer nanoreactors, *Small* **5** (22): 2545-2548

Guo, M., Jiang, M. and Zhang, G., 2008, Surface modification of polymeric vesicles via host-guest inclusion complexation, *Langmuir* **24** (19): 10583-10586

Haefele, T., Kita-Tokarczyk, K. and Meier, W., 2006, Phase behavior of mixed Langmuir monolayers from amphiphilic block copolymers and an antimicrobial peptide, *Langmuir* **22** (3): 1164-1172

Haldane, J. B. S., 1930, *Enzymes*, Longmans, Green

Hammer, D. A., Robbins, G. P., Haun, J. B., Lin, J. J., Qi, W., Smith, L. A., Ghoroghchian, P. P., Therien, M. J. and Bates, F. S., 2008, Leuko-polymersomes, *Faraday Discuss* **139** 129-141; discussion 213-128, 419-120

Hatti-Kaul, R., Tornvall, U., Gustafsson, L. and Borjesson, P., 2007, Industrial biotechnology for the production of bio-based chemicals - a cradle-to-grave perspective, *Trends Biotechnol* **25** (3): 119-124

He, N., Yi, D. and Fessner, W. D., 2011, Flexibility of Substrate Binding of Cytosine-5 '-Monophosphate-N-Acetylneuraminate Synthetase (CMP-Sialate Synthetase) from Neisseria meningitidis: An Enabling Catalyst for the Synthesis of Neo-sialoconjugates, *Adv Synth Catal* **353** (13): 2384-2398

Heimer, R. and Meyer, K., 1956, Studies on Sialic Acid of Submaxillary Mucoid, *Proc Natl Acad Sci U S A* **42** (10): 728-734

Hillebrecht, J. R. and Chong, S., 2008, A comparative study of protein synthesis in in vitro systems: from the prokaryotic reconstituted to the eukaryotic extract-based, *BMC Biotechnol* **8** 58

Hink, M. A., Griep, R. A., Borst, J. W., van Hoek, A., Eppink, M. H. M., Schots, A. and Visser, A. J. W. G., 2000, Structural Dynamics of GFP Alone and Fused With a Single Chain Fv Protein, *J Biol Chem* **275** (23): 17556

Hofmann, M. W., Peplowska, K., Rohde, J., Poschner, B. C., Ungermann, C. and Langosch, D., 2006, Self-interaction of a SNARE transmembrane domain promotes the hemifusion-to-fusion transition, *J Mol Biol* **364** (5): 1048-1060

Horsfall, L. E., Nelson, A. and Berry, A., 2010, Identification and characterization of important residues in the catalytic mechanism of CMP-Neu5Ac synthetase from Neisseria meningitidis, *Febs J* **277** (13): 2779-2790

Iskakova, M. B., Szaflarski, W., Dreyfus, M., Remme, J. and Nierhaus, K. H., 2006, Troubleshooting coupled in vitro transcription-translation system derived from Escherichia coli cells: synthesis of high-yield fully active proteins, *Nucleic Acids Res* **34** (19):

Itel, F., Chami, M., Najer, A., Lorcher, S., Wu, D. L., Dinu, I. A. and Meier, W., 2014, Molecular Organization and Dynamics in Polymersome Membranes: A Lateral Diffusion Study, *Macromolecules* **47** (21): 7588-7596

Itel, F., Najer, A., Palivan, C. G. and Meier, W., 2015, Dynamics of Membrane Proteins within Synthetic Polymer Membranes with Large Hydrophobic Mismatch, *Nano Lett* **15** (6): 3871-3878

Jain, J. P., Ayen, W. Y. and Kumar, N., 2011, Self assembling polymers as polymersomes for drug delivery, *Curr Pharm Des* **17** (1): 65-79

Jeanteur, D., Schirmer, T., Fourel, D., Simonet, V., Rummel, G., Widmer, C., Rosenbusch, J. P., Pattus, F. and Pages, J. M., 1994, Structural and functional alterations of a colicin-resistant mutant of OmpF porin from Escherichia coli, *Proc Natl Acad Sci U S A* **91** (22): 10675-10679

Karwaski, M. F., Wakarchuk, W. W. and Gilbert, M., 2002, High-level expression of recombinant Neisseria CMP-sialic acid synthetase in Escherichia coli, *Protein Expr Purif* **25** (2): 237-240

Katzen, F., Chang, G. and Kudlicki, W., 2005, The past, present and future of cell-free protein synthesis, *Trends Biotechnol* **23** (3): 150-156

Kean, E. L. and Roseman, S., 1966, The sialic acids. X. Purification and properties of cytidine 5'-monophosphosialic acid synthetase, *J Biol Chem* **241** (23): 5643-5650

Kigawa, T., Yabuki, T. and Yokoyama, S., 1999, [Large-scale protein preparation using the cell-free synthesis], *Tanpakushitsu Kakusan Koso* **44** (4 Suppl): 598-605

Kim, H., Kang, Y. J., Kang, S. and Kim, K. T., 2012, Monosaccharide-responsive release of insulin from polymersomes of polyboroxole block copolymers at neutral pH, *J Am Chem Soc* **134** (9): 4030-4033

Kita-Tokarczyk, K., Grumelard, J., Haefele, T. and Meier, W., 2005, Block copolymer vesicles - using concepts from polymer chemistry to mimic biomembranes, *Polymer* **46** (11): 3540-3563

Kittelmann, M., Klein, T., Kragl, U., Wandrey, C. and Ghisalba, O., 1992, Preparative enzymatic synthesis of activated neuraminic acid by using a microbial enzyme, *Ann N Y Acad Sci* **672** 444-450

Klermund, L., Groher, A. and Castiglione, K., 2013, New N-acyl-D-glucosamine 2-epimerases from cyanobacteria with high activity in the absence of ATP and low inhibition by pyruvate, *Journal of Biotechnology* **168** (3): 256-263

Klermund, L., Poschenrieder, S. T. and Castiglione, K., 2016a, Simple surface functionalization of polymersomes using non-antibacterial peptide anchors, *J Nanobiotechnol* **14**

Klermund, L., Riederer, A., Groher, A. and Castiglione, K., 2015, High-level soluble expression of a bacterial N-acyl-d-glucosamine 2-epimerase in recombinant Escherichia coli, *Protein Expr Purif* **111** 36-41

Klermund, L., Riederer, A., Hunger, A. and Castiglione, K., 2016b, Protein engineering of a bacterial N-acyl-d-glucosamine 2-epimerase for improved stability under process conditions, *Enzyme Microb Technol* **87-88** 70-78

Knorst, M. and Fessner, W. D., 2001, CMP-sialate synthetase from Neisseria meningitidis - Overexpression and application to the synthesis of oligosaccharides containing modified sialic acids, *Adv Synth Catal* **343** (6-7): 698-710

Kragl, U., VasicRacki, D. and Wandrey, C., 1996, Continuous production of L-tert-leucine in series of two enzyme membrane reactors - Modelling and computer simulation, *Bioprocess Eng* **14** (6): 291-297

Kuiper, S. M., Nallani, M., Vriezema, D. M., Cornelissen, J. J., van Hest, J. C., Nolte, R. J. and Rowan, A. E., 2008, Enzymes containing porous polymersomes as nano reaction vessels for cascade reactions, *Org Biomol Chem* **6** (23): 4315-4318

Kumar, M., Grzelakowski, M., Zilles, J., Clark, M. and Meier, W., 2007, Highly permeable polymeric membranes based on the incorporation of the functional water channel protein Aquaporin Z, *Proc Natl Acad Sci U S A* **104** (52): 20719-20724

Kuruma, Y., Nishiyama, K., Shimizu, Y., Muller, M. and Ueda, T., 2005, Development of a minimal cell-free translation system for the synthesis of presecretory and integral membrane proteins, *Biotechnol Prog* **21** (4): 1243-1251

Kutay, U., Hartmann, E. and Rapoport, T. A., 1993, A class of membrane proteins with a C-terminal anchor, *Trends Cell Biol* **3** (3): 72-75

Le Meins, J. F., Sandre, O. and Lecommandoux, S., 2011, Recent trends in the tuning of polymersomes' membrane properties, *The European Physical Journal E* **34** (2):

Lecommandoux, S. B., Sandre, O., Checot, F., Rodriguez-Hernandez, J. and Perzynski, R., 2005, Magnetic nanocomposite micelles and vesicles, *Adv Mater* **17** (6): 712-+

Lee, J. O., Yi, J. K., Lee, S. G., Takahashi, S. and Kim, B. G., 2004, Production of N-acetylneuraminic acid from N-acetylglucosamine and pyruvate using recombinant human renin binding protein and sialic acid aldolase in one pot, *Enzyme Microb Tech* **35** (2-3): 121-125

Lee, S., 2006, *Encyclopedia of chemical processing*, Taylor & Francis

Lee, Y. C., Wu, H. M., Chang, Y. N., Wang, W. C. and Hsu, W. H., 2007, The central cavity from the (alpha/alpha)(6) barrel structure of Anabaena sp CH1N-acetyl-D-glucosamine 2-epimerase contains two key histidine residues for reversible conversion, *Journal of Molecular Biology* **367** (3): 895-908

Liao, H. F., Kao, C. H., Lin, W. D., Hsiao, N. W., Hsu, W. H. and Lee, Y. C., 2012, N-Acetyl-D-glucosamine 2-epimerase from Anabaena sp CH1 contains a novel ATP-binding site required for catalytic activity, *Process Biochem* **47** (6): 948-952

Liese, A. and Hilterhaus, L., 2013, Evaluation of immobilized enzymes for industrial applications, *Chem Soc Rev* **42** (15): 6236-6249

Liese, A., Seelbach, K. and Wandrey, C., 2006, *Industrial biotransformations*, Wiley-VCH

Lin, J. J., Ghoroghchian, P. P., Zhang, Y. and Hammer, D. A., 2006, Adhesion of antibody-functionalized polymersomes, *Langmuir* **22** (9): 3975-3979

Lin, J. J., Silas, J. A., Bermudez, H., Milam, V. T., Bates, F. S. and Hammer, D. A., 2004, The effect of polymer chain length and surface density on the adhesiveness of functionalized polymersomes, *Langmuir* **20** (13): 5493-5500

Liu, G., Wang, X., Hu, J., Zhang, G. and Liu, S., 2014, Self-immolative polymersomes for high-efficiency triggered release and programmed enzymatic reactions, *J Am Chem Soc* **136** (20): 7492-7497

Lodish, H. F., 2003, *Molecular cell biology*, W.H. Freeman and Company

Lomas, H., Johnston, A. P. R., Such, G. K., Zhu, Z. Y., Liang, K., van Koeverden, M. P., Alongkornchotikul, S. and Caruso, F., 2011, Polymersome-Loaded Capsules for Controlled Release of DNA, *Small* **7** (14): 2109-2119

Lopez-Gallego, F. and Schmidt-Dannert, C., 2010, Multi-enzymatic synthesis, *Curr Opin Chem Biol* **14** (2): 174-183

Lu, L., Zou, Y., Yang, W., Meng, F., Deng, C., Cheng, R. and Zhong, Z., 2015, Anisamide-Decorated pH-Sensitive Degradable Chimaeric Polymersomes Mediate Potent and Targeted Protein Delivery to Lung Cancer Cells, *Biomacromolecules* **16** (6): 1726-1735

Ma, Y., Munch, D., Schneider, T., Sahl, H. G., Bouhss, A., Ghoshdastider, U., Wang, J., Dotsch, V., Wang, X. and Bernhard, F., 2011, Preparative scale cell-free production and quality optimization of MraY homologues in different expression modes, *J Biol Chem* **286** (45): 38844-38853

Martin, T. J. and Schmidt, R. R., 1993, Convenient Chemical Synthesis of Cmp-N-Acetylneuraminate (Cmp-Neu-5-Ac), *Tetrahedron Lett* **34** (11): 1765-1768

Marty, N. J., Teresinski, H. J., Hwang, Y. T., Clendening, E. A., Gidda, S. K., Sliwinska, E., Zhang, D. Y., Miernyk, J. A., Brito, G. C., Andrews, D. W., Dyer, J. M. and Mullen, R. T., 2014, New insights into the targeting of a subset of tail-anchored proteins to the outer mitochondrial membrane, *Front Plant Sci* **5**

Maru, I., Ohnishi, J., Ohta, Y. and Tsukada, Y., 2002, Why is sialic acid attracting interest now? Complete enzymatic synthesis of sialic acid with N-acylglucosamine 2-epimerase, *J Biosci Bioeng* **93** (3): 258-265

Maru, I., Ohta, Y., Murata, K. and Tsukada, Y., 1996, Molecular cloning and identification of N-acyl-D-glucosamine 2-epimerase from porcine kidney as a renin-binding protein, *Journal of Biological Chemistry* **271** (27): 16294-16299

May, S., Andreasson-Ochsner, M., Fu, Z., Low, Y. X., Tan, D., de Hoog, H. P., Ritz, S., Nallani, M. and Sinner, E. K., 2013, In vitro expressed GPCR inserted in polymersome membranes for ligand-binding studies, *Angew Chem Int Ed Engl* **52** (2): 749-753

Meeuwissen, S. A., Kim, K. T., Chen, Y., Pochan, D. J. and van Hest, J. C., 2011, Controlled shape transformation of polymersome stomatocytes, *Angew Chem Int Ed Engl* **50** (31): 7070-7073

Messager, L., Burns, J. R., Kim, J., Cecchin, D., Hindley, J., Pyne, A. L., Gaitzsch, J., Battaglia, G. and Howorka, S., 2016, Biomimetic Hybrid Nanocontainers with Selective Permeability, *Angew Chem Int Ed Engl* **55** (37): 11106-11109

Michaelis, M. and Menten, M. L., 1913, Die Kinetik der Invertinwirkung, *Biochemische Zeitschrift* **49** 333–369

Mizanur, R. M. and Pohl, N. L., 2008, Bacterial CMP-sialic acid synthetases: production, properties, and applications, *Appl Microbiol Biotechnol* **80** (5): 757-765

Morton, D., Mortezaei, S., Yemenicioglu, S., Isaacman, M. J., Nova, I. C., Gundlach, J. H. and Theogarajan, L., 2015, Tailored polymeric membranes for Mycobacterium smegmatis porin A (MspA) based biosensors, *J Mater Chem B* **3** (25): 5080-5086

Nallani, M., Andreasson-Ochsner, M., Tan, C. W., Sinner, E. K., Wisantoso, Y., Geifman-Shochat, S. and Hunziker, W., 2011, Proteopolymersomes: in vitro production of a membrane protein in polymersome membranes, *Biointerphases* **6** (4): 153-157

Nallani, M., Benito, S., Onaca, O., Graff, A., Lindemann, M., Winterhalter, M., Meier, W. and Schwaneberg, U., 2006, A nanocompartment system (Synthosome) designed for biotechnological applications, *J Biotechnol* **123** (1): 50-59

Nardin, C., Hirt, T., Leukel, J. and Meier, W., 2000a, Polymerized ABA triblock copolymer vesicles, *Langmuir* **16** (3): 1035-1041

Nardin, C., Thoeni, S., Widmer, J., Winterhalter, M. and Meier, W., 2000b, Nanoreactors based on (polymerized) ABA-triblock copolymer vesicles, *Chem Commun* (15): 1433-1434

Nehring, R., Palivan, C. G., Moreno-Flores, S., Mantion, A., Tanner, P., Toca-Herrera, J. L., Thunemann, A. and Meier, W., 2010, Protein decorated membranes by specific molecular interactions, *Soft Matter* **6** (12): 2815-2824

Neuman, B. W., Stein, D. A., Kroeker, A. D., Paulino, A. D., Moulton, H. M., Iversen, P. L. and Buchmeier, M. J., 2004, Antisense morpholino-oligomers directed against the 5 ' end of the genome inhibit coronavirus proliferation and growth, *J Virol* **78** (11): 5891-5899

Nikaido, H., 1992, Porins and specific channels of bacterial outer membranes, *Mol Microbiol* **6** (4): 435-442

Nikaido, H., 2003, Molecular basis of bacterial outer membrane permeability revisited, *Microbiol Mol Biol Rev* **67** (4): 593-656

Nomura, S. M., Kondoh, S., Asayama, W., Asada, A., Nishikawa, S. and Akiyoshi, K., 2008, Direct preparation of giant proteo-liposomes by in vitro membrane protein synthesis, *J Biotechnol* **133** (2): 190-195

Noor, M., Dworeck, T., Schenk, A., Shinde, P., Fioroni, M. and Schwaneberg, U., 2012, Polymersome surface decoration by an EGFP fusion protein employing Cecropin A as peptide "anchor", *J Biotechnol* **157** (1): 31-37

Noyori, R., 2009, Synthesizing our future, *Nat Chem* **1** (1): 5-6

O'Neil, C. P., Suzuki, T., Demurtas, D., Finka, A. and Hubbell, J. A., 2009, A novel method for the encapsulation of biomolecules into polymersomes via direct hydration, *Langmuir* **25** (16): 9025-9029

O'Reilly, E. and Turner, N. J., 2015, Enzymatic cascades for the regio- and stereoselective synthesis of chiral amines, *Perspectives in Science* **4** 55-61

Onaca, O., Enea, R., Hughes, D. W. and Meier, W., 2009, Stimuli-responsive polymersomes as nanocarriers for drug and gene delivery, *Macromol Biosci* **9** (2): 129-139

Onaca, O., Sarkar, P., Roccatano, D., Friedrich, T., Hauer, B., Grzelakowski, M., Guven, A., Fioroni, M. and Schwaneberg, U., 2008, Functionalized nanocompartments (synthosomes) with a reduction-triggered release system, *Angew Chem Int Edit* **47** (37): 7029-7031

Opsteen, J. A., Brinkhuis, R. P., Teeuwen, R. L., Lowik, D. W. and van Hest, J. C., 2007, "Clickable" polymersomes, *Chem Commun (Camb)* (30): 3136-3138

Oroz-Guinea, I. and Garcia-Junceda, E., 2013, Enzyme catalysed tandem reactions, *Curr Opin Chem Biol* **17** (2): 236-249

Ozols, J., Carr, S. A. and Strittmatter, P., 1984, Identification of the Nh2-Terminal Blocking Group of Nadh-Cytochrome-B5 Reductase as Myristic Acid and the Complete Amino-Acid-Sequence of the Membrane-Binding Domain, *Journal of Biological Chemistry* **259** (21): 3349-3354

Ozols, J., Korza, G., Heinemann, F. S., Hediger, M. A. and Strittmatter, P., 1985, Complete Amino-Acid Sequence of Steer Liver Microsomal Nadh-Cytochrome-B5 Reductase, *Journal of Biological Chemistry* **260** (22): 1953-1961

Palivan, C. G., Fischer-Onaca, O., Delcea, M., Itel, F. and Meier, W., 2012, Protein-polymer nanoreactors for medical applications, *Chem Soc Rev* **41** (7): 2800-2823

Palivan, C. G., Goers, R., Najer, A., Zhang, X. Y., Car, A. and Meier, W., 2016, Bioinspired polymer vesicles and membranes for biological and medical applications, *Chem Soc Rev* **45** (2): 377-411

Pang, Z., Lu, W., Gao, H., Hu, K., Chen, J., Zhang, C., Gao, X., Jiang, X. and Zhu, C., 2008, Preparation and brain delivery property of biodegradable polymersomes conjugated with OX26, *J Control Release* **128** (2): 120-127

Pangburn, T. O., Georgiou, K., Bates, F. S. and Kokkoli, E., 2012, Targeted polymersome delivery of siRNA induces cell death of breast cancer cells dependent upon Orai3 protein expression, *Langmuir* **28** (35): 12816-12830

Pata, V. and Dan, N., 2003, The effect of chain length on protein solubilization in polymer-based vesicles (polymersomes), *Biophys J* **85** (4): 2111-2118

Peters, R. J. R. W., Marguet, M., Marais, S., Fraaije, M. W., van Hest, J. C. M. and Lecommandoux, S., 2014, Cascade Reactions in Multicompartmentalized Polymersomes, *Angew Chem Int Edit* **53** (1): 146-150

Petersen, M. A., Yin, L. G., Kokkoli, E. and Hillmyer, M. A., 2010, Synthesis and characterization of reactive PEO-PMCL polymersomes, *Polym Chem-Uk* **1** (8): 1281-1290

Popenoe, E. A., 1959, The linkage neuraminic acid in orosomucoid, *Biochim Biophys Acta* **32** 584-585

Poschenrieder, S. T., Schiebel, S. K. and Castiglione, K., 2016a, Polymersomes for biotechnological applications: large-scale production of nano-scale vesicles, *Engineering in Life Sciences*

Poschenrieder, S. T., Wagner, S. G. and Castiglione, K., 2016b, Efficient production of uniform nanometer-sized polymer vesicles in stirred-tank reactors, *J Appl Polym Sci*

Prilipov, A., Phale, P. S., Van Gelder, P., Rosenbusch, J. P. and Koebnik, R., 1998, Coupling site-directed mutagenesis with high-level expression: large scale production of mutant porins from E. coli, *Fems Microbiol Lett* **163** (1): 65-72

Prinos, J. and Panayiotou, C., 1995, Glass-Transition Temperature in Hydrogen-Bonded Polymer Mixtures, *Polymer* **36** (6): 1223-1227

Qin, S. H., Geng, Y., Discher, D. E. and Yang, S., 2006, Temperature-controlled assembly and release from polymer vesicles of poly(ethylene oxide)-block-poly(N-isopropylacrylamide), *Adv Mater* **18** (21): 2905-+

Quast, R. B., Sonnabend, A., Stech, M., Wustenhagen, D. A. and Kubick, S., 2016, High-yield cell-free synthesis of human EGFR by IRES-mediated protein translation in a continuous exchange cell-free reaction format, *Sci Rep* **6** 30399

Ranquin, A., Versees, W., Meier, W., Steyaert, J. and Van Gelder, P., 2005, Therapeutic nanoreactors: combining chemistry and biology in a novel triblock copolymer drug delivery system, *Nano Lett* **5** (11): 2220-2224

Renggli, K., Baumann, P., Langowska, K., Onaca, O., Bruns, N. and Meier, W., 2011, Selective and Responsive Nanoreactors, *Adv Funct Mater* **21** (7): 1241-1259

Ricca, E., Brucher, B. and Schrittwieser, J. H., 2011, Multi-Enzymatic Cascade Reactions: Overview and Perspectives, *Adv Synth Catal* **353** (13): 2239-2262

Rigler, P. and Meier, W., 2006, Encapsulation of fluorescent molecules by functionalized polymeric nanocontainers: Investigation by confocal fluorescence Imaging and

fluorescence correlation Spectroscopy, *Journal of the American Chemical Society* **128** (1): 367-373

Ringe, D. and Petsko, G. A., 2009, What are pharmacological chaperones and why are they interesting?, *J Biol* **8** (9): 80

Rogers, M. J. and Strittmatter, P., 1975, The interaction of NADH-cytochrome b5 reductase and cytochrome b5 bound to egg lecithin liposomes, *J Biol Chem* **250** (14): 5713-5718

Rosenblum, G. and Cooperman, B. S., 2014, Engine out of the chassis: Cell-free protein synthesis and its uses, *Febs Lett* **588** (2): 261-268

Sachse, R., Dondapati, S. K., Fenz, S. F., Schmidt, T. and Kubick, S., 2014, Membrane protein synthesis in cell-free systems: From bio-mimetic systems to bio-membranes, *Febs Lett* **588** (17): 2774-2781

Saint, N., Lou, K. L., Widmer, C., Luckey, M., Schirmer, T. and Rosenbusch, J. P., 1996, Structural and functional characterization of OmpF porin mutants selected for larger pore size. II. Functional characterization, *J Biol Chem* **271** (34): 20676-20680

Santacoloma, P. A., Sin, G., Gernaey, K. V. and Woodley, J. M., 2011, Multienzyme-Catalyzed Processes: Next-Generation Biocatalysis, *Org Process Res Dev* **15** (1): 203-212

Sauer, M., Haefele, T., Graff, A., Nardin, C. and Meier, W., 2001, Ion-carrier controlled precipitation of calcium phosphate in giant ABA triblock copolymer vesicles, *Chem Commun (Camb)* (23): 2452-2453

Schauer, R. and Shaw, L., 1991, The Regulation of the Function of Sialic Acids by O-Acetylation, O-Methylation and N-Acetyl-Hydroxylation, *Biol Chem H-S* **372** (10): 881-882

Schmid, A., Dordick, J. S., Hauer, B., Kiener, A., Wubbolts, M. and Witholt, B., 2001, Industrial biocatalysis today and tomorrow, *Nature* **409** (6817): 258-268

Schmitt, C., Lippert, A. H., Bonakdar, N., Sandoghdar, V. and Voll, L. M., 2016, Compartmentalization and Transport in Synthetic Vesicles, *Front Bioeng Biotechnol* **4** 19

Schoonen, L. and van Hest, J. C. M., 2016, Compartmentalization Approaches in Soft Matter Science: From Nanoreactor Development to Organelle Mimics, *Adv Mater* **28** (6): 1109-1128

Sheldon, R. A., 2008, E factors, green chemistry and catalysis: an odyssey, *Chem Commun (Camb)* (29): 3352-3365

Shimizu, Y., Inoue, A., Tomari, Y., Suzuki, T., Yokogawa, T., Nishikawa, K. and Ueda, T., 2001, Cell-free translation reconstituted with purified components, *Nat Biotechnol* **19** (8): 751-755

Silvestro, L., Gupta, K., Weiser, J. N. and Axelsen, P. H., 1997, The concentration-dependent membrane activity of cecropin A, *Biochemistry* **36** (38): 11452-11460

Simon, E. S., Bednarski, M. D. and Whitesides, G. M., 1988, Synthesis of Cmp-Neuac from N-Acetylglucosamine - Generation of Ctp from Cmp Using Adenylate Kinase, *Journal of the American Chemical Society* **110** (21): 7159-7163

Sirbasku, D. A. and Binkley, S. B., 1970, Purification and Properties of N-Acetylneuraminate Lyase from Beef Kidney Cortex, *Biochimica Et Biophysica Acta* **206** (3): 479-&

Siti, W., de Hoog, H. P. M., Fischer, O., Shan, W. Y., Tomczak, N., Nallani, M. and Liedberg, B., 2014, An intercompartmental enzymatic cascade reaction in channel-equipped polymersome-in-polymersome architectures, *J Mater Chem B* **2** (18): 2733-2737

Sola-Carvajal, A., Sanchez-Carron, G., Garcia-Garcia, M. I., Garcia-Carmona, F. and Sanchez-Ferrer, A., 2012, Properties of BoAGE2, a second N-acetyl-D-glucosamine 2-epimerase from Bacteroides ovatus ATCC 8483, *Biochimie* **94** (1): 222-230

Song, J., Zhang, H., Wu, B., Zhang, Y., Li, H., Xiao, M. and Wang, P. G., 2003, Reassembled Biosynthetic Pathway for a Large-scale Synthesis of CMP-Neu5Ac, *Marine Drugs* **1** (1): 34-45

Spatz, L. and Strittmatter, P., 1971, A form of cytochrome b5 that contains an additional hydrophobic sequence of 40 amino acid residues, *Proc Natl Acad Sci U S A* **68** (5): 1042-1046

Stech, M., Quast, R. B., Sachse, R., Schulze, C., Wustenhagen, D. A. and Kubick, S., 2014, A continuous-exchange cell-free protein synthesis system based on extracts from cultured insect cells, *Plos One* **9** (5): e96635

Stoenescu, R., Graff, A. and Meier, W., 2004, Asymmetric ABC-triblock copolymer membranes induce a directed insertion of membrane proteins, *Macromol Biosci* **4** (10): 930-935

Strittmatter, P., Rogers, M. J. and Spatz, L., 1972, The binding of cytochrome b 5 to liver microsomes, *J Biol Chem* **247** (22): 7188-7194

Sührer, I., Langemann, T., Lubitz, W., Weuster-Botz, D. and Castiglione, K., 2015, A novel one-step expression and immobilization method for the production of biocatalytic preparations, *Microb Cell Fact* **14** 180

Szostak, M. and Lubitz, W., 1991, Recombinant Bacterial Ghosts as Multivaccine Vehicles, *Vaccines 91* 409-414

Szostak, M. P., Auer, T. and Lubitz, W., 1993, Immune-Response against Recombinant Bacterial Ghosts Carrying Hiv-1 Reverse-Transcriptase, *Vaccines93 : Modern Approaches to New Vaccines Including Prevention of Aids* 419-425

Szostak, M. P., Hensel, A., Eko, F. O., Klein, R., Auer, T., Mader, H., Haslberger, A., Bunka, S., Wanner, G. and Lubitz, W., 1996, Bacterial ghosts: non-living candidate vaccines, *J Biotechnol* **44** (1-3): 161-170

Tabata, K., Koizumi, S., Endo, T. and Ozaki, A., 2002, Production of N-acetyl-D-neuraminic acid by coupling bacteria expressing N-acetyl-D-glucosamine 2-epimerase and N-acetyl-D-neuraminic acid synthetase, *Enzyme Microb Tech* **30** (3): 327-333

Takahashi, S., Ogasawara, H., Takahashi, K., Hori, K., Saito, K. and Mori, K., 2002, Identification of a domain conferring nucleotide binding to the N-acetyl-D-glucosamine 2-epimerase (renin binding protein), *J Biochem-Tokyo* **131** (4): 605-610

Takahashi, S., Takahashi, K., Kaneko, T., Ogasawara, H., Shindo, S. and Kobayashi, M., 1999, Human renin-binding protein is the enzyme N-acetyl-D-glucosamine 2-epimerase, *J Biochem-Tokyo* **125** (2): 348-353

Tan, S., Tan, H. T. and Chung, M. C., 2008, Membrane proteins and membrane proteomics, *Proteomics* **8** (19): 3924-3932

Tao, F., Zhang, Y., Ma, C. and Xu, P., 2010, Biotechnological production and applications of N-acetyl-D-neuraminic acid: current state and perspectives, *Appl Microbiol Biotechnol* **87** (4): 1281-1289

Topell, S., Hennecke, J. and Glockshuber, R., 1999, Circularly permuted variants of the green fluorescent protein, *Febs Lett* **457** (2): 283-289

Uchida, Y., Tsukada, Y. and Sugimori, T., 1984, Purification and properties of N-acetylneuraminate lyase from Escherichia coli, *J Biochem* **96** (2): 507-522

van Dongen, S. F., Verdurmen, W. P., Peters, R. J., Nolte, R. J., Brock, R. and van Hest, J. C., 2010, Cellular integration of an enzyme-loaded polymersome nanoreactor, *Angew Chem Int Ed Engl* **49** (40): 7213-7216

van Dongen, S. F. M., Nallani, M., Cornelissen, J. L. L. M., Nolte, R. J. M. and van Hest, J. C. M., 2009, A Three-Enzyme Cascade Reaction through Positional Assembly of Enzymes in a Polymersome Nanoreactor, *Chem-Eur J* **15** (5): 1107-1114

van Dongen, S. F. M., Nallani, M., Schoffelen, S., Cornelissen, J. J. L. M., Nolte, R. J. M. and van Hest, J. C. M., 2008, A block copolymer for functionalisation of polymersome surfaces, *Macromol Rapid Comm* **29** (4): 321-325

van Oers, M. C. M., Rutjes, F. P. J. T. and van Hest, J. C. M., 2014, Cascade reactions in nanoreactors, *Curr Opin Biotech* **28** 10-16

van Oers, M. C. M., Veldmate, W. S., van Hest, J. C. M. and Rutjes, F. P. J. T., 2015, Aqueous asymmetric aldol reactions in polymersome membranes, *Polym Chem-Uk* **6** (30): 5358-5361

Varki, A., 2008, Sialic acids in human health and disease, *Trends Mol Med* **14** (8): 351-360

Varki, A., 2009, Multiple changes in sialic acid biology during human evolution, *Glycoconjugate J* **26** (3): 231-245

Varki, A. and Gagneux, P., 2009, Human-specific evolution of sialic acid targets: Explaining the malignant malaria mystery?, *P Natl Acad Sci USA* **106** (35): 14739-14740

Vijayan, K., Discher, D. E., Lal, J., Janmey, P. and Goulian, M., 2005, Interactions of membrane-active peptides with thick, neutral, nonzwitterionic bilayers, *J Phys Chem B* **109** (30): 14356-14364

von Itzstein, M., 2007, The war against influenza: discovery and development of sialidase inhibitors, *Nat Rev Drug Discov* **6** (12): 967-974

Vriezema, D. M., Garcia, P. M., Sancho Oltra, N., Hatzakis, N. S., Kuiper, S. M., Nolte, R. J., Rowan, A. E. and van Hest, J. C., 2007, Positional assembly of enzymes in polymersome nanoreactors for cascade reactions, *Angew Chem Int Ed Engl* **46** (39): 7378-7382

Vriezema, D. M., Hoogboom, J., Velonia, K., Takazawa, K., Christianen, P. C., Maan, J. C., Rowan, A. E. and Nolte, R. J., 2003, Vesicles and polymerized vesicles from thiophene-containing rod-coil block copolymers, *Angew Chem Int Ed Engl* **42** (7): 772-776

Wang, L. G., Chierico, L., Little, D., Patikarnmonthon, N., Yang, Z., Azzouz, M., Madsen, J., Armes, S. P. and Battaglia, G., 2012, Encapsulation of Biomacromolecules within Polymersomes by Electroporation, *Angew Chem Int Edit* **51** (44): 11122-11125

Wang, X. Q., Corin, K., Baaske, P., Wienken, C. J., Jerabek-Willemsen, M., Duhr, S., Braun, D. and Zhang, S. G., 2011, Peptide surfactants for cell-free production of functional G protein-coupled receptors, *P Natl Acad Sci USA* **108** (22): 9049-9054

Warren, L. and Blacklow, R. S., 1962, The biosynthesis of cytidine 5'-monophospho-n-acetylneuraminic acid by an enzyme from Neisseria meningitidis, *J Biol Chem* **237** 3527-3534

Whitley, P., Nilsson, I. and von Heijne, G., 1994, De novo design of integral membrane proteins, *Nat Struct Biol* **1** (12): 858-862

Wolf, S., Warnecke, S., Ehrit, J., Freiberger, F., Gerardy-Schahn, R. and Meier, C., 2012, Chemical Synthesis and Enzymatic Testing of CMP-Sialic Acid Derivatives, *Chembiochem* **13** (17): 2605-2615

Wong, D., Jeon, T. J. and Schmidt, J., 2006, Single molecule measurements of channel proteins incorporated into biomimetic polymer membranes, *Nanotechnology* **17** (15): 3710-3717

Wood, R. E., Wirth, F. P., Jr. and Morgan, H. E., 1968, Glucose permeability of lipid bilayer membranes, *Biochim Biophys Acta* **163** (2): 171-178

Woodle, M. C., Engbers, C. M. and Zalipsky, S., 1994, New Amphipatic Polymer Lipid Conjugates Forming Long-Circulating Reticuloendothelial System-Evading Liposomes, *Bioconjugate Chem* **5** (6): 493-496

Woodley, J. M., 2008, New opportunities for biocatalysis: making pharmaceutical processes greener, *Trends Biotechnol* **26** (6): 321-327

Wuu, J. J. and Swartz, J. R., 2008, High yield cell-free production of integral membrane proteins without refolding or detergents, *Bba-Biomembranes* **1778** (5): 1237-1250

Yamamoto-Otake, H., Koyama, Y., Horiuchi, T. and Nakano, E., 1991, Cloning, sequencing, and expression of the N-acyl-D-mannosamine dehydrogenase gene from Flavobacterium sp. strain 141-8 in Escherichia coli, *Appl Environ Microbiol* **57** (5): 1418-1422

Yu, H., Yu, H., Karpel, R. and Chen, X., 2004, Chemoenzymatic synthesis of CMP-sialic acid derivatives by a one-pot two-enzyme system: comparison of substrate flexibility of three microbial CMP-sialic acid synthetases, *Bioorgan Med Chem* **12** (24): 6427-6435

Zhang, X., Lomora, M., Einfalt, T., Meier, W., Klein, N., Schneider, D. and Palivan, C. G., 2016, Active surfaces engineered by immobilizing protein-polymer nanoreactors for selectively detecting sugar alcohols, *Biomaterials* **89** 79-88

Zimmer, M., 2002, Green Fluorescent Protein (GFP): Applications, Structure, and Related Photophysical Behavior, *Chemical Reviews* **102** (3): 759-782

Zimmermann, V., Hennemann, H. G., Daussmann, T. and Kragl, U., 2007, Modelling the reaction course of N-acetylneuraminic acid synthesis from N-acetyl-D-glucosamine--new strategies for the optimisation of neuraminic acid synthesis, *Appl Microbiol Biotechnol* **76** (3): 597-605

11. Abbreviations

Abbreviation	
ABTS	2,2'-azino-bis(3-ethylbenzothiazoline-6-sulphonic acid
ADH	Alcohol dehydrogenase
AGE	*N*-Acyl-d-glucosamine 2-epimerase
ATP	Adenine 5'-triphosphate
au	Arbitrary units
Bicin	2-(Bis(2-hydroxyethyl)amino)acetic acid
CalB	*Candida antarctica* lipase B
CecA	Cecropin A
CMP	Cytidine 5'-monophosphate
CMP-Neu5Ac	Cytidine-5'-monophospho-*N*-acetylneuraminic acid
CSS	CMP-sialic acid synthetase
CTP	Cytidine 5'-triphosphate
Cytb_5'	Hydrophobic domain of cytochrome b_5
EDTA	Ethylenediaminetetraacetic acid
eGFP	Enhanced green fluorescent protein
FAD	Flavin adenine dinucleotide
FDH	Formate dehydrogenase
FMN	Flavin mononucleotide
G6PDH	Glucose-6-phosphate dehydrogenase
GFP	Green fluorescent protein
GlcNAc	*N*-Acetylglucosamine
GOx	Glucose oxidase
HRP	Horseradish peroxidase
IVPS	*In vitro* protein synthesis
k_{cat}	Catalytic turn over number
K_i	Inhibition constant
K_M	Half-saturation constant
L'	Hydrophobic domain of the L protein
LDH	Lactate dehydrogenase
LeuDH	L-leucine dehydrogenase

Abbreviation	
ManDH	*N*-acetylmannosamine dehydrogenase
ManNAc	*N*-Acetylmannosamine
MMCO	Molecular mass cut-off
NAD(P)	Nicotinamide adenine dinucleotide (phosphate)
NAL	N-Acetylneuraminate lyase
Neu5Ac	*N*-Acetylneuraminic acid
OmpF	Outer membrane porin F
PAMO	Phenylacetone monooxygenase
PBD	Poly(butadiene)
PDEAM	Poly(diethylaminoethylmethacrylate)
PDMIEM	Poly(3,4-dimethylmaleinimidoethylmethacrylate)
PDMIBM	Poly(3,4-dimethylmaleinimidobutylmethacrylate)
PDMS	Poly(dimethylsiloxane)
Pe	Permeability
PEE	Poly(ethyethylene)
PEG	Poly(ethylene glycol)
PEO	Poly(ethylene oxide)
P_i	Inorganic phosphate
PIAT	Poly(isocyanoalanine(2-thiophen-3-yl-ethyl)amide)
PIB	Poly(isobutylene)
PMOXA	Poly(2-methyloxazoline)
pol	Polymersome
PolyAL	Poly(alanine-leucine)
PP_i	Inorganic pyrophosphate
PS	Poly(styrene)
TAE	Tris-acetate-EDTA
UBC6'	Hydrophobic domain of the ubiquitin conjugating enzyme 6
v	Reaction rate (velocity)
Vam3p'	Hydrophobic domain of the vacuole associated protein 3

12. Appendix A

Appendix A1 – Equipment

Table A 1 – General equipment

Equipment	Manufacturer
Analytic scale Explorer E1M213	Ohaus, Gießen, Germany
Analytic scale Extend ED124S	Satorius, Göttingen, Germany
Autoklav Varioklax 500 E H+P	E H+P Labortechnik, Oberschleißheim, Germany
Benchtop centrifuge Biofuge	Stratos Kendro-Heaeus, Lnagenselbold, Germany
Benchtop centrifuge Mikro 20	Hettich, Tuttlingen, Germany
Centrifuge Rotixa 50 RS	Hettich, Tuttlingen, Germany
Cryo mill	Retsch, Haan, Germany
Incubator Multitron II	Infors, Einsbach, Germany
Micropipette 20 µL, 200 µL, 1000 µL	Brand, Wertheim, Germany
MTP-photometer Infinite M200	Tecan, Männedorf, Switzerland
MTP-photometer EL 808IU	Bio-Tek Instruments, Bad Friedrichshall, Germany
pH-electrode BlieLine 24 pH	Schott, Mainz, Germany
pH-meter CG 843	Schott, Mainz, Germany
Photometer Genesys 20	Thermo Spectronic, Neuss, Germany
Rotary shaker	NeoLab, Heidelberg, Germany
Thermomixer comfort	Eppendorf, Hamburg, Germany
Thermishaker microtiter plates	NeoLab, Heidelberg, Germany
WiseCube shaking incubator WIS-20	Witeg Labortechnik, Wertheim, Germany
ZetaSizer Nano-S	Malvern Instruments, Malvern, UK

Table A 2 – HPLC equipment

Equipment	Manufacturer
1100 HPLC-System	Agilent Technologies, Böblingen, Germany
Aminex HPX-87H column	Bio-Rad Laboratories, München, Germany
Dual channel interface 35900E	Agilent Technologies, Böblingen, Germany
Micro-Guard Cation H Cartridge	Bio-Rad Laboratories, München, Germany
MISTRAL column oven	Spark Holland, Emmen, Netherlands
UV/Vis detector S3300	Sykam, Fürstenfeldbruck, Germany

Table A 3 – Bioreactor48 equipment

Equipment	Manufacturer
Parallel bioreactor unit	2mag, München, Germany
Milliliter single-use bioreactors	PreSens Precision, Regensburg, Germany
Control device	2mag, München, Germany
Thermostat ME-12	Julabo, Seelbarch, Germany
Cooling unit DLK-402	G. Heinemann, Schwäbisch Hall, Germany

Table A 4 – Chromatography equipment

Equipment	Manufacturer
ÄktaPilot	GE Healthcare, Uppsala, Sweden
HisTrap FF crude columns, 1 mL	GE Healthcare, Uppsala, Sweden
Butyl FF columns, 1 mL	GE Healthcare, Uppsala, Sweden
HiTrap Capto Q, 1 mL	GE Healthcare, Uppsala, Sweden
Sepharose 4B chromatography medium	GE Healthcare, Uppsala, Sweden
Laboratory column (2.5 mL)	MobiTech, Göttingen, Germany
Laboratory column (12.5 mL)	MobiTech, Göttingen, Germany
Preparative column (25x200 mm)	Kronlab, Dinslaken, Germany

Table A 5 – Cloning equipment

Type	Manufacturer, location
Mastercycler gradient	Eppendorf, Hamburg, Germany
Gelelectrophoresis chamber MGU-402T	PBS Scientific Co.
SDS-PAGE gel chamber P8DS Class II	OWI, Portsmouth, USA
Power supply E802	Consort, Fournhout, Belgium
Power supply pegPOWER E300	Peqlab, Erlangen, Germany

Appendix A2 - Consumables

Table A 6 - Consumables

Consumable	Art.-No.	Manufacturer, location
Luminescence microtiter plates (96 wells)		Brand, Wertheim, Germany
Fluorescence microtiter plates (96 wells)		Corning Inc., Corning, USA
Microtiter plates (96 wells)		Thermo Fischer Scientific (NUNC), Rochester, USA
Cuvettes		
Quartz glass cuvettes		Eppendorf, Hamburg, Germany
Microcentrifuge tubes		Eppendorf, Hamburg, Germany
Conical centrifuge tubes (15 mL)		Corning Inc., Corning, USA
Conical centrifuge tubes (50 mL)		Corning Inc., Corning, USA
PCR tubes (0.5 mL)		Eppendorf, Hamburg, Germany
Vivaspin 20 ultrafiltration unit (10 kDa)		Sartorius, Göttingen, Germany
Amicon Ultra-15 centrifugal filters (100 kDa)		Merck, Darmstadt, Germany

Appendix A3 – Chemicals

Table A 7 – General chemicals

Chemical	Purity	Art.-No.	Supplier
Acetic acid	≥ 99.8 % for analysis, ACS, ISO, Ph. Eur.	10313699	Honeywell
Agar-agar	Bacteriology	A0949	Applichem
BICIN	≥ 99 %	9162	Carl Roth
Dialysis tube ZelluTrans	MWCO: 12,000-14,000	E674	Carl Roth
Disodium hydrogen phosphate	≥ 99 %, p.a., ISO	T106	Carl Roth
1,4-Dithiothreitol	≥ 99 %, p.a.	6908	Carl Roth
Imidazole	≥ 99 %, p.a.	X998	Carl Roth
Kanamycin sulfate	≥750 I.U./mg for biochemistry	T823	Carl Roth
Magnesium chloride	≥98.5 %, water free	KK36	Carl Roth
Magnesium sulfate	≥ 99 %, Ph. Eur., USP, BP	T888	Carl Roth
Nicotinamide adenosine dinucleotide	~ 98 % for biochemistry	AE11	Carl Roth

Chemical	Purity	Art.-No.	Supplier
Peptone ex casein	tryptic digest, mikrobiology	8986	Carl Roth
Sodium chloride	≥ 99.5 %, p.a., ACS, ISO	3957	Carl Roth
Sodium dihydrogen phosphate monohydrate	pro analysi	1.06346	Merck
Sodium hydroxide	≥ 99 %, p.a., ISO	6771	Carl Roth
Sulfuric acid	30 % Pure	X876.2	Carl Roth
Sulfuric acid	95-97 % for analysis, ISO	1.00731	Emsure®Merck
Yeast extract	Powder f.d. Bacteriology	2363	Carl Roth

Table A 8 – Reactants of the biosynthesis of CMP-Neu5Ac

Chemical	Purity	Art.-No.	Supplier
Adenosine 5'-triphosphate	> 98 %	K054	Carl Roth
Cytidine 5'-triphosphate	≥ 98 %	K507	Carl Roth
CMP-*N*-acetylneuraminic acid	≥ 85 %, HPLC	C8271	Sigma-Aldrich
N-Acetylglucosamine	≥ 99 % for biochemistry	8993	Carl Roth
N-Acetylmannosamine	≥ 98 %	5525	Carl Roth
N-Acetylneuraminic acid	≥ 98 %, HPLC	110138	Calbiochem
Pyruvate	≥ 99 % for biochemistry	8793	Carl Roth

Appendix A4 – Buffer compositions

Table A 9 – Buffers for IMAC

Component	IMAC binding buffer	IMAC elution buffer
Sodium phosphate	20 mM	20 mM
Imidazole	40 mM	500 mM
Sodium chloride	500 mM	500 mM

Table A 10 – Buffers for IMAC of membrane channel proteins

Components	IMAC-MB binding buffer	IMAC-MB elution buffer
Tris-HCl	20 mM	20 mM
Imidazole	20 mM	500 mM
Sodium chloride	300 mM	300 mM
O-POE	0.6 % v/v	0.6 % v/v

Table A 11 – Buffers for hydrophobic interaction chromatography

Components	HIC binding buffer	HIC washing buffer
Sodium phosphate	20 mM	20 mM
Sodium chloride	3 M	

Table A 12 – Buffers for anion exchange chromatography

Components	AEX binding buffer	AEX washing buffer	AEX elution buffer
Tris-HCl, pH 8.0	10 mM	-	-
Bicin, pH 8.0	-	10 mM	50 mM
NaCl	-	-	300 mM
O-POE	0.6 % v/v	0.6 v/v	0.6 v/v

Table A 13 – Buffers for SDS-PAGE gel preparation

Component	Stacking gel buffer (2x)	Resolving gel buffer (4x)
Tris-HCl	250 mM, pH 6.8	1.5 M, pH 8.8
SDS	0.4 % w/v	0.8 % w/v

Table A 14 – Buffers for SDS-PAGE sample preparation

Component	Laemmli buffer (5x)	Running buffer (10x)
Tris-Hcl	300 mM, pH 6.8	250 mM
Glycerol	50 % v/v	1.92 M
SDS	10 % v/v	1 % w/v
β-mercaptoethanol	5 % v/v	-
Bromophenol blue	0.05 % w/v	-

Table A 15 – Buffers SDS-PAGE protein staining

Component	Fairbanks A	Fairbanks B	Fairbanks C
Isopropanol	25 % v/v	10 % v/v	-
Acetic acid	10 % v/v	10 % v/v	10 % v/v
Coomassie Brilliant Blue R250/G250	0.05 % w/v	0.005 w/v	-

Appendix A5 – Media

Table A 16 – Media. The pH was adjusted to 7.4.

Component	Luria broth (LB)	Terrific broth (TB)
Peptone (Casein)	10 g L^{-1}	12 g L^{-1}
Yeast extract	5 g L^{-1}	24 g L^{-1}
NaCl	5 g L^{-1}	-
Glycerol	-	4 mL L^{-1}
KH_2PO_4	-	2.13 g L^{-1}
K_2HPO_4	-	12.54 g L^{-1}

Appendix A6 – Software

Table A 17 – Software

Software	Developer
GENtle	Magnus Manske, Cologne, Germany (http://gentle.magnusmanske.de)
ImageJ 1.46r	National Institutes of Health (http://rsbweb.nih.gov/ij/)
MATLAB R2010b, R2012b	MathWorks, Natick, USA
Sigma Plot 12.3	Systat Software, Chicago, USA
MTP-photometer software Magellan v6.1	Tecan, Männedorf, Switzerland
MTP-photometer software KC Junior v.1.10	Bio-Tek Instruments, Bad Friedrichshall, Germany

Appendix A7 – Enzymes and Kits

Table A 18 – Purchased enzymes

Enzyme	Supplier, location
Antarctic Phosphatase	New England Biolabs
DNaseI	Carl Roth
Inorganic phosphatase, from baker's yeast	Sigma-Aldrich
Lactate dehydrogenase	Sigma-Aldrich
Lysozyme	Sigma-Aldrich
Phusion® High-Fidelity DNA-Polymerase	Finnymes
Proteinase K	Carl Roth
Restriction enzyme BamHI-HF	New England Biolabs
Restriction enzyme EcoRI-HF	New England Biolabs
Restriction enzyme KpnI-HF	New England Biolabs
Restriction enzyme NcoI-HF	New England Biolabs
Restriction enzyme NdeI	New England Biolabs
Restriction enzyme SalI	New England Biolabs
Restriction enzyme XhoI	New England Biolabs
T4 DNA-Ligase	New England Biolabs
Taq DNA-Polymerase	New England Biolabs

Table A 19 – Kits and standards

Kits and standards	Manufacturer	Art.-No.
Bicinchoninic acid (BCA) Protein Assay Kit	Thermo Scientific	23227
dNTP-Mix	New England Biolabs	N0447S
DNA-ladder 100 bp extended	Carl Roth	T835
GenEluteTM HP Plasmid Miniprep Kit	Sigma-Aldrich	PLN70
GenEluteTM HP Plasmid Maxiprep Kit	Sigma-Aldrich	NA0310
GenEluteTM Gel Extraction Kit	Sigma-Aldrich	NA1111
GenEluteTM PCR Clean-Up Kit	Sigma-Aldrich	NA1020
Kinase-Glo® Luminescent Kinase Assay	Promega	V6711
QuikChange® Lightning Site-Directed Mutagenesis Kit	Agilent Technologies	210518
Roti®-Mark Standard	Carl Roth	T851
Perfect ProteinTM Markers, 10 – 225 kDa	Merck	69079
Phosphate Colorimetric Kit	Sigma-Aldrich	MAK030

Appendix A8 – Genes

Table A 20 – Genes

Name	Sequence (5' → 3')
eGFP	ATGGTGAGCAAGGGCGAGGAGCTGTTCACCGGGGTGGTGCCCATCCTGGTCGAGCT GGACGGCGACGTAAACGGCCACAAGTTCAGCGTGTCCGGCGAGGGCGAGGGCGATG CCACCTACGGCAAGCTGACCCTGAAGTTCATCTGCACCACCGGCAAGCTGCCCGTG CCCTGGCCCACCCTCGTGACCACCCTGACCTACGGCGTGCAGTGCTTCAGCCGCTA CCCCGACCACATGAAGCAGCACGACTTCTTCAAGTCCGCCATGCCCGAAGGCTACG TCCAGGAGCGCACCATCTTCTTCAAGGACGACGGCAACTACAAGACCCGCGCCGAG GTGAAGTTCGAGGGCGACACCCTGGTGAACCGCATCGAGCTGAAGGGCATCGACTT CAAGGAGGACGGCAACATCCTGGGGCACAAGCTGGAGTACAACTACAACAGCCACA ACGTCTATATCATGGCCGACAAGCAGAAGAACGGCATCAAGGTGAACTTCAAGATC CGCCACAACATCGAGGACGGCAGCGTGCAGCTCGCCGACCACTACCAGCAGAACAC CCCCATCGGCGACGGCCCCGTGCTGCTGCCCGACAACCACTACCTGAGCACCCAGT CCGCCCTGAGCAAAGACCCCAACGAGAAGCGCGATCACATGGTCCTGCTGGAGTTC GTGACCGCCGCCGGGATCACTCTCGGCATGGACGAGCTGTACAAG
AGE K160I	ATGGGGAAAAACTTGCAAGCATTGGCGCAACTTTACAAAAATGCCCTCCTCAACGA CGTACTCCCGTTTTGGGAAAACTACTCCCTCGATAGTGAAGGCGGTTACTTTACTT GTCTTGATCGCCAAGGTAAGGTGTATGACACAGATAAATTTATTTGGTTGCAAAAT CGCCAAGTCTGGACTTTTTCTATGCTGTGTAACCAGCTAGAAAAACGGGAAAACTG GCTCAAAATTGCGAGGAACGGCGCTAAATTTCTTGCCCAACATGGTAGAGATGACG AGGGTAACTGGTATTTTGCCCTCACCCGTGGAGGTGAACCATTAGTACAGCCTTAC AATATTTTTTCTGATTGCTTTGCGGCGATGGCCTTTAGCCAATATGCTCTCGCCTC TGGTGAAGAGTGGTCAAAAGATGTGGCAATGCAAGCATATAATAATGTTTTGCGTC GTAAAGATAACCCCAAAGGCAAATATACCATCACCTATCCCGGCACACGCCCCATG AAAGCTTTAGCTGTGCCGATGATTTTAGCCAACCTCACTCTAGAAATGGAATGGTT GCTTCCCCAGGAGACTCTAGAAAATGTCTTGGCTGCAACCGTTCAGGAAGTTATGG GTGACTTTCTCGACCAAGAACGAGGATTGATGTATGAAAATGTTGCCCCCGATGGT TCCCACATTGATTGTTTTGAAGGTCGGCTGATTAACCCCGGTCACGGTATTGAAGC GATGTGGTTTATTATGGACATCGCCCGACGGAAAAACGACAGCAAGACTATTAACC AAGCAGTTGATGTGGTGTTAAATATCCTCAATTTCGCCTGGGATAACGAGTATGGT GGCTTGTATTACTTTATGGATGCAGCAGGTCATCCTCCACAACAATTGGAATGGGA TCAAAAATTGTGGTGGGTGCATTTAGAATCTTTGGTGGCTTTGGCGATGGGTTATC GTTTGACAGGTCGTGAAGTCTGTTGGGAATGGTATCAAAAAATGCACGATTATTCC TGGCAGCATTTTGCTGACCCAGAATATGGTGAGTGGTTTGGCTACTTAAATCGCCG TGGGGAAGTGCTGTTAAATCTCAAAGGTGGTAAATGGAAGGGATGTTTTCATGTAC CCCGTGCTTTGTATCTGTGTTGGCAACAGTTCGAGGCCTTGAGTTTACAATCAGCT TAA
NAL	ATGGCAACGAATTTACGTGGCGTAATGGCTGCACTCCTGACTCCTTTTGACCAACA ACAAGCACTGGATAAAGCGAGTCTGCGTCGCCTGGTTCAGTTCAATATTCAGCAGG GCATCGACGGTTTATACGTGGGTGGTTCGACCGGCGAGGCCTTTGTACAAAGCCTT TCCGAGCGTGAACAGGTACTGGAAATCGTCGCCGAAGAGGCGAAAGGTAAGATTAA ACTCATCGCCCACGTCGGTTGCGTCAGCACCGCCGAAAGCCAACAACTTGCGGCAT CGGCTAAACGTTATGGCTTCGATGCCGTCTCCGCCGTCACGCCGTTCTACTATCCT TTCAGCTTTGAAGAACACTGCGATCACTATCGGGCAATTATTGATTCGGCGGATGG TTTGCCGATGGTGGTGTACAACATTCCAGCCCTGAGTGGGGTAAAACTGACCCTGG ATCAGATCAACACACTTGTTACATTGCCTGGCGTAGGTGCGCTGAAACAGACCTCT GGCGATCTCTATCAGATGGAGCAGATCCGTCGTGAACATCCTGATCTTGTGCTCTA TAACGGTTACGACGAAATCTTCGCCTCTGGTCTGCTGGCGGGCGCTGATGGTGGTA TCGGCAGTACCTACAACATCATGGGCTGGCGCTATCAGGGGATCGTTAAGGCGCTG AAAGAAGGCGATATCCAGACCGCGCAGAAACTGCAAACTGAATGCAATAAAGTCAT TGATTTACTGATCAAAACGGGCGTATTCCGCGGCCTGAAAACTGTCCTCCATTATA TGGATGTCGTTTCTGTGCCGCTGTGCCGCAAACCGTTTGGACCGGTAGATGAAAAA TATCTGCCAGAACTGAAGGCGCTGGCCCAGCAGTTGATGCAAGAGCGCGGGTGA

Name	Sequence (5' → 3')
CSS	ATGGAAAAACAAAATATTGCGGTTATACTTGCGCGCCAAAACTCCAAAGGATTGCC ATTAAAAAATCTCCGGAAAATGAATGGCATATCATTACTTGGTCATACAATTAATG CTGCTATATCATCAAAGTGTTTTGACCGCATAATTGTTTCGACTGATGGCGGGTTA ATTGCAGAAGAAGCTAAAAATTTCGGTGTCGAAGTCGTCCTACGCCCTGCAGAGCT GGCCTCCGATACAGCCAGCTCTATTTCAGGTGTAATACATGCTTTAGAAACAATTG GCAGTAATTCCGGCACAGTAACCCTATTACAACCAACCAGTCCATTACGCACAGGG GCTCATATTCGTGAAGCTTTTTCTCTATTTGATGAGAAAATAAAAGGATCCGTTGT CTCTGCATGCCCAATGGAGCATCATCCACTAAAAACCCTGCTTCAAATCAATAATG GCGAATATGCCCCCATGCGCCATCTAAGCGATTTGGAGCAGCCTCGCCAACAATTA CCTCAAGCATTTAGGCCTAATGGTGCAATTTACATTAATGATACTGCTTCACTAAT TGCAAATAATTGTTTTTTTATCGCCCCAACCAAACTTTATATTATGTCTCATCAAG ACTCTATCGATATTGATACTGAGCTTGATTTACAACAGGCAGAAAACATTCTTAAT CACAAGGAAAGCTAA
OmpF	GCAGAAATCTATAACAAAGATGGCAACAAAGTAGATCTGTACGGTAAAGCTGTTGG TCTGCATTATTTTTCCAAGGGTAACGGTGAAAACAGTTACGGTGGCAATGGCGACA TGACCTATGCCCGTCTTGGTTTTAAAGGGGAAACTCAAATCAATTCCGATCTGACC GGTTATGGTCAGTGGGAATATAACTTCCAGGGTAACAACTCTGAAGGCGCTGACGC TCAAACTGGTAACAAAACGCGTCTGGCATTCGCGGGTCTTAAATACGCTGACGTTG GTTCTTTCGATTACGGCCGTAACTACGGTGTGGTTTATGATGCACTGGGTTACACC GATATGCTGCCAGAATTTGGTGGTGATACTGCATACAGCGATGACTTCTTCGTTGG TCGTGTTGGCGGCGTTGCTACCTATCGTAACTCCAACTTCTTTGGTCTGGTTGATG GCCTGAACTTCGCTGTTCAGTACCTGGGTAAAAACGAGCGTGACACTGCACGCCGT TCTAACGGCGACGGTGTTGGCGGTTCTATCAGCTACGAATACGAAGGCTTTGGTAT CGTTGGTGCTTATGGTGCAGCTGACCGTACCAACCTGCAAGAAGCTCAACCTCTTG GCAACGGTAAAAAAGCTGAACAGTGGGCTACTGGTCTGAAGTACGACGCGAACAAC ATCTACCTGGCAGCGAACTACGGTGAAACCCGTAACGCTACGCCGATCACTAATAA ATTTACAAACACCAGCGGCTTCGCCAACAAAACGCAAGACGTTCTGTTAGTTGCGC AATACCAGTTCGATTTCGGTCTGCGTCCGTCCATCGCTTACACCAAATCTAAAGCG AAAGACGTAGAAGGTATCGGTGATGTTGATCTGGTGAACTACTTTGAAGTGGGCGC AACCTACTACTTCAACAAAAACATGTCCACCTATGTTGACTACATCATCAACCAGA TCGATTCTGACAACAAACTGGGCGTAGGTTCAGACGACACCGTTGCTGTGGGTATC GTTTACCAGTTCTAA
OmpF G119D	GCAGAAATCTATAACAAAGATGGCAACAAAGTAGATCTGTACGGTAAAGCTGTTGG TCTGCATTATTTTTCCAAGGGTAACGGTGAAAACAGTTACGGTGGCAATGGCGACA TGACCTATGCCCGTCTTGGTTTTAAAGGGGAAACTCAAATCAATTCCGATCTGACC GGTTATGGTCAGTGGGAATATAACTTCCAGGGTAACAACTCTGAAGGCGCTGACGC TCAAACTGGTAACAAAACGCGTCTGGCATTCGCGGGTCTTAAATACGCTGACGTTG GTTCTTTCGATTACGGCCGTAACTACGGTGTGGTTTATGATGCACTGGGTTACACC GATATGCTGCCAGAATTTGATGGTGATACTGCATACAGCGATGACTTCTTCGTTGG TCGTGTTGGCGGCGTTGCTACCTATCGTAACTCCAACTTCTTTGGTCTGGTTGATG GCCTGAACTTCGCTGTTCAGTACCTGGGTAAAAACGAGCGTGACACTGCACGCCGT TCTAACGGCGACGGTGTTGGCGGTTCTATCAGCTACGAATACGAAGGCTTTGGTAT CGTTGGTGCTTATGGTGCAGCTGACCGTACCAACCTGCAAGAAGCTCAACCTCTTG GCAACGGTAAAAAAGCTGAACAGTGGGCTACTGGTCTGAAGTACGACGCGAACAAC ATCTACCTGGCAGCGAACTACGGTGAAACCCGTAACGCTACGCCGATCACTAATAA ATTTACAAACACCAGCGGCTTCGCCAACAAAACGCAAGACGTTCTGTTAGTTGCGC AATACCAGTTCGATTTCGGTCTGCGTCCGTCCATCGCTTACACCAAATCTAAAGCG AAAGACGTAGAAGGTATCGGTGATGTTGATCTGGTGAACTACTTTGAAGTGGGCGC AACCTACTACTTCAACAAAAACATGTCCACCTATGTTGACTACATCATCAACCAGA TCGATTCTGACAACAAACTGGGCGTAGGTTCAGACGACACCGTTGCTGTGGGTATC GTTTACCAGTTCTAA
CecA	ATGAAATGGAAGTTATTTAAAAAGATAGAAAAAGTTGGTCAGAATATTAGAGATGG TATAATCAAAGCTGGACCAGCTGTTGCAGTAGTAGGGGGAGCAACACAAATTGCAA AA
Cytb_5'	CTGAGCAAACCGATGGAAACCCTGATTACCACCGTGGATAGCAATAGCAGCTGGTG GACCAATTGGGTGATTCCGGCGATTAGCGCGCTGATTGTGGCGCTGATGTATCGTC TGTATATGGCGGATGAT

Name	Sequence (5’ → 3’)
L’	CCATTCAAACATGAGGATTACCCATGTCGAAGACAACAAAGAAGTTCAACTCTTTA TGTATTGATCTTCCTCGCGATCTTTCTCTCGAAATTTACCAATCAATTGCTTCTGT CGCTACTGGAAGCGGTGATCCGCACAGTGACGACTTTACAGCAATTGCTTACT
UBC6’	GTGTATATTGGCATTGCGATTTTTCTGTTTCTGGTGGGCCTGTTTATGAAA
Vam3p’	GTGACCCTGATTATTATTATTGTGGTGTGCATGGTGGTGCTGCTGGCGGTGCTGAG C
PolyAL	ATGGCGAACATGCTCGCAGCGTTGCTGGCCCTGCTTGCTGCGCTGTTGGCGCTGTT AGCCGCGTTACTGGCACTGCTGGCAGCTCTGCTCGCC

Appendix A9 – Oligonucleotides

Table A 21 – Primers for eGFP fusion proteins. Restriction sites are underlined.

Name	Sequence (5’ → 3’)	Tm
eGFP_for (NdeI)	GAT ACA CAT ATG GTG AGC AAG GGC GAG GAG	60.5
eGFP_for (EcoRI)	GAT ACA GAA TTC GTG AGC AAG GGC GAG GAG	60.5
eGFP_rev (EcoRI)	GAT ACA GAA TTC CTT GTA CAG CTC GTC CAT G	56.7
eGFP_rev (XhoI)	GAT ACA CTC GAG CTT GTA CAG CTC GTC CAT G	56.7
CecApA_for (NdeI)	GAT ACA CAT ATG AAA TGG AAG TTA TTT AAA AAG ATA G	51.5
CecApA_rev (EcoRI)	GAT ACA GAA TTC GGC AGC TGC AGC CGC A	59.4
CecApA_assembly_1	GAT ACA CAT ATG AAA TGG AAG TTA TTT AAA AAG ATA GAA AAA GTT GGT CAG AAT ATT AGA GA	70.0
CecApA_assembly_2	CTA CTA CTG CAA CAG CTG GTC CAG CTT TGA TTA TAC CAT CTC TAA TAT TCT GAC CAA CTT TTT CTA TCT TTT	77.0
CecApA_assembly_3	CCA GCT GTT GCA GTA GTA GGG GGA GCA ACA CAA ATT GCA AAA GCT GCT GCG GCT GCT GCG	89.0
CecApA_assembly_4	TAA TAC GAC TCA CTA TAG ATA CAG GAT CCG GCA GCT GCA GCC GCA GCA GCC GC	84.0
Cytb5_for (EcoRI)	GAT ACA GAA TTC CTG AGC AAA CCG ATG GAA AC	57.3
Cytb5_rev (XhoI)	GAT ACA CTC GAG TTA ATC ATC CGC CAT ATA CAG AC	58.9
UBC6_for (EcoRI)	GAT ACA GAA TTC ATG GTG TAT ATT GGC ATT G	50.2
UBC6_rev (XhoI)	GAT ACA CTC GAG CTA TTT CAT AAA CAG GCC CAC	55.9
PolyAL_for (NdeI)	GAT ACA CAT ATG GCG AAC ATG CTC GCA G	62.1
PolyAL_rev (EcoRI)	GAT ACA GAA TTC GGC GAG CAG AGC TGC CAG CA	65.5
Vam3p_for (EcoRI)	GAT ACA GAA TTC GTG ACC CTG ATT ATT ATT ATT GTG GTG	60.4
Vam3p_rev (XhoI)	GAT ACA CTC GAG TTA GCT CAG CAC CGC CAG	62.8

Name	Sequence (5' → 3')	Tm
	CAG	
L'_for (EcoRI)	GAT ACA GAA TTC CCA TTC AAA CAT GAG GAT TAC CCA TG	61.6
L'_rev (XhoI)	GAT ACA CTC GAG TTA AGT AAG CAA TTG CTG TAA AGT CGT C	60.7
10xAla_for (EcoRI/EcoRI)	GATA GAA TTC GCT GCT GCG GCT GCT GCG GCT GCA GCT GCC GAA TTC TATC	-
10xAla_rev (EcoRI/EcoRI)	GATA GAA TTC GGC AGC TGC AGC CGC AGC AGC CGC AGC AGC GAA TTC TATC	-

Table A 22 – Primers for NAL and CSS fusion proteins. Restriction sites are underlined.

Name	Sequence (5' → 3')	Tm
CSS_for (NdeI)	GAT ACA CAT ATG GAA AAA CAA AAT ATT GCG GTT ATA CTT G	60.2
CSS_rev (EcoRI)	GAT ACA GAA TTC GCT TTC CTT GTG ATT AAG AAT GTT TTC TG	60.2
NAL_for (NdeI)	GAT ACA CAT ATG GCA ACG AAT TTA CGT GGC	53.7
NAL_rev (EcoRI)	GAT ACA GAA TTC CCC GCG CTC TTG CAT	53.3
Cytb5_for (SalI)	GAT ACA GTC GAC CTG AGC AAA CCG ATG GAA AC	57.3
Cytb5_rev (XhoI)	GAT ACA CTC GAG TTA ATC ATC CGC CAT ATA CAG AC	58.9
UBC6_for (SalI)	GAT ACA GTC GAC ATG GTG TAT ATT GGC ATT G	50.2
UBC6_rev (XhoI)	GAT ACA CTC GAG CTA TTT CAT AAA CAG GCC CAC	55.9
Vam3p_for (SalI)	GAT ACA GTC GAC GTG ACC CTG ATT ATT ATT ATT GTG GTG	60.4
Vam3p_rev (XhoI)	GAT ACA CTC GAG TTA GCT CAG CAC CGC CAG CAG	62.8
L'_for (SalI)	GAT ACA GTC GAC CCA TTC AAA CAT GAG GAT TAC CCA TG	61.6
L'_rev (XhoI)	GAT ACA CTC GAG TTA AGT AAG CAA TTG CTG TAA AGT CGT C	60.7
10xAla_for (EcoRI/SalI)	GATA GAA TTC GCT GCT GCG GCT GCT GCG GCT GCA GCT GCC GTC GAC TATC	-
10xAla_rev (EcoRI/SalI)	GATA GTC GAC GGC AGC TGC AGC CGC AGC AGC CGC AGC AGC GAA TTC TATC	-

Table A 23 – Primers for OmpF mutagenesis, MBP-TEV-PolyAL-eGFP and colony PCR. Restriction sites are underlined.

Name	Sequence (5' → 3')	Tm
OmpF G119D_mut_for	CTG TAT GCA GTA TCA CCA TCA AAT TCT GGC AGC ATA TC	78.4
OmpF G119D_mut_rev	GAT ATG CTG CCA GAA TTT GAT GGT GAT ACT GCA TAC AG	78.4
PolyAL-eGFP_for (NcoI)	GAT ACA CCA TGG GCG AAC ATG CTC GCA G	62.1
PolyAL-eGFP_rev (KpnI)	GAT ACA GGT ACC CTT GTA CAG CTC GTC CAT G	56.7
T7	TAA TAC GAC TCA CTA TAG GG	-
T7 terminator	CTA GTT ATT GCT CAG CGG T	-

Appendix A10 – Vectors

Table A 24 - Vectors

Name	Supplier, location
pET21a(+)	Novagen, San Diego, USA
pET28a(+)	Novagen, San Diego, USA
pETM41a(+)	EMBL, Heidelberg, Germany
pET28a(+)-AGE K160I	Dr. Kathrin Castiglione, TU München
pET28a(+)-NAL	Dr. Kathrin Castiglione, TU München
pEGFP	Prof. Andreas Groll, TU München
pKKS-CSS	Prof. Wolf-Dieter Fessner, TU Darmstadt
pCytb5'-UBC6'-L'	Dr. Kathrin Castiglione, TU München

Appendix A11 – *E. coli* strains

Table A 25 – *E. coli* strains

Name	Genotype	Supplier, location
E. coli BL21 (DE3)	F-*omp*T *gal dcm lon hsd*SB(rB-mB-) λ(DE3[lacI lacUV5- T7 gene 1 *ind*1 *sam*7 *nin*5])	Novagen, San Diego, USA
E. coli BL21 (DE3) *omp8*	F-*omp*T *gal dcm lon hsd*SB(rB-mB-) λ(DE3[lacI lacUV5- T7 gene 1 *ind*1 *sam*7 *nin*5]) Δ*lamB ompF*::Tn5 Δ*ompA* Δ*ompC*	Prilipov *et al.*, 1998
E. coli DH5α	F-endA1glnV44thi-1recA1relA1gyrA96deoRnupG j80dlacZΔM15(*lac*ZYA-*arg*F)U169,hsdR17(rK-mK+),λ-	Invitrogen, Carlsbad, USA
E. coli XL10-Gold®	Tetr Δ(*mcrA*)*183* Δ(*mcrCB-hsdSMR-mrr*)*173 endA1 supE44 thi-1 recA1 gyrA96 relA1 lac* Hte [F´ *proAB lacI*q*Z*Δ*M15* Tn*10* (Tetr) Amy Camr]	Stratagene, La Jolla, USA

Appendix A12 – Amino acid sequences of peptide anchors

Table A 26 – Amino acid sequences

Name	Sequence (N → C)
eGFP	MVSKGEELFTGVVPILVELDGDVNGHKFSVSGEGEGDATYGKLTLKFICTTGKLPV PWPTLVTTLTYGVQCFSRYPDHMKQHDFFKSAMPEGYVQERTIFFKDDGNYKTRAE VKFEGDTLVNRIELKGIDFKEDGNILGHKLEYNYNSHNVYIMADKQKNGIKVNFKI RHNIEDGSVQLADHYQQNTPIGDGPVLLPDNHYLSTQSALSKDPNEKRDHMVLLEF VTAAGITLGMDELYK
AGE K160I	MGSSHHHHHHSSGLVPRGSHMGKNLQALAQLYKNALLNDVLPFWENYSLDSEGGYF TCLDRQGKVYDTDKFIWLQNRQVWTFSMLCNQLEKRENWLKIARNGAKFLAQHGRD DEGNWYFALTRGGEPLVQPYNIFSDCFAAMAFSQYALASGEEWSKDVAMQAYNNVL RRKDNPKGKYTITYPGTRPMKALAVPMILANLTLEMEWLLPQETLENVLAATVQEV MGDFLDQERGLMYENVAPDGSHIDCFEGRLINPGHGIEAMWFIMDIARRKNDSKTI NQAVDVVLNILNFAWDNEYGGLYYFMDAAGHPPQQLEWDQKLWWVHLESLVALAMG YRLTGREVCWEWYQKMHDYSWQHFADPEYGEWFGYLNRRGEVLLNLKGGKWKGCFH VPRALYLCWQQFEALSLQSA
NAL	MATNLRGVMAALLTPFDQQQALDKASLRRLVQFNIQQGIDGLYVGGSTGEAFVQSL SEREQVLEIVAEEAKGKIKLIAHVGCVSTAESQQLAASAKRYGFDAVSAVTPFYYP FSFEEHCDHYRAIIDSADGLPMVVYNIPALSGVKLTLDQINTLVTLPGVGALKQTS GDLYQMEQIRREHPDLVLYNGYDEIFASGLLAGADGGIGSTYNIMGWRYQGIVKAL KEGDIQTAQKLQTECNKVIDLLIKTGVFRGLKTVLHYMDVVSVPLCRKPFGPVDEK YLPELKALAQQLMQERG

Name	Sequence (N → C)
CSS	MEKQNIAVILARQNSKGLPLKNLRKMNGISLLGHTINAAISSKCFDRIIVSTDGGL IAEEAKNFGVEVVLRPAELASDTASSISGVIHALETIGSNSGTVTLLQPTSPLRTG AHIREAFSLFDEKIKGSVVSACPMEHHPLKTLLQINNGEYAPMRHLSDLEQPRQQL PQAFRPNGAIYINDTASLIANNCFFIAPTKLYIMSHQDSIDIDTELDLQQAENILN HKES
OmpF	AEIYNKDGNKVDLYGKAVGLHYFSKGNGENSYGGNGDMTYARLGFKGETQINSDLT GYGQWEYNFQGNNSEGADAQTGNKTRLAFAGLKYADVGSFDYGRNYGVVYDALGYT DMLPEFGGDTAYSDDFFVGRVGGVATYRNSNFFGLVDGLNFAVQYLGKNERDTARR SNGDGVGGSISYEYEGFGIVGAYGAADRTNLQEAQPLGNGKKAEQWATGLKYDANN IYLAANYGETRNATPITNKFTNTSGFANKTQDVLLVAQYQFDFGLRPSIAYTKSKA KDVEGIGDVDLVNYFEVGATYYFNKNMSTYVDYIINQIDSDNKLGVGSDDTVAVGI VYQF
OmpF G119D	AEIYNKDGNKVDLYGKAVGLHYFSKGNGENSYGGNGDMTYARLGFKGETQINSDLT GYGQWEYNFQGNNSEGADAQTGNKTRLAFAGLKYADVGSFDYGRNYGVVYDALGYT DMLPEFDGDTAYSDDFFVGRVGGVATYRNSNFFGLVDGLNFAVQYLGKNERDTARR SNGDGVGGSISYEYEGFGIVGAYGAADRTNLQEAQPLGNGKKAEQWATGLKYDANN IYLAANYGETRNATPITNKFTNTSGFANKTQDVLLVAQYQFDFGLRPSIAYTKSKA KDVEGIGDVDLVNYFEVGATYYFNKNMSTYVDYIINQIDSDNKLGVGSDDTVAVGI VYQF
CecA	KWKLFKKIEKVGQNIRDGIIKAGPAVAVVGQATQIAK
Cytb_5'	LSKPMETLITTVDSNSSWWTNWVIPAISALIVALMYRLYMADD
L'	PFKHEDYPCRRQQRSSTLYVLIFLAIFLSKFTNQLLLSLLEAVIRTVTTLQQLLT
UBC6'	VYIGIAIFLFLVGLFMK
Vam3p'	VTLIIIIVVCMVVLLAVLS
PolyAL	MANMLAALLALLAALLALLAALLALLAALLA

Table A 27 – Molecular masses of eGFP and eGFP fusion proteins

Name	Molecular mass, kDa
eGFP	29.105
CecA-eGFP	32.067
eGFP-Cytb_5'	35.268
eGFP-L'	36.819
eGFP-UBC6'	33.449
eGFP-Vam3p'	32.362
PolyAL-eGFP	31.921
MBP-TEV-PolyAL-eGFP	74.340

Table A 28 – Molecular masses of NAL and CSS and their respective fusion proteins

Name	Molecular mass, kDa		Molecular mass, kDa
NAL	34.757	**CSS**	27.130
NAL-Cytb_5'	40.858	**CSS-Cytb_5'**	33.219
NAL-L'	42.409	**CSS-L'**	34.770
NAL-UBC6'	38.016	**CSS-UBC6'**	30.377
NAL-Vam3p'	37.952	**CSS-Vam3p'**	30.313

Table A 29 – Molecular masses of AGE K160I and the membrane channel proteins

Name	Molecular mass, kDa
AGE K160I	47.762
OmpF	39.933
OmpF G119D	39.991

13. Appendix B

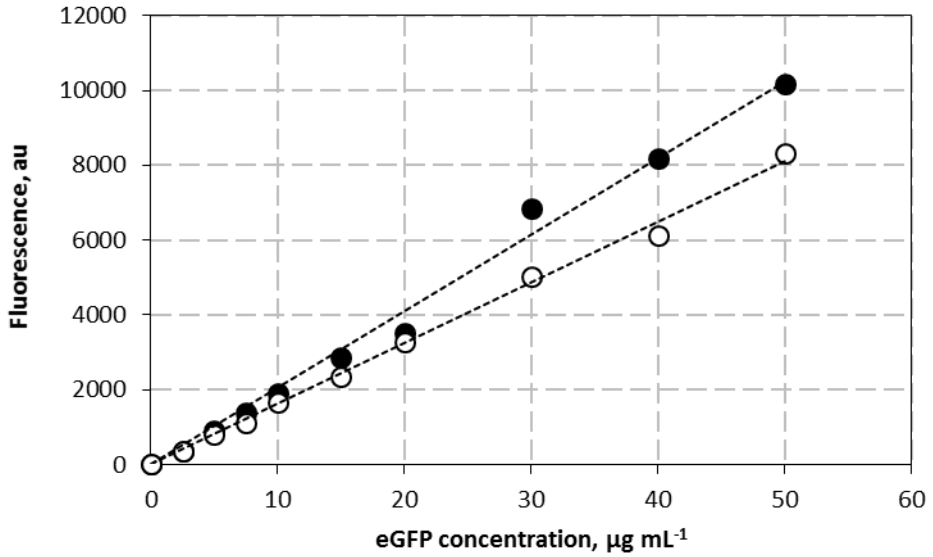

Figure B1 – Increase in fluorescence with increasing eGFP concentration with no polymersomes (*black*) and with 0.5 % w/v polymersomes (*white*).

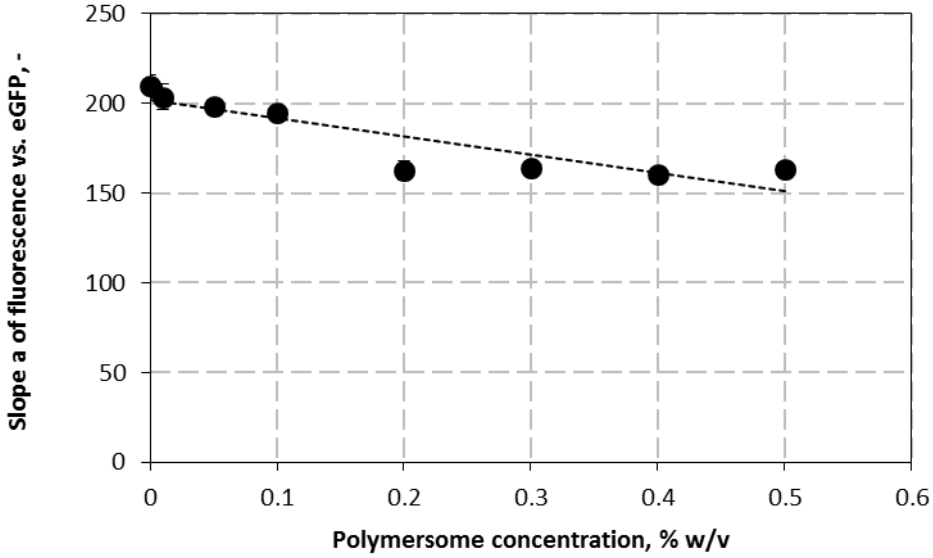

Figure B2 – Slopes of eGFP fluorescence with increasing eGFP concentration against polymersome concentration, resulting in a linear decrease of the fluorescence slope with increasing polymersome concentration.

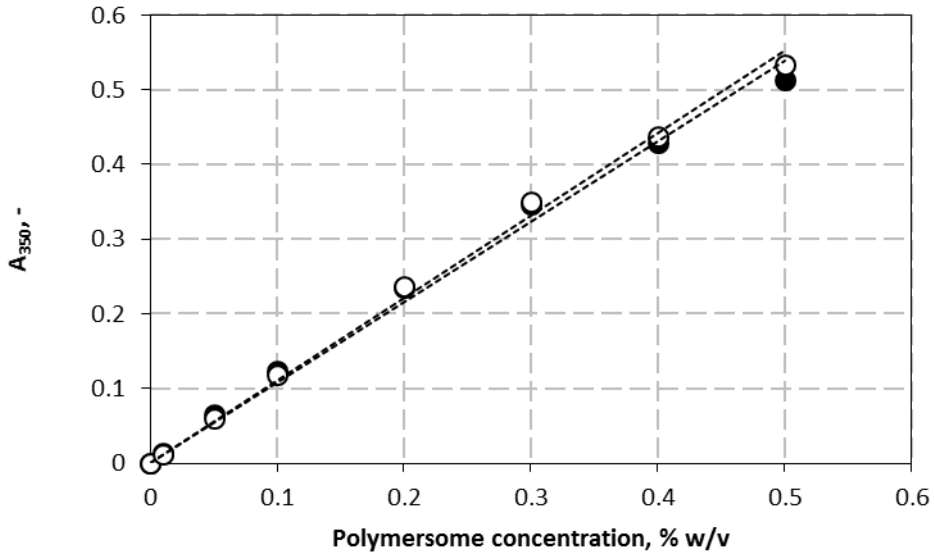

Figure B3 – Influence of eGFP concentration on the light extinction of the polymersomes at 350 nm. No change in light extinction of the polymersomes was measured when adding 0 µg mL^{-1} (*black*) and 50 µg mL^{-1} eGFP (*white*).

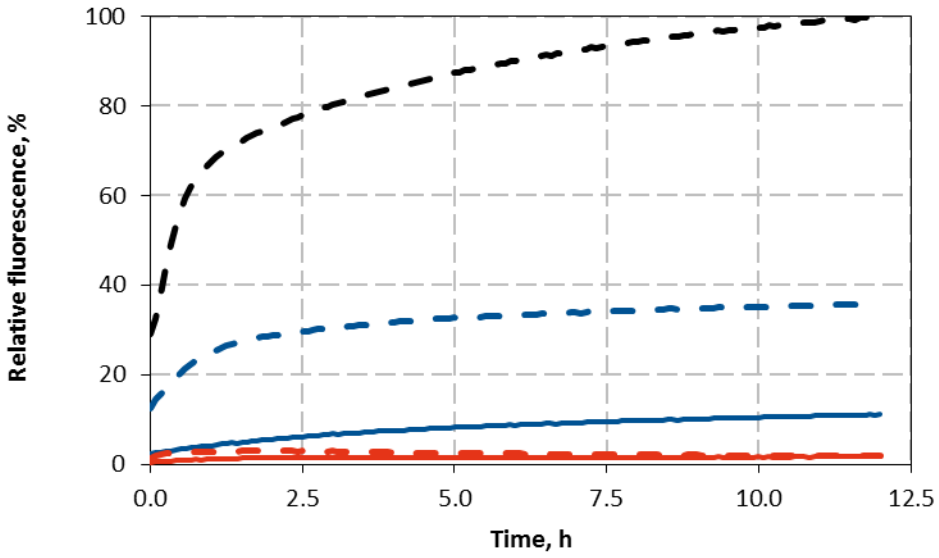

Figure B4 – Membrane integrity of calcein-loaded polymersomes in the presence of 0.75x (*solid*) and 1.5x (*dashed*) the critical micellar concentration (CMC) of NP-40 (*blue*) and 0.75 (*solid*) and 1.5x (*dashed*) the CMC of cholate (*red*). Treatment with 3 % triton X-100 is shown in *dashed black*.